RESPONSIVE POLYSACCHARIDE MACROSURFACTANTS FROM DEXTRAN BUILDING BLOCKS

DISSERTATION

Zur Erlangung des naturwissenschaftlichen Grades
„Doktor der Naturwissenschaften“
Im Promotionsfach Chemie

am Fachbereich Chemie, Pharmazie und Geowissenschaften
der Johannes Gutenberg-Universität Mainz

vorgelegt von

Diplom-Chemiker
Benjamin Bernhard Breitenbach
geboren in Bietigheim-Bissingen

Mainz, Januar 2019

– D77 –

Mainzer Dissertation

Dekan:

Erstgutachter:

Zweitgutachterin:

Tag der Einreichung: 11.01.2019

Tag der mündlichen Prüfung: 19.02.2019

EIDESSTATTLICHE ERKLÄRUNG

Die vorgelegte Dissertation wurde von April 2015 bis September 2018 am Institut für Pharmazie und Biochemie der Johannes Gutenberg-Universität in Mainz zur Erlangung des Grades „Doktor der Naturwissenschaften“ angefertigt.

Erstgutachter:

Zweitgutachterin:

Hiermit erkläre ich an Eides statt, dass ich die vorliegende Dissertation selbstständig und nur mit den angegebenen Hilfsmitteln angefertigt habe. Diese Dissertation wurde noch nicht als Prüfungsarbeit für eine andere Prüfung eingereicht. Zudem wurden bisher weder die gleiche, noch Teile der Abhandlung als Dissertation bei einer anderen Fakultät oder einem anderen Fachbereich eingereicht.

Ort, Datum Benjamin Breitenbach

ABSTRACT

Stimuli-responsive macromolecular drug delivery systems and smart nanomaterials from oligo- and polysaccharide block copolymers with amphiphilic character are emerging classes of compounds in nanomedicine. Combining a non-toxic character with controllable degradability, high biocompatibility and excellent solubility in aqueous solvents, they can serve as precisely tunable and robust nanomaterials and represent a green and sustainable alternative to artificial polymeric materials. With their inherent capacity to self-organize into micelles, rods or polymersomes they can protect and significantly improve the bioavailability of sensitive and pharmaceutically active cargo that would not be otherwise applicable in biological systems.

This thesis reports several synthetic approaches towards end group functionalized dextrans and their application in the construction of amphiphilic responsive block copolymers and starlike polysaccharide brush architectures. Key steps of the synthesis include a versatile reductive amination by a modified microwave-assisted procedure, involving a co-solvent system, and the introduction of *p*-substituted aniline derivatives. Hereby it was possible to install useful functionalities at the chain end in an effective, facile and time saving manner. This approach led us to azide- and alkyne- end-modified dextrans, which were used for the Cu-promoted synthesis of the first-ever reported amphiphilic, pH-responsive block copolymer consisting solely of polysaccharide blocks. The material has surface-activity and self-assembles in water into spherical micellar nanoparticles. This Cu-mediated transformation was then further developed to a metal-free thiol-based approach. Hereby it was possible to gain access to single- and double-stimuli-responsive polysaccharide macrosurfactants from a single starting material. Their amphiphilic nature and degradation behavior were studied in detail with a focus on drug loading capacities and triggered release. A highly potent, near-infrared (NIR) absorbing photosensitizer was encapsulated and successfully delivered into the cytosol of HeLa cells, where a phototoxic effect was triggered with controlled NIR light exposure.

The broad potential of end-on functionalized dextrans was then shown by developing dextran macromonomers for the ring-opening metathesis polymerization (ROMP) of polysaccharide brush polymers. Materials, that might become valuable intermediates in the synthesis of artificial proteoglycans for tissue engineering applications.

In summary, with our established method we can synthesize biocompatible and responsive amphiphiles from sustainable resources by metal-free polysaccharide macromonomer ligation. More generalized, the synthetic procedure should be applicable to all polysaccharide systems with an inherent reducing end, giving access to a plethora of applications at the interface of biochemistry, polymer synthesis and material science (e.g. coatings, surfactants, surfmers, block copolymers and hydrogels).

ZUSAMMENFASSUNG

Stimulus-responsive makromolekulare Drug Delivery Systeme und intelligente Nanomaterialien aus amphiphilen Oligo-, und Polysaccharid Block Copolymeren stellen eine Stoffklasse dar, die mehr und mehr Bedeutung in der Nanomedizin bekommt. Diese repräsentieren im Vergleich zu künstlichen Polymer Materialien eine grüne, nachhaltige und vielversprechende Alternative. Aufgrund ihrer geringen Toxizität, kontrollierbarer Abbaubarkeit, hoher Bioverträglichkeit und exzellenter Löslichkeit in wässrigen Lösemitteln können sie als präzise steuerbare und robuste Nanomaterialien dienen. Durch ihre charakteristische Fähigkeit zur Selbstorganisation zu Mizellen, Stäbchen oder Polymersomen ist es möglich die Bioverfügbarkeit von sensiblen, pharmazeutisch aktiven Substanzen, welche sonst nicht in biologischen Systemen anwendbar wären, durch Verkapselung zu bewahren und signifikant zu verbessern.

Die vorliegende Dissertation präsentiert verschiedene synthetische Verfahren zur Endgruppen Funktionalisierung von Dextranen und deren Verwendung zum Aufbau von amphiphilen, responsiven Block Copolymeren und sternartiger Polysaccharid Bürsten. Wir haben ein Mikrowellen-unterstütztes Verfahren abgewandelt und eine vielseitig einsetzbare Synthesestrategie entwickelt. Basierend auf reduktiver Aminierung in einem Co-Lösemittelsystem konnten *p*-substituierte Aniline am reduzierenden Ende von Dextran eingeführt werden. Dadurch wurde es möglich verschiedene nützliche Funktionalitäten am Polymer Kettenende auf eine effiziente, einfache und zeitsparende Art anzubringen. Azid- und Alkin- endgruppen modifizierte Dextrane wurden anschließend verwendet um Kupfer katalysiert, bis dahin nicht bekannte, pH-responsive Block Copolymere herzustellen, welche ausschließlich aus Polysaccharid Bausteinen aufgebaut sind. Das Material zeigte oberflächenaktive Eigenschaften und ordnete sich spontan in Wasser zu kugelartigen micellaren Nanopartikeln. Dieses Konzept wurde schließlich weiterentwickelt zu einem metallfreien, auf Thiolen basierenden Verfahren. Dadurch wurde, ausgehend von einem einzigen Edukt, der Zugang zu einfach- und doppel-stimulus-responsiven Polysaccharid Makrotensiden ermöglicht. Deren amphiphile Natur und Zersetzungsverhalten wurde im Detail untersucht, mit Fokus auf Wirkstoff Einschlusskapazität und induzierbarer Freisetzung. Ein hoch wirksamer Photo-sensibilitsator mit Absorption im Nahinfrarot Bereich konnte eingeschlossen und

erfolgreich in das Cytosol von HeLa Zellen transportiert werden. Dort konnte ein photo-toxischer Effekt durch kontrollierte Bestrahlung mit NIR-Licht ausgelöst werden.

Die breite Anwendbarkeit von endgruppen funktionalisierten Dextranen wurde anschließend durch die Entwicklung von Makromonomeren für die Ring-öffnende-Metathese-Polymerisation (ROMP) von molekularen Bürstenpolymeren aus Polysacchariden gezeigt. Diese Materialien könnten wertvolle Zwischenstufen in der Synthese von künstlichen Proteoglykanen für die Erzeugung von künstlichem biologischen Gewebe werden.

Zusammenfassend, lassen sich mit unserer etablierten Methode biokompatible und responsive Amphiphile durch übergangsmetalfreie Ligation synthetisieren, basierend auf polysaccharid Makromonomeren aus nachhaltigen Ressourcen. Im breiteren Kontext sollte das Verfahren auf alle Polysaccharide mit einem reduzierenden Ende anwendbar sein. Hiermit ergibt sich der Zugang zu einer Vielzahl an Anwendungen an der Schnittstelle zwischen Biochemie, Polymer Synthese und Materialwissenschaften (z. B. Beschichtungen, Surfactants, Surfmers, Block Copolymere und Hydrogele)

CONTENTS

1 INTRODUCTION AND BASIC CONCEPTS

During the early studies on polymer-drug conjugates, the application of pharmacologically active macromolecules as drugs or drug carrying vehicles for biological applications was regarded with skepticism.[1] It is nowadays a solid and established concept and the most promising strategy in stabilizing biologically active compounds *in-vivo*, controlling their release temporally and locally and thereby specifying their therapeutic efficacy. This is especially important for new therapy forms based on the administration of sensitive compounds such as nucleic acids, proteins, antibodies or vitamins. Highly specific pharmaceutically active cargo that requires protection of oxidizing-, pH-, and enzymatically-induced degradation during the circulation in the blood stream.

Inspired by the magic-bullet concept of Paul Ehrlich,[2] the ongoing research in the fields of biotechnology, biochemistry, polymer and material science has led to a huge leap forward in the development of new and increasingly complex drug nanocarriers. Originally proposed for chemo therapy, recent applications range from cancer treatment[3] to imaging techniques,[4] and therapy of infectous diseases.[5] Yet, it has to be considered that only few of the currently reported systems are allready applicable in medical practice. Their synthesis is often too complex for scale-up or necessitates the use of surfactants which strongly influences their later *in-vivo* fate.[6]

Among the numerous classes of materials employed for drug delivery or imaging purposes, soluble or colloidal systems based on polymer hybrid biopolymers materials gained increasing attention recently.[7] The combination of tunable macromolecular synthesis with the sustainability and biological richness of proteins, peptides or polysaccharides gives access to a plethora of multifunctional polymer materials regarding their chemical and physical properties, composition, and their ease of funtionalization.[8]

1.1 POLYMER-SUPPORTED DRUG DELIVERY

The concept of a precisely designed and pharmacologically active macromolecular compound as drug or drug conjugate was initially suggested by *Ringsdorf* and consequently refined by many research groups in academia or industry ever since.[1] The basic idea was to incorporate at least three discrete areas within a

biostable/biodegradable polymeric chain to fulfill specific tasks (**Table 1**). The first area is composed of a non-toxic block, able to solubilize the whole construct. The second area contains a fixed pharmakon or is pharmacologically active by itself and the third and last block acts as a homing device (actively targeting specific tissue or surface proteins). This concept was then further generalized to describe the ideal nanocarrier with the following characteristics:[9] a) the material has to be biocompatible and allow easy characterization and functionalization; b) it has to exhibit a significantly higher specific uptake efficiency for target cells over normal cells; c) the polymer construct has to be either soluble or colloidal under aqueous conditions; d) it should have extended circulating half-life, low rate of aggregation, and long shelf life. The success of this concept can be measured by the fact that several nanocarrier-based drugs following the originally proposed design are already on the market and more are under development or clinical trails.[9]

Table 1. Specific advantages and properties expected from polymeric drugs according to *Ringsdorf* and *Peer*.[1, 9]

Ringsdorf	*Peer et al.*
Depot effect	Protection of drug from premature degradation
Variable toxicity/solubility	Preventing non-specific interaction with biological environment
Variation in pharmacokinetics (*e.g.* release, metabolism)	Enhanced absorption in specific tissue (e.g. solid tumors)
Different body distribution (e.g. protein binding, resorption, cellular uptake)	Control pharmacokinetic and distribution profile
Polymer-specific effects	Improve intracellular penetration
Drug combinations along the polymer chain	

The most commonly reported drug carrier systems are schematically depicted in **Figure 1** and will be described briefly in terms of morphology and most recent application.

Inorganic nanoparticles describe a large class of materials, including metal-based systems such as iron oxide, gold, or manganese oxide nanoparticles but also mineral structures like mesoporous silica, and hydroxyapatite. These nanosystems offer a high control over particle size and shape (e.g. rods, spheres, cages) and are generally significantly smaller than polymeric particles (1–30 nm). However, non-specific interactions with healthy cells often lead to increased particle toxicity. Gold nanoparticles represent the most prominent

species. They offer strong optical absorption in the near infrared region (NIR) and other useful properties like photothermal activity, chemical inertness, and easy functionalization which makes them ideal candidates for combined therapy and diagnostics (theranostics).[10]

Dendrimers are monodisperse tree-like macromolecules, synthesized by iterative conjugation of heterobifunctional building blocks. They are the only polymer-based nanoparticle system with full control over the overall chemical structure. In biological applications, polyamidoamine (PAMAM) dendrimers are promising carriers. Due to their high water solubility and small size (<8 nm) these dendrimers are rapidly cleared from the bloodstream. Even though they show very promising results in many biological applications, their labour and cost-intensive production still limits a large-scale production.[11]

Micelles are self-assembly structures (15–40 nm) with a hydrophobic core and a hydrophilic corona and can be prepared from amphiphilic lipids or block copolymers. They have found wide application as carriers for hydrophobic drugs.[12]

Polymeric particles represent the most prominent drug carrier compound class and include synthetic polymers such as poly(lactic acid) (PLA) or polyethylene glycol (PEG) as well as natural polymers like chitosan or alginate. Particles from polymers can be prepared in a wide size-range (~60–800 nm), however due to polymer inherent polydispersity it is not possible to create fully monodisperse particle systems which might raise concerns in terms of material heterogeneity. Nevertheless there are many polymer-based systems in clinical development. Applications range from simple tasks such as increasing the blood circulation time of conjugated drugs to more complex features, e.g. site-directed delivery and tissue imaging.[13]

Liposomes and polymersomes are self-assembled structures that can be prepared with good control over size and particle dispersity (80–800 nm) from amphiphilic lipids or polymers. The spherical nanoparticles are composed of a bilayer shell surrounding an aqueous core. In contrast to lipid-based liposomes, polymersomes generally exhibit a higher colloidal stability. This can be referred to the lower CMC of the polymeric building blocks, induced by multiple points of interaction along the polymer chain. These delivery systems are often applied for the transport of sensitive hydrophilic compounds such as therapeutic deoxyribonucleic acid (DNA), ribonucleic acid (RNA), proteins, enzymes and antibodies.[14]

As administered drug nanocarriers actively engage with the body it is very important to create materials that behave chemically inert and/or degrade into non-immunogenic, biocompatible byproducts. The implementation of biopolymers such as peptids, proteins or polysaccharides offers an effective and simple solution and seems to be a promising approach in the development of biologically responsive next-generation drug delivery systems.

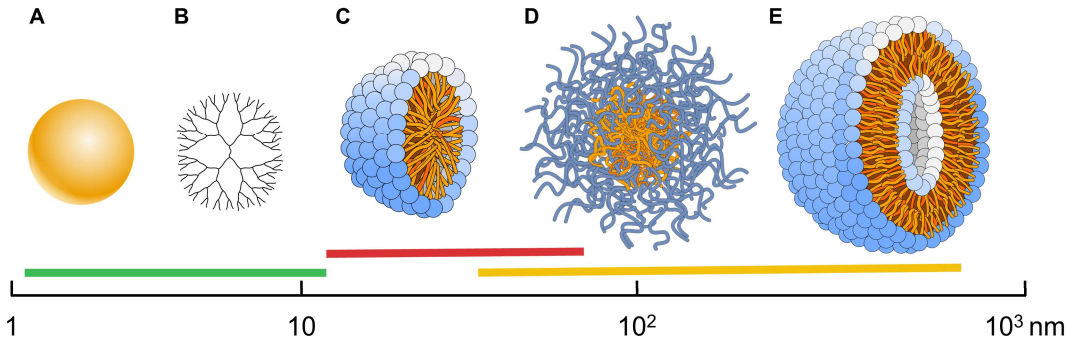

Figure 1. Most common nanoparticle systems for drug delivery and their respective sizes.[8, 15] Inorganic nanoparticles (A, green), dendrimers (B, green), micelles (C, Red), polymeric nanoparticles (D, yellow) and liposomes/polymersomes (E, yellow).

1.1.1 POLYSACCHARIDE-BASED NANOCARRIERS

The investigation of biopolymers as biologically active component in polymer architectures for applications in modern theranostics is a young and thriving field in polymer chemistry and material science. Especially polysaccharides are of interest in nanomedicine and drug delivery. They can be produced at low cost by fermentation, and are biodegradable,[16] biocompatible,[17] and robust materials that in some cases show additional bioactivity and multivalency effects.[5, 7d] (see **Chapter 1.2** and **1.3.1**)

In terms of nanoparticle design and architecture there is virtually no limit. Several groups have demonstrated successfully the formation of capsules,[18] solid particles,[19] vesicles[7d] or gels[20] from polysaccharide or polysaccharide hybrid materials. The resulting particle morphology is strongly dependent on the applied technique for polymer assembly as well as on the chemical nature of the polysaccharide material (hydrophilic, hydrophobic, amphipilic) (**Figure 2**). For example, *Alkanawati et al.* synthesized hollow nanocapsules from hydrophilic hydroxyethyl starch (HES) using microfluidics with a water-in-oil miniemulsion.[21] In the process, small HES-filled water droplets were formed in the organic phase stabilized by polyglycerol polyricinoleat (PGPR) surfactant. The hollow nanocapsules were then synthesized by crosslinking of the polymer with

2,4-toluene diisocyanat (TDI) at the droplets interface and can be loaded with hydrophilic or hydrophobic guest molecules (**Figure 2**, **A**). In a different approach, solid spherical nanoparticles were synthesized from hydrophobic acetal derivatized dextran (AcDex).[22] First an oil-in-water nanoemulsion was produced from dichloromethane (DCM) and phosphate-buffered saline (PBS) by ultrasonication. The resulting AcDex containing DCM droplets were stabilized by the surfactant poly(vinyl alcohol) (PVA). Upon evaporation of the volatile organic solvent, the residual hydrophobic polymer collapses into solid particles distributed in the aqueous phase (**Figure 2**, **B**). Depending on the type of emulsion, it is possible to encapsulate hydrophilic and/or hydrophobic compounds.[23] Amphiphilic macromolecules are mostly reported for the construction of micellar or polymersome-type architectures. The combination of a hydrophilic block (often the polysaccharide domain) and a hydrophobic block (often the artificial polymer) allows the spontaneous formation of rods, micelles, flowers or vesicles in aqueous solution.[24] Recent examples include vesicles formed by solvent displacement from an amphiphilic Dex-b-poly(γ-benzyl L-glutamate) (PBLG) block copolymer.[25] The spherical vesicles assembled in a double layer architecture and had an aqueous core and a dextran corona.

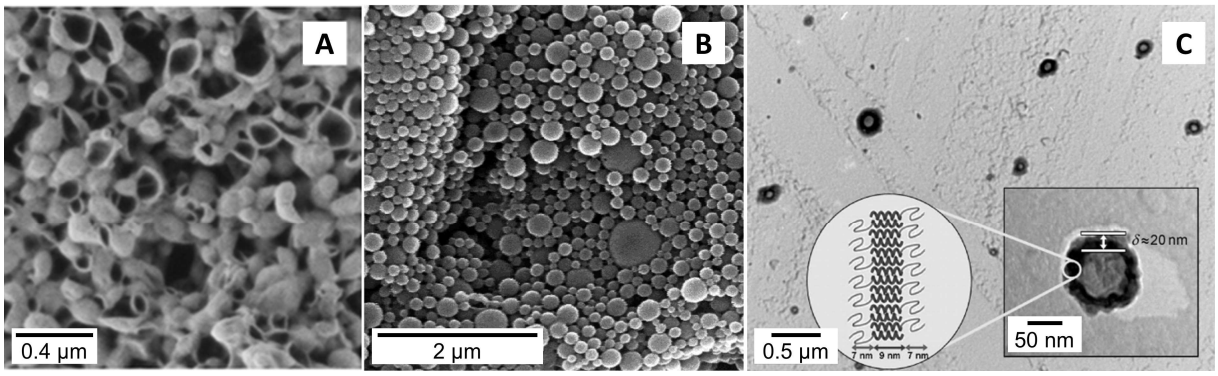

Figure 2. Images of nanocarriers prepared from different polysaccharide materials. Scanning electron microscope (SEM) image of HES capsules prepared by microfluidization (**A**) Adapted with permission from ref.[21] Copyright (2018) WILEY-VCH. SEM image of AcDex nanoparticles prepared by single emulsion (**B**). Adapted with permission from ref.[22] Copyright (2008) American Chemical Society. Transmission electron microscopy(TEM) image of self-assembled Dex-b-PBLG polymersomes prepared by solvent replacement (**C**) Adapted with permission from ref.[25] Copyright (2009) WILEY-VCH.

Moreover, polysaccharides were also reported as hydrophobic or hydrophilic building blocks to expand and improve the biological characteristics of inorganic nanoparticle systems.[10b, 26] Recently, mesoporous silica nanoparticles (MSN), functionalized with AcDex were reported as pH-responsive drug carriers. The highly porous and robust hybrid material could be loaded with the hydrophobic drug doxorubicin and showed a pH-dependent drug release profile *in vivo* where the AcDex functioned as acid-triggerable

valve.[19] Hydrophilic polysaccharide protein conjugates from Dex and bovine serum albumin (BSA) were applied to increase the blood circulation time and tissue resorption of dopamine-coated gold nanoparticles.[10a] The long circulating biopolymer hybrid anorganic material showed good accumulation in tumorous tissue and was successfully applied in photothermal therapy. In contrast, gold nanoparticles without Dex coating applied under the same conditions showed no therapeutic effect.

Essentially, the combination of polysaccharides with organic polymers and inorganic nanomaterials can result in responsive hybrid materials, in many cases with increased hydrophilicity, that can be applied for specific biological applications. In the context of drug carrier morphology, amphiphilic polysaccharide polymers are the most versatile materials. Their self-assembly properties allow for the formation of nanocarriers finely tailored for the chemical nature of the respective guest molecule. Additionally, their size and surface can be precisely controlled depending on the applied solvent and assembling technique.[27]

1.2 POLYSACCHARIDE BLOCK COPOLYMERS

Polysaccharide containing block copolymers represent a sustainable, biodegradable and non-toxic alternative to fully synthetic polymer materials. In many cases, they show higher biocompatibility, biodegradability and improved solubility in aqueous solvents than entirely petrol-based polymers which makes them ideal materials for applications such as solubilizer, foaming agents or packaging but also for vaccination and therapy.[28]

The reason why polysaccharides are so convenient to use is that they originiate from renewable recources, including microbial origin (e.g. dextran and xanthan gum), animal cartilage (e.g. chondroitin sulfate, hyaluronan and heparin) or shells of sea crustaceans (e.g. chitin and chitosan) as well as plant or allgae origin (e.g. cellulose, pectin or carrageenan) and therefore come at low cost.[29]

Depending on the polysaccharide building block, multiple chemical structures and molecular weights are available. The overall ionic nature of the polysaccharide building block can vary accordingly and range from cationic (e.g. chitin) over neutral (e.g. dextran) to anionic (e.g. chondroitin sulfate).[16] They also posses a significant number of functional groups in the polymer backbone, predominantly hydroxyl groups, but also amine, carboxy or sulfate functionalities. As a result, a large body of literature on bioorthogonal conjugation to polysaccharides can be found.[30]

In general, there are five synthetic ways to create polysaccharide block copolymer hybrid materials. The more commonly applied strategies are the conjugation (*grafting-to*) or the polymerization (*grafting-from*) of an artificial polymer onto the polysaccharide backbone and vice versa, which results in polysaccharide-graft-copolymer structures (**Figure 3**, **A** and **B**). The third strategy is the polymerization of a polysaccharide macromonomer (*grafting-through*) leading to highly rigid bottlebrush architectures with maximum grafting densities (**C**). The fourth and fifth approach include the connection of both polymer segments in a linear array to create a polysaccharide-block-copolymer AB-type architecture. Reported methods proceed either from preformed polymer building blocks (**D**) or the polymerization of the second block of one initiator-modified polymer chain end (**E**). In the following paragraph a few brief examples for polysaccharide-g-copolymer arrangements will be given.

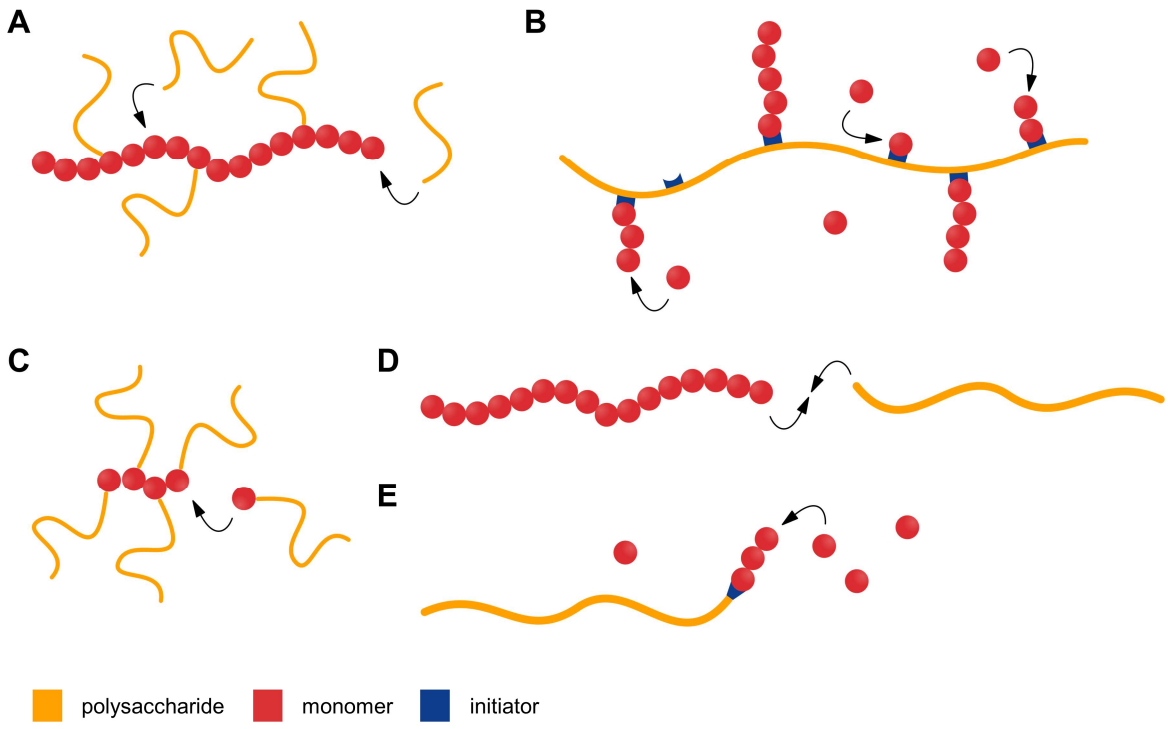

Figure 3. Possible synthetic strategies to create polysaccharide copolymers. *Grafting-to* of an end group modified polysaccharide to an artificial polymer backbone and *vice versa* (**A**). *Grafting-from* of monomers from an initiator-functionlized polysaccharide backbone (**B**). *Grafting-through* of a macromonomer consisting of a polysaccharide modified at the chainend with a polymerizable functionality (**C**). End-to-end conjugation of end group modified polysaccharide and polymer (**D**). *Grafting-from* of a monomer from an initiator-functionalized polysaccharide chain end (**E**).

1.2.1 COMB AND BRUSH ARCHITECTURES

From a synthetic point of view, the *grafting-to* method, namely the conjugation of a macromonomer onto a polysaccharide backbone (or *vice versa*) is in many cases the least

problematic approach. In general, the conjugation is carried out with high yielding "click" reactions such as CuAAC, thiol-ene or peptide-conjugation chemistry to overcome steric interactions of attached side chains and slow diffusion of unreacted macromonomer. Yet, this technique often results in limited grafting densities and necessitates difficult removal of non-conjugated polymer residues. Typically, grafting of a polysaccharide to a polymer backbone is less often reported than the reverse approach.[28] This might be due to the fact, that polysaccharides carry many functional groups in the backbone but are difficult to functionalize at the reducing end with high endgroup densities. Artificial polymers often have higher endgroup densities and are easier to funtionalize at the chain end but more difficult to polymerize with functional groups in the backbone.

Grafting-to of preformed blocks onto a polymer backbone

Ryno et al. reported an amphiphilic graft copolymer based on end-functionlized starch **2** (**Figure 4**, **A**).[31] The polysaccharide (M_n 6.5 kDa) was modified with *p*-ethynylaniline and grafted by Cu-catalyzed click chemistry onto a preformed urethane-linked polyester backbone **1** (M_n 66.6 kDa and 68.2 kDa). The modular synthesis of both components allowed a tunable starch content from 28–53% (w/w). Additionally the loading of small guest molecules into polymer thin films was shown to be a function of the starch concent. *Chen et al.* recently reported the Cu-catalyzed grafting of an azide-modified short xyloglucan (degree of polymerization (DP) 7–9; max. 1 kDa) onto a poly(propargyl methacrylate) (PPMA) polymer (M_n 23.6 kDa) with pendant alkyne-functionalities in the backbone. The brush type glycopolymer was fully characterized and could find an application as a biosensor.[32]

Marchant and coworkers grafted low molecular weight dextran (M_w 1.6 kDa) onto a poly(vinylamine) (PVAm, M_n 10.0 kDa) by reacting dextran lactone with amine groups in the PVAm side chains.[33] The polysaccharide brush had surfactant properties and showed good surface activity at the air/water and air/solid surface. A similar approach was carried out with hyaluronan conjugated to a polylysine backbone by reductive amination.[34]

The *grafting-to* of an artificial polymer onto a polysaccharide backbone was published by *Palumbo et al*. using a hyaluronic acid (HA) backbone and a preformed PLA block.[35] Activation of the terminal carboxy group of PLA with *N*-hydroxy succinimid (NHS) allowed the conjugation of the active-ester terminated polymer to amine groups in the HA

side chain. The resulting HA-g-PLA polymer was soluble in organic solvents and showed increased viscosity compared to the HA starting material. The authors suggest a possible application as hydrogel with hydrophobic domains that could be loaded with hydrophobic guest molecules. Other examples include preformed polymers such as PLA or polycaprolactone (PCL) grafted to cellulose,[36] dextran,[37] alginate,[38] and chitosan.[39]

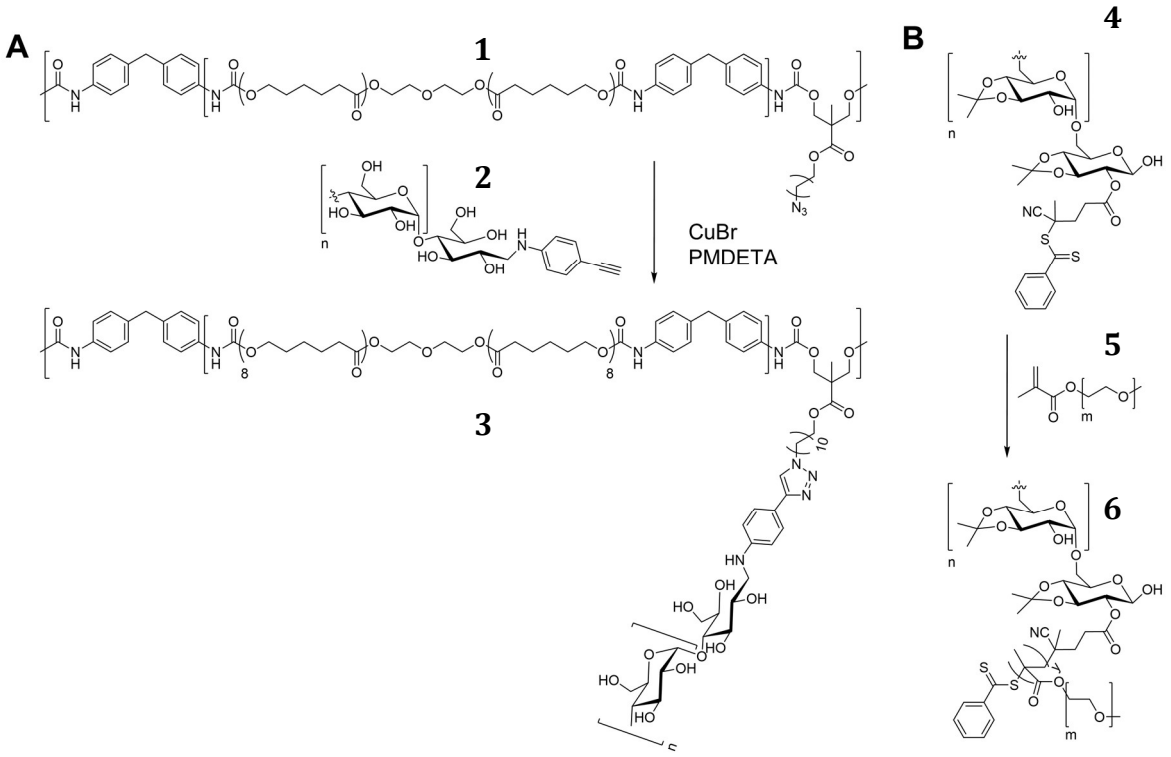

Figure 4. Chemical synthesis of polysaccharide-graft-architectures. Alkyne-modifed starch **2** was *grafted-to* an azide-functionalized urethane-linked polyester backbone **1** (**A**). Reprinted and adapted with permission from *Ryno et al.* [31] Copyright (2014) American Chemical Society. AcDex was conjugated to RAFT initiator and a PEG-methacrylate monomer **5** was polymerizied by living free radical polymerization from the polysaccharide backbone **4** (**B**). Adapted from Ref. [40]. Copyright (2012) American Chemical Society

Grafting-from of a monomer from a polysaccharide backbone

In contrast to the *grafting-to* approach, the *grafting-from* of a monomer from an initiator-modified polysaccharide backbone offers the advantage of higher grafting densities due to less steric hindrance of small molecule monomers compared to bulky macromolecules. One drawback however is the possibility of differences in final molecular weight and problematic characterization of the resulting polymer as it cannot be clearly determined whether all polymer side chains contain the same amount of monomer building blocks.

Boyer and coworkers demonstrated a succesful *grafting-from* approach of PEG-methacrylate monomers **5** from a hydrophobic acetalized dextran backbone **4** by the reversible addition-fragmentation chain transfer (RAFT) polymerization (**Figure 4**, **B**).[40]

The resulting pH-responsive comblike polymer **6** had amphiphilic properties and self-assembled in water into different morphologies such as vesicles, wormlike rods and micellar structures (depending on the time given to self-assemble). *In vitro* studies confirmed a low cellular toxicity of empty particles over three days. The material successfully delivered the encapsulated chemotherapeutic drug doxorubicin into the cytosol and showed a time-dependant release rate. Interestingly, the dox-loaded micelles had an enhanced cytotoxic effect on a SY5Y neuroblastoma cancer cell line compared to a healthy MRC5 fibroblast lung normal cell line.

More generalized, this type of polymer hybrid biomaterial is reported with many different applications in material science such as surfactants or hydrogels and nanoparticles for controlled release and can be readily synthesized with established methods. Therefore the amount of literature covers various combinations of different monomers and polysaccharides (cellulose, alginate, chitosan, hyaluronan, and dextran). Recent examples include the polymerization of poly-(2-dimethylamino)ethyl methacrylate (PDMAEMA) by atom transfer radical polymerization (ATRP) from dextran.[41] Furthermore RAFT polymerization of styrene from cellulose[42] and the free radical polymerization of *N*-vinyl-2-pyrrolidone (NVP) from crosslinked chitosan was reported recently.[43] A more detailed review on graft modifications of natural polysaccharides can be found elsewhere.[44]

Grafting-through of polysaccharide macromonomers

The synthesis of graft architectures by *grafting-through* of macromonomers has long been disfavored due to the problems arising from the polymerization of sterically demanding monomers.[45] The high molecular weight of the macromonomer results in very low concentrations of polymerizable groups and thus in kinetic and thermodynamic barriers limiting the monomer conversion and the final degree of polymerization (DP).[46] With the development of robust synthetic methods for bottle brush synthesis like ATRP,[47] RAFT[48] or ROMP[49] and the constant improvement of highly group tolerant ruthenium catalysts,[50] a toolbox of efficient polymerization techniques, capable of initiation and propargation in sterically demanding environments became available.[49] The *grafting-through* of a macromonomer is of interest in material science as it results in polymeric materials with unique physical properties such as anisotropic side chain conformation and decreased chain entanglement.[46] The densely grafted structure and steric repulsion

between side chains leads to a stretched, less flexible conformation in the side chain surface and a rigid polymer backbone.[51] In the context of polymer supported drug delivery, molecular brush polymers can be described as covalently preassembled polymeric micelles[45] and have found application as responsive nanovehicles[49, 52] and hydrogels.[53]

First simple brush polymers from unprotected maltose, lactose and maltotriose were synthesized by radical polymerization.[54] Starting with oxidation of the oligosaccharide to the respective lactone **7** and subsequent ring-opening with a *p*-vinylbenzylamine **8** led to the vinyl-terminated oligosaccharide **9** (**Figure 5**, **A**). The macromonomers were then polymerized by radical homopolymerization with azobis(isobutyronitril) (AIBN) or potassium persulfate ($K_2S_2O_8$). Unfortunately, the authors did not further characterize their polymer **11** in terms of molecular weight and polydispersity.

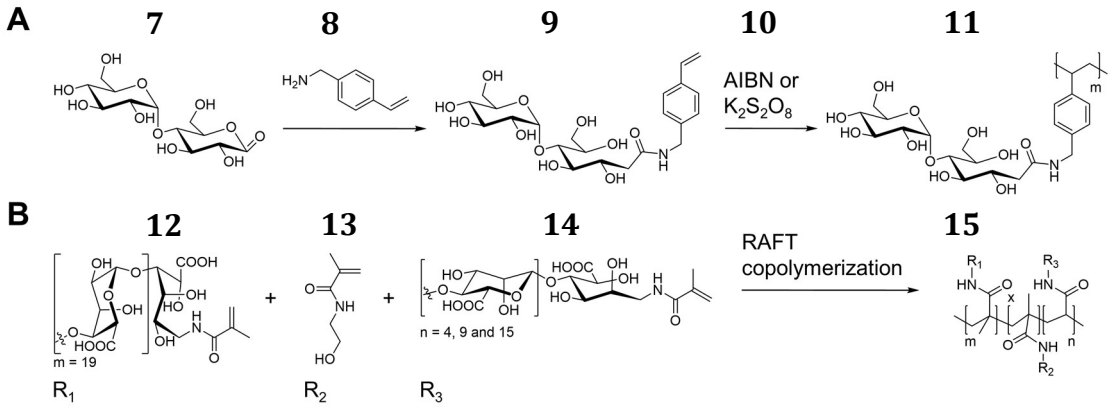

Figure 5. Free radical and controlled radical polymerization of modified oligosaccharide monomers. A maltosemonomer **9** was obtained by functionalization with *p*-vinylbenzylamine and polymerized by radical polymerization (**A**). Adapted from *Kobayashi et al.* [54] Copyright (1985) Nature. RAFT copolymerization of alginate-derived oligosaccharides L-guluronan (R_1) **12**, D-mannuronan (R_3) **14** and artificial monomer HEMAm (R_2) **13** resulted in a mixed block copolymer structure **15** with capable of ionotropic hydrogelation (**B**). Adapted from *Ghadban et al.* [20] Copyright (2012) American Chemical Society.

Further experiments based on this oligosaccharide architecture were expanding the synthetic procedure to maltopentaose in combination with enzymatic polymerization (**Figure 6**).[55] A maltopentaose monomer was therefore functionalized with *p*-vinylbenzylamine (VM5A). The oligosaccharide was then either first polymerized in the backbone (poly(VM5A)) and then *grafted-from* the poly-maltopentaose backbone enzymatically or transformed first into a macromonomer (VAA) followed by *grafting-through* with radical polymerization. Again the authors did not provide analytical data on molecular weight and polymer polydispersity. SAXS studies by *Wataoka et al.* on the homopolymerization of a oligomaltose (DP 2,3,5 and 7) and the conformation of the

resulting glycoconjugate PS revealed a "molecular bottle brush"-like behavior which is surprising regarding the small DP of the carbohydrate side chain.[54b] First results indicated that the chemical nature of the glycoconjugate PS and thus its biophysiological activity is determined by the chemical nature of the oligosaccharide as well as by its length.

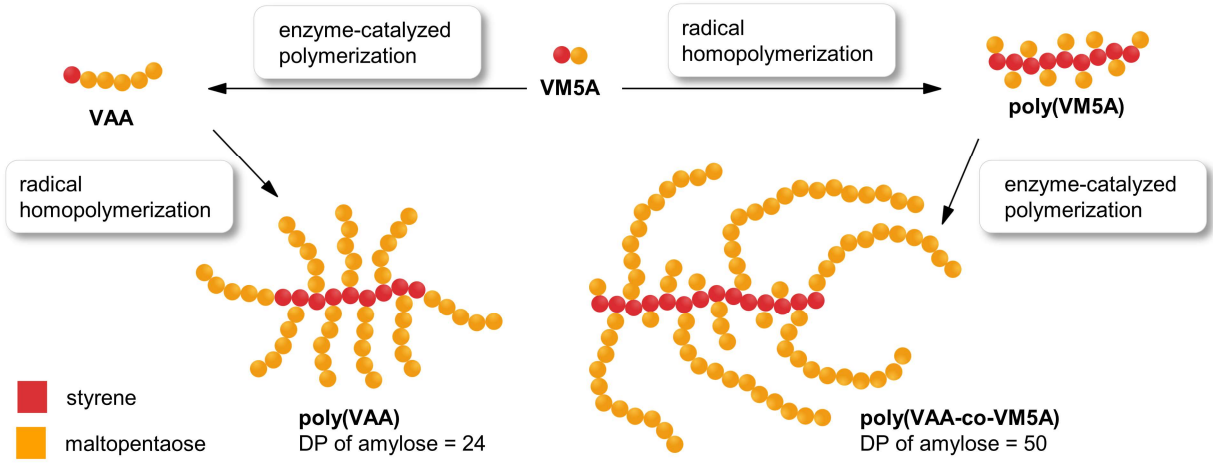

Figure 6. Schematic draft of two different types of polystyrene-graft-amyloses obtained after combining enzymatic and radical homopolymerization. Homopolymerization of macromonomer VAA leads to short brushes, whereas enzymatic-catalyzed polymerization of poly(VM5A) leads to varying sidechain length. Redrawn from *Kobayashi et al.*[55] Copyright (1996) American Chemical Society.

A controlled radical RAFT copolymerization was demonstrated recently for the unprotected alginate-based oligosaccharides D-mannuronan **14** and L-guluronan **12** (DP 5, 10, 16 and 19). The issue of steric repulsion during homopolymerization of sterically demanding oligosaccharide monomers was circumvented by copolymerization with a 2-hydroxyethyl methacrylamide (HEMAm) spacer **13**.[20, 53] The synthesis of functionalized oligosaccharide building blocks was achieved by reductive amination but also reported to be incomplete and pursued without further optimization. Ensuing RAFT block copolymerization with HEMAm led to statistical triblock copolymers (25-52 wt% saccharide, M_n 208–743 kDa, PDI 1.83–1.59) (**Figure 5, B**) with ionotropic gelation properties in the prescence of Ca^{2+}.

As discussed in the previous paragraph, the homopolymerization of complex and/or high molecular weight carbohydrate monomers is synthetically challenging and necessitates highly group tolerant polymerization techniques. To date, examples in literature only include oligosaccharide macromonomers with small DP (1–7). Even ROMP, a technique shown to be very effective in the synthesis of high molecular weight bottle brush polymers ($M_{monomer}$ 3.3–10.0 kDa)[49, 50b, 50d, 50e] was not yet applied successfully for ROMP of polysaccharide monomers.

Pioneering work on Ru-catalyzed homopolymerization of norborne-functionlized glucose monomers was carried out by *Laura Kiessling* and coworkers[56] and later refined by the application of more active Ru- and W-based catalysts by the groups of *Grubbs*[57] and *Schrock*.[58]

To the best of our knowledge, the first report of ROMP in the *grafting-through* of an oligosaccharide monomer (DP>2) was reported by *Rawat et al*.[59] A chondroitinsulfate (CS) mimicking glycopolymer **20** was synthesized in a five-step procedure involving sulfonylation of available hydroxyl groups in the saccharide monomer backbone **18** (**Figure 7**, **A**). Interestingly, the polymerization proceeded with unprotected sulfate groups with the *Grubbs* (G) 2 and *Hoveyda-Grubbs* (H-G) 2 catalysts. Due to the selective protection and deprotection of hydroxyl groups, it was possible to precisely control the site and amount of sulfate functionality and thus the overall charge of the oligosaccharide. The less reactive c*is*-cyclooctene unit **17** was installed as polymerizable unit instead of a norbornene anchor as they were described to adapt better to biological receptors.[60] By using a DCM/MeOH solvent system, it was possible to polymerize a glyco polymer with a DP of 64 (M_n 119 kDa) starting from protected, sulfated CS tetramer **16** in 51% yield. The isolated chondroitinsulfate mimick **20** inhibited outgrowth of hippocampal neurons with similar activity as natural CS polysaccharide, thus showing potential interaction with growth factors, cytokines and other proteins involved in proteoglycan signaling pathways.

Recently, two examples of heparin mimicking brush polymers from sulfated disiaccharide monomers were reported as biologically active polymer drugs. *Oh* and *Sheng et al.* adapted the DCM/MeOH solvent system approach of *Rawat et al.* and were able to polymerize sulfated oligosaccharide brushes with high molecular weights (164 kDa) and good PDI (1.61) with the G3 catalyst.[61] The authors demonstrated an anticoagulant activity which was dependent on the glycopolymer length and degree of sulfation in the saccharide backbone. Additionally, it was shown that the heparan sulfate glycopolymer could target and modulate chemokine activity, hereby influencing immune cell signaling.

The second study on heparin sulfate glycopolymers by *Loka et al.* investigated the design of a natural heparanase inhibitor based on computational studies of heparanase-heparan sulfate binding interaction.[62] Two different norbornene linker molecules were synthesized over multiple steps and conjugated by Cu-click chemistry to previously prepared azide-functionalized oligosaccharides (**Figure 7**, **B**). The authors found that the

polymerization proceeded smoothly with G2 **19** within 1 h by adding weakly coordinating 2,2,2-trifluoro-ethanol (TFE) to DCM as cosolvent system. Glycopolymers from the diantennary monomer **22** showed the best results for binding and thus potent inhibition of heparanase for a DP of 12 repeating units (M_n 12 kDa). Moreover, the glyco polymer had a very low to none anticoagulant activity.

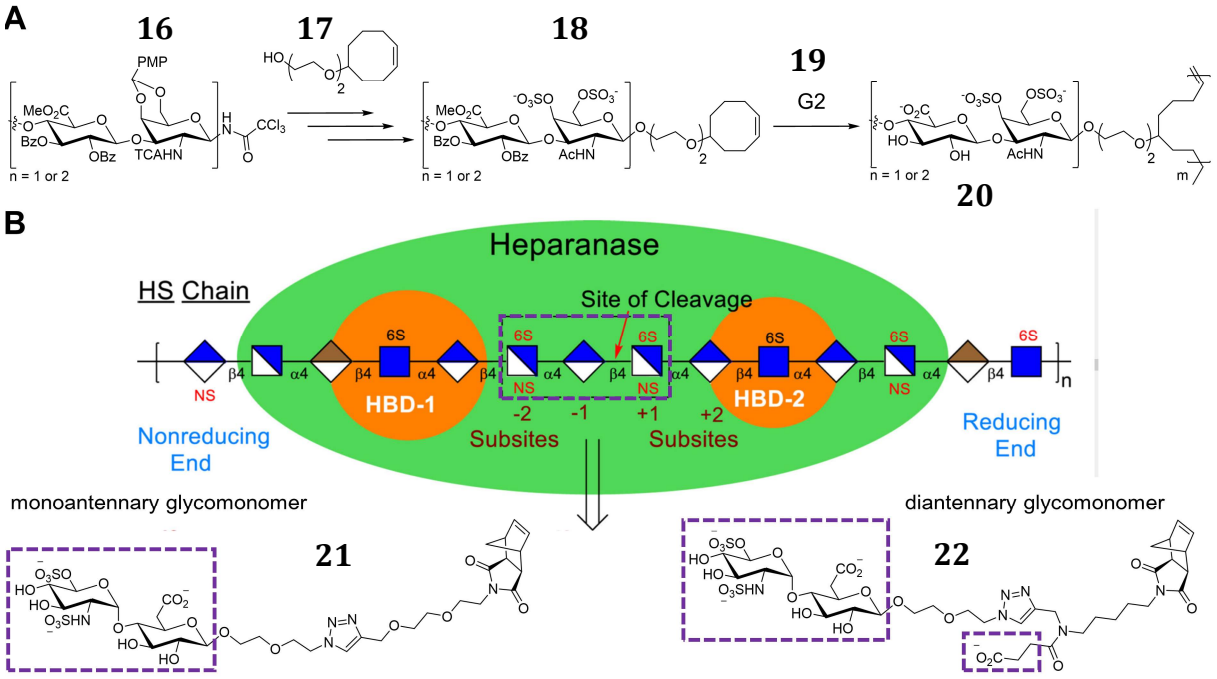

Figure 7. Neo glycopolymers by ROMP of end group functionalized di- and tetramer oligosaccharides. Chondroitinsulfate glycomimics were synthesized in a multistep procedure and polymerized in DCM/MeOH cosolvent with *Grubbs* 2 catalyst (**A**). Reprinted and adapted from *Rawat et al.* [59] Copyright (2008) American Chemical Society. Mono- and diantennary neo glycopolymers were synthesized by ROMP and evaluated for their heparanase interaction and anticoagulant activity (**B**). Reprinted and adapted from *Loka et al.* [62] Copyright (2017) Royal Society of Chemistry.

A common problem in ROMP oligosaccharide monomer polymerization is the incompatibility of solvents for monomer and catalyst. Typically, ROMP with Ru-based catalysts proceeds best in non-polar aprotic solvents[63] while most saccharides are soluble in aqueous buffers or polar solvents like MeOH. *Grubbs* and coworkers overcame this issue by emulsion polymerization of unprotected glucose monomers with dodecyltrimethylammonium bromide (DTAB) as emulsifier in a H_2O/DCM cosolvent system.[57] This approach was later adopted by *Fan et al.* and transferred to a microwave-assisted approach in Tris-buffer/DCE with H-G 2 catalyst and unprotected norbornene-functionalized glucose, manose and fucose monomers.[64] Monomer synthesis was achieved by a two-step procedure, involving nucleophilic substitution with 2-azidoethanol at the reducing alcohol of the protected saccharide and deprotection of

residual acylated hydroxyl groups. Cu-click conjugation to an alkyne-bearing norborne led to the respective carbohydrate monomer. By applying microwave irradiation, the polymerization times were reduced to 15 min and yielded high molecular weight homopolymers and statistical block copolymers (M_n 70.2–282.3 kDa, PDI 1.07–1.14). Unfortunately, the authors did not demonstrate their technique for oligo- and polysaccharide monomers.

In general, the synthesis of glycopolymers by ROMP and *grafting-through* was demonstrated for a variety of small oligosaccharide di-, tri- and tetramers including sialic acid,[65] sulfated fucose[66] and chondroitin sulfate tetramers.[59] However, the polymerization of polysaccharide macromonomers (DP > 4) has not been demonstrated so far.

1.2.2 LINEAR ARCHITECTURES

One possible alternative approach to achieve a complex macromolecule design of polysaccharide building blocks is the self-assembly of simple and synthetically easily available block copolymers. The combination of a polysaccharide with an artificial polymer by joining both segments in a linear array gives access to a variety of self-assembly structures such as micelles, rods, and polymersomes (**Figure 3**, **D** and **E**) without prior polymerization. The major advantage of this AB-type architecture over the side-chain grafting design is that all functional groups in the polymer backbone are preserved during the synthesis of the coblock. This is especially valuable in the design of highly functional and versatile polymeric materials where the feasibility of post-polymerization modifications is of great importance.

A site-specific conjugation of polymer chain ends can be achieved if both blocks carry chemo-selective antagonist groups in the polymer chain end. Polysaccharides naturally come with a single aldehyde group at the reducing end and are therefore suited for functionalization with amines, oximes or hydrazones (**Chapter 1.3.2**, **p.38**). However, the limited availability of the reducing end aldehyde[67] and its slow reaction kinetics[68] as well as the poor solubility of polysaccharides in most organic solvents resulted in a limited amount of literature using polysaccharides as copolymer blocks so far. Also, quantification and structural analysis of the modified polysaccharide chain-end by common methods such as *Fourier*-transform infrared spectroscopy (FTIR) or ^{1}H nuclear magnetic resonance (NMR) can be difficult. This is due to the wide distribution and high

intensity of all carbohydrate backbone signals, often overlaying the signal of introduced linker molecules. Only a limited amount of recent literature reports a thorough and quantitative analysis of their polysaccharide building blocks and the respective end group densities.[31, 68b, 69] The following chapter will give a short overview on recent reports of polysaccharide block copolymers and their applications.

Grafting from polysaccharide reducing end

The *grafting-from* approach in the synthesis of polysaccharide block copolymers was reported either for the polymerization of synthetic monomers from a polysaccharide block or the enzymatically catalyzed polymerization of maltose monomers from a synthetic polymer. Early studies on polysaccharide block copolymers started from functionalized polysaccharide chain ends of methyl-, ethyl-, and benzylcellulose as well as cellulose acetate and starch as starting material in a *grafting-from* approach.[70] The polymerization was based on the mechanical rupture of high molecular weight polysaccharide chains. Resulting polymeric radicals underwent subsequent reaction with polymerizable vinyl-, and acrylnitril monomers. Hereby, the authors obtained and isolated block copolymers in good yields, yet this approach is limited in the control over the length of the polymeric radical and not suited for the synthesis of well-defined polymer structures.

More recent studies, describing the polymerization of monomers from polysaccharide chain ends, exploit modern, robust synthetic techniques like RAFT, ATRP and ring-opening polymerization (ROP) to produce block copolymers with defined molecular weights and narrow PDIs. Block copolymers synthesized by *grafting-from* are only reported for polysaccharides with hyxroxy groups e.g. cellulose, dextran, maltoheptaose, and xyloglycan.[28] To the best of our knowledge, there are no reports of hyaluronan, chitosan or heparin block copolymers synthesized with these techniques. This might result from the fact that functional groups in the polysaccharide side chain could interfere with polymerization kinetics.

The polymerization of a synthetic polymer from an unprotected oligo- or polysaccharide block directly results in an amphiphilic structure and can therefore be applied for polymerization-induced self-assembly or as surfactant in emulsion-based techniques.

In this context, the RAFT polymerization from an unprotected dextran chain end was first applied in the surfactant-free emulsion polymerization of poly(vinyl acetate) (PVAc).[71]

Therefore, dextran (M_w 5 kDa) was functionalized by reductive amination with propargyl amine. Finally, a xanthate moiety was installed site-selectively at the chain end by Cu-click chemistry. The xanthate terminated dextran was then applied as macromolecular RAFT chain transfer agent (CTA). During an emulsion polymerization of PVAc, an amphiphilic dextran-b-PVAc block copolymer formed *in situ* which stabilized the polymerizing latex nanoparticles in solution over prolonged time. It was shown that 2–6wt% stabilizer was sufficient to produce narrowly dispersed nanoparticles (D_H 86–145 nm, depending on the final wt% Dex-CTA)

The site-selective introduction of a RAFT CTA at the polysaccharide chain end can be synthetically challenging due to possible hydrolysis of the CTA-moieties or necessary protection/deprotection steps. *Togashi et al.* reported a elegant Cu-free strategy involving the active-ester of a xanthate CTA and unprotected amine-terminated maltopentaose[72] In a first step, the oligosaccharide block was functionalized by reductive amination with 5-azidopentyl amine. Subsequent reduction of the azide group gave an amine-functionalized maltopentaose. In a second step, the oligosaccharide was conjugated to an NHS-activated CTA. The unprotected macro RAFT agent was applied in the polymerization of styrene, and methyl methacrylate and resulted in block copolymers with varying M_n of 5.1–20.3 kDa (PDI 1.16–1.65). Upon heating to 120–180 °C the amphiphiles self-organized into a body cubic centered morphology including micellar structures with a maltoheptaose core of 5.2–5.4 nm in diameter and a total size of 9.6–10.4 nm.

In a more general and versatile approach, acylated maltoheptose was employed as macroinitiator in ATRP for the synthesis of oligosaccharide-terminated block copolymers (M_n 10.1–16.5 kDa, PDI 1.10–1.50).[73] *Haddleton* and *Ohno* demonstrated the CuBr-mediated polymerization of a wide selection of methacrylate monomers (e.g. **26**) from a protected 2-bromoisobutyryl-modified maltoheptaose block **25** (**Figure 8**). This study is especially interesting as it validates ATRP as a successfull technique for the synthesis of full oligosaccharide glycopolymers from acetylated methacrylate-modified maltose monomers.

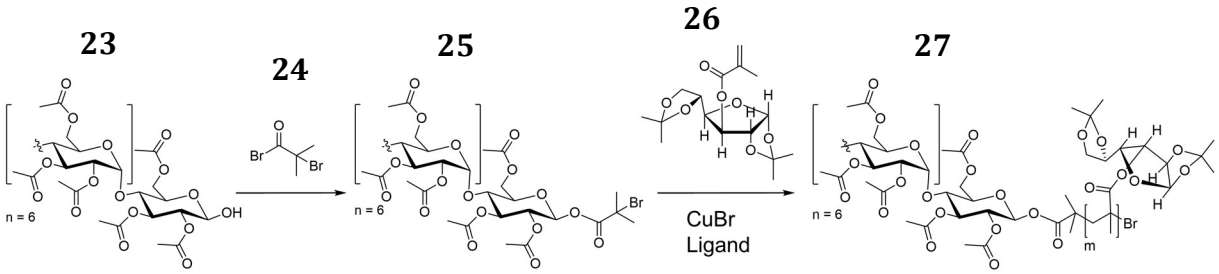

Figure 8. ATRP synthesis from initiator-terminated maltose and cellulose blocks. Protected acrylate-functionalized maltoheptaose monomers **26** were polymerized from an initiator-terminated protected maltoheptaose block **23** (**A**). Adapted with permission from *Haddleton et al.* [73] Copyright (2000) American Chemical Society.

The concept of oligosaccharide macroinitiators was then further expanded to dextran ATRP macroinitiators and their application in the polymerization of styrene as described by *Houga et al.*[74] Initially, dextran (M_n 6.6 kDa) was modified at the reducing end by reductive amination to obtain a 2-bromoisobutyramide-terminated polysaccharide block. Prior to the polymerization, all hydroxyl groups were silylated to ensure full conversion and avoid side reactions. Block copolymers with high DPs were obtained with M_n of 17.5–160 kDa. Interestingly, the particle morphology was controlled by the wt% content of polystyrene (PS) within the block copolymer **28**. Small amounts of PS content led to micelles, higher amount of PS resulted in vesicular morphologies (**Figure 9**).

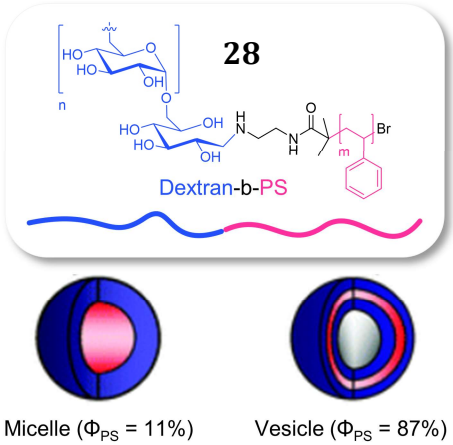

Figure 9. Dex-b-PS copolymers **28** were obtained by polymerization of styrene monomers from a silylated dextran macroinitiator. The self-assembly particle morphology could be controlled by the extend of PS within the block copolymer. Redrawn and adapted from *Houga et al.*[74] Copyright (2007) Royal Society of Chemistry.

The first report of a successfull *grafting-from* ATRP without prior protection of hydroxyl groups in the polysaccharide backbone was achieved with cellulose (M_w 10, 24, 85 kDa) **29**, modified at the reducing end by reductive amination with 2-chloroacetamide **30**. The macroinitiator **31** was then used in the polymerization of styrene monomers **32**

(**Figure 10**).[75] The polymerization proceeded at 130 °C in a controllable rate with a *N*,*N*,*N*',*N*'',*N*''-pentamethyldiethylenetriamine (PMDTA)/CuCl or an ascorbic acid/CuBr catalytic system. The symmetrical high molecular weight polymers **33** showed excellent compatibilization properties in suppression of phase separation in cellulose/PS blends.

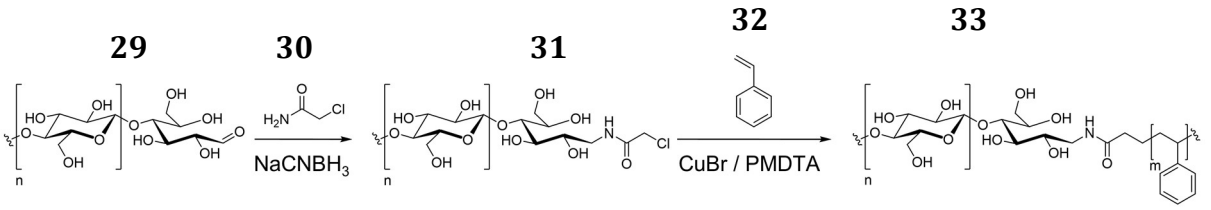

Figure 10. ATRP of styrene monomers **31** from unprotected 2-chloroacetamide terminated cellulose macroinitiator **30** (**B**). Reprinted and adapted with permission from *Yagi et al*.[75] Copyright (2010) nature polymer journal.

Novoa-Carballal et al. adapted and improved the synthetic strategy of *Haddleton* and *Houga* and achieved ATRP from an unprotected dextran macroinitiator **36** to synthesize a Dex-b-polyelectrolyte **38** from 2-(dimethylamino)ethyl metacrylate (DMAEMA) monomers **37**.[76] The modification of dextran (M_n 6, 14, 50 kDa) was achieved by oxime-click chemistry with an aminooxy group bearing ATRP initiator **35** (**Figure 11**), which allowed to reduce reaction times from 96 h to 24 h and minimize the required amount of linker molecule down to 5 equivalents (compared to 25 equivalents for reductive amination).[74]

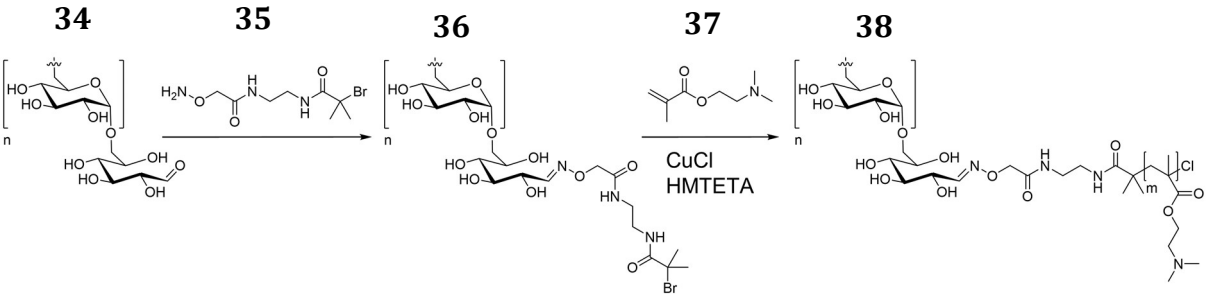

Figure 11. ATRP or enzymatically catalyzed polymerization from oligo- and polysaccharide chain ends. Dextran was modified at the reducing end by "oxime"-click chemistry and applied as unprotected macroinitiator for the polymerization of DMAEMA monomers. Adapted with permission from *Novoa-Carballal et al*. [76] Copyright (2013) Royal Society of Chemistry.

Optimized reaction conditions included a 1,1,4,7,10,10-hexamethyltriethylene tetramine (HMTETA)/CuCl system and 26 h reaction time to obtain 65% conversion. Interestingly, the hydroxy groups in the polysaccharide backbone were not protected prior to polymerization. The resulting block copolymer (M_n 33–129 kDa) Dex-b-PDMAEMA **38**

was successfully applied for the colloidal stabilization of a self-assembled interpolyelectrolyte complex with a sodium poly(styrenesulfonate) core and a dextran corona (D_H 180–260 nm in DLS, 25 nm in TEM).

While the polymerization of a synthetic block from the active end of a polysaccharide chain represents the more common approach to polysaccharide block copolymer architectures, a few studies also report the enzymatic polymerization of a saccharide monomer from a synthetic polymer. Early studies with amylase and malto-oligosaccharides found that glucose monomers can be polymerized from telechelic malto-oligosaccharide-poly(ethylene oxide)(PEO) primer.[77] Inspired by the results of *Ziegast* and *Pfannenmüller*, *Loos et al.* functionalized amine-modified PS (M_n 1, 2, 5, 100 kDa) blocks **40** with short maltoheptaose **39** (DP 7) by reductive amination (**Figure 12**).[78] The resulting amphiphilic macroinitiator **41** assembled in water into micellar aggregates with a PS core and an oligosaccharide corona. Further enzymatically catalyzed polymerization with potato phosphorylase and α-D-glucose-1-phosphate (G-1-P) **42** led to PS-b-amylose block copolymers **43** with elongated hydrophilic blocks.

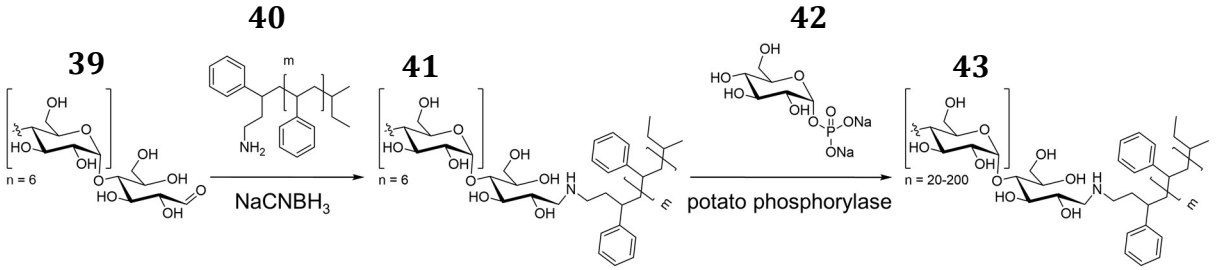

Figure 12. Functionalization of PS with oligo-maltoheptaose block and subsequent enzymatically catalyzed polymerization of amylose block. Adapted with permission from *Loos et al*.[78] Copyright (2002) American Chemical Society.

End-to-end conjugation of preformed polymer blocks

Most polymerization techniques are sensitive to functional groups in the polymer backbone or have to proceed in dry organic solvents, hereby limiting the scope of substrate starting materials. Generally, hydroxylgroups in the polysaccharide backbone are therefore often protected by acetylation or trimethylsilylation which also renders the biopolymer soluble in organic solvents. Deprotection requires harsh conditions including sodium methoxide in methanol or concentrated solutions of hydrogen chloride. Hence, the artificial polymer block and the connecting linkage between both blocks has to be robust enough not to be cleaved during deprotection. Providing that there is a common

solvent for both polymer blocks, the end-to-end coupling of preformed polymers represents a functional alternative method to the *grafting-from* of a monomer from a polysaccharide chain end. It has the advantage of precisely characterized polymer compositions and narrow PDIs in the resulting block copolymer. A drawback however is the difficult and sometimes tedious work up and separation of block copolymer product from single unmodified polymer chains. This is especially the case for block copolymerizations where the increase in molecular mass is not sufficient for separation. Often a thorough purificiation necessitates several days of dialysis and precipitation in different solvents to fully remove polymeric starting material.

First reports on end-to-end coupled polysaccharide block copolymers were describing the conjugation of oligosaccharides (DP 6–7) with *α,ω*-diamino PEO. The respective oligosaccharide was oxidized to the corresponding lactone. Subsequent ring-opening with PEO resulted in PEO-b-oligosaccharide di and triblock structures.[79] This synthetic strategy was adapted by *Marchant* and coworkers in the synthesis of maltoheptaose-, and dextran-based surfactants of ABA and AB architecture.[80]

Schatz et al. reported the first polysaccharide-b-polypeptide structure **44** from dextran and preformed poly(*γ*-benzyl L-glutamate) (PBLG) mimicking naturally occurring nano-sized vesicles such as viral capsids (**Figure 13**).[25]

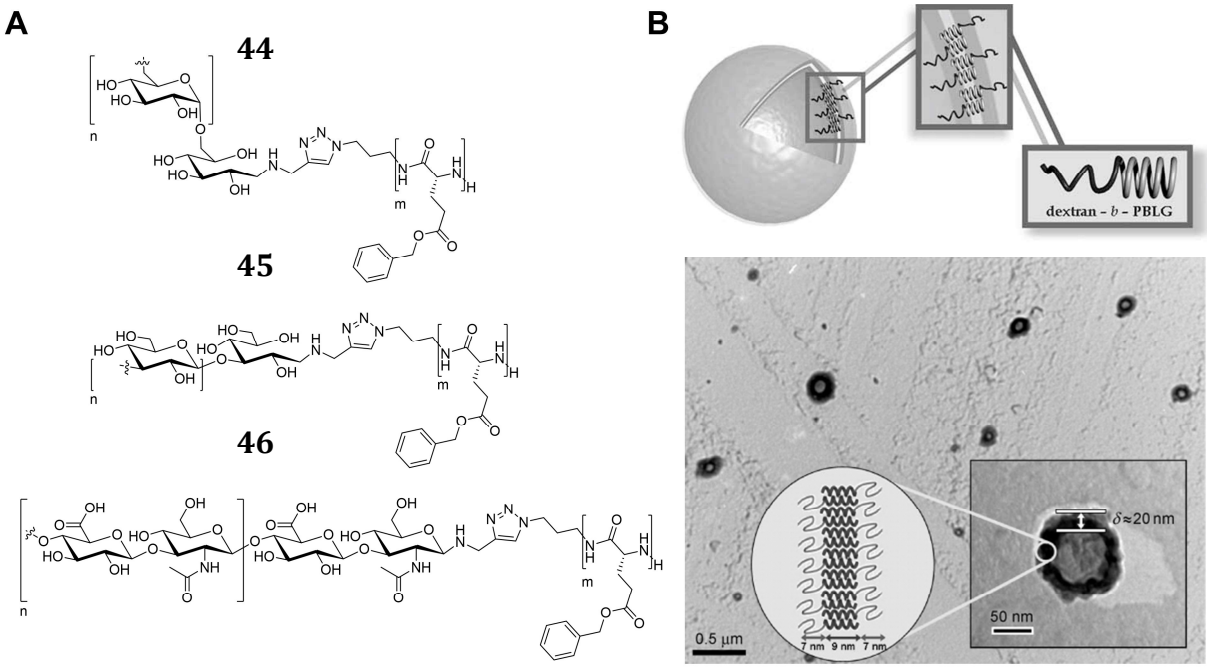

Figure 13. Polysaccharide-b-PBLG block copolymers and their self-assembled structures. Synthesized Dex-b-PBLG **44**, LA-b-PBLG **45** and HA-b-PBLG **46** block copolymers from preformed polymer blocks (**A**).[7d, 25, 81] Schematic representation of Dex-b-PLG assemblies and their observed morphology by TEM (**B**). Reprinted and adapted with permission from *Schatz et al.*[28] Copyright (2010) Wiley-VCH

The hydrophobic polypeptide block was prepared by ROP of a BLG *N*-carboxylic anhydride (NCA) initiated by 1-azido-3-aminopropane. The hydrophilic dextran block was modified by reductive amination with propargylamine and conjugated to PBLG by Cu-click chemistry. The rational design of the block copolymer involved the tendency of PBLG to adopt an α-helical conformation which favors strong side-by-side interaction of peptide-bond dipoles. This finally resulted in a bilayer structure of peptide helices next to each other with polysaccharide chains on both sides. The surface-activity and CMC were not determined, however it was shown with DLS that nanoprecipitation of the block copolymer in water induced self-assembly into hollow structures. SANS experiments further confirmed the particle morphology as polysaccharide polymersomes with a size of D_H 90 nm and a membrane thickness of $\delta \approx 20$ nm. This synthetic strategy and polymer design was later adapted by the same group changing the neutrally charged dextran with biologically active polysaccharides laminarin (LA) and HA (**Figure 13**, **A**).[7d, 81]. Alkyne-modified HA (M_w 5 kDa) and LA (M_w 5 kDa) were conjugated to azide-functionalized PBLG (M_w 6.6 kDa) by Cu-click chemistry. The LA-b-PBLG **45** and HA-b-PBLG **46** diblock copolymers where mixed in different ratios and self-assembled by coprecipitation in water. An optimized modular procedure allowed a controllable design of blend nanoparticles with a D_H of 88–92 nm and a zeta potential of $\xi = -30$ mV and −34 mV. Furthermore, the interaction of the nanoparticles with the cell surface ligand CD44 and Dectin-1 was probed with surface plasmon resonance (SPR). It could be demonstrated that HA and LA binding occurs by a multivalent effect and that the strength of interaction could be modulated by the particle morphology and composition.

Other examples of HA block copolymers include the Cu-free conjugation of HA (M_w 7.4 kDa) with poly(D,L-lactide-co-glycolide) (PLGA; M_w 5 kDa).[82] The succesfull synthesis was based on a combination of reductive amination of HA with hexamethylene diamine and subsequent conjugation to NHS-activated PLGA. The material had a low CMC (28 mg L^{-1}) and assembled in water into solid spheres with sizes of D_H 59–116 nm and a zeta potential of $\xi = -28$ mV and −0.87 mV. Encapsulation of the hydrophobic drug doxorubicin resulted in increasing particle sizes and decreasing zeta potential.

The direct comparison of these solid spherical particles with the polymersome-like structures obtained by *Upadhyay*[81] and *Duan*[7d] gives a valuable insight in the self-assembly behavior of this compound class. As all three block copolymers only differ in the artificial polymer block and connecting linkage, it becomes evident that the nature of the

hydrophobic block has a tremendous influence on the self-assembly behavior and resulting particle morphology.

The active-ester-based technique for the synthesis of a polysaccharide block copolymer was also adapted by *Verma et al.* with preformed NHS-activated PLA (Mw 10, 20, 50 kDa) and amine-modified dextran (Mw 1.5, 6, 10 kDa). Their robust and easy approach allowed a detailed investigation of the correlation between changing block lengths of Dex-b-PLA and self-assembled particle sizes.[83] Further investigation and development of the reductive amination step led to a microwave-assisted approach, significantly improving reaction times from three days to four hours (**Chapter 1.3.4**, **p.41**).[68b]

A metal-free conjugation based on polysaccharide chain degradation was reported for the synthesis of a chitosan-b-PEG copolymer (similar to the approach of *Ceresa et al.*).[84] The chitosan (mol. weight not reported) was treated with potassium persulfate to degrade the polymer chain which led to low molecular weight fractions terminated with a free radical species. Acryloyl-functionalized PEG (Mw 2 kDa) was then reacted with the chitosan chain end, unfortunately it was not clearly demonstrated wheater only one PEG chain was attached to the polysaccharide. Also the molecular weight distribution of the chitosan fragments could not be controlled. The final block copolymer showed thermogeling behviour at 36 °C.

Glycosaminoglycan (GAG)-based block copolymers were first described by *Fajardo et al.* and synthesized by a Cu-click technique.[69] Low molecular weight CS (Mw 5.7 kDa) was obtained by enzymatic degradation of the high molecular weight polysaccharide (Mw 19.3 kDa) and functionlized by reductive amination with 4-propargyloxyaniline. PLA (Mw 1.7 and 6.5 kDa) was modified by tosylation of the chain end hydroxyl group with subsequent substitution by sodium azide. Both blocks were conjugated by Cu-click chemistry. The resulting amphiphilic block copolymer had a comparably high CMC (48 and 158 mg L^{-1}) and DLS/SLS experiments indicated loosely connected hyperbranched clusters or aggregates (D_H of 35–54 nm, ρ = 0.95 and 1.16). It was not clearified by the authors whether the amphiphile assembles into classical micelles or nanoparticulate aggregates. The concept of GAG block copolymers was then expanded to CS-b-PLGA block copolymers and a Cu-free synthesis based on peptide-coupling chemistry.[7e] The CS (Mw 10 kDa) block was modified by reductive amination with adipic acid dihydrazide and coupled to NHS-activated PLGA (Mw 5, 7 and 10 kDa) of varying molecular weights. The block copolymer had an improved CMC (26–29 mg L^{-1}) when compared to earlier CS-

block copolymers and assembled into solid spherical particles (D_H 253–283 nm) with a negative zeta potential from ξ = −33.9 mV to −37.0 mV. *In vitro* studies confirmed the potential of the material to deliver doxorubicin into the cytosol of MCF-7 cells.

A very interesting example for the combination of nanomedicine and polymer chemistry is the creative approach of *Meier* and coworkers who exploited the bioactivity of heparin-b-poly(dimethylsiloxilane) (Hep-b-PDMS) polymersomes for malaria therapy (**Figure 14**, **A**).[5]

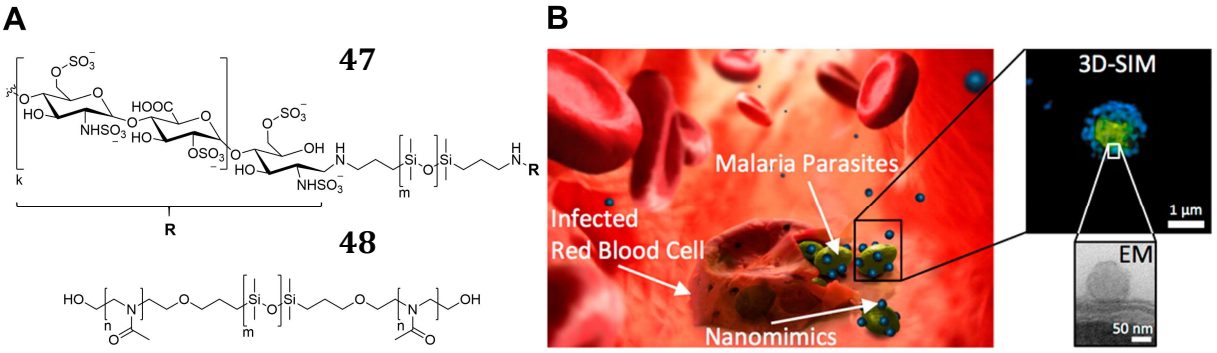

Figure 14. Nanomimics from Heparin-block copolymer blend. Chemical structure of Hep-b-PDMS-b-Hep **47** and PMOXA-b-PDMS-b-PMOXA di and triblock copolymer **48** (**A**). Schematic representation of nanomimics (blue) sticking to malaria parasites (green) and EM picture of nanomimic polymersome (**B**). Reprinted and adapted with permission from *Najer et al.*[5] Copyright (2014) American Chemical Society

Heparan sulfate acts as receptor on red blood cells for merozoites of the *P. faciparum* parasite. This allows the specific recognition and attachment of the parasite to the host cell before invasion and subsequent infection. The authors were addressing this stage of infection by modifying the closely related heparin (Mw 11 kDa) by reductive amination with a preformed telechelic PDMS (M_w max. 0.8 kDa) block. A blend of poly(2-methyl-2-oxazoline)-b-PDMS-b-poly(2-methyl-2-oxazoline) (PMOXA-b-PDMS-b-PMOXA; M_w 6.5–7.7 kDa) **48** with (25% w/w) Hep-b-PDMS-b-Hep triblock copolymer **47** led to self-assembled nanomimics with a D_H of 132 nm and a heparin corona. DLS and cryo-TEM revealed a polymersome morphology (ρ = 0.9–0.99) with a membrane thickness of $\delta \approx 11$ nm. It was also found that higher amounts of Heparin-b-PDMS amphiphile **47** (35–65% w/w) resulted in mixtures of polymersomes and aggregated micelles or worm like structures. *In vitro* experiments clearly demonstrated that the nanomimics successfully blocked an invasion of plasmodium merozoites into red blood cells by strong multivalent binding to the $MSP1_{42}$ ligand of the parasite (**Figure 14**, **B**). This approach is different from other polymer-supported nanotherapies as the macromolecule itself is the active substance without further need for an active drug or vaccine to be released.

The aforementioned studies on polysaccharide block copoylmers are clearly showing the outstanding properties and possibilities of this relatively young compound class. The following last two reports set the focus on the idea of a sustainable approach that includes carbohydrates from yet unused resources such as biomass byproducts from industrial processes.

Rosselgong et al. utilize short xyloglycan oligosaccharides (DP 6) derived from xylan (beechwood) and oleic acid.[85] Both polymer blocks were functionalized with either an azide or an alkyne group and conjugated by Cu-click chemistry. The new aspect here was that both building blocks were derived from cheap byproducts of the paper/pulp industry. With DLS/SLS as well as TEM experiments the morphology of the particles could be determined as vesicular spheres (ρ = 0.9–0.99, D_H = 90 nm). The amphiphilic block copolymer could be loaded with hydrophilic and hydrophobic cargo simultaneously. Encapulation of the antifungal compound propiconazole revealed superior activity compared to free drug. Even though this publication shows that valuable hybrid materials can be synthesized from completely biobased resources, it is noteworthy to say that the overall procedure includes the application of toxic chemicals such as sodium azide and sodium cyanoborohydride. Additionally the key step in the synthetic procedure is still based on metal catalysis. Both factors which are limiting a larger industrial application.

The thiol-ene "click" reaction of thiol-modified hydroxypropyl methyl cellulose (HMPA, M_w 5, 8 and 10 kDa) **49** and allyl-terminated PLLA (M_w 2 kDa) **50** represents a nice example for a *green* conjugation approach for the synthesis of biobased polysaccharide block copolymers (**Figure 15**).[86]

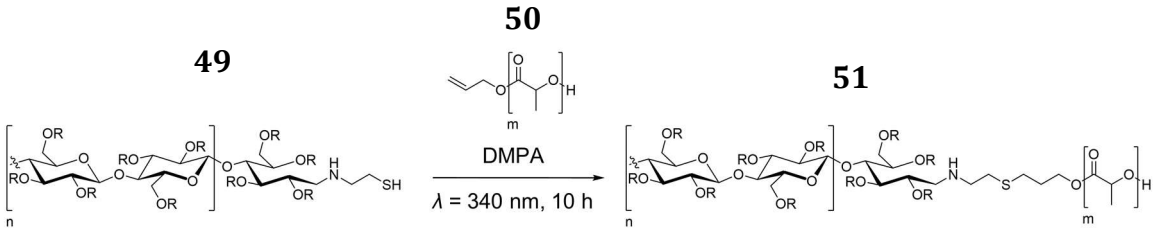

Figure 15. Photo thiol-ene conjugation of thiol-functionalized HPMA **49** and allyl-terminated PLLA **50**. Reprinted and adapted with permission from *Wang et al.*[86] Copyright (2017) Wiley-VCH

The block copolymer was obtained after 5 h irradiation at λ = 340 nm with 2,2-dimethoxy-2-phenylacetophenone (DMPA) as photocatalyst. The block copolymer **51** showed an amphiphilic character (CMC 120–150 mg L^{-1}) and assembled in water into micellar particles with a D_H of 124–240 nm. Generally, both studies provide a solid basis for further investigations but also demonstrate that there is an ongoing need for

improvement. The development of new high-performance materials with biobased elements and biodegradable/biocompatible properties is of great importance and should lead the direction of future studies from basic research in polymer material chemistry to industrial application.

1.2.3 RESPONSIVE LINEAR ARCHITECTURES

The main purpose of nanoparticle supported therapy is to deliver and release a pharmaceutically active cargo at a desired location within the body. In this context smart nanoparticulate systems have to be designed with the ability to respond to a specific external stimulus. Thereby it is possible to synthesize highly stable particles and minimize premature release of an encapsulated cargo inside the blood stream. Yet full local and temporal control over the complete cargo release can be ensured.

In an effort to optimize and refine oligo- and polysaccharide block copolymers, several reseach groups studied the effect of installed stimuli-responsive elements on the delivery and release characteristics of their copolymer architectures. Due to the fact that oligo- and polysaccharide block copolymers are still a comparably young area of research, the amount of literature is readily comprehensible. Nevertheless, there are reports of several creative block copolymer designs with the ability to respond to changes in temperature, pH, UV light, and reduction potential. Triggered by the respective external stimulus, the self-assembled particles change their morphology or solubility and degrade with subsequent release of the encapsulated guest molecule.

The application of photo-chemically sensitive micelles is of growing interest as it bears the potential for remotely controlled spatial and temporal selectivity. An ideal system would allow finetuning of these properties, depending on the type of photo-responsive group (and therefore on its selective wavelengths) but also on its location within the polymer architecture.[87] So far, the only photoresponsive polysaccharide block copolymer was reported by *Lee et al.*[88] The authors combined low molecular weight dextran (M_n 1.5 kDa) or maltodextrin (M_n 2.7 kDa) as hydrophilic block with either poly(4-methyl-*ε*-caprolactone) or poly(4-X-*ε*-caprolactone) (PXCl, X = methyl or phenyl; M_n 1.4–8.3 kDa) as hydrophobic block (**Figure 16**, **A**).

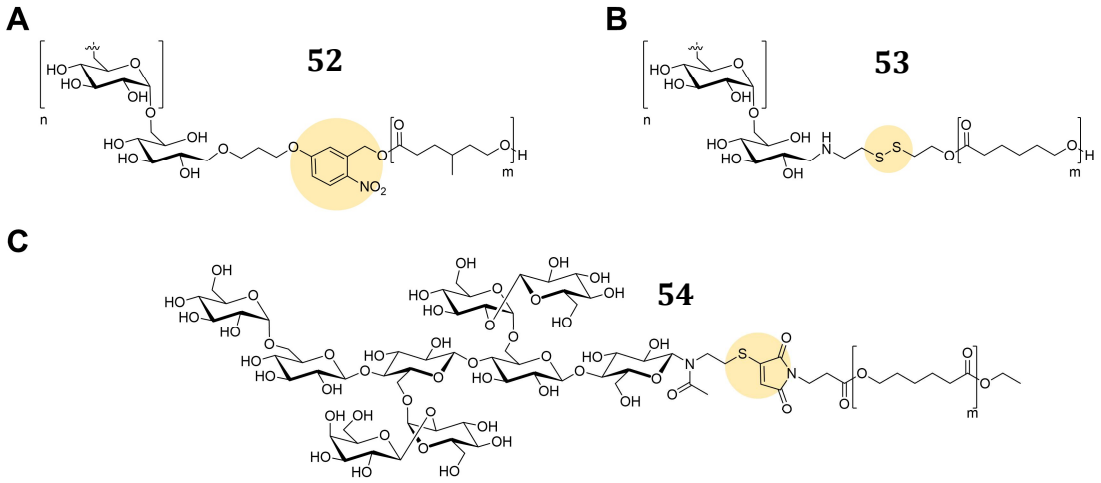

Figure 16. Responsive block copolymer architectures based on hydrophobic polycaprolactone and poly(4-methyl-caprolactone). The responsive elements are marked with yellow circles. *Lee et al.* conjugated dextran to poly(4-methyl-caprolactone) with a photo cleavable 5-hydroxy-2-nitrobenzyl alcohol (**A**).[89] *Sun et al.* performed a thiol-exchange reaction with dipyridyl dithiol activated dextran resulting in a reduction-sensitive mixed disulfide structure **53** (**B**).[90] Halila and coworkers found that *Michael* addition with 3-bromomaleimid activated polycaprolactone and thiol-modified xyloglucooligosaccharides leads to a reduction sensitive structure **54** (**C**).[91]

The PXCL domain was polymerized from 5-hydroxy-2-nitrobenzyl alcohol as initiator in a ring-opening polymerization. The oligosaccharide domain was modified at the reducing end with 3-bromo-propanol and conjugated in a nucleophilic substitution to the 5-hydroxy-benzyl group at the hydrophobic polymer chain end. This synthetic strategy is rather unusual as typically polymer end to end conjugations are performed with high-yielding and site-selective "click" techniques such as CuAAC, thiol-ene or peptide coupling reactions.[25, 68b, 92]

A major reason for this being the difficult separation of macromonomer from the block copolymer and the high amount of adjacent reactive groups in the biopolymer backbone. The resulting amphiphilic block copolymer **52** assembled in water into spherical nanoparticles with a D_H of 61–189 nm and a CMC of 2.2–50.4 mg L^{-1} (depending on the length of PXCl). Moreover, the particle system could encapsulate hydrophobic drugs such as indomethacin and doxorubicin. Irradiation at a wavelength of λ = 325 nm triggered a particle burst and release of the encapsulated cargo.

Another popular strategy in smart drug delivery is the incorporation of reduction-responsive elements into the polymer architecture. The idea is to utilize the large difference in redox potential between the extracellular ($20–40 \cdot 10^{-6}$ M) and the intracellular ($0.5–10 \cdot 10^{-3}$ M) environment as trigger for controlled micelle degradation. This phenomenon is caused by an increased intracellular level of glutathione (GSH), a

thiol-containing tripeptide generated in cell cytoplasm.[93] Especially in cancer therapy, the controlled release of guest molecules from nanocarrier systems triggered by GSH is appealing, since elevated intracellular GSH levels have been reported in many human and murine tumor cell lines.[94] In the experimental setup, the intracellular environment is often mimicked by aqueous buffer solutions containing dithiothreitol (DTT, 10 mM).[95]
The synthesis of reduction responsive polysaccharide amphiphiles can be achieved with thiol-modified polymers and was demonstrated by three groups with different conjugation strategies (**Figure 16 B**, **C** and **Figure 17 A**).
Sun et al. performed ring-opening polymerization of *ε*-caprolactone, initiated by 2-(2,4-dinitrophenyl)thioethanol to create a reduction-responsive block copolymer **5353**.[90] The fast thiol-exchange reaction between a dipyridyl disulfide-modified dextran (M_n 6 kDa) and a thiol-modified PCL (M_n 3.5 kDa) resulted in an amphiphilic mixed disulfide (**Figure 16**, **B**). Above a CMC of 9.3 mg L^{-1} the amphiphile self-assembled in water into spherical nanoparticles with a D_H of 60–80 nm. Fluorescence microscopy further confirmed the cellular uptake of doxorubicin-loaded micelles and a triggered release was shown by DLS after incubation in 10 mM DTT.

Another synthesis of a reduction-responsive oligosaccharide amphiphile based on modified PCL was reported by *Halila* and coworkers (**Figure 16**, **C**).[91] First, hydroxyl-terminated PCL (M_w 4.1 kDa) was modified in a *Steglich* esterification with 3-bromomaleimid. The conjugation to thiol-modified xyloglucooligosaccharides (M_n approx. 1 kDa) was achieved by thiol "click" *Michael* addition. The amphiphile **54** assembled in water into small micellar particles with a D_H of 30-34 nm and released encapsulated Nile red upon incubation in 10 mM DTT. As a proof of concept, smaller amounts of DTT (10 µM) simulating extracellular levels of GSH did not lead to particle degradation.
A different chemical ligation strategy was pursued by *Carvalho et al.*[7b] The two glycosaminoglycans (GAG) hyaluronan (HA, M_w 4.3 kDa) and chondroitinsulfate (CS, M_w 19.2 kDa) were modified at the reducing end by oxime "click" with 11-(aminooxy)-1-undecanethiol. The short hydrophobic alkane sequence was sufficient to install an amphiphilic character in the resulting block copolymer and induce self-assembly into micellar nanoparticles with a D_H of 146 nm (HA) and 193 nm (CS). While this approach is different and simpler than typical block copolymer formation, the GAG amphiphiles had a

higher CMC (310 mg L^{-1} and 103 mg L^{-1}) than observed for block copolymers with larger hydrophobic segments. Interestingly, the authors did not include the reduction-sensitive region in between both blocks but at the chain end of the hydrophobic domain. As a result, the chain-end thiol functionality became oxidized during the self-assembly process and formed dithiol connections, crosslinking monomers inside the micellar structure (**Figure 17**, **A**). The nanoparticles were internalized in a CD44 dependent pathway by receptor recognition. Additionally, a controlled release of the model drug Nile red was demonstrated after treatment with the reducing agent DTT (10–100 mM).

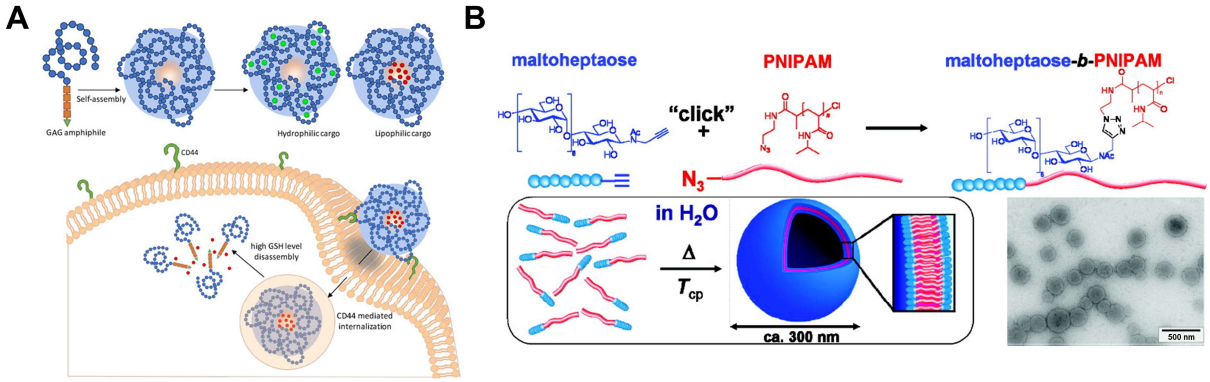

Figure 17. Responsive block copolymer nanoparticles. HA and CS (blue)were conjugated by oxime "click" to short C_9 chains (orange) with terminal thiol functionality. Self-assembling leads to thiol-crosslinking and stable particles (**A**). Reprinted with permission from *Carvalho et al.*[7b] Copyright (2018) American Chemical Society. Maltoheptaose was modified at the reducing end with propargyl amine and Cu-clicked to azide-modified PNIPAM. Hereby a thermo-responsive block copolymer was obtained (**B**). Reprinted with permission from *Otsuka et al.*[96] Copyright (2010) Royal Society of Chemistry.

Low molecular weight HA (M_w 4.3 kDa) was also used by *Niskanen et al.* for the Cu-mediated synthesis of a thermo-responsive amphiphilic block copolymer.[97] HA was functionalized with 2-(2-azidoethoxy)ethanamine by reductive amination and clicked to a hydrophilic alkyne-modified poly-(*N*-vinylcaprolactam) (PVCL, M_w 3.5 kDa). The authors demonstrated that the low cloud point temperature of PCVL (49 °C) could be transferred to the amphiphile (with a slight increase to 51 °C), introducing a reversible solubility switch into the polymer architecture. Heating the amphiphile above the new cloud point temperature induced micellation into hollow polymersome structures. Since the particle size was a function of the heating rate, the final polymersome size was controllable by adjusting the time to reach the final temperature. Fast heating produced larger particles with a D_H of 443 nm. Slow heating lead to 275 nm-sized nanoparticles.

By changing PVCl to poly-*N*-isopropylacrylamid (PNIPAM), the group of *Borsali* could significantly lower the cloud point temperature of their amphiphilic maltoheptaose-based

block copolymer (**Figure 17**, **B**).[96] In a first step they performed ATRP to synthesize azide-modified PNIPAM blocks of different sizes (M_n 3.3–25.1 kDa). Subsequent conjugation to alkyne-functionalized maltoheptaose led to a family of amphiphilic block copolymers that underwent phase transition above a cloud point temperature of 39.4–73.9 °C (depending on the DP of PNIPAM). Self-assembling in water resulted in well-defined nanoparticles with vesicular morphology of 300 nm.

In contrast to the reversible amphiphilic character of thermoresponsive block copolymers, most acid-sensitive polysaccharide block copolymers can not undergo multiple cycles of assembling and disassembling. The main purpose of this compound class in nanomedicinal applications is to exploit increased pH-levels in tumorous tissue as external stimulus for controlled particle degradation and cargo release. Typically, the design of the respective block copolymers is based on the combination of a hydrophilic and a pH-responsive hydrophobic block.

A prominent example for an acid-responsive polymer block is acetalated dextran. The fine-tuning of acetal content in the polysaccharide backbone allows for a precise adjustment of the rate of hydrolysis and has been extensively researched by *Bachelder et al*.[22, 98] The first pH-responsive linear polysaccharide block copolymer was reported by *Zhang et al.* (**Figure 18**, **A**).[99]

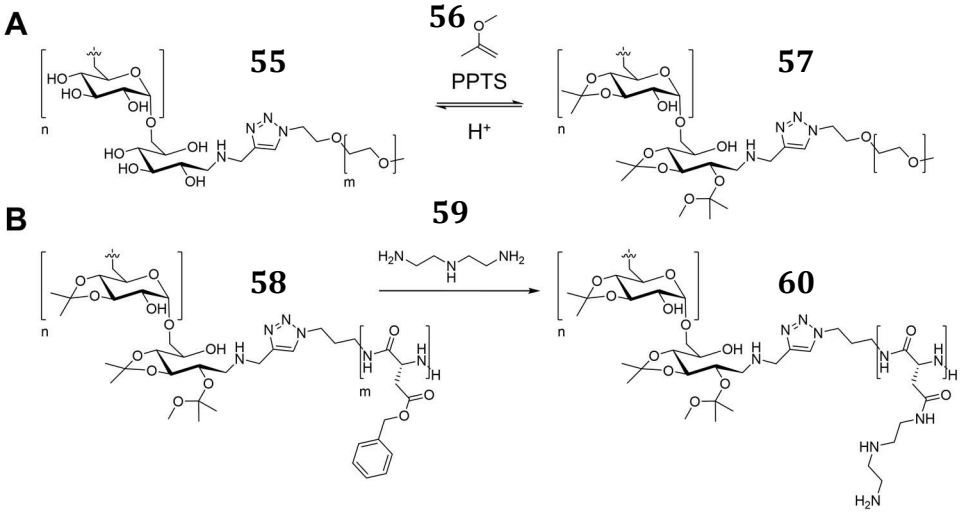

Figure 18. Synthesis of a responsive AcDex-b-PEG block copolymer **57** by acetalization of double hydrophilic Dex-b-PEG block copolymer **55** (**A**) Post polymerization modificatio of an AcDex-b-polypeptide amphiphile **57**. A cationic AcDex-b-PAsp(DET) block copolymer **60** was prepared by aminolysis of an AcDex-b-PBLA double hydrophobic block copolymer (**B**) Redrawn from ref.[99-100]

Even though the design is very simple, the authors presented an elegant synthetic strategy based on Cu-catalyzed conjugation of two hydrophilic chain end functionlized polymer

blocks. Dextran (M_n 6.0 kDa) was modified with propargylamine at the reducing end by reductive amination and conjugated to azide-terminated PEG (M_n 5.0 kDa). Since the amphiphilic PEG block contains no functional groups in the backbone, the acetalization reaction can only occur in the hydrophilic backbone of the dextran domain, giving the whole polymer an amphiphilic character. It was found that the degree of acetalization not only had an influence on the speed of particle degradation but also on the CMC (7.2–80.2 mg L^{-1}) and particle size (D_H 144–248 nm). Furthermore, the cellular uptake of doxorubicin-loaded nanoparticles was faster and more efficient compared to self-assembled non-responsive dox-loaded PEG-b-PLA nanoparticles.The amphiphile design of *Zhang et al.* was then further developed by *Li et al.* adding a positively charged hydrophilic block (**Figure 18**, **B**).[100] This synthetic procedure was inspired by the former approach of *Lecommandoux* and coworkers who synthesized Dex-b-PBLG block copolymers.[25] The modified synthesis included the combination of an alkyne-functionalized AcDex (M_w 7.3 kDa) and a hydrophobic poly(γ-benzyl L-aspartic acid) PBLA (M_w 3.6 kDa) by Cu-click chemistry. Subsequent aminolysis of the γ-benzylic ester **58** resulted in a positively charged hydrophilic domain. The cationic amphiphile **60** was able to complexate plasmid DNA (pDNA) in combination with the hydrophobic drug doxorubicin (dox). An optimization of the ratio of negative to positive charge (N to P) led to pDNA/dox-loaded cationic nanoparticles with a D_H of 308 nm and a zeta potential of 7.9 mV. Unfortunately, the surface-activity was not determined. However, it was clearly demonstrated that the particle system exhibited pH-responsive release characteristics and allowed gene transfection with an efficiency of 4.2% in the BEL-7402 cell line.

Huang and coworkers reported a design for acid-responsive polysaccharide block copolymer based on the synergistic interplay of supramolecular recognition and hydrophobic adenine-terminated AcDex **61** (**Figure 19**).[101] The authors combined reductive amination with Cu-click chemistry to functionalize AcDex (M_w 6.0 kDa) with the nucleobase adenine. When incubated in THF with a telechelic thymine-terminated PEG (M_w not reported), an ABA triblock amphiphile was formed, that self-assembled in water into flower micelles. Variations of the amount of acetal coverage in the dextran backbone resulted in different particles sizes (D_H 143–173 nm) and CMCs (3.5–5.9 mg L^{-1}). The double pH-sensitive supramolecular micelles were efficiently loaded with doxorubicin and showed rapid release of their cargo below pH 5. Additional *in vivo* experiments with

HeLa cells further confirmed cellular uptake and inhibition of proliferation as a direct pharmaceutical effect of doxorubicin.

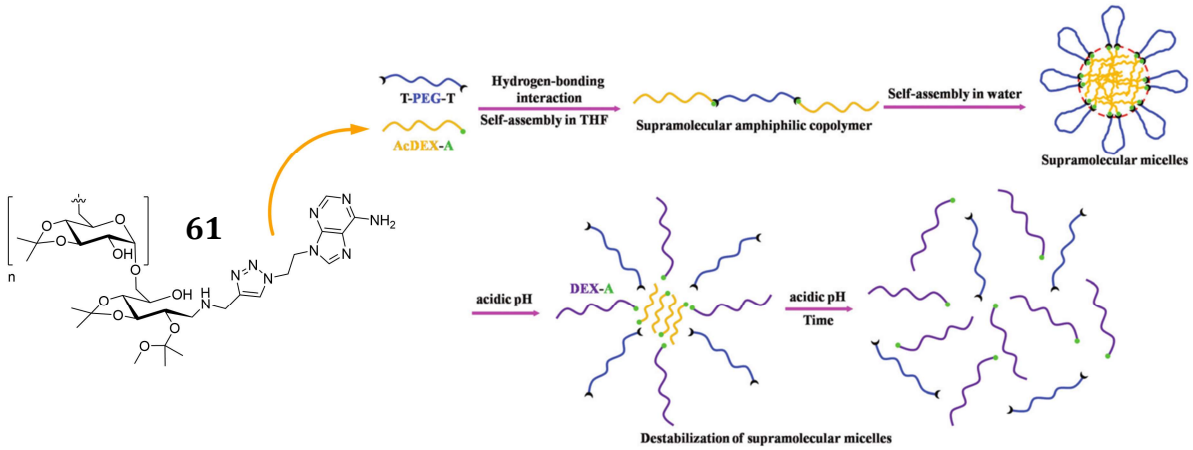

Figure 19. Supramolecular assembly of adenine-modified AcDex **61** with telechelic thymine-functionalized PEG. The flower micelles are stabilized by multiple hydrogen bonds and the hydrophobic effect. Lowering the pH disrupts the supramolecular interaction between complementary nucleobases and cleaves-off acetals in the dextran backbone. Reprinted and adapted with permission from *Kuang et al.*[101] Copyright (2015) Royal Society of Chemistry.

1.2.4 FULL OLIGO- AND POLYSACCHARIDE LINEAR BLOCK COPOLYMERS

The material class of polysaccharide block copolymers combines the biocompatibility, bioactivity and low toxicity of biopolymers with the benefits of precisely tunable composition and structure of synthetic polymer chemistry.[28] While their physicochemical properties make them interesting and promising biomaterials for future applications in nanomedicine, there is yet some limitation in the use of artificial polymers. Not all polymer types are fully biocompatible and in some cases induce immune responses by being recognized as foreign material by the immune system.[102] Consequently, the development of amphiphilic structures solely consisting of oligo-, and polysaccharide blocks represents one possible solution. Interestingly, despite the biological richness and diversity of polysaccharide structures and functionality, only few reports can be found in literature describing the general concept of full oligosaccharide amphiphilic block copolymers.

In an attempt to investigate the surface-activity of nonionic methylcellulose, *Kamitakahara et al.* synthesized the first amphiphilic diblock co-oligomers from tri-*O*-methylated and unmodified cello-oligosaccharides **62**.[103] The cellulose amphiphiles were synthesized by stepwise glycosylation as unsymmetrical trimer, pentamer or

hexamer with only one or two hydrophilic cellulose monomers per amphiphile (**Figure 20**, **A**). Despite the fact that all oligomers showed promising surfactant effectiveness (γ = 29 mN m^{-1}), their CMCs were relatively high (500 mg L^{-1}). Additionally, their synthesis involved labour-intensive work-up procedures such as multiple protection-deprotection steps including transition metal catalysts and preparative thin layer chromatography (PTLC) which made them impractical for larger application.

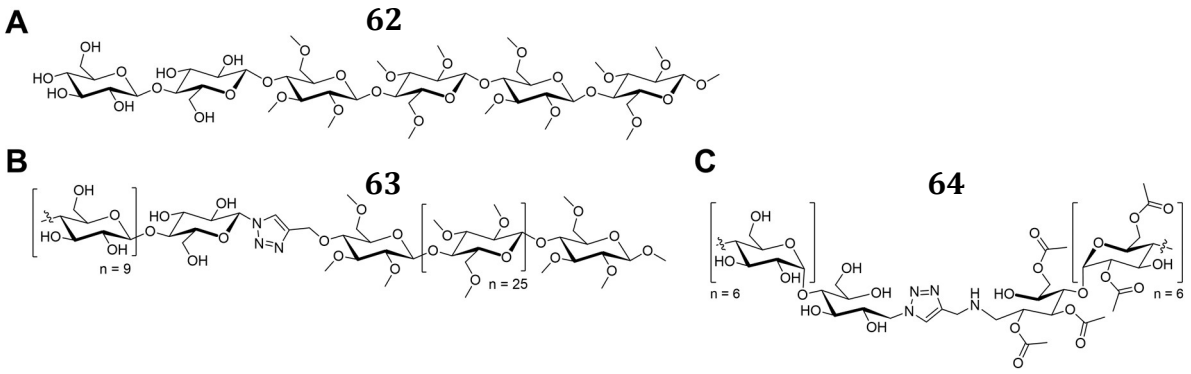

Figure 20. Surface-active hexamer of methylcellulose and cellulose by stepwise glycosylation as reported by *Kamitakahara et al.* (**A**). Thermogeling unsymmetrical cellulose-block-methylcellulose copolymer by Cu-click of *Takano et al.* (**B**). Symmetrical Cu-clicked maltoheptaose-block-acetylated maltoheptaose by *Halila* and coworkers (**C**).[103b, 104]

A further developed, simplified procedure was later reported independently by the groups of *Halila* and *Takano*.[104] Both groups synthesized the hydrophilic and hydrophobic block separately from azide and alkyne end group modified oligosaccharides and conjugated the blocks in a final step with Cu-click chemistry. *Takano* and coworkers did not explore the surface-activity of their unsymmetrical low molecular weight cellobiose (DP∼7) amphiphile **63**, however they found unusual thermogeling behavior at 25 °C (**Figure 20**, **B**). The group of *Halila* discovered the potential of symmetrical maltoheptaose amphiphiles to self-assemble in aqueous solution into micellar nanoparticles (**Figure 20**, **C**). The maltoheptaose-b-acetylated maltoheptaose copolymer **64** had a comparably low CMC (100 mg L^{-1}) and formed nanoparticles with a D_H of 56 nm. A successful degradation study with maltose-hydrolyzing glycoamylase enzyme, revealed a possible application as biodegradable and biocompatible nanocarrier. Extending the work of *Halila* and coworkers, we recently reported a Cu-mediated synthesis of a pH-responsive full dextran amphiphile. The material self-assembled in aqueous solution into micellar nanoparticles with D_H of 100 nm and decomposed below a pH of 6. The project is distinguishable from earlier approaches as it applied low molecular

weight polysaccharide dextran (30 AGU, M_w approx. 5 kDa) instead of oligosaccharides, which led to a drastic decrease in the CMC (12 mg L^{-1}) and therefore increase in thermodynamic stability of the assembled micelles. A trend commonly observed when comparing polymeric surfactants to their low molecular weight counterparts.[105] Furthermore, the protection of hydroxyl groups in the polysaccharide backbone with acid-labile acetals instead of acyl groups introduced a stimulus-responsive solubility switch. The concept of acid-catalyzed transformation of hydrophilic dextran to hydrophobic acetalated dextran was developed by *Bachelder et al.* and applied by several groups so far.[19, 22, 99-100]

A similar pH- and reduction-responsive block copolymer from maltoheptaose **39** and acetalated maltoheptaose **69** was reported recently by *Cheng et al.* (**Figure 21**).

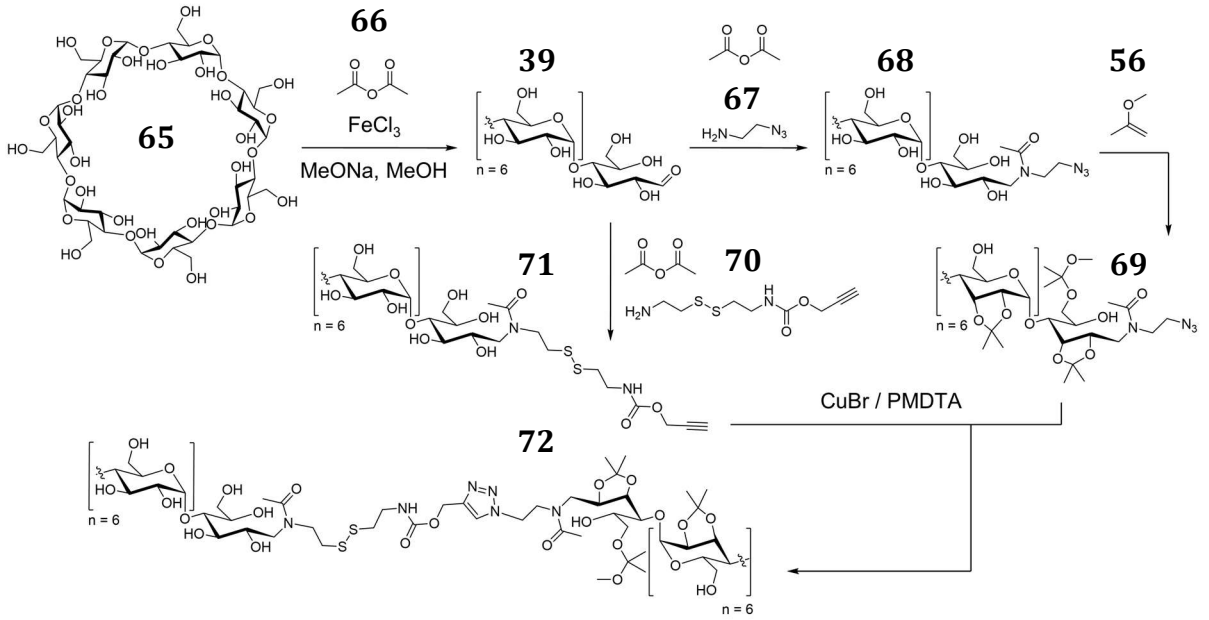

Figure 21. Synthesis of maltoheptaose-S-S-acetalated maltoheptaose amphiphile **72** (MH-S-S-AcMH). Starting from *β*-cyclodextrin **65** a maltoheptaose block is obtained and modified by reductive amination with 3-azido propylamine **67** and subsequent acetalization. The hydrophilic block is obtained by reductive amination with a propargyl cystamine linker **70**. Cu-mediated conjugation results in double responsive MH-S-S-AcMH **72**. Reprinted and adapted with permission from *Cheng et al*.[106] Copyright (2018) Royal Society of Chemistry.

Although also relying on Cu-click conjugation, the authors could introduce reduction-responsiveness additional to the pH-sensitive properties by modifying one maltoheptaose block with a propargyl cystamine linker **70**. The block copolymer **72** self-assembled in aqueous solution into micellar nanoparticles with a D_H of approx. 119 nm, unfortunately the surface-activity was not probed. However, the authors demonstrated

the encapsulation and a triggered release of the chemotherapeutic drug doxorubicine. Moreover, the nanocarriers were readily internalized by HeLa cells.

In summary, the synthesis of linear polysaccharide block copolymers has been described in literature with various oligo-, and polysaccharides and monomer substrates. Reported procedures apply either *grafting-from* chain polymerization or end-to-end coupling of preformed blocks. Both methods however led to hybrid biomaterials with promising qualities such as biocompatibility, bioactivity, surface-activity and self-assembly properties. Regardless of the fact that they proceed from different substrates, all synthetic strategies in the foregoing chapter include at some stage the introduction of a reactive functionality at the reducing end of the respective oligo- or polysaccharide block. In this context, polymer properties of dextran and the basic principles for site-selective modification at the reducing end will be described briefly in the following chapter.

1.3 General aspects of endgroup modification

The ideal polymer material for nanocarriers should be well characterized, easily functionalized, and biocompatible.[9] A detailed knowledge of the physico-chemical properties of a macromolecule is necessary to describe more complex assemblies of macromolecular structures such as micellar particles or the polymer conformation on coated surfaces. Herein we summarize our findings on reported properties of low molecular weight dextran to facilitate future characterizations of nanomaterials containing dextran as building block.

1.3.1 Dextran, a natural polymer building block

Dextran is a neutrally charged homoglycan, composed of α-1,6 glycosidic-linked glucose units (**Figure 22**). Typically, the monomer repeating unit in polysaccharides is referred to as the anhydroglucose unit (AGU). The polysaccharide is industrially produced from sustainable resources, more specifically, by fermentation of sucrose by lactic bacteria of the *leuconostoc* and *streptococcus* species.[107] Depending on the producing bacteria, the molecular weight and branching density can vary from 1–200 kDa and 3–50%.[17] Side chains are linked mainly by α-1,3, occasionally by α-1,2 and α-1,4 glycosidic bonds.[107] Dextrans used in this thesis were produced from *leuconostoc* species with a narrow M_w of 4.5–5.5 kDa and a low branching densitiy (5%).[108]

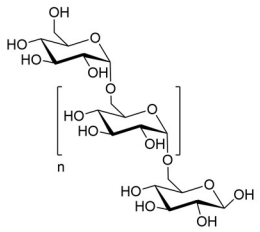

Figure 22. Structure of dextran. All glucose units are linked by α-1,6 glycosidic bonds.

Dextrans are soluble in a variety of aqueous and organic solvents, including H_2O, DMSO, DMF/LiCl (2 % w/v), ethylene glycol, aqueous solutions of urea (6 M) and glycine (2 M).[108-109] Most common solvents in literature are H_2O and DMSO but we found that mixtures of organic solvents and water such as DMF/H_2O (3:1), MeOH/H_2O (1:1) and THF/H_2O (1:1) were suitable as well.{Styslinger, 2012 #208;Rosselgong, 2018 #485} Generally, the good solubility is a result of the α-1,6 linkage between each AGU which creates a low rotational barrier and allows high chain mobility in solution.[108] Dextran can be considered a rather flexible polymer, compared to other polysaccharides which can also be found in the short persistence length (L_P = 1.5–1.8 nm) (**Table 2**).[110] In aqueous solution, the polymer chains prefer the conformation of a random coil structure. Increasing the concentration in solution forms bigger aggregates with random coils interpenetrating other polymer chains, finally leading to a more complex coil structure. Below a molecular weight of 2 kDa the polysaccharide appears rod-like.[28, 110]

Table 2. Relevant dextran polymer properties (see text for literature resources). L_P is a measure which describes the distance along the polymer backbone over which the chain can be considered fairly straight. R_h describes the radius of a solid sphere with the same diffusion behaviour as the polymer in free solution.

M_w (kDa)	L_p (nm)	r_h (nm)	r_d (nm)	$\bar{\nu}$ (cm^3 g^{-1})	L_{AGU} (nm)
9.5–10	1.5–1.8	0.19–0.23	0.27	0.61	0.44–0.45

The partial specific volume of dextran in aqueous buffer (0.5 N Na_2HPO_4 and 0.05 N NaH_2PO_4) was determined to be $\bar{\nu}$ = 0.61.[111] The *Stokes* radius (r_s) or radius of hydration (r_h) was determined by *Granath* and *Fisher* as 0.19–0.23 nm (10 kDa).[112] Unfortunately, the r_h is a measure of the polymer coil size in solution and therefore dependant on the molecular weight. By computing the radius of the polysaccharide fibre (r_d = 0.27 nm) as the radius of a cylinder having the same contour length and specific volume as dextran, *White* and *Deen* found a polymer describing value independent of molecular weight. It has to be considered though, that the authors were calculating with a monomer length of 1.0 nm from X-ray diffraction analysis of α- and β-D-glucose.[113]

A more precise value for the glucose monomer length (0.44–0.45 nm) was determined by several groups in more recent studies by single molecule atomic force microscopy (AFM).[114]

In terms of pharmacokinetics, conjugates of dextran with therapeutic agents were reported to show prolonged pharmalogical effects, alteration of the toxicity profile and a reduction in the immunogenicity of the respective drug or protein.[17]

Several studies describe dextran-coated materials as having superior colloidal stability compared to PEG-coated particles [90, 115] paired with very low- to non-specific cell binding and good resistance to protein adsorption.[100, 116] Due to its good biocompatibility, biodegradability and hydrophilicity the polysaccharide is a commonly used biomaterial in drug delivery applications and nanomedicine.[16-17, 28-30, 98, 108]

The circulation time and elimination of dextran from the human body was shown to be a function of molecular weight. Low molecular weight dextrans (<40 kDa) are filtered by the kidneys and thus have shorter circulation times.[117] They are known to be non-toxic and chemically inert.[118] Whereas higher molecular weight dextrans show longer blood circulation times before they become cleared in the spleen and liver by the mononuclear phagocytic system.[119] The macromolecule is biodegradable by dextran-1,6-glucosidase, an enzyme found in spleen, liver, lungs, kidneys and muscle tissue.[120]

In medicinal therapy, high molecular weight dextrans (most commonly 40–70 kDa) are applied as synthetic blood volume expander. As an example, Dex 70 is used as a 6% solution in saline buffer for the treatment of shock symptomatics arising from hemorrhage or surgery.[121] It is also reported to reduce thrombosis and consequently the risk of post-operative pulmonary emboli.[122]

Generally, dextran is considered a non-toxic and safe biopolymer for medicinal therapy, however possible immunologic events have to be considered in *in vivo* applications. Adverse immunological side effects such as anaphylactoid reactions were described after therapy with high molecular weight dextrans (40–70 kDa).[123] The unwanted effect of immunological reactions can be reduced when low doses of 1 kDa dextran solutions are administered prior to treatment with Dextran 40 or Dextran 70. In this case, the short oligosaccharide can act as a hapten and interferes with the formation of antibody-dextran complexes.

1.3.2 SITE-SELECTIVE CONJUGATION

Polysaccharides represent a complex and functionally diverse group of polymer building blocks in polymer material chemistry.[28] Despite their well documented merits[16] and functionalities[30] that allow them to compete as equals with their artificial counterparts, their application as polymer building blocks is still not as established in polymer chemistry as the latter.[16-17] One possible reason for their minor application is the more complex production compared to petrol-based polymers. Additionally, the overall polymer architecture and therefore molecular weight distribution is not as finely tunable. However, with the accelerating progress in biotechnology and the growing public interest in *green* and sustainable polymer materials, these arguments become less and less substantial. Creating polysaccharide block copolymers in a bottom-up approach requires the site-selective functionalization of the polymer chain end. This is possible by exploiting the aldehyde group at the reducing end, resulting from the mutarotation phenomenon (**Figure 23**). Since only the last glucose unit at every chain end can form the open or closed conformation, polysaccharides with a negligible low degree of branching contain only one aldehyde group within the whole polymer. The concentration of aldehyde in solution for *α*-D-glucose was reported to be 0.0024%,[124] for low molecular weight dextran (M_w 3.5–6 kDa), a concentration of 0.024% aldehyde was observed.[67]

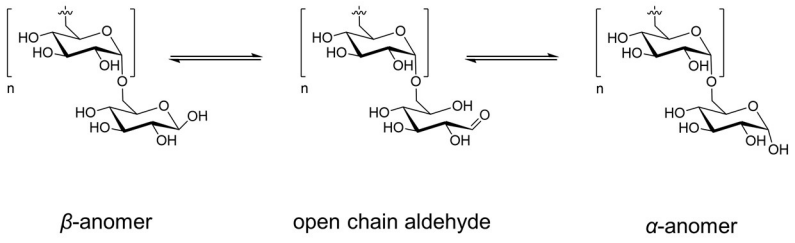

Figure 23. The mutarotation phenomenon describes among others the reaction of *α*-D-glucose into the *β*-D-glucose anomer by open- and closing the glucose ring structure.[125] The resulting transistion state aldehyde group enables site-selective functionalization.

Generally, there are three common synthetic strategies reported in literature to transform the aldehyde functionality into a more reliable anchor group for further conjugation chemistry. In **Figure 24**, the most prevalent synthetic methods for a site-selective modification of polysaccharide reducing ends are shown: One possibility is the modification of the aldehyde with an aminooxy compound forming an oxime.[7b]

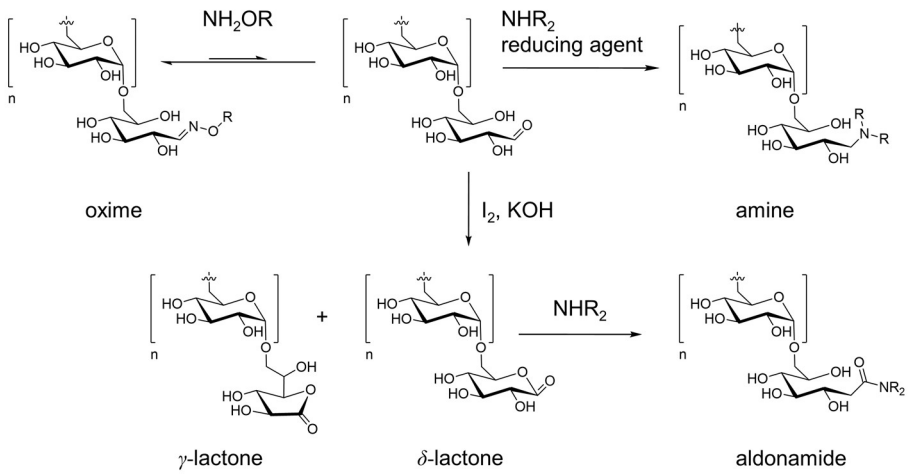

Figure 24. The most common synthetic strategies in polysaccharide end group functionalization proceed by oxime formation, amination or lactonization chemistry. By applying aminooxy ligation chemistry, no reduction of the formed oxime is necessary. The reaction of the free aldehyde group with an amine under reductive conditions leads to an amine conjugate. Oxidation of the open-chain aldehyde group to the respective aldonic acid gives a lactone. The lactone can then be transformed into an aldonamide by nucleophilic ring-opening with an amine.

By organocatalysis or sample freezing, almost quantitative conversion can be achieved in very short reaction times.[126] However, molecules containing aminooxy functionalities often require multiple step preparations or have limited commercial availability. A more convenient synthetic strategy involves the amination of the aldehyde group with a primary or secondary amine, often in the prescence of $NaCNBH_3$, $NaBH(OAc)_3$ or $NaBH_4$ as reducing agents. Amine-bearing building blocks are widely commercially available and can easily be introduced into linker molecules or polymers. While this is the simplest and fastest way to install a functionality on a polysaccharide end, it often requires a large excess of amine and reducing agent.[31, 127] The third synthetic strategy is a two step procedure. First, the aldehyde at the reducing end is oxidized to its corresponding lactonic acid using I_2 or Br_2 in KOH. With the removal of water by freeze drying, a five- or six-membered (γ, or δ)-lactone ring is formed. Subsequent reaction with an amine, results in an aldonamide structure.[80a, 128] In terms of sustainability and also for industrial applications, the oxidation/aldonamide formation is preferred over the first two synthetic routes.[129] Neither a reducing agent, nor labour-intensive syntheses of aminooxy compounds are required. Unfortunately, this reaction is also the most time intensive, due to the two-step process, the slow ring opening of the lactone group and the tedious work-up with anionic exchange resins.[80a, 128a]

1.3.3 REDUCTIVE AMINATION AT THE CHAIN END

Functionalizing the polysaccharide on the reducing end by reductive amination in order to achieve end-on ligation is the most important tool applied in this thesis. Therefore, the general reaction mechanism and common strategies applied in oligo- or polysaccharide modification relying on this method will be discussed shortly.

The one-pot reductive amination using sodium cyanoborohydride is often represented as a one step reaction type. From a chemical point of view, it is actually a two step reaction consisting of an amination and a reduction step (**Figure 25**). First, nucleophilic addition of an amine to the aldehyde group forms an imine, or *Schiff* base in an equilibrium with the free aldehyde functionality. Second, the resulting imine is reduced by hydride transfer to the sp^2-carbon atom. As discussed in the previous paragraph, the aldehyde functionality is only present in low concentrations, therefore the observed rate of reaction is limited by the rate of tautomeric conversion of the last glucose unit.[130]

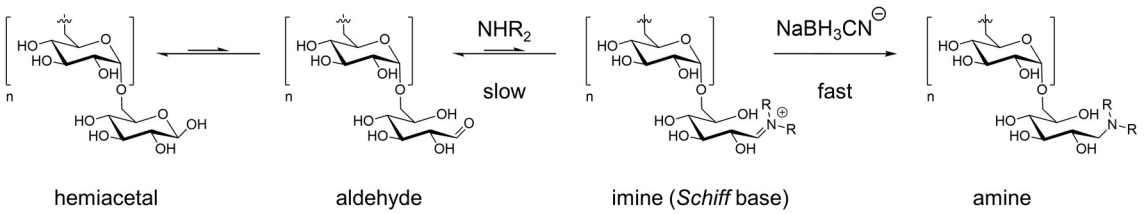

Figure 25. General mechanism for the reductive amination of a polysaccharide reducing end with a cyanoborohydride ion (adapted from ref [28, 131]). The reaction is a two step process consisting of a kinetically slow amination and subsequent fast reduction of the formed imine (*Schiff* base).

In general, the reaction is preferably performed in buffered solutions. As reducing agent $NaCNBH_3$ is very popular, due to its selectivity towards imines, allowing a one-pot reaction setup.[131] It is also favored because of its high stability in aqueous solutions. The acid-catalyzed rate of hydrolysis at pH 7 was reported to be less than 0.5% in 24 h and the reducing agent was found to be fairly stable in acidic solvents until pH 3.[132] Although reductive amination can be performed from pH 5–10, *Borch et al*. suggest an optimum between pH 6–8.[131] *Moreau et al*. narrowed the range further down to an optimum at pH 7.[68a] At this pH, reduction of the imine proceeds much faster than the reduction of the aldehyde. Below pH 4 the rate of carbonyl reduction increases rapidly, outperforming the imine reduction rate.[131] In summary, two important aspects have to be considered regarding the effect of the pH on the reductive amination. First, a sufficient concentration of protons has to be present to support the formation of protonated oxygen species to

facilitate imine formation. Second, the primary aliphatic amine species will be protonated to a high degree at a pH <5, leading to a decrease of its nucleophilicity.

Contrary to the findings mentioned before, most reports in literature use NaOAc-buffer at pH 5 and up to 100 equivalents of amine. Typical protocols use reaction times of 2–3 days at 50–60 °C.[31, 99-100, 133] On one hand, the use of a large excess of amine is beneficial for suppressing the formation of double aminated side products and for shifting the equilibrium between aldehyde and imine towards the imine species. On the other hand, this type of reaction has a of poor atom economy. Another major problem arising from long reaction times at elevated temperatures is that it is limiting the method to very robust biopolymers. Sensitive proteins like antigens or small molecules, e.g. arylazides are not stable under these reaction conditions and are therefore not compatible with this method. The key to overcome this difficulty is the use of microwave dielectric heating.

1.3.4 TUNING REACTION KINETICS WITH MICROWAVE POWER

Microwave-enhanced reductive amination with neutrally charged polysaccharides necessitates the use of aqueous sodium borate-buffer (SBB) solvent systems. Hydroxy groups in the polysaccharide backbone chelate the borate ions, consequentially introducing a net charge into the polymer, giving it a dipol character (**Figure 26**).[134]

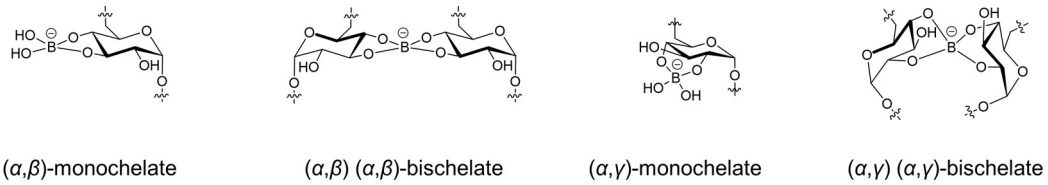

Figure 26. The complexation of boric acid with hydroxyl groups units in polysaccharide backbones can form different chelate species, depending on the binding positions. Borate binds either to adjacent- (α, β), to alternative- (α, γ) or to mixed (not shown) (α, β) (α, γ) hydroxyl groups forming mono-, or bischelate complexes (adapted from ref.[134c]).

The overall dipol moment allows the molecule to move in the alternating field of microwaves, leading to a dramatic increase in reaction kinetics. This implies that all chemical modifications on neutrally charged polysaccharides involving microwave irradiation have to include a borate buffer system and hence either water soluble reagents or a cosolvent, miscible with the aqueous phase. Additionally, post functionalization modification of the polysaccharide backbone requires desalting by dialysis or gel permeation chromatography to fully remove buffer salts and obtain free hydroxyl groups.

Pagnotta et al. describe the accelerated reaction of *α*-D-glucose to *β*-D-glucose in D_2O:EtOH mixtures as a result of an intrinsic microwave effect.[125, 135] *Turnbull* and coworkers reported microwave influenced accelerated reaction rates rather as a solvent-mediated heating effect, concomitant with an increased rate of mutarotation.[136] Their findings were based on results for the attachment of sugars to aminosilane-derivatized glass surfaces in various DMF/H_2O mixtures. Both studies were carried out on different model systems and therefore can not be compared directly. Furthermore, both groups missed to compare reaction rates at high temperatures with kinetics at room temperature in order to clearly differentiate between an intrinsic or a solvent mediated heating effect. Nevertheless, the final outcome in both studies supports the hypothesis of a microwave-induced acceleration of the rate of mutarotation, thereby increasing the concentration of the open chain aldehyde functionality. As a result, *Moreau et al.* could show that the extent of amination after 1 h exposure of microwave irradiation is comparable to the degree of modified chains after incubating the dextran in a preheated water bath for 48 h.[68a] *Verma et al.* could significantly reduce reaction times from 72 h for conventional heating to 4 h when applying microwave irradiation. As a model reaction they performed a reductive amination at the chain-end of dextran with *N*-Boc ethylenediamine at room temperature.[68b]

Compared to other techniques for site-selective functionalization of the polysaccharide reducing end (**Chapter 1.3.3**, **p.40**), the microwave-assisted one-pot procedure is the fastest and simplest method available and yields equally high endgroup densities.

2 MOTIVATION AND AIM OF THE WORK

Increasing interest in nanotechnology and associated applications in nanomedicine enhanced the use of block copolymers as suitable components for smart nanomaterials significantly in the last decade.[137] The conjugation of a hydrophilic polymer block with a hydrophobic polymer block has become a popular method to create structures with the ability to self-assemble. Their amphiphilic nature and capacity to self-organize into micelles, rods or polymersomes enables manifold applications such as nano-sized catalytic environments,[138] nanoparticles for drug delivery,[91, 139] or solution stabilizing surfactants.[115, 140] Especially in the field of drug delivery, there is a need for the development of non-toxic and biocompatible high-performance polymer materials with stimuli-responsive release characteristics. The motivation for this thesis was to explore the utility of dextran as non-toxic, green polymer building block and its application in the synthesis of stimuli-responsive polysaccharide nanomaterials.

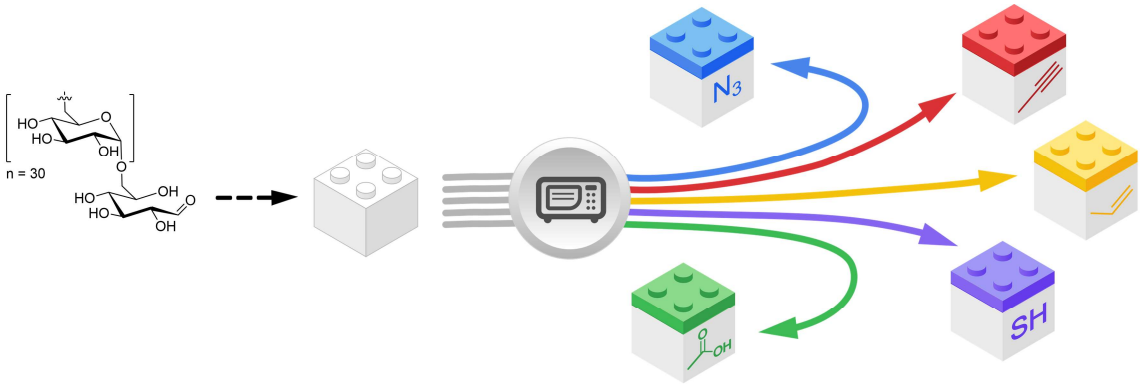

Figure 27. Microwave-assisted end-group functionalization of dextrans to reach high end-group densities.

The first project was therefore focused on the design of a general, fast and efficient synthetic method for the introduction of various functional groups at the polysaccharide chain-end (**Figure 27**). This should allow the use of dextran for end-on conjugation as biopolymer building block alternative to artificial polymers. Key issues were on the one hand, the limited availability of the reducing chain-end aldehyde (< 0.02%)[28, 67] and its slow reaction kinetics.[68, 127b, 136] On the other hand, the development of a method for the thorough quantification and structural analysis of the modified polysaccharide chain-end. This should help to clarify the often vaguely published structure analysis by ^{1}H NMR

caused by the wide distribution and high intensity of all glucose backbone proton signals.[25, 93c, 99]

Despite the vast number of published articles on polymer supported drug delivery, many artificial polymers show limited biocompatibility and many particle systems require stabilization by non-biodegradable surfactants. This is problematic, as for some polymers there are first reports of unintended immune responses.[102] Furthermore, surfactants like poly(vinyl alcohol) (PVA) were shown to remain in the nanoparticle system in high amounts even after purification.[141] Residual surfactant can significantly alter the particle surface properties, determining the adsorption and composition of the protein corona and thus the *in vivo* fate of the nanocarrier system.[6]

Surface-active polymer systems containing only oligo-, or polysaccharide blocks represent a functional, non-immunogenic and sustainable solution to this problem.[107]

In the second project, it was investigated whether the combination of an end group functionalized hydrophilic dextran with an end group functionalized hydrophobic acetalized dextran resulted in a pH-responsive polysaccharide macrosurfactant (**Figure 28**). The amphiphile should be able to self-assemble into micellar nanoparticles, omitting the need for non-biodegradable surfactants like PVA. It was planned to study its surface activity, self-assembly and acid triggered degradation. Afterwards, the hydrophobic drug curcumin could be encapsulated to evaluate loading capacities and triggered release as well as the stabilizing effect on the model drug in aqueous solution.

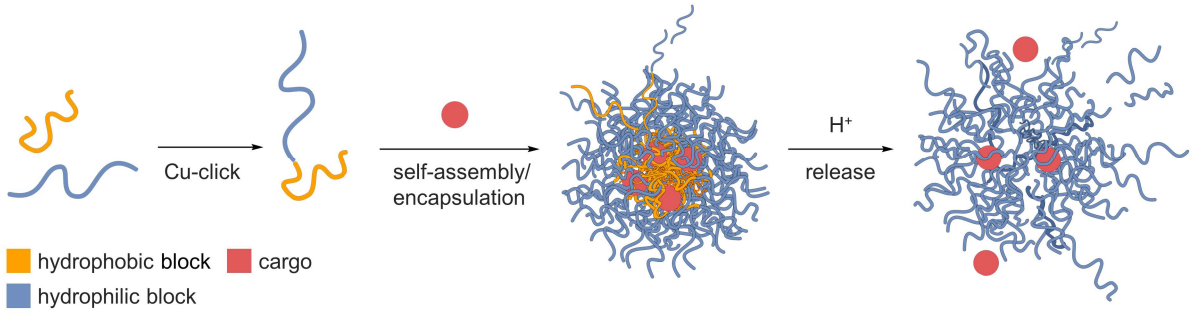

Figure 28. Hydrophilic and hydrophobic dextran building blocks are combined with Cu-click chemistry to form an acid-responsive polysaccharide block copolymer with amphiphilic properties.

The concept of smart full polysaccharide block copolymers was then further developed in the third project. The goal was to establish an improved, metal-free ligation strategy based on thiol-modified dextran. Hereby it should be possible to create a double-stimulus-responsive block copolymer from a single starting material. The morphology of the self-assembled particles and their degradation induced by different external stimuli could

then be studied in detail. With the encapsulation of a photosensitizer molecule, it should be explored whether the macrosurfactant can successfully deliver and release a functional cargo into the cytosol of cells (**Figure 29**).

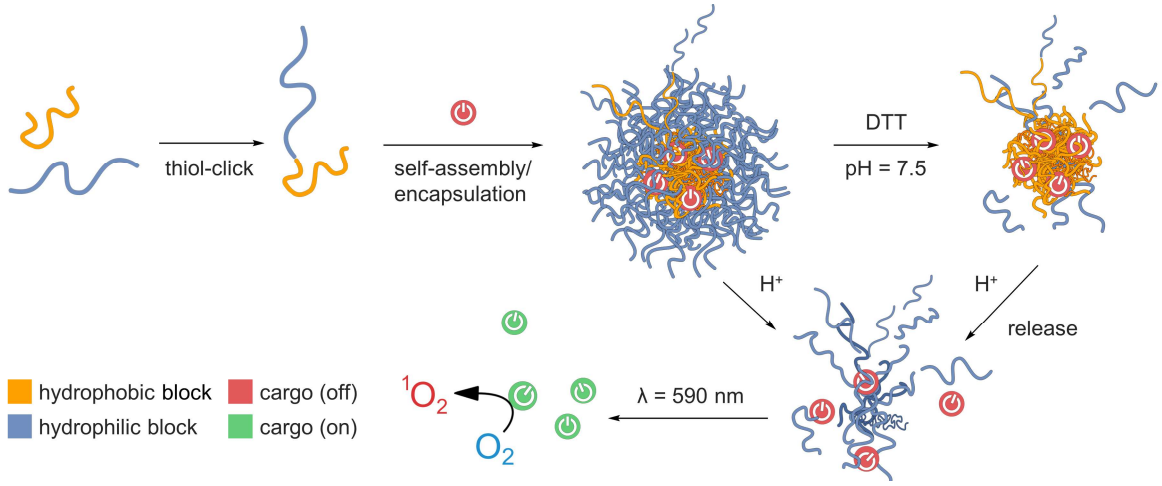

Figure 29. The acid and reduction-responsive dextran amphiphile should be applied as macrosurfactant for the stabilization and delivery of a hydrophobic 2nd generation photosensitizer into the cytosol of HeLa cells. Hereby inducing a phototoxic effect, triggered by NIR-light.

To fully exploit the possibilities of metal-free thiol-based ligation, it was planned to conjugate the two polysaccharide blocks with thiol-ene chemistry and the resulting material should be compared to the 1st generation pH-responsive amphiphile. Furthermore, the influence of the ligation chemistry on the surface properties of all prepared surfactants should be investigated with a focus on the increasing flexibility in the linkage, connecting both blocks (**Figure 30**).

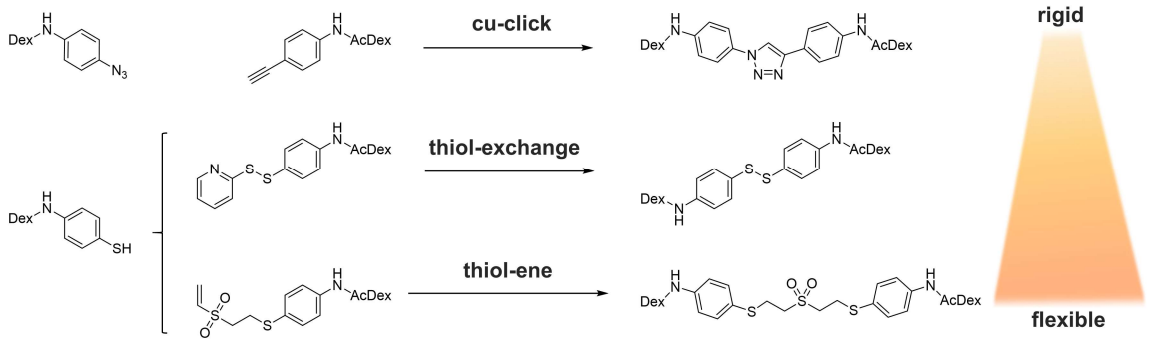

Figure 30. Since the three different ligation strategies result in different degrees of linkage flexibility, it was planned to study the influence of the altering architecture on the surface activity and self-assembly characteristics.

In addition to nanomedicine and drug delivery, tissue engineering is an emerging field in polymer chemistry where polysaccharide materials can contribute substantially. To prove the versatility of our technique, we were interested if end-group modified dextran

could also be applicable as macromonomer in the synthesis of more complex polymer architectures like proteoglycan-type structures. It was therefore decided to synthesize starlike brush polymers by ring-opening metathesis polymerization (ROMP) (**Figure 31**). The goal was to prepare polysaccharide brushes with low molecular weight dextran side chains and a maximum grafting density. Therefore, norbornene containing linker molecules were envisioned for a conjugation with dextran. The resulting macromonomer should be polymerized in a *grafting-through* approach and the influence of increasing catalyst activity on the polymerization should be studied. Hereby, the focus was set on the optimization of monomer conversion and final molecular weight of the brush.

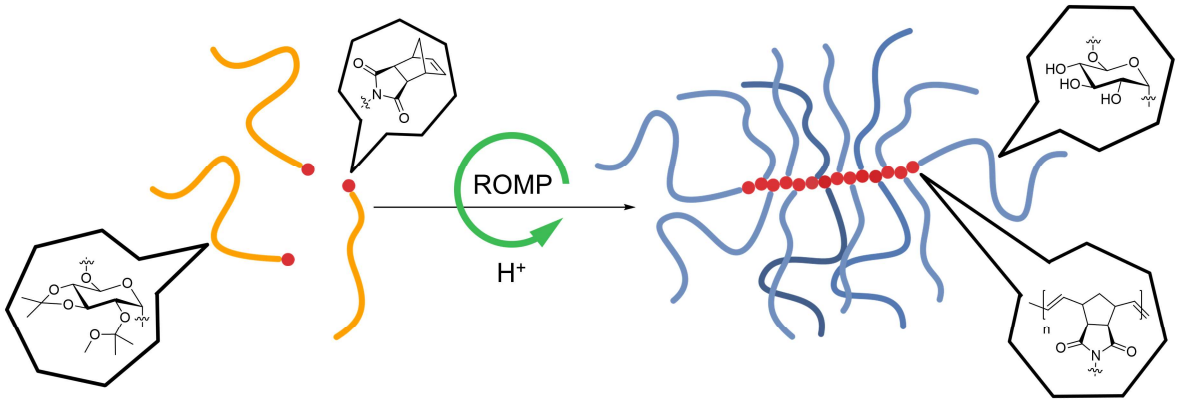

Figure 31. AcDex will be functionalized with a norbornene functionality at the reducing end. ROMP with the resulting macromonomer and subsequent acidic work up leads to water-soluble polysaccharide brush polymers.

3 RESULTS AND DISCUSSION

3.1 DEXTRANS AS MULTIFUNCTIONAL BUILDING BLOCKS

In this first chapter we explored the development and optimization of a general synthetic route for the introduction of valuable functionalities on the reducing end of dextran. The focus was on achieving maximum end group densities and reproducible analytics of the chain end modification with a minimum of required amount of amine.

3.1.1 TWO-STEP APPROACH: ALIPHATIC AMINES AS HOMOBIFUNTIONAL LINKER

In order to create polysaccharide building blocks for a bottom-up polymer synthesis, dextran (M_w 10 kDa) was modified on the reducing end, following the microwave-enhanced reductive amination strategy reported by *Gu* and coworkers.[68b] The use of aliphatic amines in the reductive amination reaction on the dextran reducing end proved to be problematic because of the unreliable analysis of the end group density. Dextran with a M_w of 10 kDa has on average 60 anomeric protons and 360 glucose ring protons. The introduction of a small molecule linker with two chemically identical protons from a CH_2 group is hard to trace in ^1H NMR because of the weak signal intensity compared to the glucose proton signals. Additionally, the glucose signal covers the area from 2.90–3.75 ppm and from 4.25–5.17 ppm (in DMSO-d_6), or from 3.38–3.99 ppm and from 4.96–5.30 ppm (in D_2O). Thus, the signal of the installed functional group has to be more low field shifted, in the aromatic region, or towards the higher field, e.g like in methyl resiudes. By using *N*-Boc ethylenediamine (*tert*-butyl *N*-(2-aminoethyl) carbamate) as amine it was in fact possible to circumvent this problem. Boc contains nine chemically and magnetically identical protons which are well visible in ^1H NMR spectroscopy at 1.4 ppm and provide a sufficiently strong proton signal, well separated from the glucose backbone signals (**Figure 78**, supplemental).[68b] The conversion of amine-modified dextran with activated benzoic esters resulted in low conversion and dextran conjugated esters as side products. Because this strategy was limited to direct modification with amine functionalities and afforded several synthetic steps to the final product, it was discarded.

Instead, we decided to use dextran with a lower molecular weigth of 5 kDa (**34**) to facilitate the visibility of a small molecule, next to the AGU protons. First, 1-amino-11-azido-3,6,9-trioxaundecane **73** was examined. Unfortunately, in the FTIR spectrum of the

isolated product **74**, there was no trace of a characteristic azide band. Instead, the success of the end group modification was observed by the disappearance of the signal for the α-anomeric proton (δ = 6.7 ppm) and the β-anomeric proton (δ = 6.3 ppm) by ^1H NMR. While this indicated quantitative conversion, it did not allow to calculate the exact amount of modified chains (mc) at the reducing end. The functional end-group density of **74** had to be probed in a model click reaction with 4-ethinyl benzoic acid **75** (**Figure 32**). Subsequent quantification of **76** with ^1H NMR revealed a signal at 8.29 ppm from the formed triazole proton and two multipletts at 7.78 ppm and 6.97 ppm from the benzoic acid. Calculating the ratio of the aromatic benzoic acid protons to the anomeric protons of dextran gave a moderate end group functionalization of 47%mc.

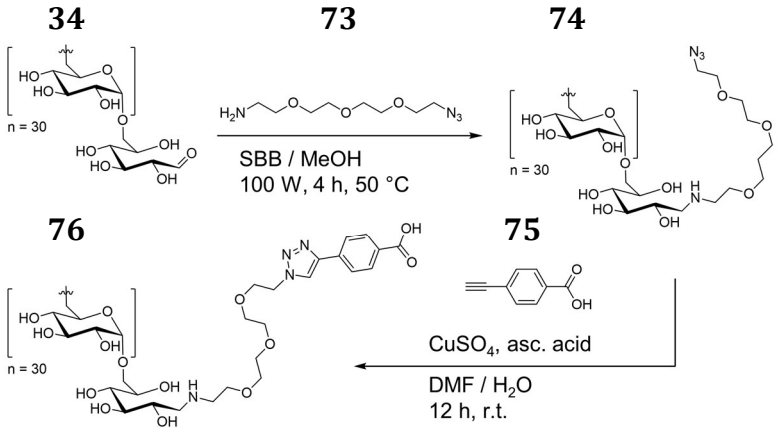

Figure 32. Modification of dextran **34** by reductive amination and probing of the end group functionality. Functionalization was carried out in a microwave vessel at 50 °C, 4 h, $B(OH)_3$-buffer/MeOH and 10 eq. amine. The click reaction was performed at rt in DMF/H_2O, 12 h with 0.2 eq. $CuSO_4 \cdot 5\ H_2O$, 2.5 eq. ascorbic acid and 2.0 eq. benzoic acid derivative **75**.

3.1.2 SINGLE-STEP APPROACH: ANILINES AS HETEROBIFUNCTIONAL LINKER

We decided therefore to use aniline as small molecule linker (**Figure 33**). The aromatic primary amine was reported to function as organocatalyst in amination reactions, but also to overcome the issue of slow reaction kinetics in reductive amination.[127b] Moreover, the introduced aromatic system allowed tracking of the reaction progress by UV-absorption signals as well as direct analysis of introduced end groups by ^1H NMR.[31, 69] As discussed in **chapter 1.3.4** (**p.41**), borate ions are essential for the interaction of dextran with the alternating field of microwaves. A test reaction solely in DMSO (the only organic solvent suitable for dextran) showed no conversion and therefore confirmed the assumption that the method was limited to aqueous buffers.

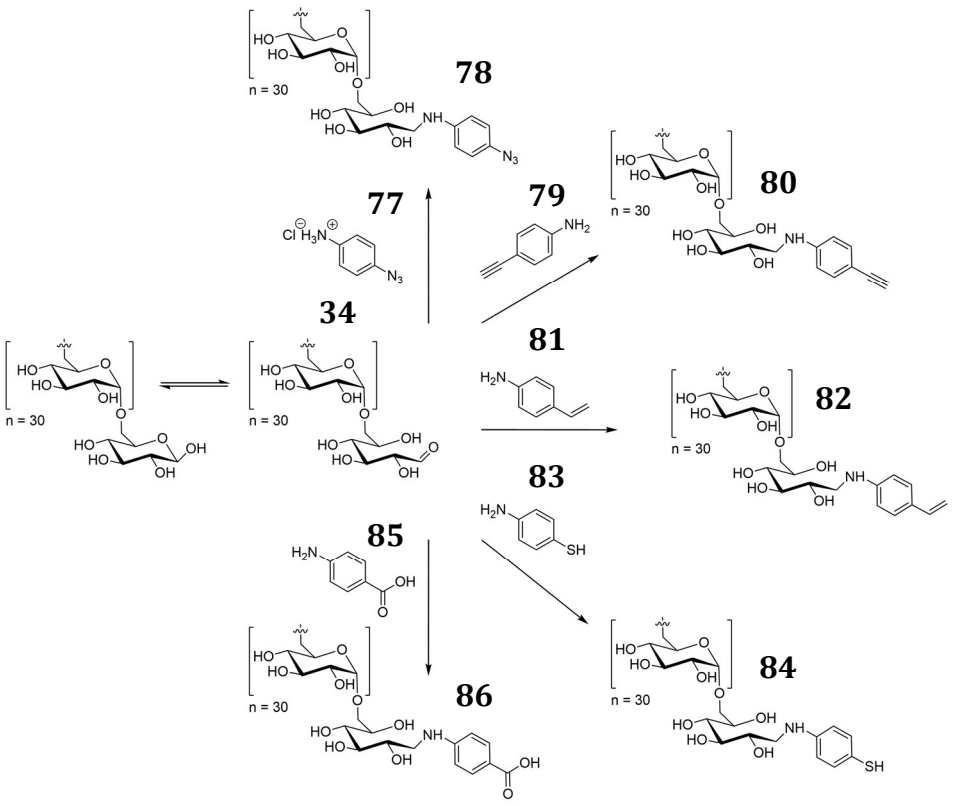

Figure 33. Microwave-enhanced reductive amination on the reducing end of 5 kDa dextran **34**. Using 10 eq. of aniline gives the end-group modified dextran (75–94%mc, depending on the according aniline). Reaction conditions include either a SBB/MeOH mixture of 1:1 or 4:1 (in the case of azido aniline hydrochloride **77**). Dextran and the aniline were dissolved in a concentration of $2.5 \cdot 10^{-5}$ mol mL^{-1} and $2.49 \cdot 10^{-5}$ mol mL^{-1}, respectively.

Table 3. Applied cosolvents in the microwave enhanced reductive amination of dextran with *p*-azido aniline hydrochloride.

cosolvent	%mc
DMSO	no conversion
DMF	no conversion
THF	85–90
MeOH	89–93

Table 4. Conjugated *p*-substituted anilines and the respective p*K*a values in H_2O of the protonated species.[142],*

R	p$K_{a\,amine}$	p$K_{a\,Residue}$
azide	4.74	–
alkyne	4.30	23
vinyl	4.82	–
thiol	4.47	6.86
carboxyl	4.77	2.69

**also calculated with marvin sketch V.*

Due to the fact that most applied aniline derivatives are either not fully water soluble or not water soluble at all at a basic pH, organic solvents, misciple with the aqueous phase were tested as cosolvents (**Table 3**). Finally, the best results were obtained for a SBB/MeOH system, hence MeOH was applied as an organic cosolvent in further experiments. After first promising results with *p*-azidoaniline **77**, the minimally required amount of amine concentration was reexamined. Starting from 20 equivalents, as

reported by *Verma et al*.[68b], the initial concentration of amine was decreased to 10 equivalents with no significant loss in chain-end density in the isolated product **78**. However, when further decreasing the amount of amine from 10 equivalents to 5 equivalents, the degree of substitution decreased from 89%mc to 57%mc.

Synthesis of azide-funtionalized dextran

First experiments for the functionalization of dextran **34** with *p*-azido aniline **77** were conducted at 50 °C for 4 h. Unfortunately, they all led to the degradation of *p*-azido aniline **77**. When performing the reductive amination above 30 °C, the reaction solution turned from light orange to dark red-black and a black gum-like lump was isolated. The samples were not analyzed due to their indissoluble character in H_2O and DMSO. A possible explanation is the acid-, photo- and heat-sensitivity of arylazides or their basic catalyzed hydrolysis to the corresponding thiol.[143] Heating to elevated temperatures (> 50–60 °C) over longer time periods might also result in elimination of N_2 from the aryl azide, producing a reactive nitrene species that will undergo a rearrangement reaction. The nitrene can then form an azaepine ring which can react with any nucleophile nearby, e.g other anilines.[144] It is also mentioned in literature, that *p*-substituents with electron donating properties (like amines) can enhance a photo- or thermolysis reaction.[145] Therefore, the end-group modification of dextran **34** with azidoaniline hydrochloride **77** was conducted at 30 °C and in the prescence of 11 equivalents triethylamine (TEA) to ensure complete deprotonation of the reactive amine species (**Figure 34**).

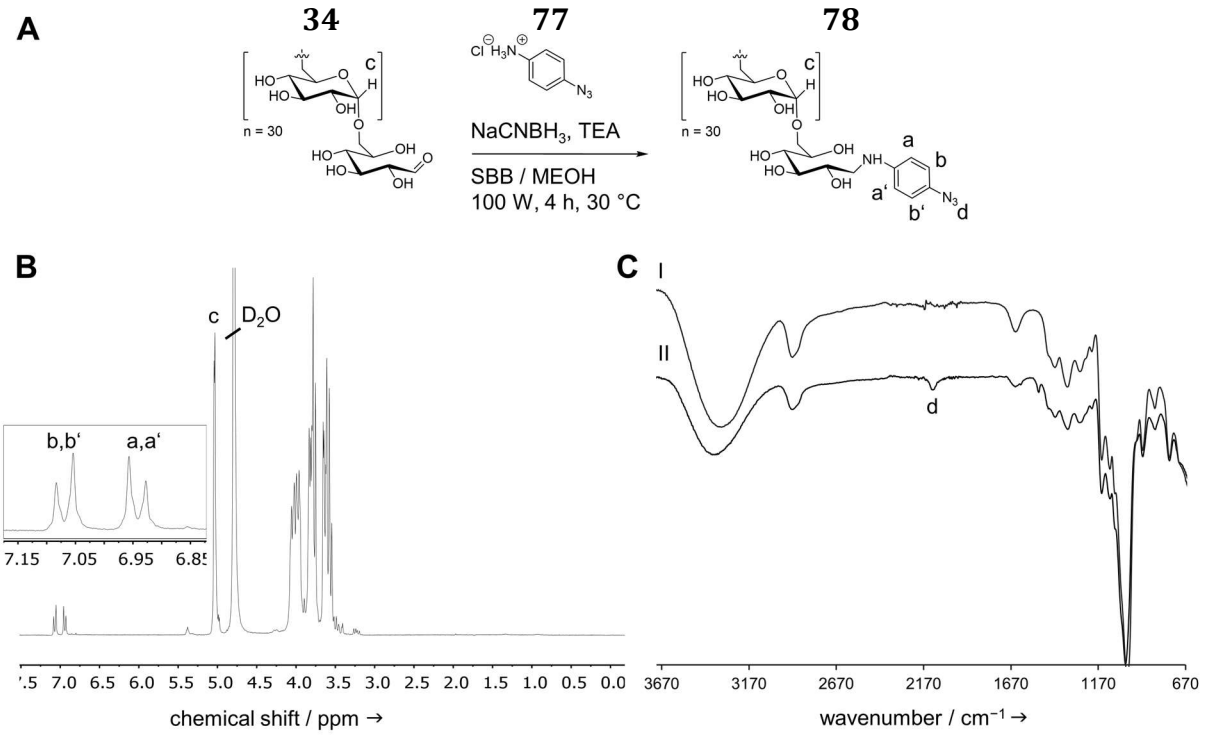

Figure 34. Microwave-assisted reductive amination of dextran **34** with *p*-azidoaniline hydrochloride **77** (**A**). ^1H NMR (D_2O, 300 MHz) of azide-modified dextran **78**, showing characteristic signals for the introduced aromatic protons (a,a' and b,b') and for the anomeric proton (c) (**B**). The FTIR spectrum of Dex-N_3 **78** (II) shows a characteristic absorption band at 2113 cm^{-1} for the azide group d. In the spectrum of unmodified dextran **34** (I), no absortion is visible in the same region (**C**).

Attempts to dissolve azidoaniline hydrochloride **77** without TEA led to a drastic decrease of the pH to 3. *Smith et al.* reported the reduction of phenylazide with $NaBH_4$ to the corresponding aniline as a quantitative reaction.[146] In order to exclude the possibility of a side reaction of azidoaniline **77** with the excess of $NaCNBH_3$, but also because of the qualitative analysis by FTIR, the azide functionality was probed in a model click reaction with *N*-propargylmaleimide **87**. The isolated product Dex-click-Mal **88** was analysed by ^1H NMR and FTIR and an end-group density of 93%mc was ascertained (**Figure 35**, **A–C**). The appearance of a singlett at 8.33 ppm (^1H NMR) belonging to the formed triazole was a strong indicator for a successful reaction. Furthermore, the FTIR signal for the azide group (2113 cm^{-1}) disappeared and a characteristic carbonyl stretch band at 1705 cm^{-1} was observed.

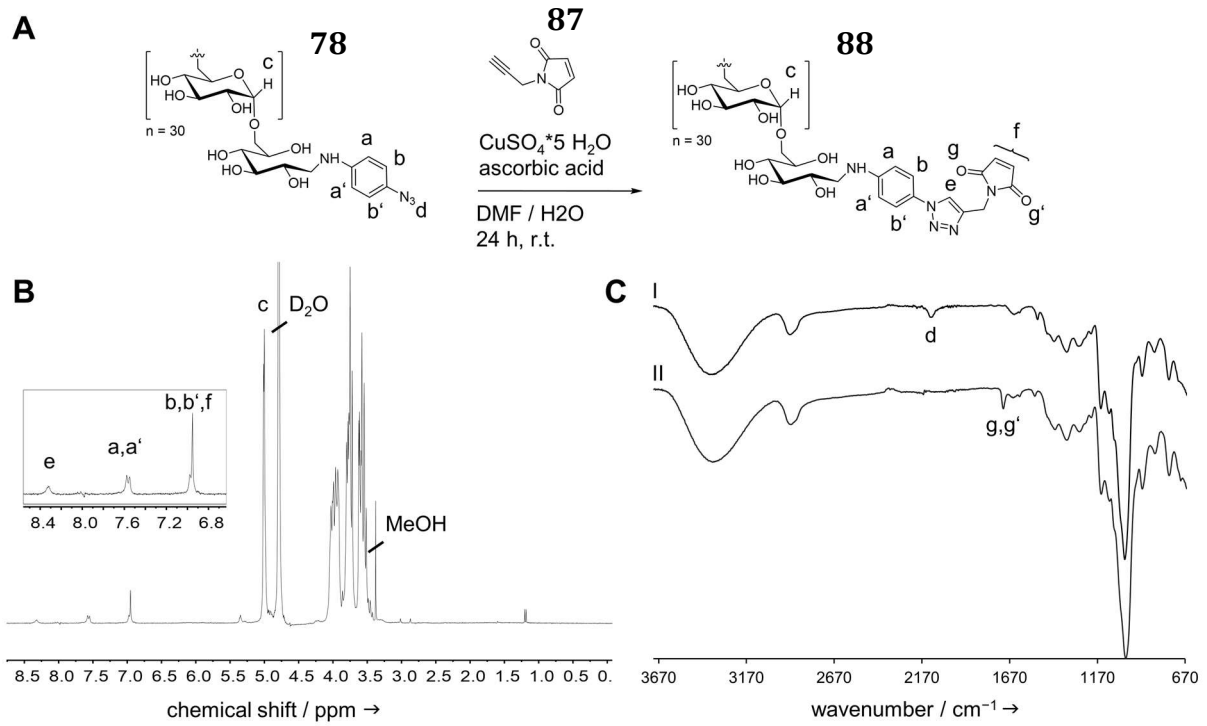

Figure 35. The free azide functionality on the reducing end was probed with the model compound *N*-propargyl maleimide **87** in a cu-catalyzed click reaction (**A**). Analysis of the ^1H NMR (D_2O, 300 MHz) of **88** shows the appearance of a proton signal (e, 8.33 ppm) of the newly formed triazole ring as well as a new signal for the maleimide group (f, 6.93 ppm) (**B**). Also the characteristic FTIR signal for the azide group (spectrum I, 2113 cm^{-1}) disappears after the click reaction, indicating a full consumption of the azide group. At 1705 cm^{-1} (spectrum II), the absorption peak for both carbonyl C=O stretches in the introduced maleimide groups appear (C).

Synthesis of alkyne-functionalized dextran

Dextran with an alkyne-functionality was prepared by reacting dextran **34** with *p*-ethynylaniline **79**. Compared to the synthesis of the azido derivative, the reaction temperature was raised to 50 °C, as suggested by *Moreau et al.*[68a] Additionally, the ratio of MeOH to $B(OH)_3$-buffer had to be changed to 1:1, due to the inferior solubility of *p*-ethynylaniline **79** in aqueous solution. The isolated Dex-alkyne **80** was analyzed by ^1H NMR as described for Dex-N_3 **78** and an end group density of 73%mc was determined (**Figure 36**, **B**). The lower degree of modification might be due to the weaker +M effect of the alkyne function. Sp-hybride orbitals of the alkyne carbon have only 50% p-orbital character and since only the p-orbitals can overlapp with the aromatic ring orbitals to donate electron density, they can compensate the electron withdrawing effect of the aromatic ring on the amine function to a lesser extend.[147] This is also the reason why **79** has a stronger acidic character than the other anilines (see **Table 4**, **p.50**).

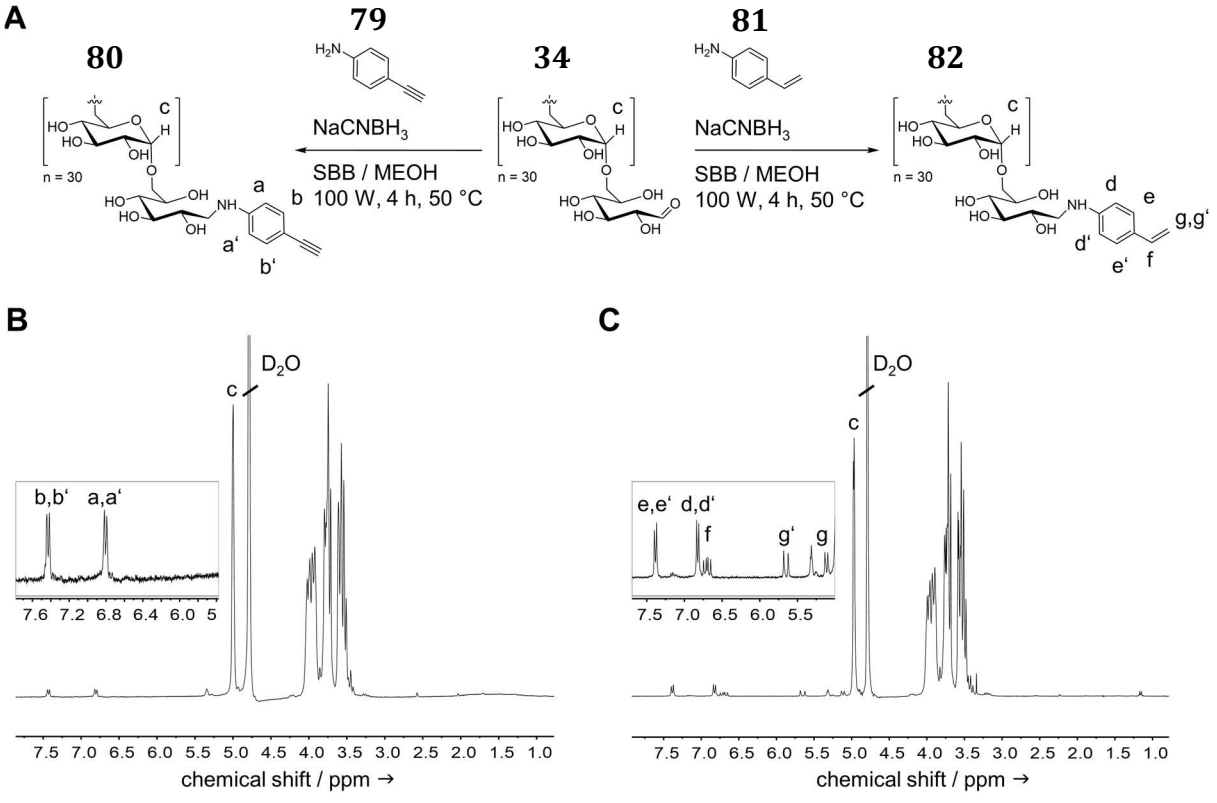

Figure 36. Functionalization of Dex **34** with *p*-ethynylaniline **79** or *p*-vinylaniline **81** (**A**). ^1H NMR (D_2O, 300 MHz) of modified dextran **80** (**B**) and modified dextran **82** (**C**).

Synthesis of vinyl-functionalized dextran

The vinyl end group functionalized dextran **82** was synthesized, using the established microwave-assisted method. The amount of dextran carrying a vinyl group could be

calculated by comparing the signal of the introduced benzene ring (e, e', d, d'; 7.40–7.37 ppm and 6.84–6.81 ppm) with the well visible protons of the vinyl group (f, g, g'; 6.75–6.65 ppm, 5.68–5.62 ppm and 5.14–5.10 ppm) and the anomeric proton (c, 4.98 ppm) (**Figure 36**, **C**). Although *p*-vinylaniline **81** was poorly soluble in the solvent mixture, the end group density was good with 83–92%mc. We assume that compared to *p*-ethynylaniline **79**, the sp^2 orbitals of the vinyl group have a stronger p-character and therefore overlap better with the aromatic ring orbitals. This might partially compensate the electron withdrawing effect of the aromatic ring on the amine group and is also visible in the p*K*a of the primary amine. The isolated Dex-vinyl **82** was fully water-soluble.

Synthesis of thiol-functionalized dextran

Even though the synthesis of thiol-terminated dextran was reported by other groups before, recently published methods turned out to be not compatible with our microwave assisted approach.[90, 148] Therefore, we introduced a *p*-substituted aniline due to its compatibility with our established microwave assisted synthesis, the easy quantification by ^1H NMR and the low pK_a of the aromatic thiol **83** (**Table 4**, **p.50**). We assumed that, compared to an aliphatic derivative, the aryl thiol would be present in a more reactive thiolate anion state at neutral pH.[142a, 142c] Succesfull synthesis of thiol-terminated Dex-SH **84** was achieved with *p*-aminothiophenol (4-ATP) and microwave-enhanced reductive amination. Under the applied reaction conditions, some of the 4-ATP **83** was oxidized to a bright yellow colored disulfide **89** to a certain extend, due to the alkaline pH and the microwave irradiation in the prescence of air (**Figure 37**, **A**). As shown in **Figure 37**, **B** and **C**, the UV absorption- and the ^1H NMR spectrum of Dex-SH changed after reduction with either tris(2-carboxyethyl)phosphine (TCEP) or DTT which indicates a change at the free thiol group and the aromatic ring. Upon reduction of the formed disulfide, the aromatic system becomes smaller and absorbs light mainly in the UV region at 280 nm. In the UV spectrum the broad absorption band between 305 nm and 405 nm is decreasing significantly in intensity, while increasing in intensity at 280 nm. This was also observed by a sharp change in color of the reaction solution from bright yellow to colorless. Hereby, the reduction of the thiol endgroup was easily monitored qualitatively. The ^1H NMR signal of the aromatic protons before the reduction shows a broad multiplett with overlapping signals from 7.61 ppm to 7.33 ppm, but changed into two sharp multipletts at 7.26–7.24 ppm and 6.80–6.77 ppm, after the reduction (**Figure 37**, **B**).

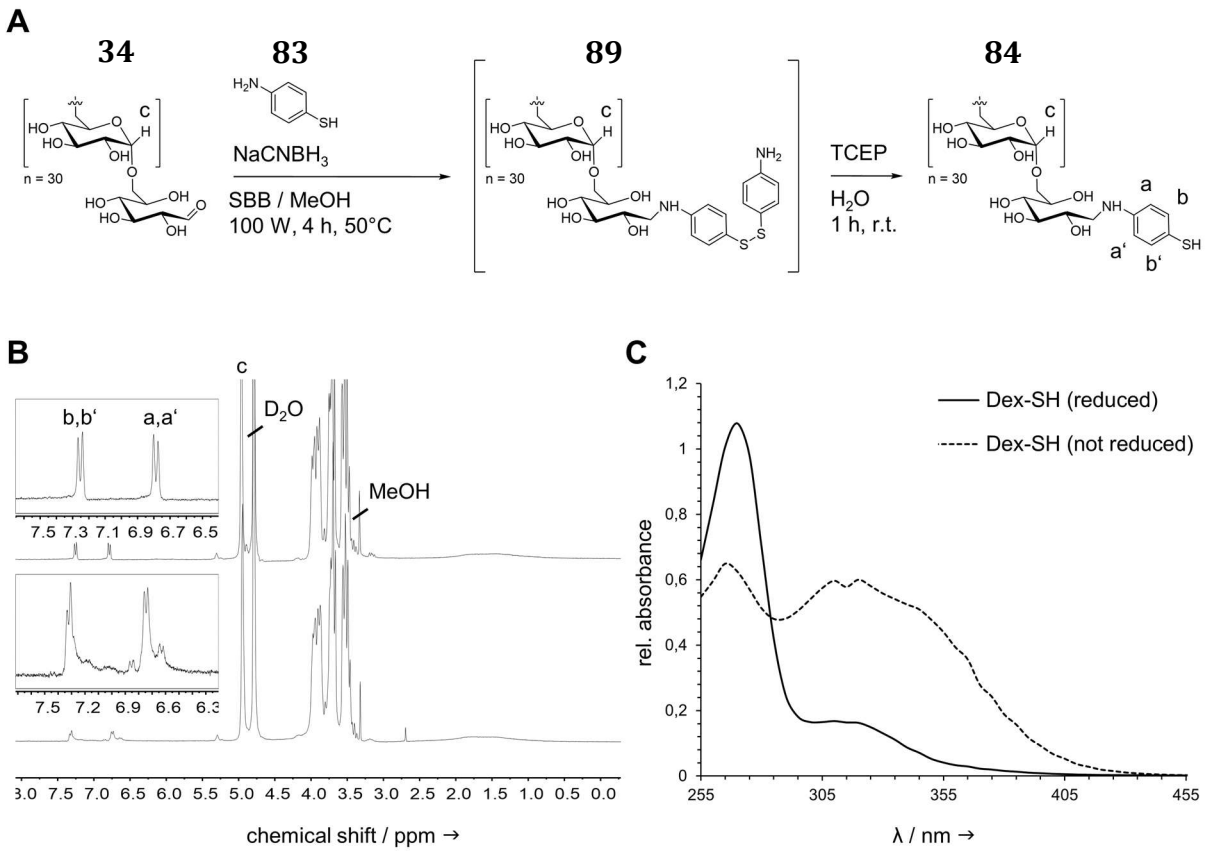

Figure 37. Reductive amination of dextran **34** with 4-ATP **83** results in a mixture of oxidized intermediate **89,** Dex-S-S-Dex disulfide and Dex-SH **84**. Subsequent reduction of the reducing end thiol gives Dex-SH **84** (**A**). ^{1}H NMR in D_2O (300 MHz) of isolated intermediate **89** prior to (lower spectrum) and after (upper spectrum) treatment with TCEP shows a distinct change in the proton signal from broad multiplett signal to two sharp multipletts (**B**). The reduction of the free thiol group was also monitored with UV spectra analysis prior to (dotted line) and after reduction (straight line). The change from a broad to a more sharp absorption signal indicates a change in the benzene substitution pattern (**C**).

The prescence of a free thiol group was also confirmed by *Raman* spectroscopy, where the S-H stretching mode was clearly observed at 2456 cm^{-1} (**Figure 49**, **C, p.76**). Reduction of Dex-SH **84** was attempted with $NaBH_4$, DTT, and TCEP. The reduction with $NaBH_4$ was not efficient due to either fast hydrolysis of the reducing agent at acidic pH or fast reoxidation of the thiol under alkaline conditions. Reduction with TCEP proved to be faster and gave a higher content of reactive thiol in the product (90–95%mc) compared to reduction with DTT (78–84%mc).[149] While the reaction mixture was fully decolorized after 1 min when TCEP was used, it took about 2 h when using DTT. Additionally, with the use of TCEP as reducing agent, the possibility of DTT competing with the S–H at the dextran end for the thiol activating agent can be circumvented.[149b] To avoid reoxidation of the introduced sulfhydryl group, the thiol-modified dextran **84** was isolated as quickly as possible by precipitation and freeze-drying. Work up by dialysis had to be carried out

either before the reduction step or after protecting the free thiol group with 2,2'-dipyridyl disulfide (DPDS) **95** or divinylsulfone (DVS) **98**.

Carboxy-functionalized dextran

As discussed in **chapter 1.3.2** (**p.38**), a carboxylic acid group can be introduced at the polysaccharide reducing end by selective oxidation of the aldehyde to an aldonic acid with I_2 and KOH. However, this reaction is time consuming (<24 h), affords additional work up with ion exchange resins[80a] and the introduced end group is difficult to quantify. In order to speed up modification times and simplify the reaction setup, *p*-amino benzoic acid (4-ABA) **85** was applied to introduce a carboxyl functionality on the reducing end of dextran **34** (**Figure 38**, **A**).

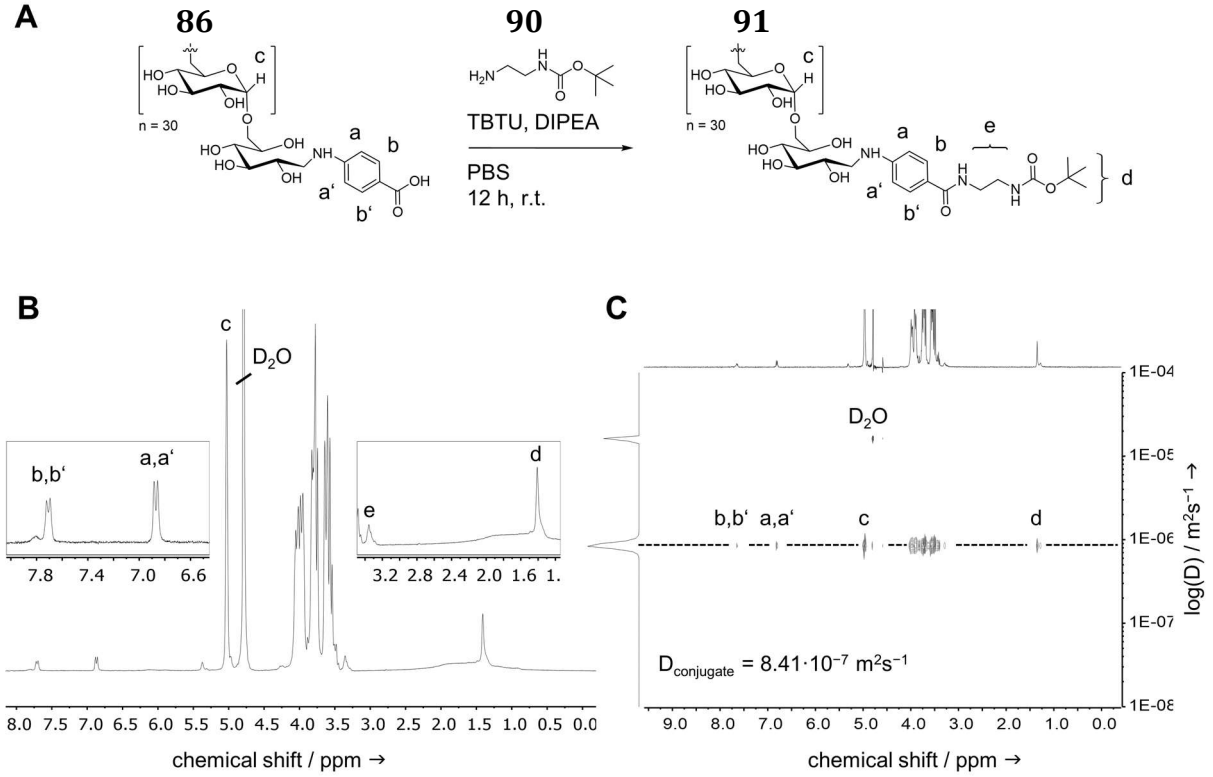

Figure 38. The end-group functionality of Dex-COOH **86**was probed by a model peptide coupling reaction with *N*-Boc-ethylenediamine **90** (**A**). The successful conjugation and therefore the availability of a free carboxyl group was observed by ^1H NMR in D_2O(300 MHz). This was observed by the appearance of the Boc proton signal (d, 1.39 ppm) and the ethylene proton signals (e, 3.33 ppm) next to the aromatic protons (a, a', 7.80–7.67 ppm and b, b', 6.86–6.84 ppm) (**B**). The dosy spectrum (D_2O, 400 MHz)of **91** shows all observed proton signals aligned at a single diffusion coefficient, which indicates that they are part of the same molecule (**C**).

This also adds the additional benefit of a UV active group to facilitate detection in gel permeation chromatography (GPC) analysis and purification, compared to the oxidation approach. The succesfull modification was monitored by ^1H NMR and gave end group

densities of 89%mc. Although this is lower than the end group density achieved with the selective oxidation method (up to 96%mc) the reductive amination process proceeds much faster (4 h). The availability for bioconjugation of the carboxyl group at the reducing end was probed with *N*-Boc-ethylenediamine **90.** Typically, in amide coupling reactions with *N,N,N′,N′*-Tetramethyl-*O*-(benzotriazol-1-yl)uronium tetrafluoroborate (TBTU) the carboxyl group is first deprotonated.[150] The selective amine-to-carboxyl ligation in the prescence of a large excess of free hydroxyl groups on the glucose backbone requires a fine tuning of the reaction pH to avoid esterification as side reaction. Therefore, the low p*K*a of the carboxyl group (**Table 4**, **p.50**), compared to an aliphatic derivative, is probably beneficial for this type of reaction. The modification of **86** was possible in good to moderate yields (78–85%mc).The ^{1}H NMR and DOSY (**Figure 38**, **B** and **C**) spectra of **91** show the appearance of a Boc signal at 1.39 ppm with the same diffusion coefficient as the aromatic protons at 6.86–6.84 ppm and the anomeric proton at 5.00 ppm. It can therefore be concluded that the reaction was succesfull and that Dex-COOH **86** can be used as building block for Cu-free bioconjugation.

In this first chapter a new method for the chain end functionalization and a quantification strategy was developed. Key steps of the synthesis include a versatile reductive amination by a modified microwave-assisted procedure, involving a co-solvent system, and the introduction of *p*-substituted aniline derivatives. Low molecular weight dextran **34** was selectively functionalized with an azide, alkyne, vinyl, thiol, and carboxyl group on the reducing end (73–95%mc). The varying degree of modification can be attributed to the different substituents at the benzene ring and the resulting solubility in the SBB/MeOH solvent system. Furthermore, the mesomeric effect of the aniline substituents has to be considered as it influences the nucleophilicity of the opposing amine. The modification with 4-ATP **83** gave the highest degree of modification (90–95%mc) while modification with *p*-ethynylaniline **79** was only possible with 73%mc. The modification with *p*-azidoaniline hydrochloride **77**, *p*-vinylaniline **81** and 4-ABA **85** was proceeding in good yields and gave similar end group densities (85–90%mc). In terms of functionality and use in bioconjugation, the Dex-SH building block **84** is preferred over the other conjugates due to its high degree of modification and its usefulness in a plethora of copper-free and site-selective bioconjugation reactions.[151] As a rule of thumb the following principles should be considered when using microwave-assisted reductive amination with dextran and aniline:

1) Conjugations work best with electron-donating groups in *p*-position (e.g. vinyl group) or if the aniline is good soluble under reaction conditions (e.g. thiolate or carboxylate groups).
2) The solvent system has to contain aqueous borate buffer (0.1M, pH 7–8). Possible cosolvents are MeOH and THF. DMF and DMSO are not suitable.
3) At least 10 equivalents amine have to be introduced in order to reach sufficiently extensive modification of the reducing end.
4) Before the backbone hydroxyl groups can be conjugated in a next reaction step, the borate buffer has to be removed by dialysis (at least 12 h) or short gel columns (e.g. sephadex G25).
5) In general, the size of the polysaccharide is not a critical parameter when performing reductive amination.[68a] However, the introduction of functional groups becomes very hard to identify already with 10 kDa Dextran. It is indeed possible to see aromatic protons of introduced anilines in the ^{1}H NMR spectrum, but the detection of a characteristic signal of an azide function or a thiol group in FTIR and *Raman* spectroscopy is not possible due to the high intensity of the many polysaccharide-related stretching modes.

3.2 CU-BASED SYNTHESIS OF MACROSURFACTANTS

The above introduced chain end functionalized polysaccharides can be versatile building blocks in the bottom-up synthesis of new responsive biopolymer nanomaterials. As a proof of concept, a full polysaccharide amphiphilic block copolymer was prepared from the building blocks Dex-N_3 **78** and Dex-alkyne **80**, using copper-mediated azide-alkyne click chemistry in a *grafting-to* approach. The combination of a hydrophilic dextran block with a hydrophobic acetalated dextran block results in an amphiphilic structure that turns water-soluble upon decreasing the pH. The material was characterized with ringtensiometry, GPC, DOSY-, ^{1}H NMR, and FTIR. The self-assembly properties were examined and characterized with DLS and TEM. Furthermore, the loading capacity and release properties as well as the cellular uptake characteristics were probed with the hydrophobic pharmaceutically active drug curcumin. The results presented in this chapter were published in *Biomacromolecules* (*Breitenbach et al.*[152]) and are discussed here in detail.

3.2.1 SYNTHESIS OF ACDEX-ALKYNE

With the newly established microwave-assisted method, azide-, and alkyne-modified dextrans were synthesized as hydrophilic building blocks for the preparation of an amphiphilic macrosurfactant. Consequently, the hydrophilic alkyne-modified dextran **80** was transformed into a hydrophobic building block. Following a procedure of *Fréchet* and coworkers, the hydroxyl groups on the polysaccharide backbone of Dex-alkyne **80** were protected with acid-degradable acetals (**Figure 39**, **A**).[22-23, 153] It was mandatory for the successful reaction to fully remove all residual buffer salts from the previous reductive amination reaction (**Figure 36**, **A** and **B**, **p.54**). Acetalization was achieved by adding 2-methoxypropene **56** and catalytic amounts of PPTS to a stirred solution of **80** in DMSO. The protection of the free hydroxyl groups in the polysaccharide backbone introduced an adjustable solubility switch, enabling an acid-triggered change from a hydrophobic to a hydrophilic polymer. Depending on the reaction time, the amount of cyclic (e) vs. acyclic acetals (f) can be controlled. Less stable acyclic acetals (f) are formed more quickly but rearrange over time into more stable cyclic acetals (e). Hereby degradation kinetics can be finely tuned, as acyclic acetals would degrade faster, whereas cyclic acetals hydrolyse slower. The extent of protection and ratio of cyclic to acyclic acetals could be determined by ^1H NMR in D_2O/DCl. At the time of acidic hydrolysis, acyclic acetals decompose into

acetone and methanol, while cyclic acetals give only acetone (**Figure 39**, **B**). The reaction was also monitored by FTIR (**Figure 39**, **C**). Protection of the free hydroxyl groups was observed by the disappearance of the O–H stretching signal at 3583–3086 cm^{-1}.

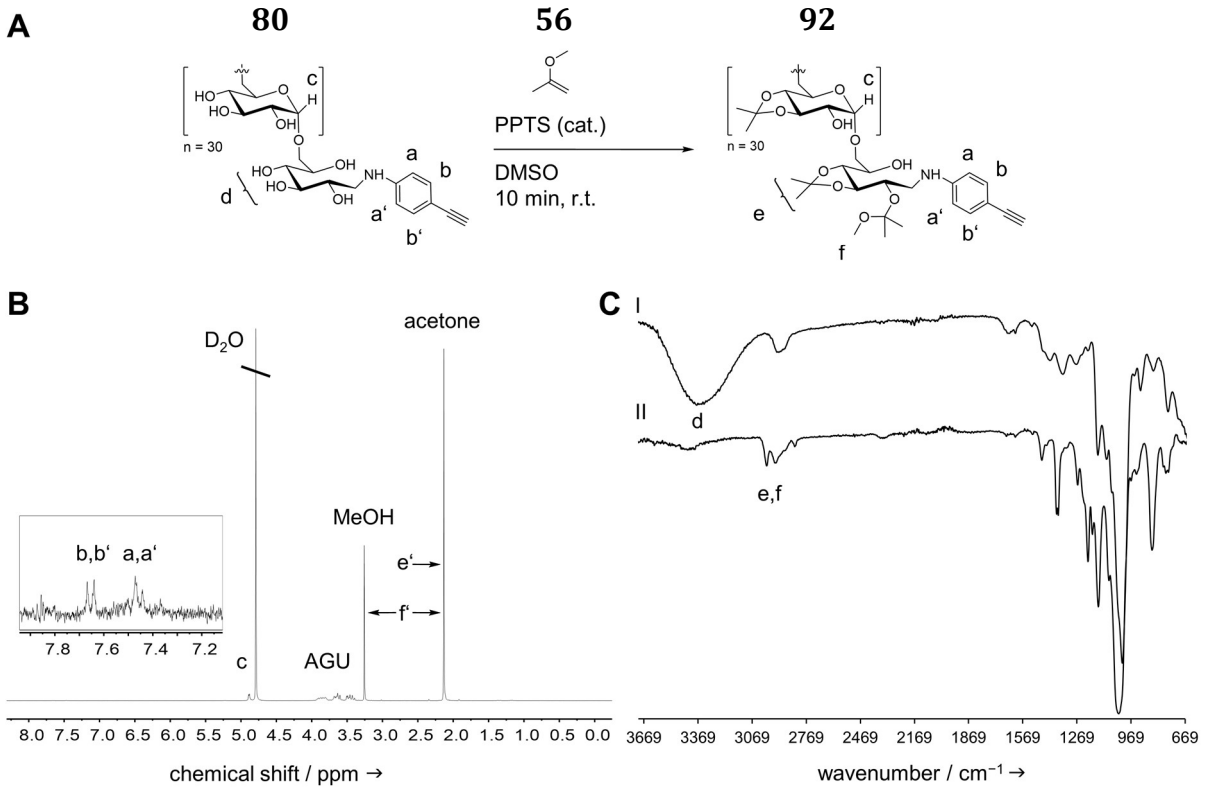

Figure 39. Acetalization of Dex-alkyne **80** turns the hydrophilic building block into a hydrophobic and acid responsive building block (**A**). ^1H NMR of AcDex-alkyne **92** in D_2O/DCl (300 MHz) shows the degradation of acyclic acetals (f) into methanol and acetone (f') whereas cyclic acetals (e) decompose to give only acetone (e') (**B**). The FTIR of acetalated dex-alkyne **92** (II) shows no O–H stretching signal (d), whereas C–H stretch signals (e) and (f) from the introduced acetals appear, confirming the consumption of free hydroxyl groups (**C**).

After a reaction time of 10 minutes, a hydrophobic material was obtained , which was soluble in organic solvents like MeOH or DCM with a total acetal coverage of 66.1%, whereof 42.6% were acyclic and 23.5% were cyclic acetals. From the ratio of cyclic and acyclic acetals, the average molecular weight of AcDex-alkyne **92** could be calculated with **eq. 9** and **eq. 10** (**chapter 5.2**, **p.142**). Considering the total amount of 30 repeating units within a 5 kDa dextran chain, the molecular weight of AcDex-alkyne **92** was determined with 6069.39 g mol^{-1}. In conclusion, a total of 70.4% of hydrophobic material could be recovered. The M_w (weight average molecular weight), was 5164.06 g mol^{-1} (determined by GPC). However, GPC measurements in DMF were calibrated with PEG standards and

therefore allow no direct conclusion from molecular weight to the retention time of the polymer.

3.2.2 SYNTHESIS OF DEX-CLICK-ACDEX BY CUAAC

The hydrophobic AcDex-alkyne **92** and the hydrophilic Dex-N_3 **78** were conjugated by the copper(I) mediated azide-alkyne cycloaddition (CuAAC). The cu-catalyzed click reaction of an azide- and an alkyne-functionalized macromonomer is a popular ligation strategy in bioconjugation and polymer chemistry due to its high chemoselectivity and compatibility with other functional groups.[154] Therefore it is also a commonly applied synthetic method for polysaccharide-to-polymer ligation.[69, 99-100] First attempts to run the click reaction in DMF/H_2O mixtures and a Cu(II)SO_4/ascorbic acid system, as applied for Dex-click-Mal **88**, did not lead to any conversion. Thus, we decided to use a combination of copper bromide (CuBr) and PMDTA in DMSO. Despite the different solubility of both blocks in aqueous- and organic solvents, all reactants were soluble in DMSO. The amine PMDTA **93** serves both as a reaction promoting base and as a chelator additive for the reactive Cu(I) species. By deprotonation of the alkyne residue, it provides acetylide anions for the formation of a reactive Cu-acetylide complex.[155] Furthermore, it also chelates the Cu(I) species and protects the catalyst from oxidation in the prescence of residual oxygen, thus providing a steady and high concentration of reactive Cu(I) throughout the reaction. Copper halydes are known to form stable clusters in solution and require the prescence of an amine base or elevated temperatures to return to a non-clustered reactive state.[156] To ensure a quantitative conversion, the reaction was performed with 2 equivalents PMDTA **93** at 50 °C over 3 days, as described by *Schatz et al*.[25] When increasing the temperature, the triazole proton signal intensity in the ^1H NMR of **94** at 8.55 ppm (**Figure 40** and **Figure 41**, (d)) became weaker, indicating side reactions. In early experiments at higher temperatures (>60°C) the formation of a product with amphiphilic properties but no formation of a triazole ring (or in such small quantities that it was not detectable by ^1H NMR) was observed. As described in **chapter 3.1.2** (**p.52**), arylazides are sensitive to heat or photolysis. At higher temperatures over long time periods (72 h), the aryl azide possibly decomposes in small quantities, followed by a rearrangement. This reactive intermediate could then react with the dextran- or acetalated dextran block in an uncontrolled way, leading to different non-characterized side-products.[157] However, these products did not self-assemble into micellar nanoparticles. By keeping our

temperature relatively low (40–50°C), the above-mentioned side reactions could be minimized and the desired copolymer **94** was obtained in good to excellent yields. *Koberstein* and coworkers recently published a sceptical article on the yields obtainable in click ligation of polystyrene polymers. Despite the excellent performance of the CuAAc reaction, polymer ligation did not yield 100% conversion and necessitated extensive work-up and thorough analysis of the product .[158] To facilitate the work-up and ensure a full conversion of the higher modified Dex-N_3 block **78**, a small excess of 1.5 equivalents AcDex-alkyne block **92** was applied. The unreacted hydrophobic polymer was removed by precipitation in H_2O-dd (pH 8 with TEA). Excess copper and unmodified dextran **34** were removed by extensive dialysis against H_2O-dd (pH 8 with TEA) over 3 days.

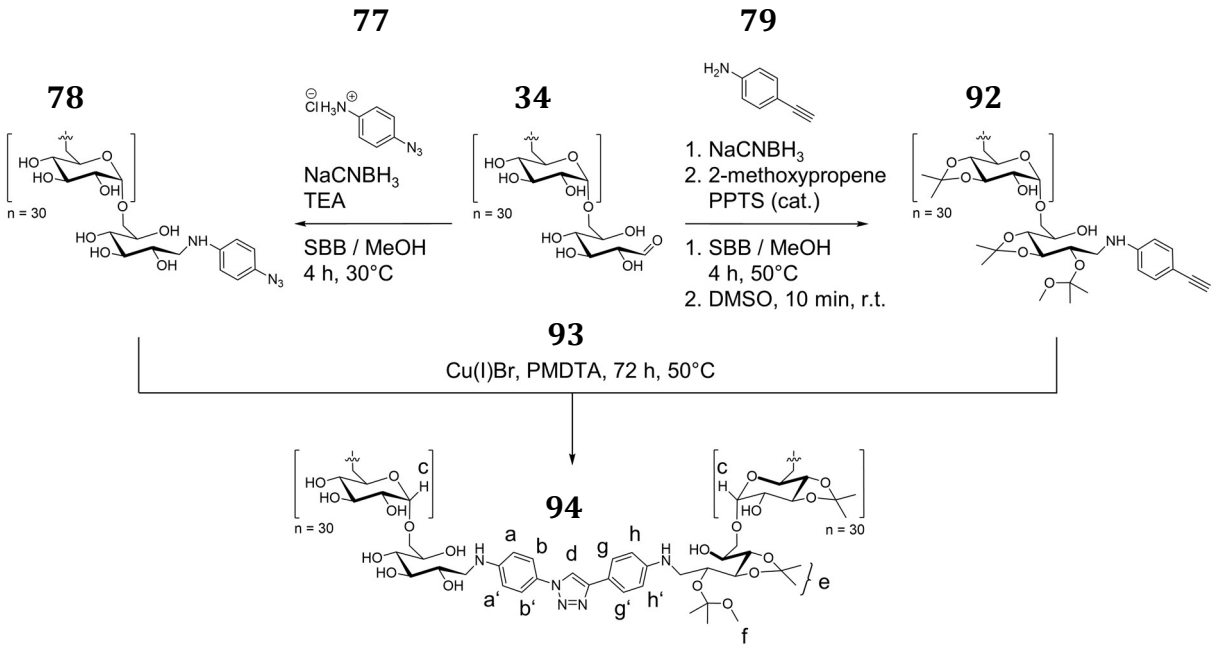

Figure 40. Synthetic route towards the amphiphilic Dex-b-AcDex block copolymer **94** by Cu(I)-mediated click reaction of a hydrophilic Dex-N_3 block **78** with a hydrophobic AcDex-alkyne block **92**. Adapted from ref.[152]. Copyright (2017) American Chemical Society.

The successful synthesis and purification of block copolymer **94** was confirmed by ^1H NMR, diffusion ordered spectroscopy (DOSY), FTIR and size exclusion chromatography (SEC). The disappearance of the azide stretching mode at 2112 cm^{-1} in the FTIR spectrum (**Figure 83**, supplemental) qualitatively indicates a complete consumption of azide-modified dextran **75**. Furthermore, the ^1H NMR spectra of Dex-click-AcDex **94** in D_2O (**Figure 41**, **B**) shows the acetals of the hydrophobic block at 1.50 ppm (e) and 3.20 ppm (f), in comparison to the spectra after treatment with D_2O/DCl (**Figure 41**, **A**). The proton signals of both aniline derivatives are visible at 7.00 ppm,

7.65 ppm and 7.75 ppm (a, a', b, b', g, g', h, h'). Another prove for the the successful click reaction was the formation of a triazole ring, characterized by the appearance of a single signal at 8.55 ppm (d).

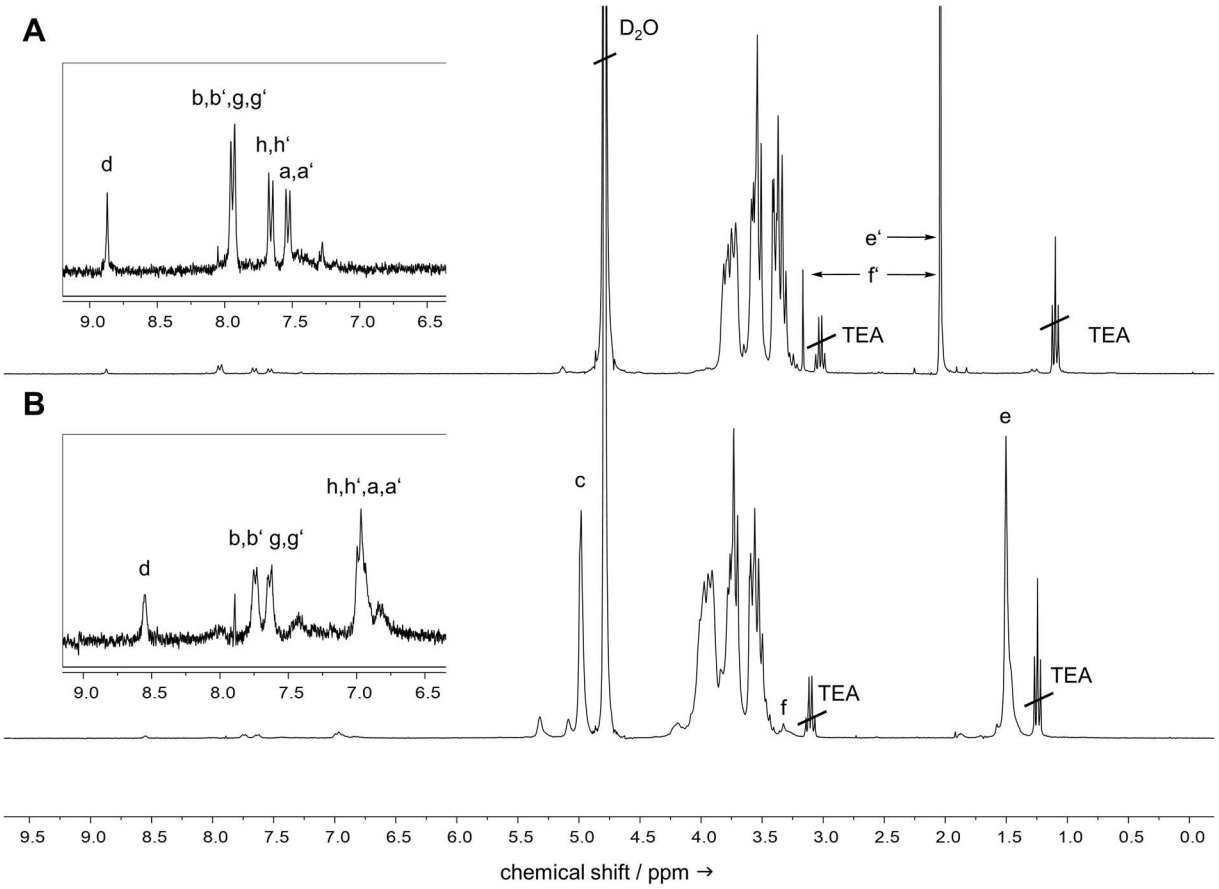

Figure 41. ^{1}H-NMR (300 MHz) spectra of Dex-click-AcDex block copolymer **94** in D_2O+DCl (**A**) and D_2O (**B**). Spectrum **B** shows the characteristic signal of the acetal protons (e, f), both benzene ring protons a–h' and the formed triazole proton d. Adding a few drops of DCl cleaves the acetals and forms methanol and acetone (e' and f' in spectrum **A**). Adapted from ref.[152] Copyright (2017) American Chemical Society.

An increase in molecular weight was observed with SEC and DOSY. The SEC column retention times were 8.69 min for the copolymer **94** and 8.86 min for the hydrophilic Dex-N_3 block **78** (**Figure 42**, **A**). As expected, the larger block copolymer passed the column faster than the smaller monomer, but the block copolymer eluted at later retention times than a 10 kDa dextran standard. *Zhang* and *Marchant* suggested, that the retardation in retention times of polymer-polysaccharide amphiphiles can be induced by interaction of the hydrophobic segment and the column matrix and is not necessarily linked to the molecular weight.[80a] The diffusion coefficient of Dex-click-AcDex **94** ($7.7 \cdot 10^{-7}$ m^2 s^{-1}) measured with DOSY was lower than the diffusion coefficient obtained for Dex-N_3 **78** ($9.1 \cdot 10^{-7}$ m^2 s^{-1}). Typically, larger molcules diffuse slower than small molecule species

and therefore have a lower diffusion coefficient and *vice versa*. As comparison, *Viel et al.* reported diffusion coefficients of $11.6 \cdot 10^{-11}$ m^2 s^{-1} for 5.8 kDa pullulan and $8.0 \cdot 10^{-11}$ m^2 s^{-1} for a 12 kDa pullulan.[159] The data obtained by SEC and DOSY strongly supports the fact that a product with higher molecular weight than the starting material was obtained. The hydrophobic block **91** does not dissolve in aqueous solution and cannot be compared under the same SEC and DOSY conditions.

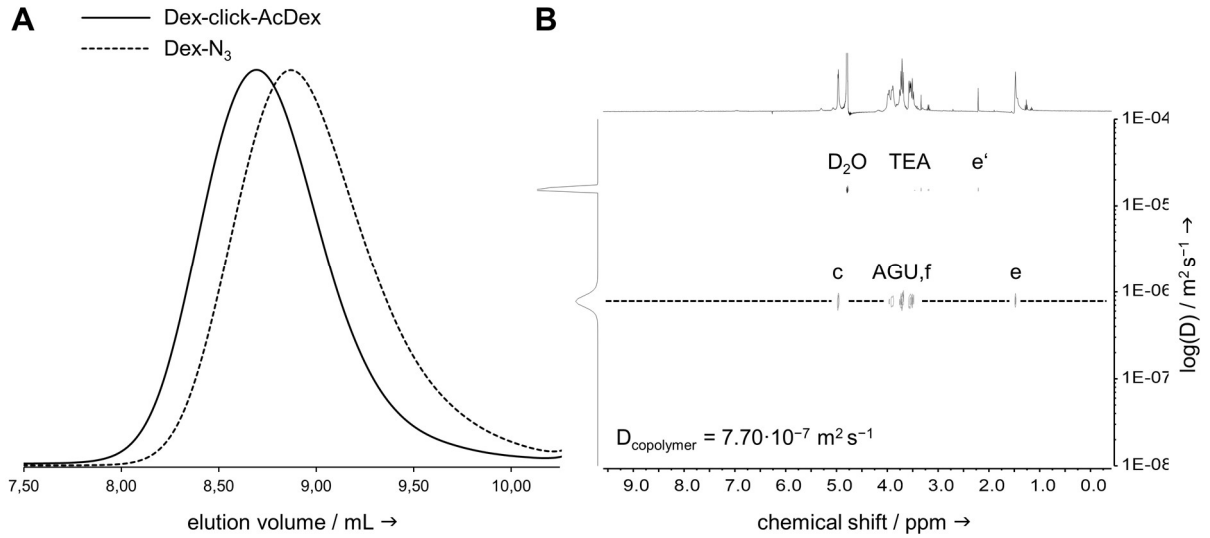

Figure 42. The SEC elugram of Dex-click-AcDex **94** (straight line) and Dex-N_3 **78** (dotted line) in H_2O (0.1 M $NaNO_3$, 1 mL min^{-1}) shows shorter retention times for the block copolymer, which is consistent with an increase in molecular weigh (**A)** Adapted from ref.[152] DOSY spectrum (D_2O, 400 MHz) of the block copolymer (**B**). The signals for the acetal protons (e, f) align at the same diffusion coefficient as the signals for the anomeric, and the AGU ring protons. The block copolymer has a smaller diffusion coefficient than single block Dex-N_3 ($9.08 \cdot 10^{-7}$ m^2 s^{-1}) as expected for a larger molecule.

Table 5. Acetal coverage of hydrophobic starting material and isolated block copolymer as determined by ^{1}H NMR (D2O/DCl, 300 MHz). The theoretical Mw was calculated from 1H NMR and with gel permeation chromatography (GPC). The block copolymer was analyzed by aqueous GPC (dextran standard), the starting material by DMF GPC (PEO standard).

polymer	total (%)	cyclic (%)	acyclic (%)	$M_{w,NMR}$ (g mol^{-1})	$M_{w,GPC}$ (g mol^{-1})
AcDex-alkyne	66.1	23.5	42.6	6069.39	5164.06
Dex-click-AcDex	22	12.5	9.5	11069.39	6908.48

The resulting amphiphilic character of copolymer **94** was also confirmed by the self-assembly and formation of micellar particles during the aqueous work-up after the click reaction (observed with DLS and TEM) (**Figure 90**, supplemental). The isolated polymer contained 22% acetals, whereas 9.5% had acyclic- and 12.5% had cyclic character (**Table 5**). Although the starting material AcDex-alkyne **91** had an acetal coverage of 66%, the

resulting block copolymer **94** contains 11% less protected hydroxyl groups than expected for a 1:1 coupling. The fact that all stable cyclic acetals were present in the product after work up, but the acyclic acetals were hydrolysed underlines the assumption that the loss in acetal structures might be attributed to the long dialysis time and the hydrolysis of acetals even under neutral conditions.

3.2.3 SELF-ASSEMBLING OF DEX-CLICK-ACDEX BLOCK COPOLYMER

Micellar nanoparticles were assembled from lyophilized material **94** by a solvent exchange method. Spherical particles formed upon slowly removing DMSO (the solvent which both blocks are soluble in), increasing the water content and therefore the overall polarity of the solvent. This process is driven by the strive of the hydrophobic block to minimize the contact area of the hydrophobic region with the surrounding aqueous media. The micelle formation was observed with dynamic light scattering (DLS) and transmission electron microscopy (TEM). The obtained nanoparticles had a narrow size distribution, represented by a PdI of 0.107 and a neutral zeta potential (**Table 6**, **Figure 43**). A fully stretched glucose molecule was reported to have an average chain length of approx. 0.45 nm.[114b, 114c] When calculating with 30 repeating units in a 10 kDa dextran, this would add up to a length of 27 nm. DLS measurements of the micellar particles show a D_H of 68 nm, suggesting that under the applied conditions the copolymer forms spherical nanoparticulate assemblies rather than classical micelles. By using TEM, the morphology of the nanoparticles can be described more precisely as closed, filled spherical assemblies with an average size below 100 nm (**Figure 43**). With this information in hand, the aggregation number (amount of polymer chains forming a nanoparticulate structure) can be estimated to be approx. 51027 chains per micelle (**eq. 12** and **eq. 13, Table 6**).

Table 6. Results for the particle characterization of self-assembled Dex-click-AcDex micelles. Samples were measured with empty particles or cargo-encapsulated (cur-loaded) particles. Z-Average (Z-Ave) describes the average size of all particles in the sample; intensity describes the particle size distribution within the sample, depending on their scattering intensities; number represents the size of the particles forming the largest population in the sample (adapted from [152]). The aggregation number (N_{Ag}) describes the amount of polymer chains in one micelle. Particles were empy (−) or curcumin-loaded (+). The ζ-potential describes the overall charge on the particle surface. Polydispersity Index (PdI) is a dimensionless parameter to describe the particle size distribution.

particles	PdI	Z-Ave (d.nm)	intensity (d.nm)	number (d.nm)	ζ-potential (mV)	N_{Ag}
–	0.107	103.3±0.4	112.3 ± 1.7	66.88 ± 2.5	2.83 ± 5.22	$5.10 \cdot 10^4$
+	0.098	98.9±0.7	109.8 ± 1.8	68.71 ± 0.8	–6.11 ± 6.31	-

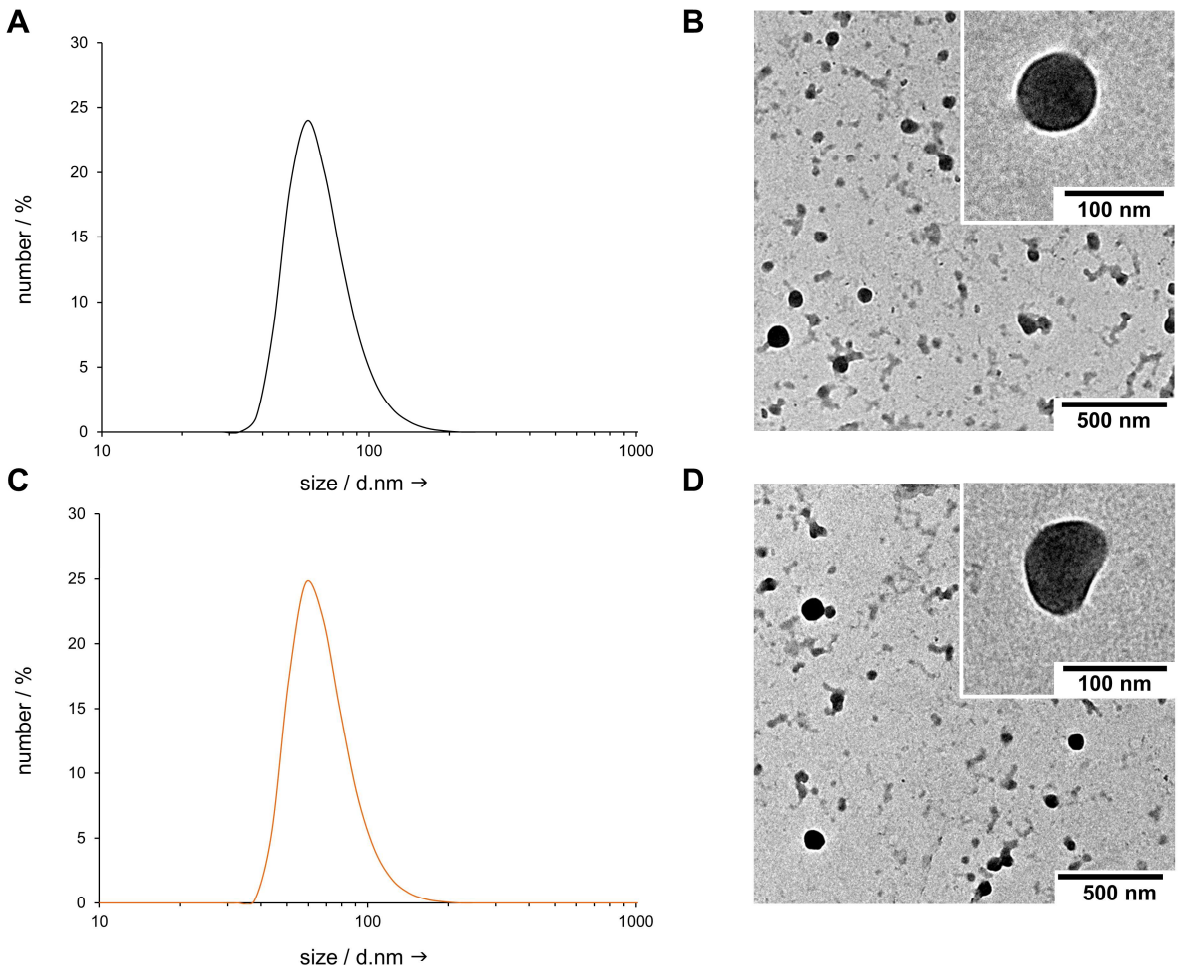

Figure 43. DLS measurement (**A**) and TEM analysis (**B**) for size determination of empty micellar nanoparticles. Curcumin-loaded micelles were also observed in DLS (**C**) and TEM (**D**). The self-assembled structures of loaded (**B**) and empty (**A**) particles show no significant differences in size. Both samples have a narrow size distribution and a hydrodynamic diameter (D_H) of approx. 100 nm (where 69 d.nm represents the largest particle population by number). As TEM analysis proceeds under harsh conditions, particles can possibly disassemble or be destroyed. This might lead to the light gray artifacts in the background. Adapted from ref.[152] Copyright (2017) American Chemical Society.

It is hypothesized that the amphiphiles assemble into knot-like structures where the hydrophobic blocks entangle with several amphiphilic polymers to form a tightly packed core with a surrounding hydrated dextran corona. Similar micellar nanoparticle assemblies have been described in the literature previously.[160] Self-assembly is a thermodynamically driven process. The ability of amphiphiles to self-assemble into micellar nanostructures is mostly depending on the ratio of hydrophobic to hydrophilic content within the polymer and the rate of transition from favored to unfavored solvent.[128c] The critical micelle concentration (CMC) can be a very helpful indicator for the particle stability. A lower CMC value often correlates with a higher thermodynamic stability of the particle system (considering only simple, non-sterically hindered AB block copolymer amphiphiles). This is especially important in drug delivery applications. Upon

injection in the blood stream, micelles have to withstand high dilution and therefore should favorably have a CMC as low as possible. The CMC of Dex-click-AcDex **94** was determined to be sufficiently low, with a concentration of 12 mg L^{-1} (**Figure 98**, supplemental). *Zhang et al.* reported a AcDex-b-PEG block copolymer for drug delivery with CMCs of approx. 82 mg L^{-1} and 7.2 mg L^{-1}, depending on the ratio of PEG to hydrophobic AcDex.[99] Dextran as the hydrophilic block was reported in Dex-b-PCL conjugates with CMCs ranging from 6.8 to 50.4 mg L^{-1}. With an increasing PCL block length, the CMC decreases.[89-90] An amphiphile built solely from maltoheptaose and acylated maltoheptaose was reported by *Modolon et al.* with a CMC of 100 mg l^{-1}.[104a] In contrast to these and other reported polysaccharide-containing amphiphilic AB block copolymers, the Dex-click-AcDex amphiphile has a CMC in the lower range and thus particles show a comparably high stability.

3.2.4 MICELLE DEGRADATION UNDER ACIDIC CONDITIONS.

A site-specific payload release is desirable for non-systemic drug delivery applications. In particular, small changes in the pH of the surrounding tissue can be exploited for a triggered particle degradation and thus controlled drug release. Environments of slightly lower pH values (5–6) are for instance endosomal/lysosomal compartments within cells, but also tumor tissue or sites of inflammation decrease their pH due to changes in their metabolism.[161] To observe the acid-triggered decomposition of our micellar system, Dex-b-AcDex particles were incubated in either H_2O-dd with neutral pH (**Figure 44**, **B** vials A) or sodium acetate buffer at pH 5.5 (**Figure 44**, vials B). Samples analyzed by DLS at time point t=0 h showed a maximum particle population between 70–80 d.nm. During the first 2 h, the micellar nanoparticles begin to lose their organized structure. This is caused by the pH-induced cleavage of acetals and the associated loss of amphiphilic nature of the material. To visualize this process, both samples were placed in vials and illuminated with a green laser. The weakened intensity of back-scattered green laser light from the particle solution in vial B over time (**Figure 44**, **B**) can be matched to the decrease in particle size distribution by DLS towards 50–60 nm (**A**). After 4 h, the particles further degraded to sizes of 30–40 nm. At this point, the intensity of the green laser beam in vial B has significantly decreased, due to the limited amount of remaining particles that can scatter the laser light. After 24 h, the laser beam is not visible anymore in vial B supporting the results of the DLS measurement where only random aggregates smaller than 5 nm were

found. This confirms that the micellar structures respond to a decrease in the pH by disassembling. The acid-labile nature of the nanoparticle material **94** results in a change of solubility towards water-soluble material over time under mild acidic conditions. In comparison, particles incubated at pH 7 (vial A) can still be visualized by scattered laser light.

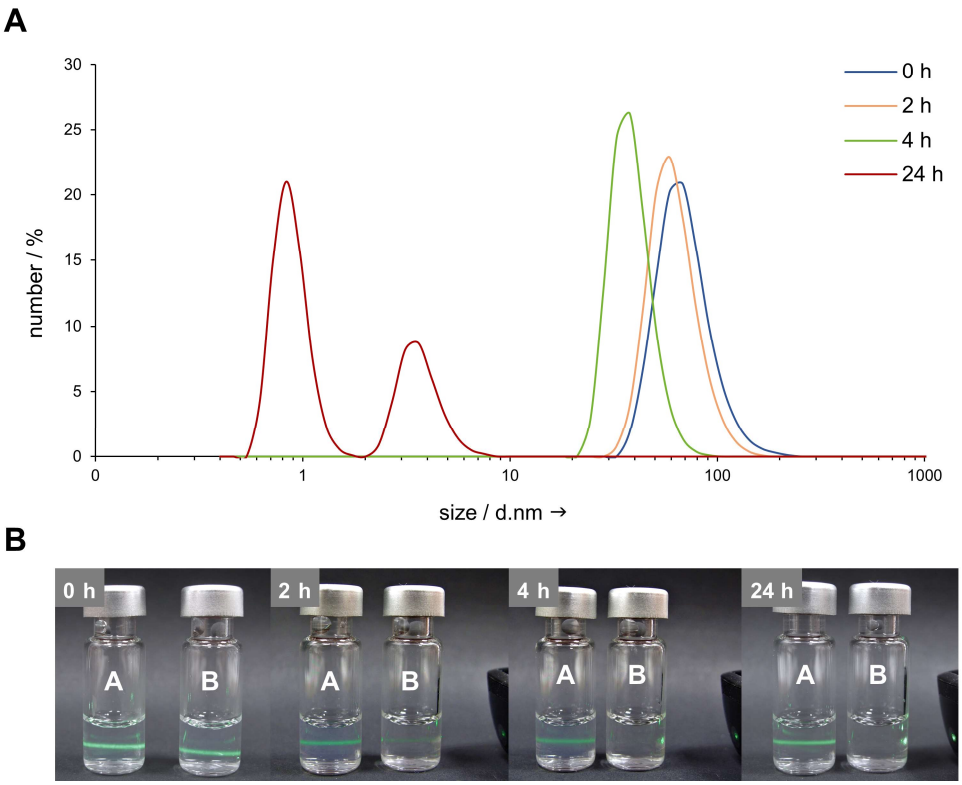

Figure 44. The degradation of Dex-click-AcDex micelles incubated under acidic conditions (NaAc-buffer, pH 5.5, 24 h) was followed by DLS (**A**) and laser beam scattering (**B**). During the first 2 h, particles at pH 5 start to disassemble (vial B), leading to smaller populations and limited backscatter compared to particles incubated at neutral pH (vial A). After 24 h, particles incubated at pH 5 are completely degradet. Reprinted with permission from ref.[152] Copyright (2017) American Chemical Society.

3.2.5 CURCUMIN LOADING, STABILITY AND RELEASE

The amphiphilic block copolymer **94** can function as a tool to drastically increase the bioavailability of hydrophobic drugs by encapsulation in micellar particles and stabilization in aqueous solution. As a proof of concept, the hydrophobic model compound curcumin **99** (**Figure 77**, **A**) was loaded into the self-assembled micellar nanoparticles. Curcumin is a light sensitive, bright-yellow colored diarylheptanoid and the main constituent of the turmeric plant (*curcuma longa*, part of the ginger family). The hydrophobic compound is heavily discussed as possible natural product drug and was recently shown to be pharmaceutically active in cancer treatment and for the treatment of cystic fibrosis.[162] In order to achieve a sufficient bioavailability and stabilization in

polar environment, the poorly water soluble compound **99** has to be encapsulated in nanoparticle carriers.[163] Therefore, curcumin was incubated with block copolymer **94** in DMSO overnight. The bright yellow solution was precipitated in H_2O-dd, all water-insoluble precipitates were removed by centrifugation. The clear yellow solution was dialyzed over 2 d to ensure a full removal of DMSO. During the solvent replacement, stable micelles formed and the concentration of the curcumin-loaded micelle solution was determined to be 1.42 mg mL^{-1}. Particles with encapsulated drug were characterized with TEM and DLS (**Figure 43**, **Table 6**). *Stenzel* and coworkers recently reported a shrinking in particle size with increased cargo loading[164], however no significant change in size compared to empty particles was observed. Curcumin was encapsulated in the micellar nanoparticles with a loading ratio of 0.93 mol per mol carrier material (corresponding to an EE of 23% and a LC of 3%; **eq. 12** and **eq. 13**). By using the same dialysis technique, it was also attempted to dissolve pure curcumin in water (**Figure 45**, vial B) as a comparison to solutions of curcumin stabilized by the amphiphile (vial A). The suspension of pure curcumin in water contains large visible aggregates directly after preparation as a direct result of the poor solubility in aqueous media. After 24 h, almost all curcumin precipitated and formed a thin yellow film at the bottom of vial B. The supernatant became colorless. In comparison, no precipitate formed in the polymer-stabilized solution (vial A). Even after 4 months of storing in the fridge, no precipitate was observed, confirming the long-term stability of the nano-formulation (**Figure 45**).

The release kinetics of the hydrophobic model compound curcumin **99** were observed in a dialysis experiment. First, curcumin-loaded nanoparticles were prepared and characterized, then dialyzed against either sodium acetate buffer at pH 5.5 or H_2O-dd at pH 7. At pH 5, curcumin **99** was released fast initially upon hydrolysis of the acetals in the hydrophobic block. Between 8–24 h, the release flattened off over time (**Figure 46**) as residual curcumin **99** was slowly washed out of the few remaining and mostly degraded micelles. After 24 h, approx. 95% of the hydrophobic drug was released from the particles. Particles incubated at pH 7 also showed a release of curcumin **99** over time, but at a slower and more stready rate, when compared to particles incubated under acidic conditions. After 2 h 20.5%, about half as much cargo is released from the micelles compared to when incubated at lower pH. After 4 h 27% of the cargo is released and ca. 40% after 8 h. After 24 h at neutral pH, the particles released ca. 70% of their cargo. We are not sure whether the release is due to slow degradation of the particles under neutral

conditions or if the hydrophobic membrane of the dialysis bag offers a more hydrophobic environment for the curcumin to adhere to. Since no precipitation of free curcumin **99** was observed, even after 4 month storage in glas vials in the fridge, it seems more likely that the interaction of curcumin **99** with the hydrophobic surface of the dialysis bag was favored over the hydrophobic micellar core.

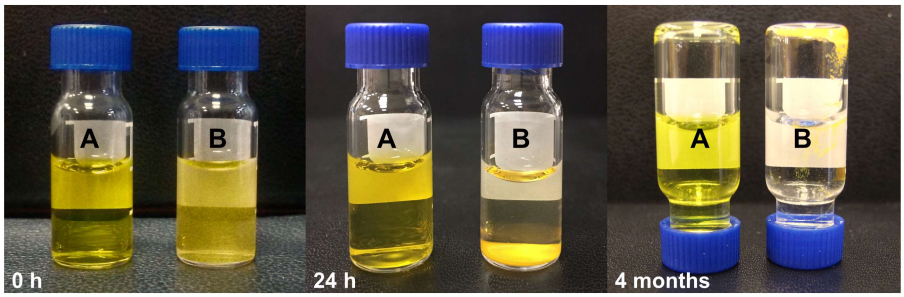

Figure 45. Aqueous solution of curcumin **99** stabilized with Dex-click-AcDex **94** (vial A) and without copolymer addition (vial B). The micellar solutions (vial A) are stable for prolonged times (up to 4 months) compared to pure curcumin **99** in water (vial B). Without additive large aggregates and precipitates form over time. Reprinted from ref. [152] (Copyright 2017) American Chemical Society.

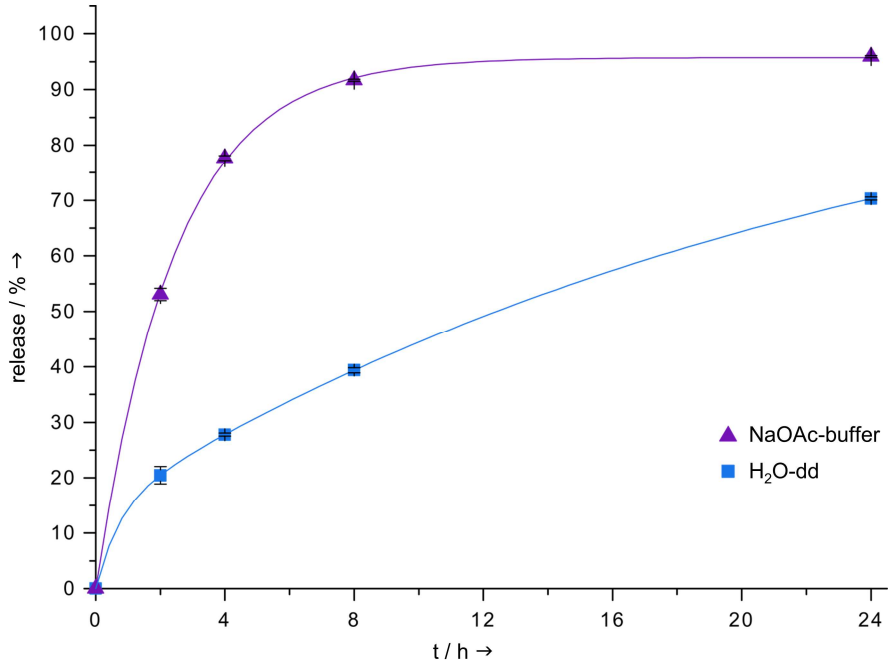

Figure 46. The amount of encapsulated curcumin **99** was determined photometrically after 0, 2, 4, 8, and 24 h for samples incubated at pH 5.5 (purple) and pH 7 (blue). The percent of release was calculated starting from 100% encapsulated curcumin content at time point 0. At pH 5.5, after 2 h 53% of encapsulated curcumin **99** was released. After 8 h 92% of encapsulated cargo was released from the particle material until after 24 h, 96% of all encapsulated curcumin **99** was released from the micelles. This release can be described burst-like. The initial fast release can be explained by the quick cleavage of acetals from the dextran, rendering much of the carrier material water-soluble. Adapted from ref.[152] Copyright (2017) American Chemical Society.

3.2.6 TOXICITY OF THE MICELLAR NANOPARTICLES

It is known that removing copper after click reactions can be a difficult task and often insufficient due to coordination of the catalyst to functional groups or chelation with the formed triazol ring.[165] Traces of residual Cu-catalyst can be toxic to cells and organisms even in micromolar concentrations and have to be fully removed when considering a biomedical application of the material.[166] Therefore, residual copper salts were removed by extensive dialysis. The *in vitro* toxicity of empty and curcumin-loaded micellar nanoparticles was evaluated by the MTT assay (**Figure 47**). After 48 h, empty particles show no toxicity on HeLa cells up to high concentrations of 500 µg mL^{-1}. In comparison, curcumin-loaded particles show a concentration-dependent inhibition of cell growth starting at particle concentrations of around 250 µg mL^{-1} (corresponding to a curcumin concentration of 20.41 µmol·L^{-1}). These chemotherapeutic effects are comparable to literature known results using nanoparticles with curcumin concentrations of 10–30 µmol L^{-1}.[167] The *in vitro* experiments confirm the biocompatibility of the particle material and exemplify its potential as drug carrier with the successful stabilization and delivery of curcumin **99**.

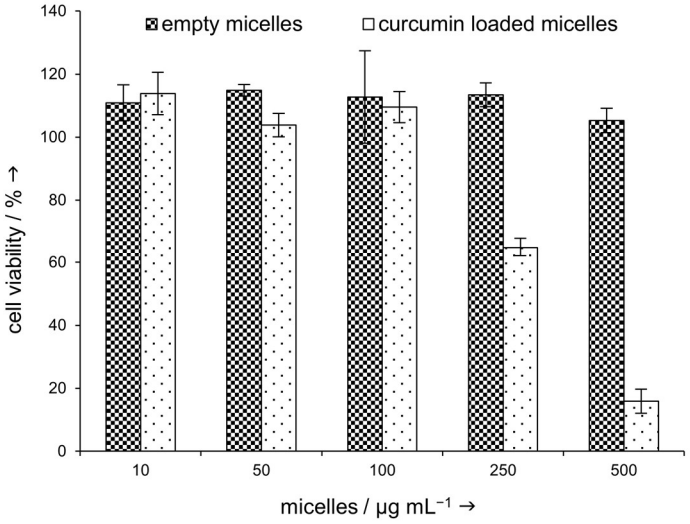

Figure 47. *In vitro* studies confirm the non-toxicity of the empty Dex-click-AcDex micellar nanoparticles when incubated with HeLa cells over 48 h. Micelles loaded with curcumin **99** inhibit the growth of the HeLa cancer cell line. Adapted from ref.[152] Copyright (2017) American Chemical Society.

In this chapter, we demonstrated that it is possible to synthesize amphiphilic, pH-responsive block copolymers composed only of modified polysaccharide blocks. The material was synthesized using Cu-mediated click chemistry. As a result, a *green* macrosurfactant could be isolated and was characterized with ringtensiometry, ^1H and

DOSY NMR, FTIR, and GPC. Due to a low CMC of 12 mg L^{-1} (12 ppm), self-assembly of **94** resulted in narrowly dispersed micellar nanoparticles particles with a diameter of approx. 70 nm. The micelles were shown to be stable over 24 h at neutral pH, but decomposed with decreasing pH. The biocompatibility and non-toxicity by sufficient removal of residual copper was confirmed with *in vitro* experiments. As possible future therapeutic application, the hydrophobic and pharmaceutically active drug curcumin **99** was encapsulated in the polysaccharide micelles and stabilized in aqueous solution. With varying pH, a fast and burst-like or slow and steady release of the drug was accomplished. The compound class of full polysaccharide block copolymers represents a particular interesting system in cases where biomedicinal applications have become difficult due to polymer induced immune responses.[102] Due to their high biocompatibility, degradability and low toxicity they represent a valuable addition to the toolbox of biodegradable artificial polymers. In addition, in contrast to many synthetic block copolymers, these natural biopolymers also offer functional groups in the backbone of both blocks. This allows for a variety of modifications for future smart biopolymer materials with applications in drug delivery or surfactant chemistry.

3.3 THIOL-BASED SYNTHESIS OF MACROSURFACTANTS

Cu-catalyzed click reactions are highly efficient coupling reactions and have found wide application in the conjugation of macromonomer building blocks.[156] However, in order to create biocompatible and non-toxic amphiphilic block copolymers for biological applicatios, it is necessary to reduce the application of transition metal catalysis and minimize the amount of toxic reagents and solvents to a necessary minimum. Consquently, we explored an alternative coupling strategy for both blocks to omit the use of copper in the conjugation process.

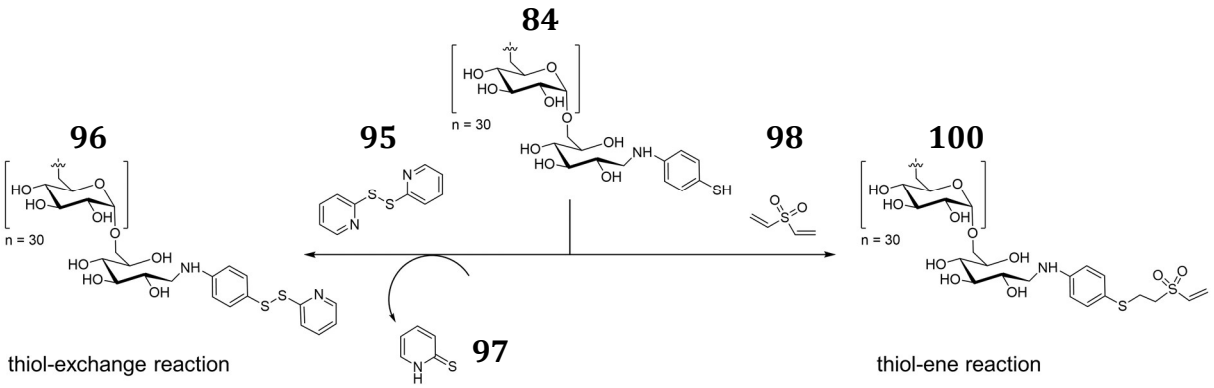

Figure 48. Based on thiol-modified dextran, two different building blocks can be prepared. The mixed disulfide Dex-S-S-Py **96** block represents an electrophilic activated thiol. Upon reaction with other thiols, a reductively cleavable mixed disulfide can be formed through thiol-exchange. The vinylsulfone-modified dextran **100** can react selectively with thiol-, amine- or alcohol groups, depending on the pH of the buffered solution in a fast thiol-ene reaction.

The modification of dextran with a thiol group on the reducing end offers benefits over other nucleophilic functionalities. Thiols, in contrast to other biorthogonal linkers, such as the arylazide group, are cheaper, easier to introduce, and show better stability. Additionally, thiols are very soft nucleophiles compared to amines or alcohol functionalities. In the context of a polysaccharide polymer backbone with 3 available hydroxyl groups on each monomer, the precise indistinguishability of the nucleophilic anchor group is mandatory for site- and chemoselective reactions addressing the reducing end. The introduction of a thiol functionality leads to a versatile dextran building block as it gives access on the one hand to a polymer with a nucleophilic end group (Dex-SH, **84**). On the other hand the dextran chain can be further modified with an electrophilic vinyl sulfone end group to yield dextran **100** or with a reductively cleavable thiol-reactive pyridyldisulfide to obtain dextran **96** (**Figure 48**). Consequently, a single-, and a double-stimulus-responsive polysaccharide block copolymer was prepared from the respective dextran building blocks. The following chapter will describe the synthesis

and application of a pH- and reduction-responsive disulfide-connected polysaccharide block copolymer. The pH-responsive vinyl sulfone derivative **107** will be discussed as a copper-free alternative in the synthesis of single-stimulus-responsive amphiphile in the subsequent chapter.

3.3.1 SYNTHESIS OF DEX-S-S-PY

Thiol-modified dextran was prepared as described in **chapter 3.1.2** (**p.54**).The activation of the thiol group at the reducing end on the dextran polymer chain was carried out in degassed DMSO under Argon atmosphere with DPDS **95** (**Figure 49**, **A**). The activation of Dex-SH **84** was first performed in diluted solution (2.9 mM) and a 10-fold excess of DPDS **95** to avoid the dimerization of dextran as a side reaction. A single diffusion coefficient in the DOSY spectrum of Dex-S-S-Py **96** (**Figure 81**, supplemental) as well as a matching ratio in the ^{1}H NMR integrals of the proton signals (**Figure 49**, **B**) (a,a',b,b',g) and (f) showed that no dimerization occured. We later found that activation with DPDS **95** can be performed directly after the reduction step without isolation of Dex-SH **84**, allowing a fast synthesis of Dex-S-S-Py **96** over three steps on one day. Moreover, the reaction proceeds quantitatively with a small excess of 2 eq and in much higher concentration (15 mM). Within the first minute of the reaction, a bright yellow color emerged. The yellow color is a result of the cleavage of the disulfide bridge in DPDS **95**, producing a pyridine-1-thione dye **97** with a characteristic absorption band at 375 nm (**Figure 48**).[168] However, due to the very fast reaction as well as the broad UV absorption background of the aniline ring in Dex-SH **84** and the formation of the product **96**, it was not possible to monitor the increasing absorption of the nascend dye **97** (data not shown). Thus it was not possible to track the reaction kinetics and optimize reaction times or follow the proceeding reaction photometrically.[159, 169] The consumption of the free thiol groups was followed qualitatively by comparing the *Raman* spectra of Dex-SH **84** and Dex-S-S-Py **96** (**Figure 49**, **C**). During the reaction with DPDS **95**, the S–H stretching mode at 2456 cm^{-1} disappeared. Additionally, the signal of both aromatic protons in the ^{1}H NMR spectrum shifted from 7.28 to 7.45 ppm and from 6.82 to 6.74 ppm while the characteristic signal of a pyridyl group appears at 8.42, 7.90 and 7.35 ppm. Integration of all proton signals allowed the calculation of the end group density of 90–95% for Dex-S-S-Py **96** (**Figure 49**, **B**).

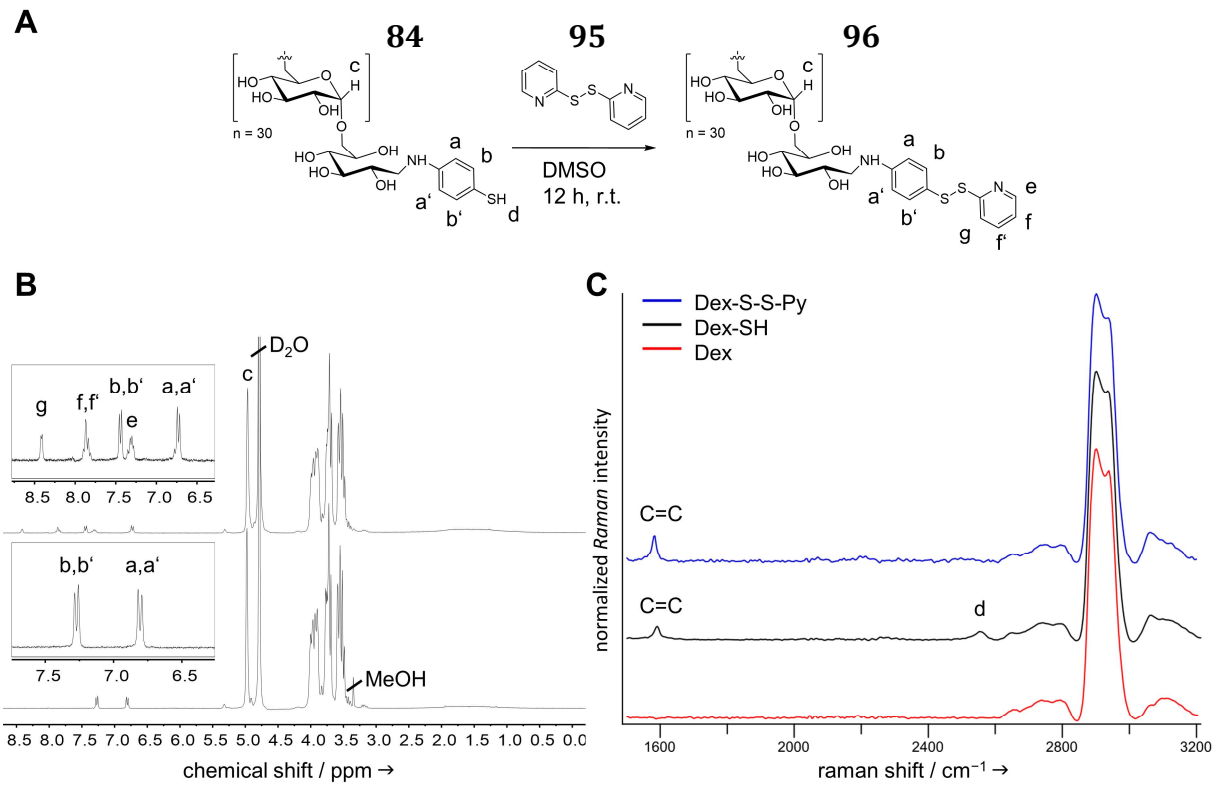

Figure 49. Scheme for the activation of thiol-modified dextran with dipyridyl disulfide **95** (**A**). ^{1}HNMR (D_2O, 300 MHz) of Dex-SH **84** and Dex-S-S-Py **96** shows the introduction of a pyridyl-residue (**B**). The *Raman* spectrum (H_2O-dd, 0.5 mg µL^{-1}) of dextran **34** and Dex-SH **84** shows the appearance of a characteristic S–H stretching mode at 2456 cm^{-1} as well as the C–H ring breathing mode at 1584 cm^{-1}. The disappearance of the S–H stretching mode indicates a full consumption of all thiol groups at the reducing end (**C**). Adapted from ref.[170] Copyright (2019) Royal Society of Chemistry.

3.3.2 SYNTHESIS OF ACETALATED ACDEX-S-S-PY

Acetalated Dex-S-S-Py **101** was prepared and characterized, like described for AcDex-alkyne **92** in **chapter 3.2.1** (**p.60**). The reaction of the OH groups of each dextran monomer was confirmed by the disappearance of the O–H vibration at 3593–3078 cm^{-1} in the FTIR (**Figure 84**, supplemental). Also, a new C–H stretch from the acetal CH_3 signal appeared at 2987–2831 cm^{-1}.[19] The new molecular weight and content of introduced acetals was determined by integration of the proton signal of generated acetone and MeOH during acidic cleavage of the acetals in the ^{1}H NMR (D_2O/DCl, 300 MHz). The isolated product had a molecular weight of 6102 g mol^{-1} and contained 77.6% acetals, whereas 45.9% were cyclic and 31.7% were acyclic acetals.

The wider application of AcDex-S-S-Py **101** was shown in the synthesis of a responsive enzyme-S-S-AcDex conjugate. The material, was applied in our lab in the synthesis of stimuli-responsive biopolymer hybrid nanoparticle in the master thesis of Pia Winterwerber.[171]

3.3.3 SYNTHESIS OF DEX-S-S-ACDEX BY THIOL-EXCHANGE LIGATION

The crucial design for our block copolymer was determined by the fact that the copolymer ligation reaction had to be highly group tolerant and forming little side products. By consequently removing the need for metal-catalysis and simplifying the synthetic procedure, the material should find application as drug delivery platform that is compatible with therapeutic applications in clinical settings. Thiol ligation chemistry offers a variety of metal-free, highly selective and group tolerant procedures, such as thiol-ene or thiol exchange reactions.[151, 172] Additionally, the formation of block copolymers by thiol exchange ligation allows the introduction of a reductively cleavable disulfide bridge.[90, 92, 159] In an attempt to develop a shortened and simplified synthesis, Dex-SH **84** was selected as starting material for both blocks. The hydrophobic block could then be synthesized by modification of the hydrophilic block over two steps.

Typically, the ligation of two polymer blocks in a thiol-exchange reaction with pyridyl-activated thiol groups is catalyzed by the addition of few equivalents of acetic acid.[90, 159, 173] Due to the acid sensitive nature of the hydrophobic block **101**, a simple transfer of this approach to our ligation strategy was not possible. However, the low pKa of thiophenol **83** (ca. 6.5) compared to an aliphatic derivative (ca. 8.5) leads to a higher concentration of reactive thiolate anion at neutral pH. Therefore, the addition of 1.2 equivalents Dex-SH **84** was sufficient to provide enough reactive species for a good conversion with the activated AcDex-S-S-Py **101** over 24 h (**Figure 50**). The FTIR spectrum of the block copolymer product **102** shows two characteristic signals of both blocks. More precisely, the signal of an O–H stretch at 3593–3078 cm^{-1} from the Dex-SH block as well as the CH_3 stretch of the AcDex-S-S-Py block from 2983–2825 cm^{-1} can be determined (**Figure 84**, supplemental). Furthermore, the ^1H NMR (D_2O, 300 MHz) of the isolated product shows the acetal proton signals of the hydrophobic block **101** at 3.30 ppm and 1.47 ppm. The disappearance of the pyridyl group signals with two residual aromatic proton signals left at 7.53 ppm and 6.78 ppm indicates a complete thiol exchange (**Figure 51**, **A**). Recent examples in literature show that DOSY NMR spectroscopy can be applied to differentiate between mixtures of polymers or polysaccharides of varying molecular weight.[174] DOSY experiments confirmed a successful ligation, as the signals for the aromatic protons of Dex-S-S-AcDex as well as the AGU backbone protons and the acetal signal align at the same diffusion coefficient ($D = 6.05 \cdot 10^{-7}$ m^2 s^{-1}; **Figure 51**, **B**). The diffusion coefficient of the

hydrophilic block Dex-SH **84** ($D = 9.09 \cdot 10^{-7}$ m^2 s^{-1}; **Figure 80**, supplemental) was distinguishably different.

It has to be mentioned that the block copolymer structure contains less acetals than expected for a 1:1 coupling (**Table 7**). Since the characterization of the acetal structure is carried out by comparing signal intensities of the polysaccharide backbone, acetone and MeOH in the ^1H NMR spectrum, unremoved Dex-SH starting material **84** could lead to the misinterpretation of a loss in acetal coverage. However, residual staring material would cause two diffusion coefficients in the DOSY spectra. It is therefore more likely that partial hydrolysis of cyclic (e) or acyclic acetals (f) occurred during the thiol exchange reaction.[175]

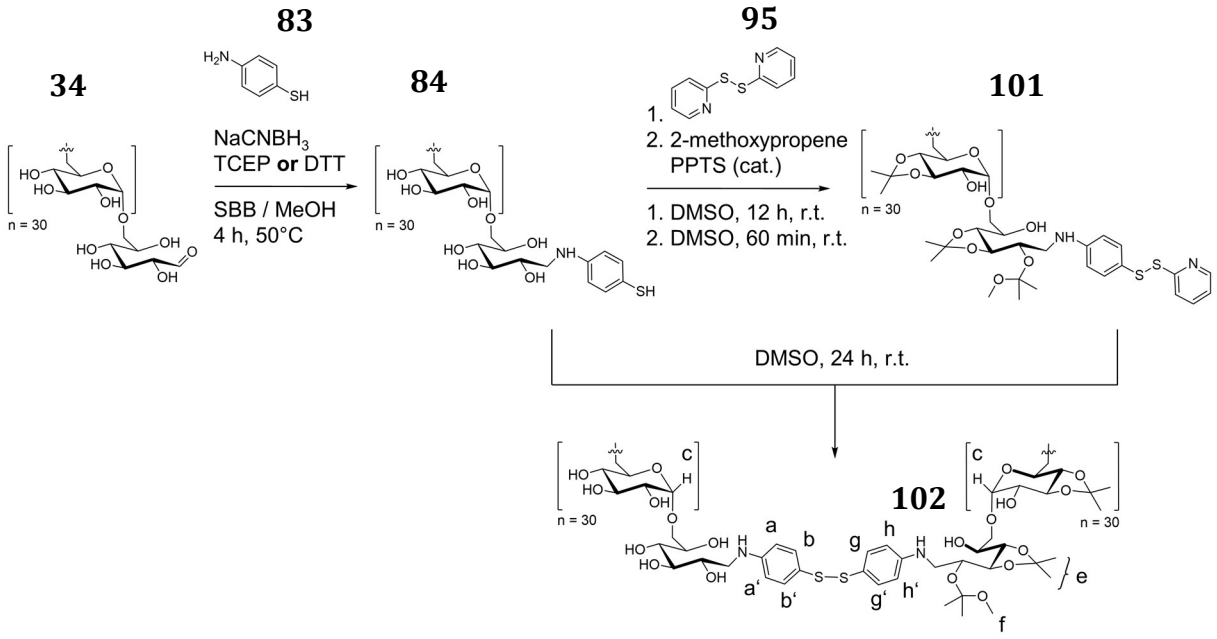

Figure 50. The hydrophilic thiol-modified dextran block is synthesized by reductive amination of commercially available dextran. Reaction of the thiol moiety with DPDS **95** and subsequent acetalization with 2-methoxypropene **56** gives the hydrophobic block AcDex-S-S-Py **101**. Combination of both blocks in a thiol-exchange reaction results in the formation of a mixed disulfide amphiphile Dex-S-S-AcDex **101**. Adapted from ref.[170] Copyright (2019) Royal Society of Chemistry.

Table 7. Acetal structure and content determined by ^1H NMR (300 MHz, D_2O/DCl). The theoretical molecular weight of hydrophobic block AcDex-S-S-Py **101** and block copolymer Dex-S-S-AcDex **102** was determined by ^1H NMR and GPC. AcDex-S-S-Py **101** was examined in DMF against PEO standard. Dex-S-S-AcDex **102** was examined in H_2O (0.1 M $NaNO_3$) against a dextran standard.

	total acetal (%)	cyclic (%)	acyclic (%)	$M_{w,NMR}$ (g mol^{-1})	$M_{w,GPC}$ (g mol^{-1})
AcDex-S-S-Py	77.6	45.9	31.7	6102.09	6601.48
Dex-S-S-AcDex	25.6	18.0	7.6	10246.81	8236.29

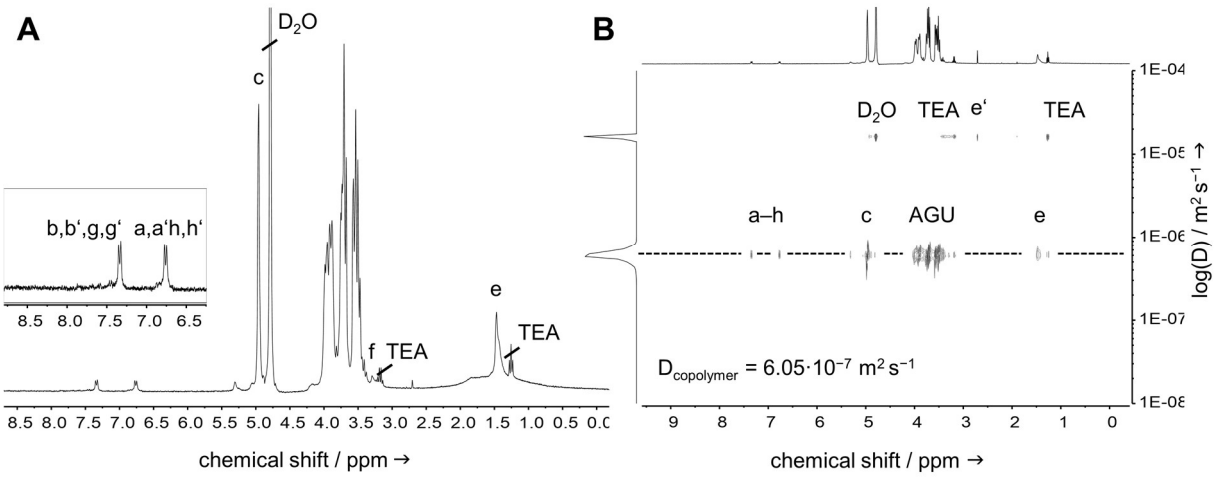

Figure 51. ^1H NMR (300 MHz, D_2O) of Dex-S-S-AcDex **102** showing the signals of cyclic acetal (e) and aromatic proton signals (a,a',b,b',g,g' and h,h'). There are no proton signals of the pyridyl group visible (**A**). DOSY spectrum (400 MHz, D_2O) with two diffusion coefficients. The upper signal combines traces of D_2O, TEA and acetone (e') from auto-hydrolyzed acetals. The lower diffusion coefficient of the block copolymer includes the signals of the aromatic linker with the signals of the acetals and the polysaccharide backbone (AGU). Adapted from ref.[170] Copyright (2019) Royal Society of Chemistry.

3.3.4 Self-assembly of Dex-S-S-AcDex block copolymer

Self-assembly of the Dex-S-S-AcDex amphiphile **101** into micellar nanoparticles was achieved by using a solvent exchange method like described in **chapter 3.2.3** (**p.69**).[25] The reaction solution in DMSO was precipitated into a 10-fold excess of H_2O-dd and unreacted residual AcDex was removed by centrifugation. The supernatant was then dialyzed (MWCO 6–8 kDa) to slowly remove the common solvent for both blocks and increase the polarity of the solvent to induce micellation. The surface activity and CMC of block copolymer **101** was determined by ringtensiometry. In contrast to Dex-click-AcDex **94**, the amphiphile **101** had a slightly higher CMC (12.6 mg L^{-1}; **Figure 100**, supplemental). As discussed in the previous chapter for Dex-click-AcDex **94**, the comparably low CMC (12.6 ppm) is at the lower range of recently reported polysaccharide containing amphiphiles.[69, 90, 99]

The particles were studied with- and without loading of the 2nd generation photosensitizer (PS) phthalocyanine zinc (PC(Zn)) **103** (**Figure 77**, **B** experimental) by dynamic light scattering. Empty particles had an average hydrodynamic diameter (2 R_H) of 88 nm, whereas loaded particles were slightly larger (117 nm). Both particle systems shared a reasonably unimodal distribution in size, characterized by a PdI of 0.14 (empty), and 0.13 (loaded) (**Table 8**). The size of self-assembled polymer systems is difficult to compare to other micellar polymer particles. It can vary significantly and depends on the ratio of hydrophilic to hydrophobic block length, as well as on the type and overall size of

the polymer. Reported examples of block copolymer nanoparticles with polymers of similar molecular weight include hydrodynamic radii from 60–181 nm.[3, 12, 90, 99, 106] Determining the R_H of a micellar nanoparticle can lead to a better understanding of the particle morphology. The length of a fully stretched 10 kDa dextran block copolymer with 60 AGU can be estimated to be approx. 27 nm.[114c] A typical micellar architecture with a block copolymer monolayer would therefore result in a smaller diameter than the one obtained by DLS. To specify our findings, the radius of gyration (R_G) and the radius of hydration (R_H) were measured by static light scattering (SLS) and multiangle dynamic light scattering (DLS). The ρ-ratio (R_G/R_H) was calculated as ρ = 0.85 for empty and ρ = 0.83 for loaded particles. This is close to the reported ρ-ratio for homogeneous spheres ρ = 0.778,[176] and it was therefore concluded that the micellar assemblies resemble a tightly packed polymer particle rather than a hollow sphere (ρ = 1).

Table 8. Data obtained by fixed angle DLS. Self-assembled Dex-S-S-AcDex particles without (−) and with cargo (+). Micelles were resuspended in aqueous NaCl (10 mM) in concentrations used in cell experiments (2.5 mg mL^{-1}). PdI is a dimensionless parameter to describe the particle size distribution. Z-Ave describes the average size of all particles in the sample. Intensity describes the population by scattering intensity. Number describes the largest population within the particle solution. The ζ-potential describes the overall charge on the particle surface.

particles	PdI	Z-Ave (d.nm)	intensity (d.nm)	number (d.nm)	ζ-potential (mV)
−	0.141	88.10 ± 0.82	103.16 ± 1.67	51.82 ± 2.80	−1.84
+	0.137	117.6 ± 0.37	137.03 ± 0.46	75.50 ± 3.02	−0.74

TEM images of air-dried samples further confirmed our assumption (**Figure 52**, **C**-**D**) that the micellar nanoparticles form packed, homogeneous spheres during the self-assembly process. An investigation by CRYO TEM was not possible because particles strongly adhered to the tissue during the removal of the aqueous solution and became detached from the grid. As a direct consequence of the the very polar polysaccharide corona, the nanoparticles are not strongly bound to the unpolar copper grid surface and preferentially adhere to the cellulose membrane of the plotting seal. Attempts to remove the excess particle solution from a single side of the grid led to large cluster structures caused by particles traveling with the flow of the solvent (**Figure 96**, supplemental).

The amount of polymers within one micelle, described by N_{ag} was calculated using **eq. 12** and **eq. 13**. With an R_H of 53.2 nm, the micellar particles contain an average of $6.06 \cdot 10^4$ copolymers/micelle (**Table 9**).

Table 9. Data obtained from multiangle dynamic light scattering and static light scattering of assembled particles. The R_H describes the radius of hydration, the R_G the radius of gyration. The quotient of R_H/R_G is termed as ρ-ratio and can describe the particle morphology. The N_{ag} describes the amount of polymer chains within one micellar particle.

particle	R_H (nm)	R_G (nm)**	R_G/R_H	N_{ag}*
empty	53.2±1.2	45.1±4.5	0.85	$6.08 \cdot 10^4$
loaded	64.5±3.8	53.4±5.3	0.83	-

*Calculated using **eq. 12** and **eq. 13**; **standard deviation of 10% experimental accuracy.

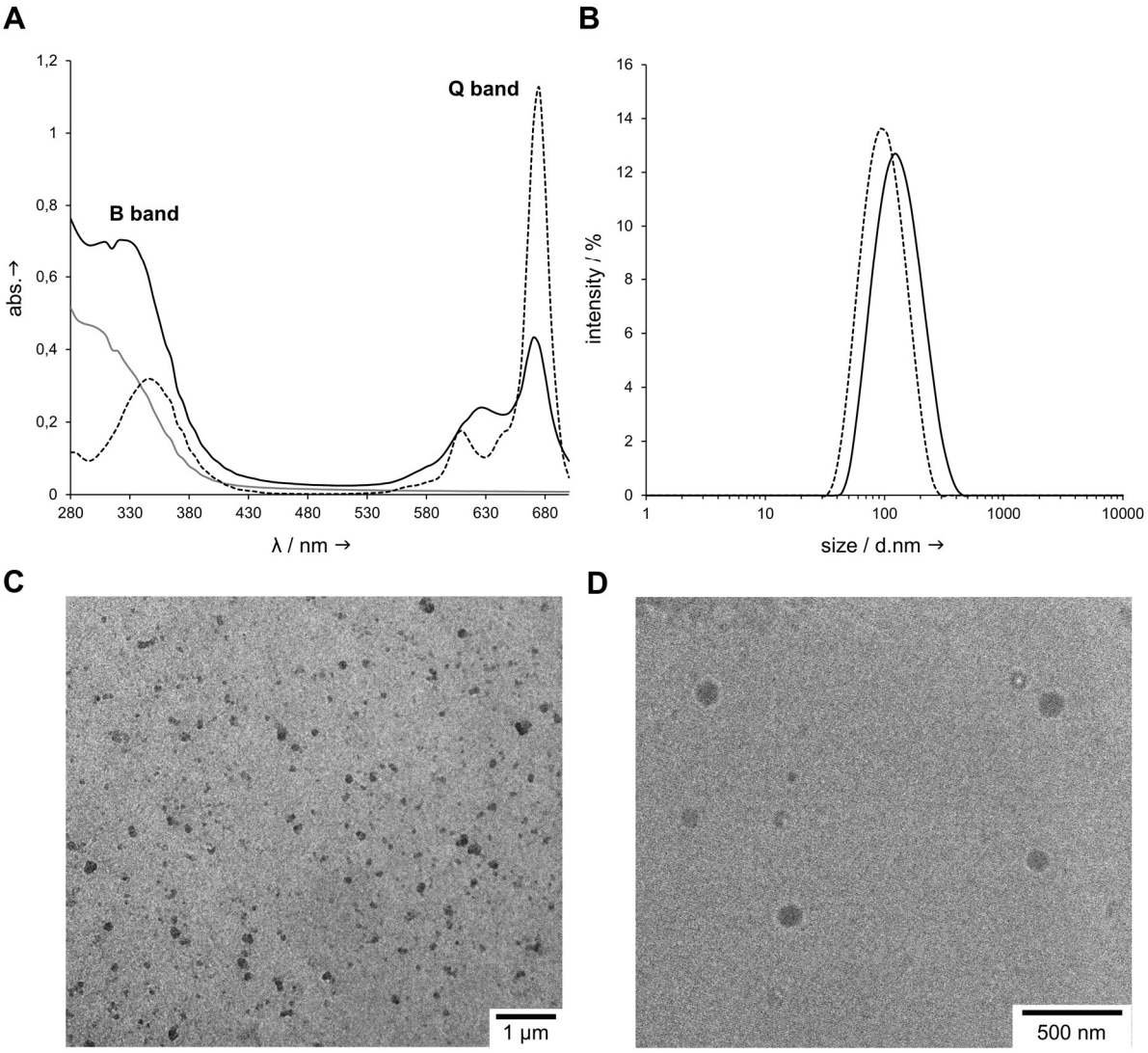

Figure 52. Absorption spectra of free dye in DMSO-water (9/1, v/v) and PC(Zn) (0.14 mM) (grey line), PC(Zn)-loaded particles in water with PC(Zn) (0.05 mM) (black line) and empty particles in water (dotted line). Feeding ratio of PC(Zn) in particles is 2.2 wt% with the B band at 300–400 nm and Q band between 650–750 nm. Broadening of the Q band indicates beginning aggregation of the cargo (**A**). DLS of PC(Zn)-loaded Dex-S-S-AcDex micelles (black line) and empty Dex-S-S-AcDex micelles (dotted line) in NaCl (10 mM). Sizes are shown in intensities as $2 \cdot R_H$ and scattering angle 90° (**B**). TEM image of PC(Zn)-loaded Dex-S-S-AcDex micelles showing filled, solid spheres. Adapted from ref.[170] Copyright (2019) Royal Society of Chemistry.

Typical aggregation numbers for polymeric micelles are reported as hundrets per micelle, however there are few reports with thousands per micelle (e.g. *Shi et al.*, N_{ag} 4.1 10^3).[177] It can be assumed that the flexible disulfide bridge between both polymer blocks facilitates and increases the chance of polymer chains intertwining during the self-assembly process. The hydrophobic blocks, entangled with several amphiphilic block copolymers, form a tighly packed core surrounded by a water-swollen dextran corona. The assumption of a compact knot-like bundle was further supported by the fact that the micelles were stable during the freeze-drying process and would not fall apart upon removal of the water. Also in SEC experiments a high molecular weight fraction (nanoparticles) and a lower molecular weight fraction (block copolymer) was observed (**Figure 87**, supplemental). However, ultrasound treatment using the sonication bath would disrupt the micellar particles and result in ill-defined aggregate structures in DLS and TEM.

3.3.5 PC(Zn) LOADING AND RELEASE BY NANOPARTICLE DEGRADATION.

The PS was encapsulated by combining a stock solution of PC(Zn) **103** in DMSO with a solution of amphiphile **101** in DMSO. The mixture was treated like described for the micellation of empty particles. During the solvent replacement process, the hydrophobic block of the amphiphile **101** assembles with the hydrophobic PC(Zn) **103**, driven by the increasing polarity of the surrounding solvent. Simultaneously, the hydrophilic dextran block forms a stabilizing corona around the hydrophobic guest molecule, trapping it in the micellar core. The loading capacity (LC) of the polysaccharide nanoparticle system was probed, with changing feed of PC(Zn) **103** from 0.76–3.30% (**Table 10**). We found, that the LC could be varied from 0.53–2.46% without precipitation of the cargo during the dialysis work up. Higher loadings were not further examined, as the material was already very effective on HeLa cells in low concentrations (0.15 $mol_{PCZn}/mol_{polymer}$). Additionally, recent literature suggests that high loadings of PC(Zn) **103** might decrease the PS performance.[178] High local concentrations of PC(Zn) **103** should be avoided in nanoparticle systems due to its strong tendency to aggregate and crystallize. At a feed of 2.2 wt% cargo, we observed a broadening in the Q band of the UV spectrum of the loaded PC(Zn) compared to the free dye (**Figure 52**, **A**). Peak broadening is often described as an indication for aggregation (or stacking) of PC(Zn) **103** inside the nanoparticle, resulting in a reduction of photoactivity.[179] Therefore all cell culture tests were performed with

micellar particles prepared with a max. feed of 1.76 wt% (0.15 $mol_{PCZn}/mol_{polymer}$). Prior to examining the cellular uptake, the particle stability in neutral aqueous solution (NaCl, 10 mM) and DMEM-buffer was monitored with DLS over 24 h. During the measurement, the polydispersity and the particle concentration (estimated by the derived count rate) did not change significantly (**Table 11**;**Figure 91**, **B** supplemental).

Table 10. Optimization of PC(Zn) loading into Dex-S-S-AcDex micellar nanoparticles. The encapsulation efficiency (EE) and loading capacity (LC) were calculated with **eq. 14** and **eq. 15**. The amount of PC(Zn) was determined by a fluorescence-based assay in DMSO against a PC(Zn) standard (ex. 610 nm, em. 690 nm). The amount of polymer was calculated from the isolated freeze-dried nanoparticles and amount of PC(Zn).

feed (wt%)	$mol_{cargo}/mol_{polymer}$	EE (mol%)	LC (mol%)
0.76	0.09	65.56	0.53
1.76	0.15	66.06	0.85
2.20	0.28	82.45	1.58
3.30	0.45	84.81	2.46

Table 11. Characterization of self-assembled, loaded Dex-S-S-AcDex nanoparticles (1.76 wt%), observed over 24 h in aqueous 10 mM NaCl or DMEM-buffer after resuspension of lyophilized samples. The concentration was 10 mg mL^{-1}. PdI is a dimensionless parameter to describe the particle size distribution. Intensity describes the particle size distribution within the sample, depending on their scattering intensities; number represents the size of the particles forming the largest population in the sample.

	initial size			after 24 h		
medium	PdI	intensity (d.nm)	number (d.nm)	PdI	intensity (d.nm)	number (d.nm)
DMEM	0.151	142.9±1.9	70.5±5.8	0.155	153.0±5.2	77.8±4.4
NaCl (10 mM)	0.160	140.6±3.6	69.9±1.7	0.155	167.9±23.7	76.8±2.9

The dual-responsiveness of the particles was investigated by incubation in acidic or reductive environments and the decomposition behavior was analyzed in terms of degradation speed and aggregate formation. We found, that the particles incubated in NaOAc-buffer at pH 5 degraded in a slow process over 24 h (**Figure 53**, **B**). Acid-catalyzed cleavage of acetals in the hydrophobic backbone block results in a loss of the amphiphilic character of block copolymer **102** which becomes fully water-soluble. Particle sizes tracked by DLS show a shift towards smaller hydrodynamic diameters after 8 h incubation time. Furthermore, the polydispersity of the samples increases (from a PdI of 0.2 to 0.4) while the derived count rate decreases, indicating a loss of the colloidal character of the solution (**Figure 91**, **A** and **B** supplemental).

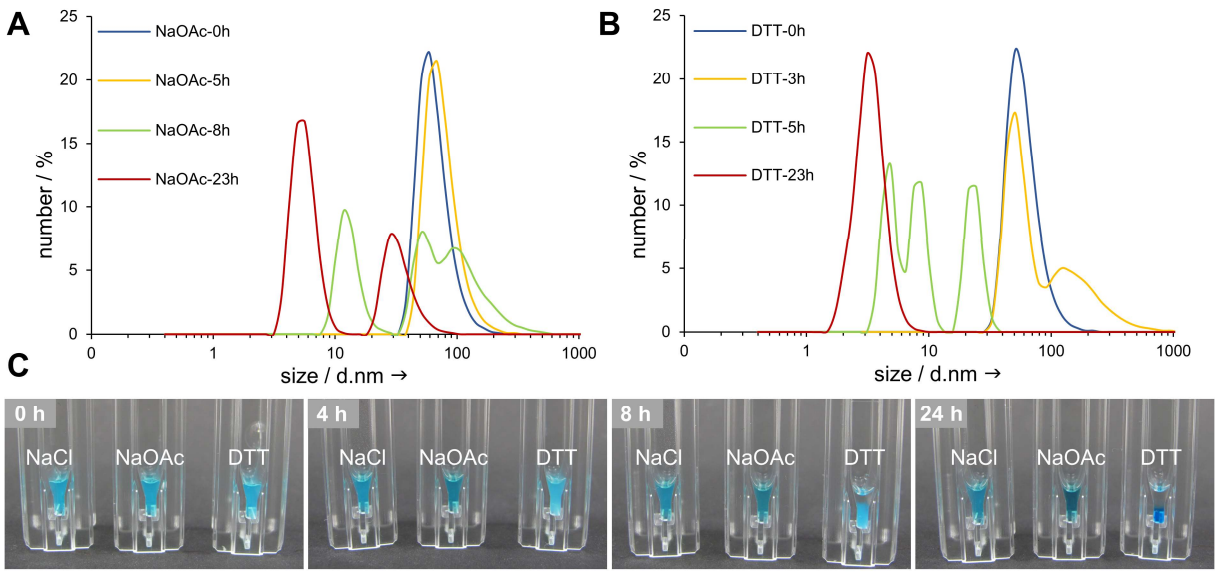

Figure 53. DLS data of particles incubated in 50 mM NaOAc-buffer (5 mg mL^{-1}) at pH 5 shift in size towards a larger R_H after 8 h. The particles become more polydisperse as the acetals in the hydrophobic block are cleaved-off (**A**). Particles incubated in 10 mM DTT/NaCl (5 mg mL^{-1}) at pH 7 start to precipitate rapidly and sediment beginning after 3 h. Parts of the corona forming hydrophilic dextran blocks are reductively cleaved, resulting in a loss of steric repulsion. This induces aggregation of the residual hydrophobic particles and aggregation into larger structures. Finally, most of the material precipitates and only smaller particles are detected in the DLS measurements (**B**). These different mechanisms of degradation can also be observed visually in microcuvettes. The particle solution at pH 5 (NaOAc, middle) becomes darker over time, while the block copolymer dissolves very slowly, leaving PC(Zn) nanoaggregates surrounded/stabilized by residual hydrophobic polysaccharide. The particle solution under reductive conditions (DTT, right) becomes cloudy at first, which indicates the fast formation of large aggregates. After 23 h, all material precipitated together with PC(Zn) to the bottom of the cuvette. (**C**). Reprinted from ref.[170] Copyright (2019) Royal Society of Chemistry.

Since we found that the amphiphile dissolution under acidic conditions is a slow and steady process, we hypothesize that the precipitation of the hydrophobic cargo is hindered by the continuous stabilizion with residual amphiphile.

Particles incubated at neutral pH with the addition of a reducing agent (H_2O-dd, NaCl/DTT, 10 mM) show a different decomposition behavior. Within the first 3 hours, a change in particle size together with an increase in polydispersity can be monitored by DLS (**Figure 53**, **A**; **Figure 91**, **A** supplemental). The formation of larger aggregates can also be observed visually in the increasing turbidity of the solution from 3–5 h (**Figure 53**, **C**). Particle sizes and derived count rate further decrease as AcDex and PC(Zn) **103** form aggregates and start to precipitate. Residual particles, tracked in DLS, have small sizes below 50 d.nm (**Figure 53**. **A**, **Figure 91**, **A** supplemental). Finally, all cleaved AcDex and PC(Zn) cargo is precipitated after 23 h. This different degradation behavior is caused by the disulfide cleavage point, connecting the two blocks. DTT is an effective small molecule reducing agent. The reduction of the polymer block connecting disulfide leads to a fast loss of the amphiphilic character and a removal of the the stabilizing hydrophilic

dextran corona around the particle core as both polymer blocks are cleaved. The destabilized "naked" hydrophobic particles aggregate quickly, which can be monitored by the sharp increase in polydispersity within the first 3 hours after incubation. Since the hydrophobic block remains intact at neutral pH, unsoluble clusters of AcDex block and PC(Zn) **103** form until they are too heavy and large in size to be stable in solution and precipitate.

Additional to the particle degradation studies, the ability of the particle system to release the cargo upon an external stimulus was tracked over 24 h with gel permeation chromatography (GPC) (**Figure 54**). Time points for sample quantification measurements were matched to the measurement intervals of the degradation study.

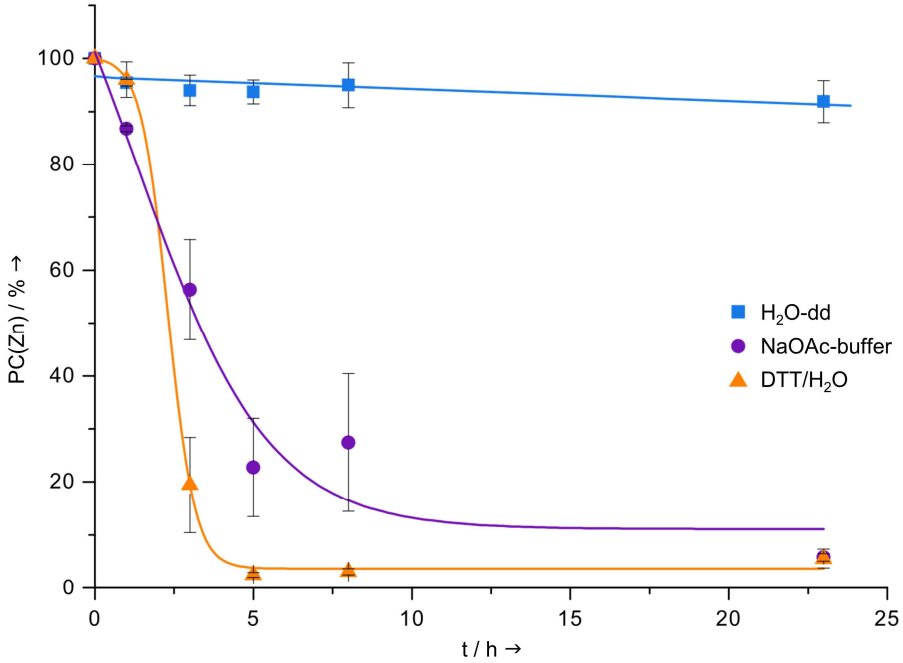

Figure 54. Release of PC(Zn) **103** from loaded micelles determined by GPC. Signals are normalized to 100% for the signal t = 0 h. Particles incubated in neutral solution (NaCl, 10 mM) show only minimal loss of cargo (>90% after 23 h). In NaOAc buffer (pH 5, 50 mM) particles slowly release cargo within the first 5 hours. After 23 h, a complete release of PC(Zn) can be observed. Reduction with DTT (10 mM) results in insoluble aggregates and removal of almost all PC(Zn) from the aqueous phase within the first 5 h. Reprinted from ref.[170] Copyright (2019) Royal Society of Chemistry.

At neutral pH, particles remain stable and show only minimal PC(Zn) release (< 5%) over 24 h (**Figure 54**, blue squares). Particles at pH 5 however, show a decrease in the concentration of encapsulated PC(Zn) of 13% after 1 h incubation time. The release continues to increase up to 43% after 3 h, until after 5 h ca. 72% of encapsulated cargo is removed from the particle system (**Figure 54**, purple circles). It is interesting to see that although the DLS measurement showed an acid-triggered particle degradation at a later

time point (7–8 h) (**Figure 53**, **B**), some PC(Zn) **103** is released after 1 h. Possibly, the high pressure and flow rate during the GPC experiment results in a wash out of cargo from partially degraded micelles. Incubation of particles in reducing conditions (NaCl/DTT, 10 mM) results in a rapid release of PC(Zn) **103** of up to 80% within the first 3 hours (**Figure 54**, orange triangles). While technically, there is no real release and particle degradation at neutral pH, this observation can be explained by the fast cleavage of disulfide bridges. As discussed in the previous section, the acetalated dextran and encapsulated PC(Zn) **103** molecules form unsoluble aggregates. This finally leads to precipitating aggregates which cannot pass the sephadex gel column. The majority of the encapsulated PC(Zn) **103** (96%) is precipitated from solution after 5 h and cannot be tracked by GPC detection anymore.

3.3.6 INTRAZELLULAR PC(ZN) RELEASE AND CONTROLLED PHOTOTOXICITY

For an efficient nanoparticle supported therapy it is desirable to obtain full control over delivery and release of a pharmaceutically active cargo within a specific tissue. In addition, the nanoparticle system has to ensure stabilization and protection of the cargo from premature aggregation and subsequent loss of function. In this context, the efficient cellular delivery of PC(Zn) **103** and the subsequent probing of its photosensitizer activity was performed on HeLa cells. In first experiments, the uptake of the micellar nanoparticles was tracked by flow cytometry and later confirmed with fluorescence microscopy (**Figure 55**). HeLa cells incubated for 24 h with PS-loaded micelles (0.25 mg ml^{-1} micelles; 8.5 µg ml^{-1} PC(Zn)) showed a significant shift in fluorescence intensity, whereas cells incubated with empty micelles showed only a weak autofluorescence signal (**Figure 55**, **B** both signals in one graph). Additionally, no mixed fluorescence signal was observed, demonstrating a full cellular uptake of all micelles. Fluorescence microscopy imaging after 23 h incubatiuon time revealed PC(Zn) **103** homogenously distributed in the cytosol of all HeLa cells around the 4′,6-diamidino-2-phenylindole (DAPI)-stained nucleus (**Figure 55**, **A**). Hereby it was possible to distinguish between unspecific adsorption onto the cell membrane and real cellular uptake of the micellar particles. At the applied dye concentration, imaging turned out to be difficult, due to the fact that upon irradiation with laser light at 630 nm (near the Q band), the photosensitizer would produce toxic reactive oxygen species (ROS), among others singlet oxygen. Hence, shortly after irradiating the samples, the cells died.

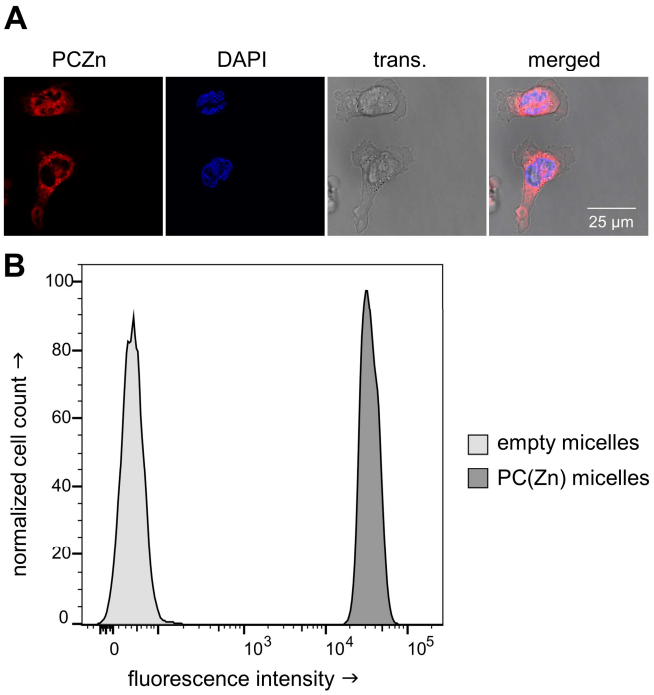

Figure 55. Representative fluorescence microscopy images of HeLa cells incubated for 24 h with PC(Zn)-loaded micellar nanoparticles (0.25 mg mL^{-1}). From left to right the panels show PC(Zn) **103** fluorescence in cells (red), DAPI stained cell nuclei (blue), the transmitted light image and an overlay of all three images (**A**). Flow cytometry profile of HeLa cells incubated for 24 h with particles shows a significant shift in fluorescence intensity caused by particle uptake (**B**). Reprinted from ref.[170] Copyright (2019) Royal Society of Chemistry.

This effect of induced phototoxicity was probed in a WST assay. HeLa cell samples were either treated in dark or after irradiation with light in the NIR. Incubation in the dark with both, empty and PC(Zn)-loaded micelles did not lead to a decrease in cell-viability, irrespective of the applied concentration. However, when cells were irradiated at a wavelength of 590–630 nm for 15 min with a light dose of approx. 1 mW cm^{-1} (0.88 J cm^{-1}) (**eq. 16**), a toxic effect was clearly observed. Hereby we can cleary demonstrate a photo-induced toxicity of the PC(Zn)-loaded micelles (**Figure 56**, **B**). Cells incubated with empty micelles were not affected by cellular damage after irradiation. This confirms the non-toxicity of the Dex-S-S-AcDex material **102** as well as the solely photo-inducible toxicity of the encapsulated PC(Zn) **103**. When incubated with 0.25 mg ml^{-1} micelles (3.63 µM PC(Zn) respectively), only 41±8% of all cells survived the phototreatment. In contrast, *Hirohara et al.* reported a slightly lower phototoxicity with a RAFT polystyrene-b-PPEGA copolymer. However, they applied PC(Zn) in higher concentrations (3.9 µM) with higher light doses 30 J cm^{-2}.[180] *Wang* and coworkers reported an optimized setup based on a PEG-b-PAA-b-PS nanoparticle system with fast irradiation times of 2 min. They achieved similar toxicity but at the cost of higher

concentrations of PS and light doses (5 μM PC(Zn) and 2.4 J cm^{-2}).[181] Compared to other reported drug delivery systems in photodynamic therapy, the Dex-S-S-AcDex amphiphile **102** combines the benefits of biodegradable, non-toxic material with high loading capacities and stimuli-responsiveness.

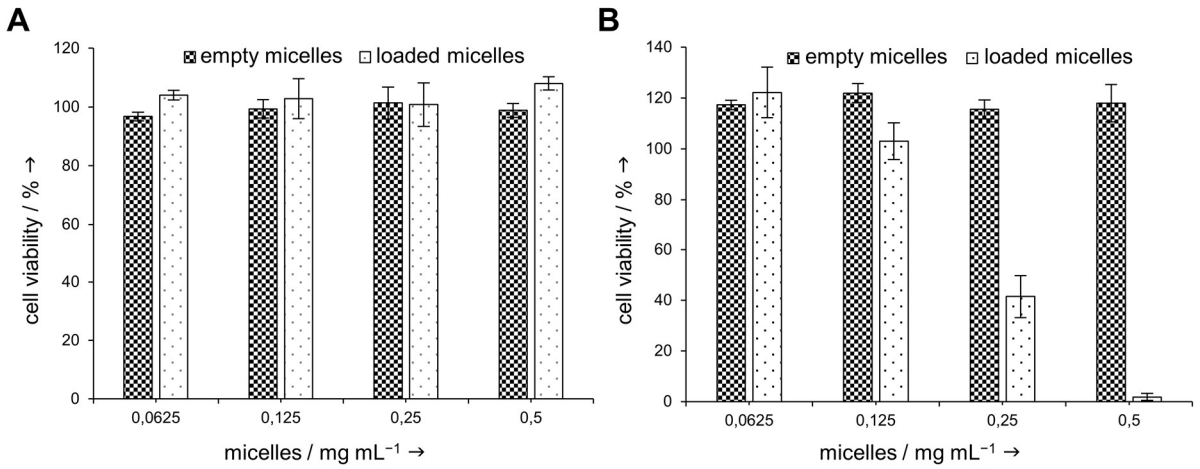

Figure 56. Cellular toxicity of PC(Zn)-loaded micellar nanoparticles determined by WST assay, HeLa cells were incubated with particles over 24 h in the dark (**A**) After irradiation of all cells for 15 min at 590–600 nm (1 mW cm^{-1}), the PC(Zn) containing particles show photo-induced toxicity (**B**). Reprinted from ref.[170] Copyright (2019) Royal Society of Chemistry.

In this chapter, the synthesis of an amphiphilic polysaccharide block copolymer was further refined. By switching from a CuAAc-based to a Cu-free click strategy a reduction-sensitive disulfide bridge was incorporated into the block copolymer architecture as a second stimulus-responsive moiety. The thiol exchange reaction between a thiol-modified dextran **84** and dipyridyl dithiol acetalated dextran **101** allowed ligation of both blocks in an efficient and time saving manner. The isolated pH- and reduction-sensitive amphiphile **102** was surface-active, had a low CMC of 12.6 mg L^{-1} and self-assembly properties (of comparable efficiency to the 1st generation Dex-click-AcDex **94**). Self-assembling yielded micellar nanoparticles with a R_H of 53–64 nm (empty and loaded) and a reasonably narrow size distribution (PdI 0.13–0.14). The polysaccharide particles were shown to stabilize the 2nd generation photosensitizer PC(Zn) **103** in H_2O-dd (10 mM NaCl) or cell culture medium DMEM over 24 h and could be stored over long term as freeze-dried powder. The material degraded in pH ranges below pH 5, or upon addition of a reducing agent, e.g. DTT (10 mM) in biologically relevant concentrations. The triggered particle disintegration led to a time-dependent release of the hydrophobic cargo. This feature is especially interesting for drug delivery applications. In a model experiment

PC(Zn)-loaded Dex-S-S-AcDex micelles were taken up and internalized by cells. When irradiated at 590–600 nm, a controllable and concentration-dependent toxicity could be induced.

Although the Cu-catalyzed synthesis of a double-stimulus responsive full oligosaccharide amphiphile was reported previously, this short and simplified synthesis should be seen as an extension to existing, more complex syntheses.[106, 159] In this protocol, we circumvent the use of metal catalysis and provide usefull reactive dextran intermediates, applicable to other bioconjugation procedures. More generalized, the synthetic strategy should be applicable to all polysaccharide systems with an inherent reducing end.

3.4 VINYLSULFONE - A CU-CLICK ALTERNATIVE

In this chapter, the Cu-free synthesis of a pH-responsive dextran block copolymer is described. The product is then compared to the other block copolymers prepared in **chapter 3.2** and **3.3** in terms of surface activity, CMC and self-assembly properties. The main purpose of this project was to develop a catalyst-free synthesis for a single stimulus-responsive polysaccharide macrosurfactant, hereby expanding the toolbox of Cu-free clickable dextran building blocks. Vinylsulfone-terminated dextrans represent valuable polysaccharide building blocks that allow chemo-selective modification at the reducing end with thiol, amine or hydroxyl groups. To the best of our knowledge, there are no reports of vinylsulfone end group-modified dextrans and linear vinylsulfone-linked pH-responsive polysaccharide block copolymers. We propose that they will broaden the applicability of full polysaccharide block copolymers as responsive biomaterial for biological and biomedicinal applications.

3.4.1 VINYLSULFONE-MODIFIED DEXTRAN

The modification of Dex-SH **84** with divinylsulfone **98** (**Figure 48**, **p.74**) was performed similarly to the synthesis of Dex-S-S-Py **96** with the exception that all reactants were water-soluble and the reaction was performed in PBS (10 mM EDTA). As demonstrated for modified dextran **96**, a four-fold excess of the homobifunctional DVS linker **98** was sufficient to achieve complete thiol consumption without crosslinking of two dextran chains. GPC measurements confirmed that no unmodified Dex-SH **84** reacted with already modified Dex-S-VS **100** (**Figure 88**, supplemental) during the reaction. It was shown by ^{1}H NMR that the thiol groups were converted quantitatively (**Figure 57**, **B**). Yet, the quantification of the end group was not clearly ascertainable since the proton signals of the vinyl group (h) of Dex-S-VS **100** (6.96–6.74 ppm, 6.52–6.28 ppm) could not be clearly distinguished from the aromatic aniline protons (7.41 ppm and 6.96–6.74 ppm). Therefore, the reactivity and functionality of the vinylsulfone was probed in a model reaction with *N*-Boc-aminoethanethiol **104** (**Figure 57**, **A**). We found that the vinylsulfone group is reactive enough to achieve full conversion with 1.2 eq thiol at room temperature over 12 h. Moreover, integration of the signals of the dextran anomeric proton and the Boc-group revealed a conversion of >95% of all vinylsulfone groups.

Vinylsulfone-modified polymers can be valuable building blocks in the synthesis of peptide- or protein/enzyme conjugates[182] as well as in block copolymers and surface-

coated nanoparticles.[183] Depending on the pH of the buffered reaction system, the vinylsulfone group can be selectively addressed by thiols (pH 6–8), amines (pH 8–10) or hydroxyl groups (pH >10).[184]

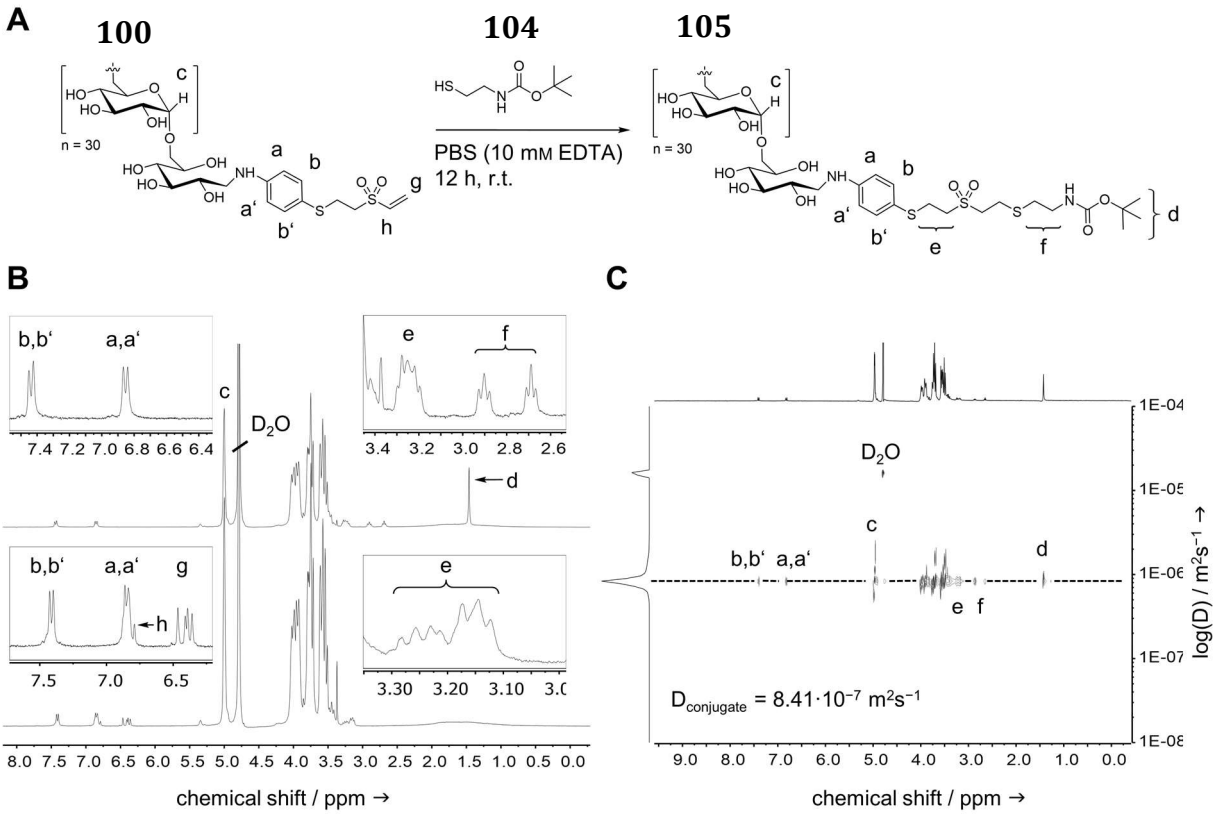

Figure 57. The vinylsulfone functionality of Dex-S-VS **100** was probed with *N*-Boc-aminoethanethiol **104** in a *Michael*-type reaction (**A**). In the ^1H NMR (300 MHz, D_2O) of the starting material (lower spectrum), the proton signals of the vinyl group (g, h) disappear while in the product spectrum (upper spectrum) the characteristic signal of the Boc group (d) and the ethylene protons (f) of the linker molecule appear. Integration of the signals of the anomeric proton in the polymer backbone and the Boc signal suggests full conversion of all thiol groups (**B**). The DOSY spectrum (400 MHz, D_2O) of Boc-modified Dextran **105** demonstrates the covalent attachment of the aliphatic thiol to the vinylsulfone functionality.

3.4.2 Synthesis of AcDex-S-VS block and Dex-S-VS-S-AcDex amphiphile

The synthesis and analysis of acetalated Dex-S-VS **106** was carried out as described for AcDex-alkyne **92** and AcDex-S-S-Py **101** with a varying acetal content from 67–82%. AcDex-S-VS **106** was then applied as hydrophobic block along with Dex-SH **84** as hydrophilic block in the synthesis of a polysaccharide block copolymer. The conjugation of both blocks was achieved under the same conditions as for Dex-S-S-AcDex **101** (**Chapter 3.3.3**, **p.77**). The resulting pH-responsive amphiphile Dex-S-VS-S-AcDex **107** was isolated with an acetal content of 20–38%, depending on the nature of the AcDex-S-VS block **106** (**Figure 58**). The block copolymer was analyzed analogous to Dex-click-AcDex **94** and Dex-S-S-AcDex **102** with FTIR, ^1H NMR, DOSY and GPC and will not be

further discussed in detail here (**Figure 79**, **Figure 82**, **Figure 85**, **Figure 89** supplemental). Compared to the synthesis of the pH-responsive Dex-click-AcDex block copolymer **94**, it was not possible to obtain a vinylsufone-linked block copolymer with low acetal loading (20–23%) and surfactant properties. Attempts to perform vinylsulfon-*Michael* addition with AcDex-S-VS **106** with an acetal content of <67% (and a higher ratio of acyclic acetals) gave a block copolymer with <20% acetals in the hydrophobic block. With the addition of 1 eq TEA, it was possible to obtain an amphiphile with similar acetal content as Dex-click-AcDex **94** (23%). However, it was not possible to determine a CMC and micellation experiments led reproducibly to small, unstable aggregates with a R_H of 10–15 nm (by DLS). Increasing the acetal content of the hydrophobic building block **106** to 78–83% (with a majority of cyclic acetals) resulted in a surface-active block copolymer **107** with an acetal content of 30–38% in the isolated product and a strong tendency to form micellar nanoparticles during the dialysis work-up. Surprisingly, it was not possible to fully characterize the amphiphile with the highest acetal content in the hydrophobic block (38%) either. Although the material was soluble to give a stable solution with no precipitation over time, CMC values could not be ascertained reproducibly and varied from 19–40 mg L^{-1} (**Table 15**; **Figure 102**, supplemental) This phenomenon will be further discussed in **chapter 3.4.4**.

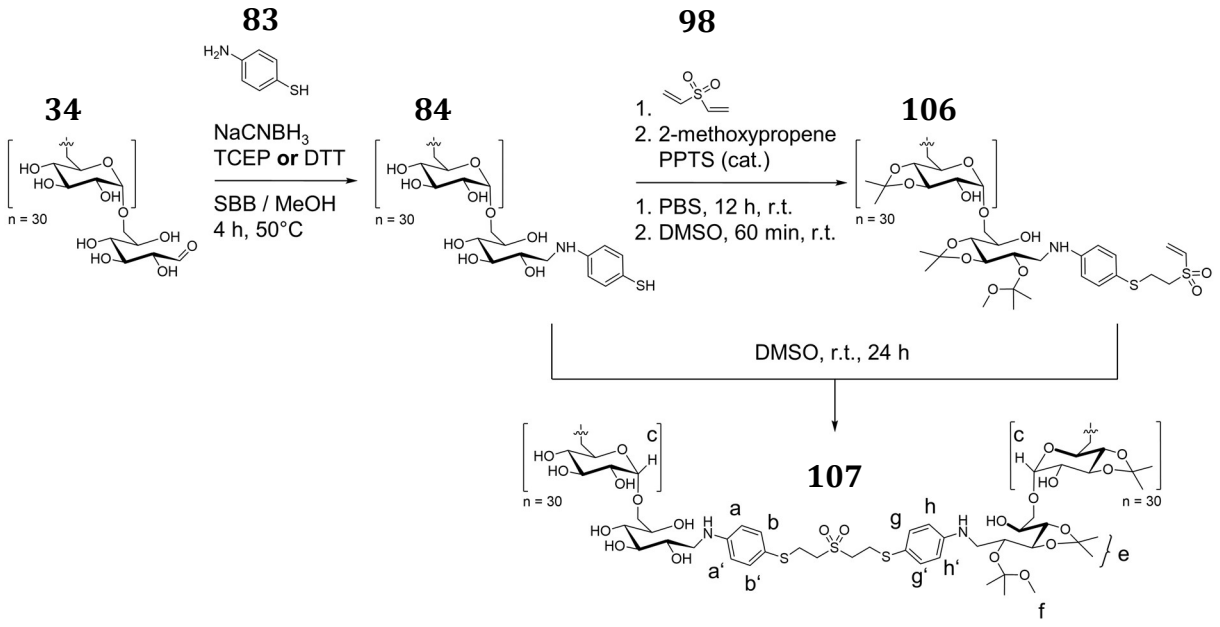

Figure 58. Catalyst-free synthesis of a pH-responsive polysaccharide amphiphile by thiol-vinylsulfone ligation of a hydrophilic thiol-modified dextran **84** and a vinylsulfone-terminated hydrophobic acetalated dextran **106**. The resulting block copolymer Dex-S-VS-S-AcDex **107** was investigated for its surface-active properties and self-assembly ability.

3.4.3 MICELLATION, DRUG-LOADING AND TRIGGERED DEGRADATION

In order to establish a quick test to clarify whether a synthesized block copolymer had the desired amphiphilic character, its surface activity was probed with the hydrophobic dye Nile red **108** (**Figure 77**, **C**). This allowed to quickly screen the synthesized products, for the aforementioned property, omitting a time-intensive complete work-up by dialysis over three days. Consequently, a small sample of the reaction solution (5 mM in DMSO) was added to Nile red **108** to achieve a final concentration of the dye of 0.6 mM. The resulting intensely purple colored solution was added dropwise to a 10-fold excess of H_2O-dd, water-insoluble precipitates were removed by centrifugation and the resulting solution dialyzed over two days against H_2O-dd (pH 8, with TEA). Samples in which the dye completely precipitated within the first 3–4 h of dialysis were discarded. Interestingly, unlike in micelles from Dex-click-AcDex **94** and Dex-S-S-AcDex **102**, we found that an acetal content of 23% was not sufficient to stabilize and encapsulate a hydrophobic guest molecule with loading capacities higher than 0.39% (**Table 12**). These samples also had to be filtered before cargo quantification due to precipitation of Nile red **108** during the solvent exchange overnight. Only in samples of block copolymer **107** with an acetal content of 30–38%, Nile red **108** aggregation and precipitation was successfully prevented and good loading capacities were achieved.

Table 12. Selected dye loadings achieved with Dex-S-VS-S-AcDex **107** with varying acetal content and model compound Nile red **108** determined by absorption assay at 550 nm. With increasing acetal content, the hydrophobicity of the AcDex-S-VS block **106** increases and thus the ability to stabilize Nile red **108**.

sample	acetal content (%)	LC %	EE %	comment
I	15.73	0.12	2.82	precipitation
II	20.68	0.39	15.25	precipitation
III	33.76	1.81	48.09	stable
IV	39.30	1.82	55.45	stable

Compared to micelles from Dex-click-AcDex **94**, the empty and loaded particles from copolymer **107** were stable over 72 h in neutral aqueous solution, but also during the freeze-drying process (**Table 13**). The higher stability of nanoparticles was also confirmed by GPC where two fractions eluted from the column. The first fraction represented very high molecular weight species and was possibly assembled nanoparticles. The second fraction at longer elution times was block copolymer **107** (**Figure 89**, supplemental). The size distribution of the micellar particles can be described

as moderately monodisperse with a PdI of 0.14 (empty) and 0.12 (loaded).[185] Similar polydispersities were achieved in micelles from Dex-S-S-AcDex **102**. Micelles from Dex-click-AcDex **94** could be assembled with a more monodisperse distribution (0.10–0.11). Typically, self-assembled micellar polymer particles from block copolymers are reported with polydispersities such as 0.12 (PEG-b-PLA)[3], 0.39 (PEG-b-PCL)[186] or from 0.14–0.34 depending on the hydrophobic block length (Dex-b-PMCL).[89] However, size distributions in self-assembled nanoparticle systems can strongly vary with the applied assembling method as well as the nature of the polymers and therefore can not be directly compared.[187]

Table 13. DLS data obtained with Dex-S-VS-S-AcDex **107** (38% acetals) redissolved from lyophilized samples. Micelles contain either Nile red **108** as cargo (+) or were empty (–). Particle sizes and PdI illustrate the degradation of particles over 24 h, depending on the pH of the incubation buffer. Micelles were either incubated in NaOAc-buffer (pH 5) or NaCl-solution (10 mM, pH 7).

		initial size			after 24 h		
cargo	pH	PdI	intensity (d.nm)	number (d.nm)	PdI	intensity (d.nm)	number (d.nm)
–	7	0.141	148.36±3.4	74.69±6.6	0.130	143.43±3.8	80.29±1.9
–	5	0.131	138.36±1.8	74.66±2.1	0.770	15–189*	1–8*
+	7	0.123	130.80±5.1	75.81±5.9	0.167	133.90±1.5	70.06±0.2
+	5	0.134	136.67±3.7	70.18±6.8	1	21–30*	0.8–30*

*Multiple particle size populations were observed.

Due to the little surface-activity and poor micellar stability of Dex-S-VS-S-AcDex **107** with low acetal content, all further experiments were conducted with amphiphile containing 30–38% acetals ([cyclic acetals]>[acyclic acetals]) in the hydrophobic block.

The observation that empty micellar particles are larger (D_H 148 d.nm) than loaded particles (D_H 130 d.nm) can be attributed to the fact that the cargo loading slightly increases the hydrophobicity of the micellar core while promoting the expelling of water. Hence, the hydrophobic acetalated polysaccharide chains in the micellar core are less swollen and become compressed more tightly which results in shrinking of the micelles. A phenomenon recently observed and described by *Stenzel* and coworkers for fructose-PLA-b-PMMA block copolymer micelles.[164] The overall size diameter of micellar particles assembled from the vinylsulfone-linked block copolymer **107** was similar to micelles from Dex-S-S-AcDex **102** (ca. 140–142 d.nm), but larger than micelles from Dex-click-AcDex **94** (98–105 d.nm). The largest population of micelles in all samples however had

the same diameter of ca. 69–75 d.nm (by number) which suggests that all block copolymers can be assembled in micellar structures of comparable size.

The high content of stable cyclic acetals resulted in longer degradation times than observed for the Dex-click-AcDex micelles. This is an attractive property for long-acting drug conjugates to enable less-frequent administration resulting in improved patience compliance.Time-dependent DLS measurements demonstrated that micellar particles incubated at pH 5 showed no change in size for the first 9 h (**Figure 92**, supplemental). Images of Dex-S-VS-S-AcDex micelles with Nile red **108** loading show that after 24 h incubation at acidic pH the particles are decomposed to an extend that the released Nile red cargo **108** can not be stabilized in solution anymore and precipitates. Yet there is still residual acetalated dextran present, forming large structures with the released dye at the bottom of the vial (**Figure 59**). Particles kept at neutral pH were stable and showed no precipitation of the cargo when left to stand for 48 h. Particles in NaOAc-buffer were fully decomposed into water soluble dextran and residual hydrophobic Nile red **108** at the bottom of the vial.

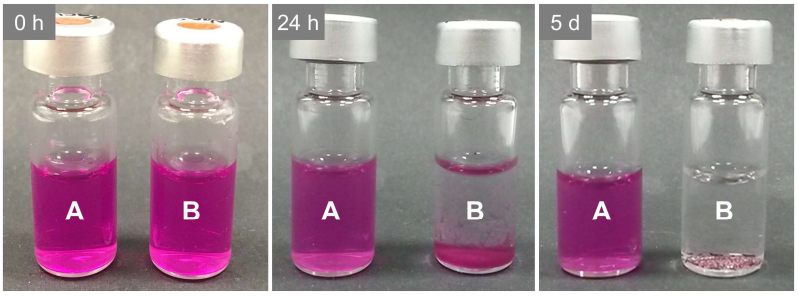

Figure 59. Nile red-loaded Dex-S-VS-S-AcDex micelles (5 mM) dispersed in either pH 7 (10 mM NaCl, **A**) or pH 5 (50 mM NaOAc, **B**). After 24 h, micelles incubated at acidic pH have formed large aggregates with Nile red **108** and precipitated. After 5 d, particles incubated at neutral pH are still stable, the material incubated at pH 5 is fully decomposed into water-soluble dextran and residual hydrophobic Nile red **108**.

In conclusion, it can be summarized that a single-stimulus-responsive dextran block copolymer was synthesized using a *Michael*-type thiol-vinylsulfone reaction. The synthesis also led to valuable vinylsulfone-terminated intermediates **100** and **106**. We show, that the Dex-S-VS-S-AcDex material **107** can substitute Dex-click-AcDex **94** as pH-responsive amphiphile (circumventing the need for metal catalysis during the synthesis) with the restriction to slowly degrading material. Additionally, it was shown that the hydrophobic model compound Nile red **108** could be encapsulated and stabilized in aqueous solution over longer time periods and be released upon a decrease in the pH to pH 5 (**Figure 59**). This is especially interesting and useful in the formation of long

circulating drug carriers. Amphiphiles prepared from fast degrading AcDex-S-VS **106** with a lower acetal content (≤ 23%) and a higher degree of acyclic acetals, showed low loading capacities and formed either unstable micelles or did not self-assemble at all (**Table 12**).

The surface-activity and surfactant properties of the Dex-S-VS-S-AcDex material **107** was investigated in the context of changing acetal content and directly compared to the other polysaccharide macrosurfactants Dex-click-AcDex **94** and Dex-S-S-AcDex **102**. It will be therefore discussed in more detail in the following additional chapter.

3.4.4 SURFACE ACTIVITY AND MICELLATION OF BLOCK COPOLYMERS

Amphiphilic block copolymers or macrosurfactants[188] are popular polymer architectures in nanomedicinal applications due to their chemical and physical properties. Polymeric surfactants generally show the phenomenon of very small critical micellar concentrations (CMC) compared to small molecule surfactants. This is especially desirable for drug delivery as micelles injected in the bloodstream have to withstand high dilution. The significant decrease in CMC is caused by the fact that long polymer chains have a greater likelihood of interaction and entanglement than their low molecular weight counterparts.[105] As the different nature of polymer chains in a merged block copolymer can have a strong influence on its properties it can also have a great impact on the assembling characteristics of micellar nanostructures built from these polymer blocks.[81-82, 188] It is therefore vital to identify several characteristics to distinguish between the surface-activity and micellation properties of different polymeric surfactants in order to compare and evaluate their self-assembly behavior in aqueous solution. Parameters described in literature include the standard free *Gibbs* energy of micellation ($\Delta G^{\circ}_{\mathrm{mic}}$), the maximum surface excess concentration of surfactant at the air/water interface (Γ_{max}) and the surface area occupied by each surfactant molecule (A). The adsorption of surfactant at the air/water interface results in depression of the surface tension (γ) with increasing surfactant concentration and peaks at a maximum at a decline by 20 mN m^{-1}.[189] This behavior is defined as the surfactant efficiency (pC_{20}) and described by the negative logarithm of the bulk concentration necessary to reduce the surface tension by 20 mN m^{-1}(**eq. 1**).[190]

$$pC_{20} = -\log(c_{20}) \qquad \text{eq. 1}$$

The free energy decrease for the transfer of an amphiphile unimer (solo subunit of a surfactant micelle)[191] from the bulk phase into the micelle is described by the *Gibbs* free energy of micellation. For micelles with a large N_{ag} it can be approximated with the simplified **eq. 2**, with R as the ideal gas constant (in J mol^{-1}) and T the absolute temperature (K).[192]

$$\Delta G° = RTln(CMC) \qquad \text{eq. 2}$$

The maximum surface excess concentration (Γ_{max} in mol cm^{-2}) describes the area-related maximum concentration of a tenside at an interface and can be extracted from the slope of the surface tension (γ) vs. log(amphiphile)-plot with **eq. 3**, derived by *Rosen et al.* (**Figure 61**).[189] Here, R is denoted with (erg mol^{-1} K^{-1}).

$$d\gamma = -2.303RT\Gamma_{max}\, d\log(c_{amphiphile}) \qquad \text{eq. 3}$$

$$A = 1/\Gamma_{max}\mathrm{N} \qquad \text{eq. 4}$$

The surface area A occupied by a surfactant molecule (in Å^2), can then be acquired from **eq. 4**, where N is the *Avogadro* constant (in mol^{-1}). **Note:** Å^2 was later converted to nm^2 for reasons of comparability. The average radius of the occupied surface area can be calculated with **eq.5**.

$$r = \sqrt{A/\pi} \qquad \text{eq.5}$$

The maximum reduction in surface tension (in mN m^{-1}) at the CMC is defined as the surfactant effectiveness (πCMC) and can be determined directly from the plot of surface tension vs. surfactant concentration in the experimental data with **eq. 6** (supplemental data) or calculated by **eq. 7**, derived by *Rosen et al.*[189]

$$\pi CMC_{found} = \gamma_0 - \gamma_{CMC} \qquad \text{eq. 6}$$

$$\pi CMC_{calc.} = 20 + 2.303RT\Gamma \log(CMC/c_{\pi=20}) \qquad \text{eq. 7}$$

It was pointed out multiple times in literature that the overall molecular architecture (type of grafted side chains, chain lengths, ratio of hydrophilic to hydrophobic block, chemical nature of blocks etc.) of a block copolymer has an influence on its surface activity and micellation properties.[80b, 187, 189, 193] Therefore, all three synthesized polysaccharide macrosurfactants were examined under the aspect of their diverse conjugation chemistry and the consequently resulting difference in spacer length and flexibility (**Note:** the flexibility of the linkages was not calculated. Estimates are based on the chemical structures and the resulting degrees of rotational freedom). All three surfactants are

constructed with the same building blocks dextran and acetalated dextran. However, the CuAAC ligation of Dex-N_3 **78** and AcDex-alkyne **92** in the 1st generation macrosurfactant **94** leads to a more rigid and flat aromatic linkage between both polymer blocks. The disulfide linkage and the dialkylsulfone bridge in the 2nd generation macrosurfactants **102** and **107** on the other hand, introduce a growing degree of flexibility between the hydrophilic and the hydrophobic domain (**Figure 60**).

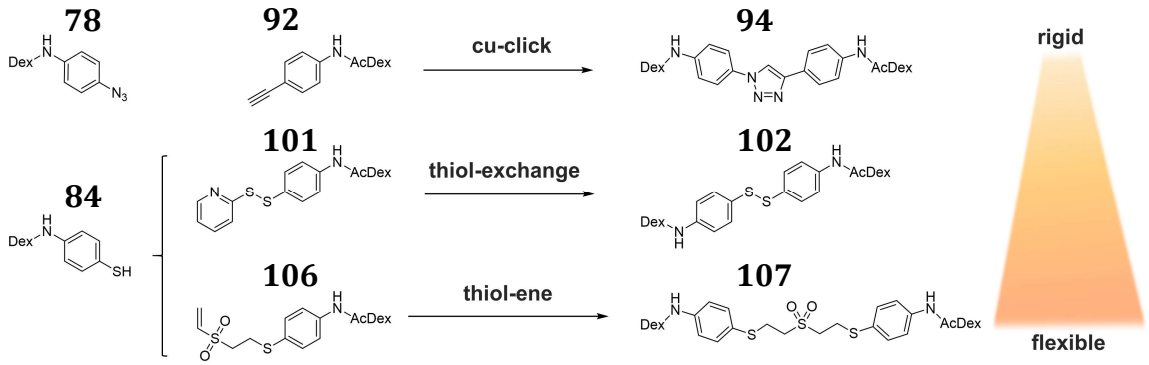

Figure 60. Depending on the conjugation chemistry, the hydrophilic and hydrophobic polysaccharide blocks are conjugated with an increasing degree of flexibility (estimates about flexibility are based on the chemical structure and the different resulting rotational degrees of freedom for single or double bonds).

Therefore, the three block copolymers were synthesized with similar acetal content (25.6–30%) and surface-activity parameters were attained and compared to other published polymer macrosurfactants. No obvious trend was observed for the CMC values. The dialkylsulfon-linked block copolymer **107** had a higher CMC of 21 mg L^{-1} compared to the mixed disulfide **102** (12.6 mg L^{-1}) or the clicked amphiphile **94** (14.6 mg L^{-1}) (**Table 14**, supplemental data **Figure 99–100**).

Table 14. Surface-active properties of prepared polysaccharide amphiphiles. The Dex-click-AcDex **94** and Dex-S-VS-S-AcDex **107** had an acetal content of 30%. Dex-S-S-AcDex **102** had an acetal content of 25.6% in the hydrophobic block.

polymer	CMCx10^6 (mol L^{-1})*	Γx10^{10} (mol cm^{-2})	area/molecule (nm^2)	efficiency pC_{20}	πCMC_{found} (mN m^{-1})	$\pi CMC_{calc.}$ (mN m^{-1})
94	1.46	9.23	0.18	5.93	25	23
102	1.26	8.30	0.2	5.98	30	24
107	2.10	12.08	0.14	5.81	31	29

*Calculated with an average molecular weight of 10 kDa.

In general, the critical micelle concentration for all three amphiphiles is very low compared to other polysaccharide containing block copolymer systems. *Zhang* and *Marchant* reported N-alkyl maltonamides (C_6 to C_{12}) with CMCs from 36.6–0.16 g L^{-1} and a *N*-alkyl dextranaldonamid (1 kDa Dex) with 0.55 g L^{-1}.[128c] Other reported nonionic

surfactants such as Mal-b-AceMal (100 mg L^{-1}), PEG-b-PLLA (4 mg L^{-1}), PCL-b-dexran (9.2 mg L^{-1}), or HEMA-b-PNIPAM (100 mg L^{-1}) illustrate that low CMC values are not uncommon for similar sized copolymer systems but that there is also a wide space to explore by changing the composition and chemical nature of the conjugated blocks.[90, 104a, 159, 194].

The negative ΔG°_{mic} of approx. −32 kJ mol^{-1} to −33 kJ mol^{-1} at 25°C (**eq. 2**) shows that micellation is thermodynamically equally favored for all three amphiphile systems. The values are in the range of commercial poly(ethylene oxide)-poly(propylene oxide) (pluronic®) block copolymers of equal molecular weight (from −28.5 to −28.8 kJ mol^{-1}) or SDS (−21.2 kJ mol^{-1}).[195]

For all prepared amphiphiles, a similar surfactant efficiency (pC_{20}) was observed (**eq. 1**, **Table 14**). However, a small difference in surfactant effectiveness from rigid to flexible architecture was observed. Dex-S-VS-AcDex **107** had the highest effectiveness (31 mN m^{-1}, **Table 14**, **eq. 6**). Except for the πCMC_{found} of Dex-S-S-AcDex **102**, the data is in good agreement with the calculated values (πCMC_{calc}, **eq. 7**, **Table 14**). Possibly, the CMC of **102** needs to be recalculated. Regarding the surface excess concentration of surfactant, also a small difference in terms of surface packing was observed (data extracted from **Figure 61**).

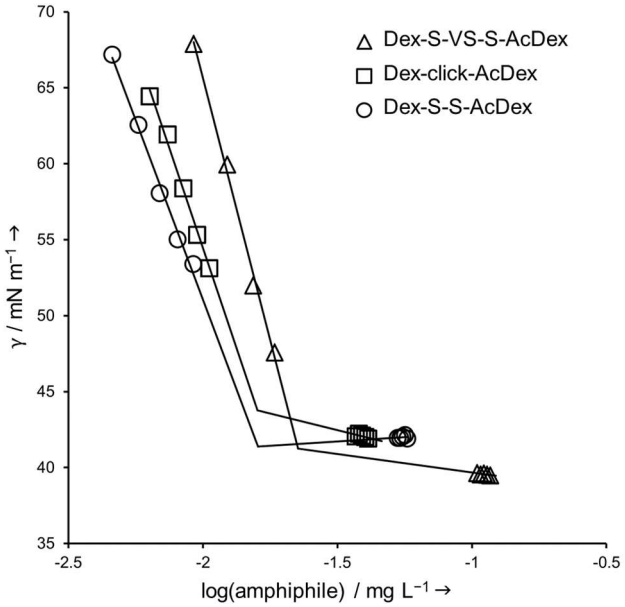

Figure 61. SFT (γ) vs. common logarithm of amphiphile konzentration-plot derived from ringtensiometric measurements in aqueous solution. The block copolymers Dex-S-VS-S-AcDex **107** and Dex-click-AcDex **94** had an acetal content of 30% in the hydrophobic block. Dex-S-S-AcDex **102** had only 25.6% acetals in the hydrophobic block. The three macrosurfactants have a similar effectiveness in reducing surface tension but different CMCs and slopes (important for calculation of surface excess concentration).

The most flexible dialkysulfone-linked amphiphile **107** showed the largest surface concentration and the smallest surface area per molecule of 0.14 nm² (**Table 14**, **eq. 3**, slope of **Figure 61**). The amphiphiles **94** and **102** showed lower surface area concentrations and also slightly larger surface areas per molecule (A = 0.18–0.2 nm², **Table 14**). This is in agreement, with the fact that the surfactant with the highest surface excess concentration Γ_{max} (Dex-S-VS-S-AcDex **107**) has the highest effectiveness (πCMC) as the flexible linkage allows a tight packing of the hydrophobic AcDex-block at the air/water interface. The bulky geometry of Dex-S-S-AcDex **102** and the rigid conformation of Dex-click-AcDex **94** result in larger occupied areas at the air/water interface. This phenomenon was also described by *Zhang* and *Marchant* when comparing Maltose- and Dextran-based surfactants.[80b]

What is also apparent is the generally very low Γ_{max} and A of all three block copolymers. When comparing the reported calculated *Stokes* radius of a dextran coil (M_w 5–10 kDa, r = 1.66–2.28 nm, **Table 2**, **p.36**) with the average radius from the surface area occupied with 1st or 2nd generation macrosurfactant (**Table 14**, **eq.5**, r = 0.21–0.25 nm) and the reported radius of an unmodified dextran fibre (r = 0.27 nm, **Table 2**, **p.36**)[110, 196], it becomes apparent that the amphiphile chains are most likely assembled in a very closely packed arrangement.[112b, 112c, 197] More general, the area at the air water interface occupied by a single block copolymer macrosurfactant is much smaller than expected from reported radii for a hydrated dextran chain of the same molecular weight. Hence, we hypothesize that the acetalated dextran chains of the amphiphile are forced into an extendet conformation into the air phase. This is consistent with the findings of *Gref et al.* who reported a "brush"-like orientation of their PEG-b-PLA copolymers (r = 0.2–0.5 nm²) at the air-water interface as a direct result of tight packing.[197] In comparison, *Marchant et al.* reported loosely packed *N*-alkyl maltonamides (C_{10}) with 0.36 nm² surface area/molecule.[80b] Yet, low molecular weight glycoside non-ionic surfactants were also reported with very small surface areas of 0.16–0.23 nm².[198] One could assume that the larger Γ_{max} and smaller A of amphiphile **107** is a results of its flexible linkage between the hydrophobic and the hydrophilic chain, however the amount of data is not sufficient to allow for a detailed interpretation of the findings.

It was expected, that an increase in acetal content and therefore an increase in hydrophobicity of Dex-click-AcDex **94** (from 23% to 30%) and Dex-S-VS-S-AcDex **107** (from 30% to 38%) would lead to a decrease of the CMC or an increase of the effectiveness

πCMC (**Table 15**).[187] While this is true for the effectiveness of Dex-click-AcDex **94**, this trend was not observed for Dex-S-VS-S-AcDex **107**. Interestingly, it was found that the surfactant efficiency as well as the effectiveness of Dex-S-VS-S-AcDex **107** rather decreased, with higher acetal content.

Table 15. Surface-active properties of prepared polysaccharide amphiphiles Dex-click-AcDex **94** with low acetal content (23%, quickly degrading) and Dex-S-VS-S-AcDex **107** with high acetal content (38%, slowly degrading).

acetals (%)	CMCx10^6 (mol L^{-1})*	Γx10^{10} (mol cm^{-2})	area/molecule (nm^2)	efficiency pC_{20}	πCMC_{found} (mN m^{-1})	ΔG_{mic} (kJ mol^{-1})
23	1.20	1.66	1.02	4.17	21	−33.76
38	1.92–3.04	4.17–11.10	0.15–0.39	5.42–5.66	25–27	−30.67–−32.59

*Calculated with an average molecular weight of 10 kDa.

During the measurement, the decrease in surface tension with increasing surfactant concentration was fluctuating strongly (**Figure 102**, **B**; supplemental data). However, the surfactant effectiveness was relatively stable at 25–27 mN m^{-1}.

It was shown before for poly(acrylic acid)(PAA) block copolymer systems that amphiphiles containing strongly hydrophobic blocks, like PS show a decreased surface-activity compared to block copolymers that contain mildly hydrophobic blocks such as poly(*n*-butyl acrylate) (PBA) or poly(diethylene glycol ethyl ether acrylate) (PDEGA). According to the authors, block copolymers with a higher hydrophobicity show a slower equilibrium between unimere in micelle or in solution and prefer the micelle conformation over adsorption at the air/water interface. This could lead to a decrease in surface tension not consistent with the increase of amphiphile concentration in solution.[193c] It was not possible to determine a consistent value for the CMC with freeze-dried material **107** (38% acetals), due to a changing behavior in surface reduction (**Table 15**). The recorded reduction in surface tension throughout the ringtensiometric measurement of **107** (38% acetals) might result from small amounts of unimer released from preassembled micelles.

In summary, first results indicate that the conjugation strategy has a weak influence on the surface activity of the resulting block copolymer. Compared to the Dex-click-AcDex **94** and Dex-S-S-AcDex **102** (25–30% acetals), the Dex-S-VS-S-AcDex **107** (30% acetals) was more effective in reducing surface tension but had a higher CMC. Additionally, an increase

from 30% to 38% acetals (hence overall hydrophobicity of the AcDex block) had no positive effect on the surface activity and CMC of Dex-S-VS-S-AcDex **107**.

Once assembled, micelles from Dex-SH-based 2nd generation macrosurfactants displayed a higher stability compared to the 1st generation amphiphile micelles. Particles from amphiphile Dex-S-S-AcDex **102** and Dex-S-VS-S-AcDex **107** did not break apart and could be eluted as high molecular weight fraction during size-exclusion chromatography, clearly separated from free unimer (**Figure 87**, **Figure 88**, supplemental data). This higher stability was further exploited for drug formulation and storage. Hydrophobic drugs (curcumin, phthalocyanine zinc and nile red) were loaded into particles, freeze-dried and stored as powder for later use. Stock solutions were easily prepared by simply redissolving the material in the desired concentration and medium/buffer (**Figure 62**).

Figure 62. Image of Nile red- (left, purple) and curcumin-loaded micellar nanoparticles (right, yellow) from Dex-S-VS-S-AcDex **107** to illustrate the benefits of a stable nanoformulation. Images were taken directly after drug loading (left), then micelles were freeze-dried (middle) and redissolved in a higher concentration (right).

Attempts to redissolve micelles from Dex-click-AcDex **94** led to precipitation of the cargo and highly polydisperse particle size distributions visible in DLS (data not shown). Since all three amphiphiles had comparable CMCs and surface-activities, it is hypothesized that higher particle stability is a consequence of the flexible disulfide-, or alkylsulfone linkage between both blocks. The stronger entanglement finally results in a tighter conformation during the self-assembly process and more polymer chains interwoven into a knot-like bundle.

Another important aspect is the simplified conjugation strategy. While the 1st generation amphiphile **94** was built from two different starting materials (Dex-N_3 **78** and Dex-alkyne **80**) and conjugated by Cu-catalysis, the 2nd generation amphiphiles **102** and **107** can be synthesized from thiol-modified dextran **84** without added catalyst. More precisely, this means that four different building blocks (**96**, **100**, **101** and **106**) and two different macrosurfactants (**102** and **107**) can be synthesized from one single starting material

Dex-SH **84**. The catalyst-free conjugation then proceeds either by fast thiol-exchange or a *Michael*-type thiol-vinylsulfone reaction.

Their simple preparation, good surface activity and low CMC make dextran block copolymers a versatile and tunable platform for applications in surfactant chemistry and drug delivery.

3.5 DEXTRAN BRUSH POLYMERS

In order to explore the possibilities of more complex polymer architectures besides AB block copolymers from low molecular weight polysaccharides, norbornene end group–functionalized acetalated dextran macromonomers (AcDex MM) were synthesized. In this chaper, AcDex MMs were polymerized by ring-opening metathesis polymerization (ROMP) in a *grafting-through* approach with the aim of creating proteoglycan-like biopolymer bottlebrushes (BB) (**Figure 31**, **p.47**). Two AcDex MM (5 kDa) with varying spacer length between norbornene function and AcDex chain were synthesized and polymerized. In the course of the project, several obstacles hampering the polymerization process were identified and explored.

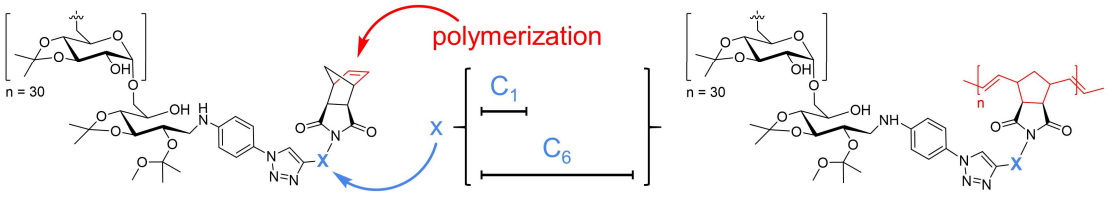

Figure 63. Schematic presentation of an acetalated dextran macromonomer with a polymerizable Norborne unit at the chain end. The connecting linker between AcDex and norbornene was varied in length.

3.5.1 SYNTHESIS OF ACDEX MM WITH SHORT C_1 LINKER

The first synthetic strategy was designed with the aim of creating a fast and easy access to MM **111** (**Figure 64**). Therefore it was decided to follow a Cu-click strategy similar to the preparation of Dex-click-Mal **88** (p.52).[199] The 5-norbornene-2,3-*exo*-dicarboximide residue as polymerizable anchor group was chosen due to three reasons. First, the high ring strain of the norbornene residue allows polymerization at room temperature and mild conditions with a *Grubbs* catalyst. Second and third, they are easily and cheap synthetically accessible from commercially available pure *exo*-monomer starting materials. This is important as the *exo*-monomers are reported to have higher reactivity than the *endo*-analogue in ROMP, thereby the rate of polymerization can be tuned solely by the choice of the monomer.[50a] The short click-C_1-norbornene linker **109** was prepared in a one-step procedure, as described in literature from *cis*-5-norbornene-*exo*-2,3-dicarboxylic anhydride **117** and propargylamine.[200] Subsequent conjugation to Dex-N_3 **78**, was achieved using a Cu(II)SO_4/ascorbic acid catalytic system. The reaction was monitored qualitatively by the disappearance of the azide stretch signal at 2113 cm^{-1} and the appearance of a carbonyl stretch at 1687 cm^{-1} in the FTIR spectra (**Figure 65**, **C**).

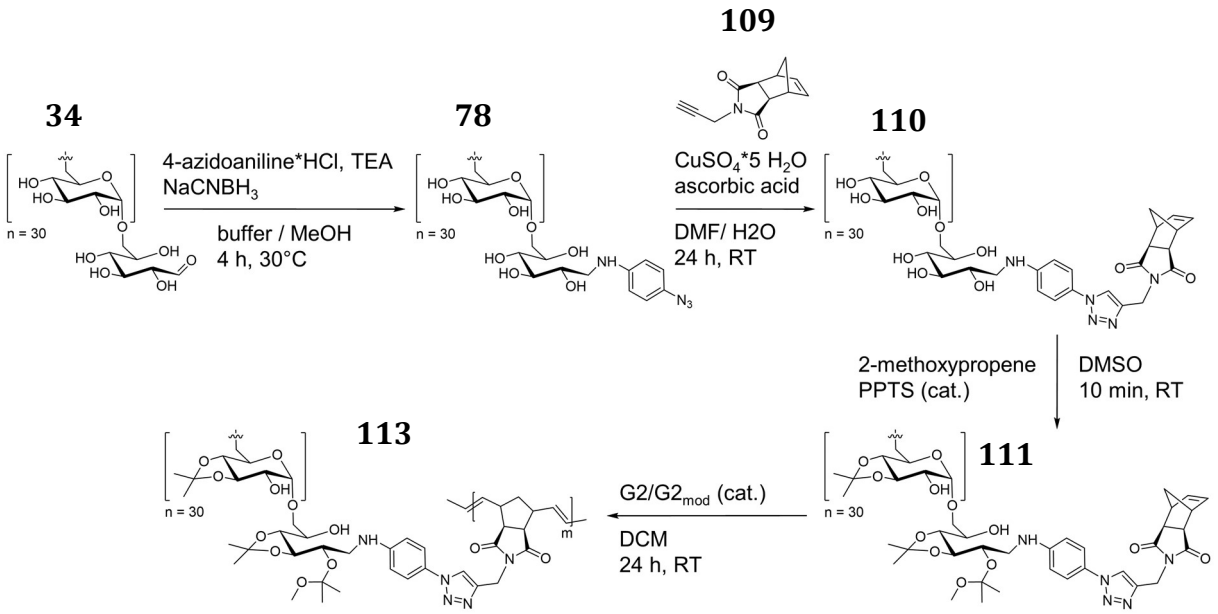

Figure 64. Synthesis and polymerization of AcDex-click-C_1-Norb MM **111** with C_1 linker. Norbornene **109** was synthesized as described in literature and conjugated to Dex-N_3 **78**.[200] After acetalization of the dextran backbone, the hydrophobic AcDex-C1-Norb **111** was polymerized with either *Grubbs* 2 or modified *Grubbs* 2 ($2_{mod.}$) catalyst. *Grubbs* 2_{mod} catalyst was prepared from *Grubbs* 2 and pyridine, as described by several groups.[201]

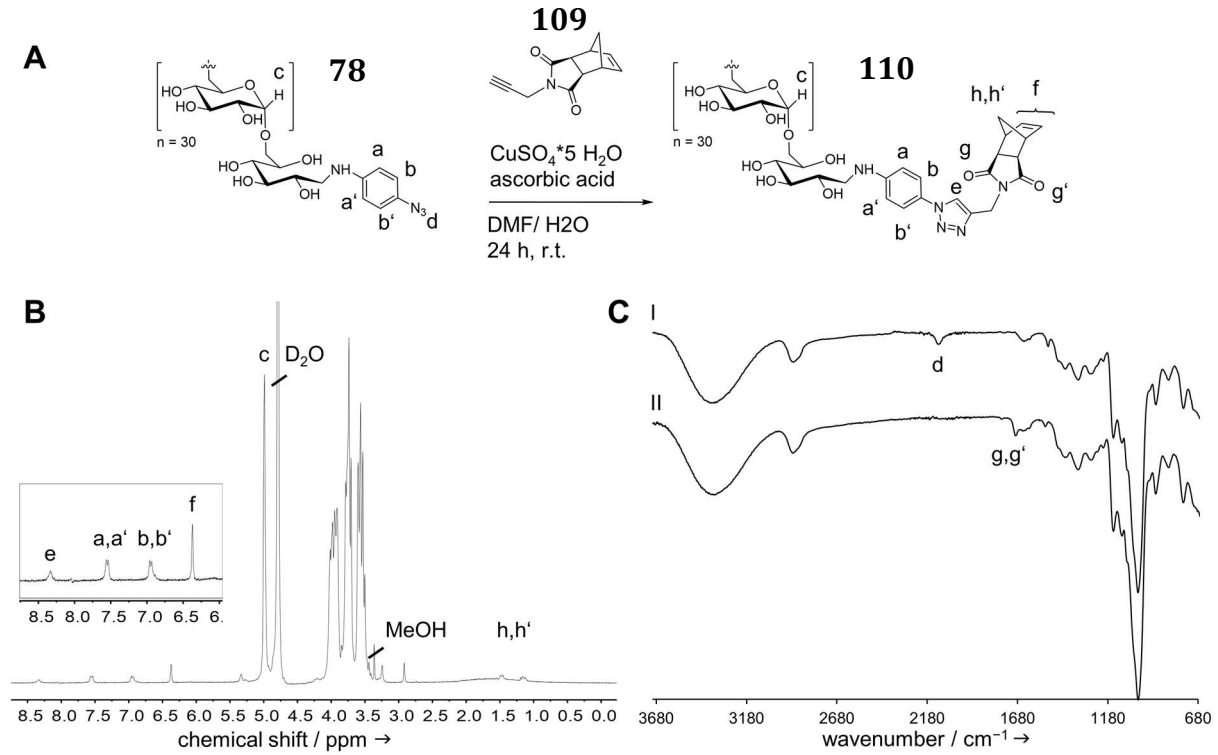

Figure 65. Synthesis of Dex-click-C_1-Norb MM **107** (**A**). ^1H NMR (300 MHz, D_2O). The norbornene end group density was quantified by calculating the ratio of anomeric proton (c) to norbornene proton (f) (**B**). The FTIR spectrum of Dex-N_3 **78** (I) and Dex-click-C_1-Norb **110** (II) shows the consumption of the azide functionality (d) during the click reaction and the appearance of a C=O stretch from the carbonyl bond of the introduced norbornene linker **109** (**C**).

In the *^1H* NMR spectra, integration of the triazole proton signal (8.33 ppm), the anomeric proton signal (4.98–5.00 ppm) and the characteristic norbornene-alkene group signals (6.37 ppm) allowed to determine an end group density of 86%mc for the Dex-click-C_1-Norb MM **113**. Since it was planned to use a Ru-based *Grubbs* catalyst (**Figure 67**) as initiator for the polymerization, the acetalization of the water-soluble MM was necessary to minimize the amount of free hydroxyl groups coordinating with the metal center of the catalyst. Additionally, the MM is turned soluble in organic solvents and can be deprotected under mild acidic conditions (pH<6, r.t.). This is desirable, as ROMP polymerizations with *Grubbs* 1–3 catalyst (G1–3) typically proceed best in dry, polar and non-coordinating solvents (e.g. DCM, EtOAc or toluene) but the product is supposed to be water soluble.[63] Acetalization of the backbone hydroxyl groups was achieved as described in the previous **Chapters 3.2.1** and **3.3.2.** The resulting AcDex-click-C_1-Norb MM **111** had an acetal coverage of 79% (54% cyclic, 25% acyclic) and a molecular weight of approx. $M_{w.NMR}$ 6603 g mol^{-1} ($M_{w,GPC}$ 4589 g mol^{-1}; PDI of 1.26).

3.5.2 ROMP OF ACDEX-CLICK-C_1-NORB MM

First attempts for the polymerization of AcDex-click-C_1-Norb macromonomer **111** were carried out in high concentration (0.05 M) with a ratio of macromonomer [MM] to initiator [I] of 100:1 and *Grubbs* 2nd generation catalyst (G2) **19** (**Table 16**).[200] After 24 h, the reaction solution had turned into a gel. A small amount of DCM had to be added, the polymerization was quenched by adding 10 equivalents of ethyl-vinyl ether and the product was precipitated in H_2O-dd. GPC analysis of the isolated crude material revealed, that only 19% of the MM **111** was converted to the bottle brush polymer (BB) **113**, resulting in a final molecular weight of 35 kDa and a degree of polymerization (DP) of 7. General reported reaction times for ROMP polymerizations of MMs with G2 vary from 3–10 h.[50a, 50c] As the polymerization proceeded over 24 h without full conversion, we concluded that either limited catalyst lifetime, steric repulsion at the propagating chain end or gelation of the reaction mixture might be a limiting factor, suppressing full polymerization. If limited catalyst lifetime was the reason for residual MM fractions in the SEC trace, the amount of MM would most likely vary with the concentration of G2 **19**.[202] Gelation caused by a too high reactant concentration would slow down the diffusion of monomer to the propagating chain end but just as steric crowding it would not be influenced by changing the catalyst concentration [I]. A series of polymerizations was

therefore conducted with varying ratio of [MM]:[I] under diluted conditions (0.02 M). Interestingly, all isolated products of this series had a final M_w of approx. 20–25 kDa but increasing conversion from the lowest to the highest amount of catalyst (up to 61%) (**Figure 66**, **A**). These results were consistent with the reports of other groups, where ROMP at [MM]<0.05 M led to poor monomer conversion [50a, 50d, 203] but also supported our hypothesis that steric hindrance of the reactive chain-end by the increasing density of polysaccharide side chains slow down rates of initiation and thus hamper the synthesis of higher molecular weight products.[204]

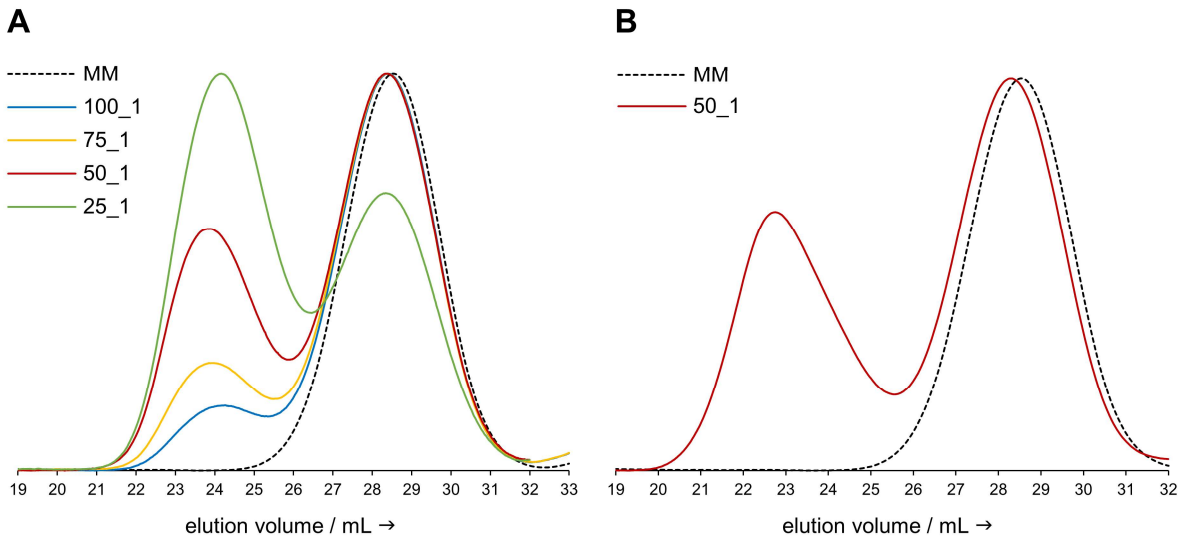

Figure 66. Normalized GPC traces of MM AcDex-click-C_1-Norb **108** and Polymer **110** (DMF, RI Detection, mPEG Std.). The ratio of MM to catalyst (I) in the reaction solution was adjusted as depicted in the key on the left. Polymerization over 24 h with G2 catalyst and [MM] 0.02 M (**A**). Polymerization 24 h with $G2_{mod}$ catalyst and [MM] 0.05 M (**B**).

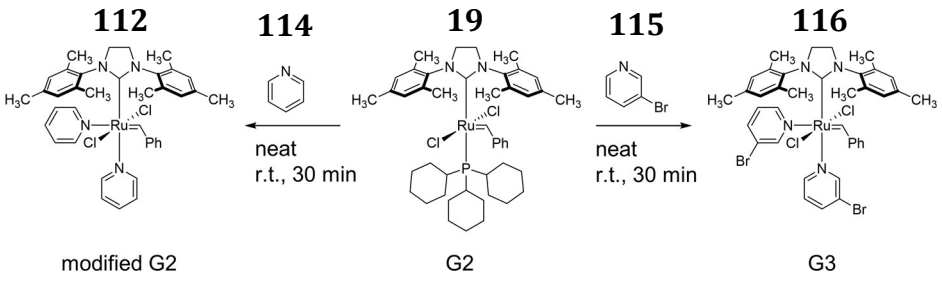

Figure 67. Ligand exchange on *Grubbs* 2nd generation catalyst (G2) **19** with pyridine **114** or 2-bromo pyridine **117** leads to the more reactive modified G2 ($G2_{mod}$) **112** and G3 **116**. The reaction proceeds in neat ligand as solvent. G3 **116** represents the most reactive Ru-based catalyst for ROMP to date and was received from commercial suppliers. Adapted with permission from *Love et al.*[201] Copyright (2002) American Chemical Society.

In an attempt to speed up reaction times and increase the rate of initiation and chain propagation, the phosphine ligand on G2 **19** was exchanged with a more labile pyridine ligand **114** like described by *Grubbs* and coworkers (**Figure 67**).[201] By using the more

reactive modified *Grubbs* 2nd generation catalyst ($G2_{mod}$) **112** it was assumed, that if the rate of polymerization surpasses the catalyst degradation rate, polymerizations can be pushed towards higher monomer conversion and thus higher molecular weights.

Therefore, the following polymerization was conducted at higher initial concentration of MM **111** (0.05 M) and $G2_{mod}$ **112** (MM:I, 50:1). SEC analysis of the product revealed that it was possible to increase the molecular weight of the BB **113** product above the initial 35 kDa, however only up to a final M_w of 45 kDa and a DP of 9, respectively (39% conversion; **Table 16**; **Figure 66**, **B**). Changing the solvent from DCM to toluene in order to avoid solvent loss by evaporation over the reaction time had no effect on the final DP but MM conversion dropped to 20%. It was not possible to achieve polymerization of high molecular weight bottlebrush polymers with MM **111**. First results indicate that a major factor for poor monomer conversion is the slow rate of polymerization known for bulky and sterically demanding macromonomers.[50b, 50c] Consequently, we decided to change the MM design towards less steric repulsion near the active site of polymerization by increasing the length and flexibility of the spacer between the dextran side chain and the norbornene functionality.

Table 16. Selected results for the polymerization of MM **111**. The DP was not changed by a variation in the ratio of [MM]:[I]. A change in the reactant concentration and catalyst activity (from *Grubbs* 2 **19** to modified *Grubbs* 2 **112**) showed the strongest influence. All reactions were performed in DCM under an athmosphere of argon at r.t.

conc. (mol L^{-1})	cat.	[MM]:[I]	$M_{w,GPC}$ (kg mol^{-1})	BB Đ*	DP	conversion* (%)
0.05	G2	100:1	35	1.26	7	19.3
0.02	"	100:1	20	n.d	5	14.1
"	"	75:1	"	n.d	"	17.6
"	"	50:1	"	n.d	"	39.4
"	"	25:1	"	n.d	"	61.0
0.05	$G2_{mod.}$	50:1	45	1.30	9	39.0

*Ascertained by SEC using absolute M_w determined by RI detection and the signal ratio of MM to BB.

3.5.3 SYNTHESIS OF ACDEX MM WITH C_6 LINKER

First attempts in the ROMP polymerization of the polysaccharide macromonomer **111** showed moderate conversion and a maximum possible DP of 9. Ideally, an optimized reaction would allow the polymerization of either low **or** high molecular weight bottlebrush species depending on the desired application. A DP of 20–30 (100–150 kDa

for a 5 kDa polymer) would be desirable for short BB, whereas a DP of 100–200 (500–1000 kDa, respectively) would be interesting for long brushes. In the context of polymer supported drug delivery, short molecular brush polymers are ideal drug carrier candidates as they can be described as covalently preassembled polymeric micelles. Just like dendrimers, they are synthesized with full control over structure, architecture and functionalization and yield particles with very low polydispersities. High molecular weight brushes are interesting for tissue engineering applications such as rigid biopolymer hydrogels and proteoglycan-mimicking structures (e.g. artificial cartilage substitute or coatings).

In order to further explore the scope of the ROMP of a polysaccharide BB, it was therefore decided to reduce steric repulsion at the active site of polymerization. A second, norbornene-containing linker molecule elongated by a linear aliphatic C_6 chain was installed at the dextran chain end (**Figure 68**) to improve reaction kinetics. When calculating with a CH_2–CH_2 bond length of l_{max} = 0.25 nm,[205] changing from a C_1 to a C_6-spacer results in an increase of roughly 1.25 nm distance between the dextran sidechain and the norbornene functionality (not including C–N bonds). Moreover, the C_6 spacer **119** should result in a higher flexibility of the polymer sidechain compared to the C_1 spacer. It was hypothesized that the new macromonomer design would further reduce steric crowding/repulsion along the polymer backbone during polymerization. Ideally, a sterically less hindered polymerization proceeds faster and thus enables higher rates of conversion and molecular weights.[50b]

The click-C_6-*N*(Ac)-Norb linker **119** was synthesized with little modifications after a procedure of *Johnson et al*. (**Figure 68**).[49]

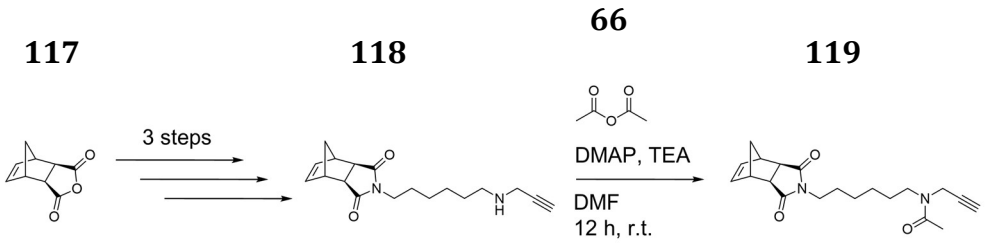

Figure 68. Synthesis of click-C_6-Norbornene linker **119**. The intermediate **118** was prepared as reported elsewhere.[49] The secondary amine was then acylated with acetic anhydride **66** to avoid chelation and deactivation of the ruthenium center of the *Grubbs* catalyst.

First, the propargylamin-C_6-norbornene linker intermediate **118** was prepared from *cis*-5-norbornene-*exo*–2,3-dicarboxylic anhydride **117** over three steps. Subsequent *N*-

acylation of the secondary amine was necessary to avoid coordination to the Ru-catalyst metal center during polymerization and therefore a loss in activity, a known phenomenon in ROMP.[206] As a proof of principle, AcDex MM terminated with norbornene linker **118** (data not shown) was polymerized in a model reaction, however no conversion was observed.

The click-C_6-*N*(Ac)-Norb linker **119** was then conjugated to azide-terminated dextran **78** as described for Dex-click-Mal **88** and Dex-click-C_1-Norb **111** (**Chapter 3.1.2**, **p.52**) and (**Chapter 3.5.1**, **p.104**) (**Figure 69**). The successful reaction was followed qualitatively by FTIR. A quantitative determination of end group densities was achieved by ^1H NMR. Integration of the triazole proton signal (8.27 ppm), the anomeric proton signal (4.98–5.00 ppm) and the characteristic norbornene-alkene group (6.20 ppm) signals in the ^1H NMR allowed to determine an end group density of 90–95%mc for Dex-click-C_6-*N*(Ac)-Norb **120**.

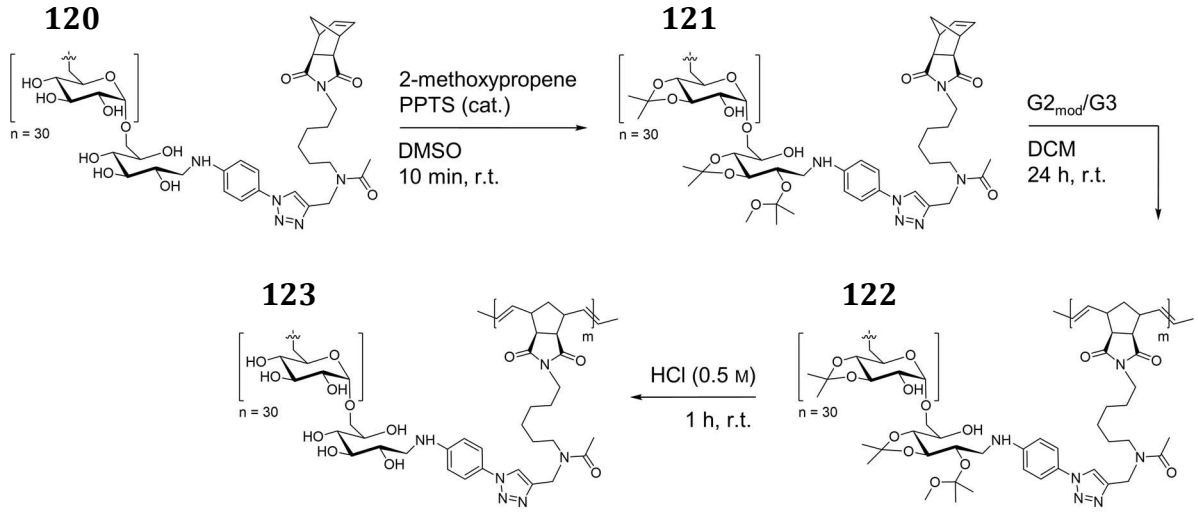

Figure 69. Synthesis of dextran bottlebrush **123** containing a prolonged click-C_6-*N*(Ac)-Norb linker **119**. The linker was Cu-clicked to Dex-N_3 **78** and the resulting MM **120** was acetalized. Polymerization of the hydrophobic AcDex-C_6-*N*(Ac)-Norb **121** was carried out with either *Grubbs* 2_{mod} **112**, or *Grubbs* 3 catalyst **116**. Subsequent deprotection in HCl gives the polysaccharide BB **123**.

Interestingly, the C_6-dextran MM **120** showed a strong foaming ability when dissolved in water, indicating surface-active properties. It has been reported before by *Zhang* and *Marchant* that the combination of low molecular weight dextrans (Mw 1600 g mol^{-1}) with either a C_6- or C_{12} aliphatic chain is sufficient to produce molecules with surfactant characteristics.[80] We did not further investigate the properties of MM **120**, however a dextran surfactant with polymerizable end group functionality would be an interesting

molecule with possible application as polysaccharide surfmer (a surface active polymer with polymerizable functionality, see outlook **p.116**).[207] The MM **120** was then acetalized and characterized as reported for MM **111** (**p.104**). The resulting hydrophobic AcDex MM **121** had an acetal coverage of 81% (51% cyclic, 30% acyclic) and a molecular weight of approx. $M_{w,NMR}$ 6559 g mol^{-1} ($M_{w,GPC}$ 5382 g mol^{-1}; PDI 1.31).

3.5.4 ROMP OF ACDEX-CLICK-C_6-N(AC)-NORB MM

The polymerization of MM **121** under similar conditions than for the MM **111** (DCM, 24 h, G2$_{mod}$ **112**) resulted in a brush **122** with slightly higher molecular weight (DP 11, approx. 55 kDa, **Table 17**). Unfortunately, an increase in spacer length between the AcDex side chain and the norbornene functionality did not lead to an improved monomer conversion, like initially expected. It was therefore investigated whether increasing the molar amount of catalyst or diluting the reaction mixture had an influence on the rate of polymerization.

Table 17. Selected results for the polymerization of MM **121**. The highest M_w was obtained for a concentration of 0.05 M with the G3 catalyst . All reactions were performed under an athmosphere of argon at r.t.

conc. (mol L^{-1})	solvent	cat.	[MM]:[I]	$M_{w,GPC}$ (kg mol^{-1})	BB Đ*	DP	conversion* (%)
0.05	DCM	G2$_{mod.}$	50:1	55	1.42	11	32.5
"	"	"	30:1	45	1.37	9	51.4
0.025	"	"	50:1	35	1.27	7	32.2
0.005	"	"	"	5	1.35	1	0
0.050	DCM	G3	50:1	70	1.42	14	24
"	EtOAc	"	"	50	1.32	10	11.1
"	DMF	"	"	35	1.20	7	7.5

*Ascertained by SEC using absolute Mw determined by RI detection and the signal ratio of MM to BB.

Although the more reactive catalyst G2$_{mod}$ **109** was employed, the obtained results were similar to earlier results described in **Chapter 3.5.2.** The maximum DP and conversion of MM **121** decreased when diluting the reaction mixture with concentrations of MM below 0.05 M, until no conversion was observed concentrations of 0.005 M (**Table 17**). This result is puzzling since BB polymers with high molecular weights (500–5000 kDa) and 70–90% conversion have been reported for MM concentrations between 0.005–0.02 M (PS $MM_{5\,kDa}$, $_{DP\ 100}$[50d]; p-(*tert*-butyl acrylate $MM_{17\,kDa}$, $_{DP\ 300}$[48]; PEG-sialic acid $MM_{4\,kDa}$, $_{DP\ 100}$[65]). Possibly, AcDex MM **121** takes on a random coil-like conformation in

solution with the active norbornene function hidden by a surrounding acetalated glucose backbone. Upon higher dilution it becomes more difficult for the propagating catalyst-monomer species to reach the active norbornene residue of an adjacent MM. When changing the ratio of MM:I from 50:1 to 30:1, monomer conversion could be improved up to 51%, however the final DP decreased from 11 to 9 (corresponding to a new M_w of 45 kDa, respectively) (**Figure 70**, **A**). The high MM concentration increases the viscosity of the solvent, thereby worsen the diffusion speed of monomer to the propagating species. At the same time, an increase in the amount of catalyst leads to an increase in the amount of initializing species while decreasing the concentration of free macromonomer neighboring the monomer-catalyst complexes. This could finally lead to the result of a smaller DP but higher monomer conversion.

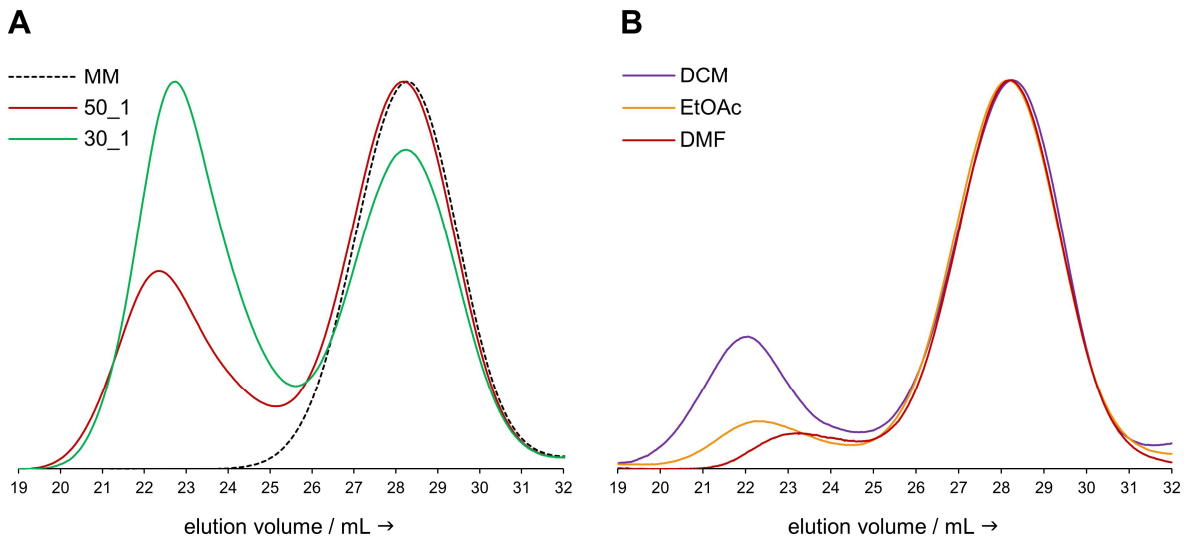

Figure 70. Normalized GPC traces of MM **121** and BB **122** (DMF, RI Detection, mPEG Std.). Polymerization over 24 h with $G2_{mod}$ **112** and varying ratio of [MM]:[I] (**A**). The effect of solvent polarity on the conversion with [MM]:[I] of 50:1 was then examined for ROMP with G3 catalyst **116** (**B**).

As suggested by *Matson et al.*, major factors limiting the maximum DP are most likely either the rate of propagation of the polymerization, or limited lifetime of the active catalyst species. Consequently, incomplete MM conversion is a result of slow propagation, as polymerization rates exceed the catalyst lifetime.[50d]

It was decided to change the catalyst from the modified G2 **112** to the more reactive 3rd generation *Grubbs* (G3) catalyst **116** (**Figure 67**) and explore the effect of different solvents on the outcome of the polymerization process. G3 has been reported as the most active of a ruthenium-based catalyst to date, with high rates of initiation and propagation.[201] First polymerizations with G3 **116** in DCM (r.t., 24 h, 0.05 M) resulted in

a BB **122** with the largest mol. weight achieved so far for the homopolymerization of a polysaccharide macromonomer (M_w 70 kDa, DP 14)(**Figure 70**, **B**). The conversion of MM **121** to BB **122** reached 24%. Polymerizations in EtOAc or DMF, solvents reported earlier as good alternate ROMP solvent, led to a significant decline in MM conversion and BB molecular weight.[50e, 65]. However, it is unclear whether the bad performance of G3 **116** in EtOAc and DMF was due to strong coordination of solvent molecules to the catalyst or because both solvents had slightly higher water content than the DCM.

Polymerization of the MM **121** was therefore conducted in DCM with G3 **116** (MM:I, 50:1) and isolated by precipitation in H_2O-dd. GPC analysis of the crude product **122** (**Figure 70**, **B**) revealed a M_w of 70 kDa and a PDI of 1.4 (monomer PDI 1.3). The acetalated OH groups of BB **122** were deprotected in 0.5 M HCl (1 h, r.t.), and residual MM **120** was removed in a centrifugal filter unit (MWCO 30 kDa, 4x10 min). Analysis of the isolated deprotected dextran BB **123** by ^1H NMR (**Figure 71**, **A** upper spectrum) showed no signal of alkene protons of the norbornene functionality at 6.20 ppm. SEC measurements further confirmed that residual MM **120** was fully removed (**Figure 71**, **B**).

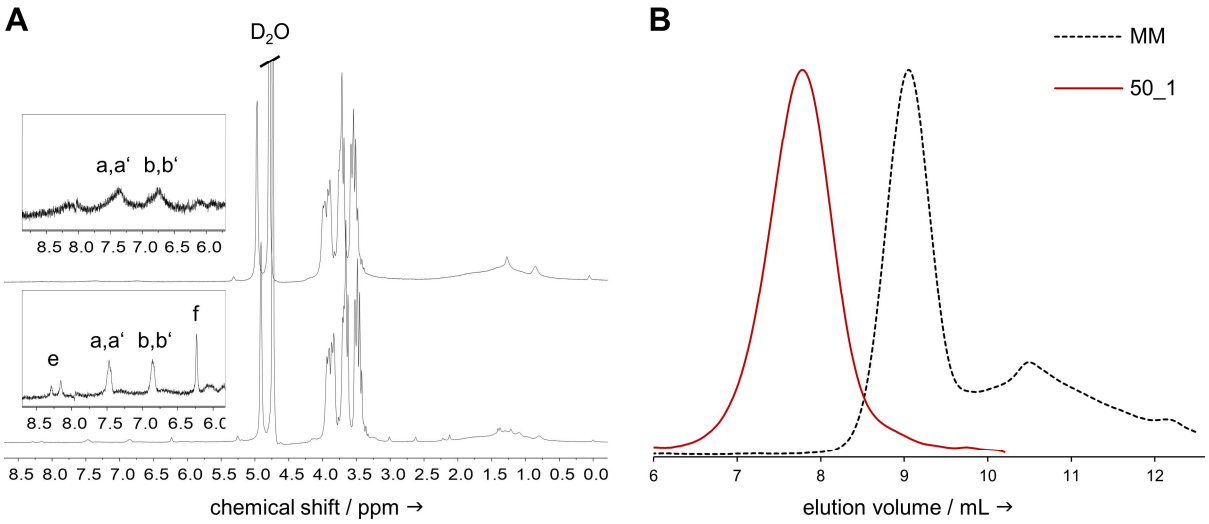

Figure 71. ^1H NMR (300 MHz, D_2O) of crude BB (lower spectrum) and purified BB **123** (upper spectrum). It is notable that the proton signal of the alkene group in the norbornene residue (**f**) is missing in the spectrum of the purified product **123** (**A**). The GPC traces (0.1 M $NaNO_3$, RI Detection, Dex Std.) of MM **120** and BB **123** show clearly a successful purification of the BB polymer.

The aqueous GPC analysis of deprotected Dex BB **123** revealed a PDI of 2.6 and a Mw of 128 kDa (monomer PdI was 1.52). However, this does not correlate with the results from GPC measurements in DMF for the crude acetalated material. *Bowden* and coworkers pointed out, that size determination of BB polymers with traditional SEC and RI detection can be problematic due to the tendency of the polymers to form shapes like rods or

random coils.[50a] Other groups reported anomalous elution times and separations.[51] Therefore further experiments should include dynamic light scattering measurements to precisely determine the molecular weight of the deprotected dextran BB **123**.

In overall summary for this project, the synthesis of two norbornene-end group-functionalized AcDex MM **111** and **121** with varying spacer length was established with high end group densities of 86–96%mc. The reactivity of the *exo*-norbornene functionality was investigated in ROMP polymerizations with the G2/G2$_{mod}$ and G3 catalyst and the first star-like polysaccharide brush polymers with M_w from 50–70 kDa were prepared (corresponding to a DP of 10–14). To the best of our knowledge, there are no reports of *grafting-through* ROMP of polysaccharide macromonomers. After deprotection, a fully water-soluble polysaccharide brush polymer was isolated, hence this represents the first polymerization of a polysaccharide MM and a BB polymer with polysaccharide side chains. Despite the fact, that additional analytical data would be beneficial to fully elucidate the obtained BB polymer structure, this project yields some very exciting and promising results. Future studies bear the potential of dextran BB polymers as functional and versatile biopolymer nanomaterials. Short brushes (~100–200 kDa) are conceivable as virus capsid-mimicking nanocarriers for drug delivery. Longer brushes of 500–1000 kDa offer exciting applications as coatings or lubricants for high performance materials or artificial cartilage in tissue engineering.

4 SUMMARY AND OUTLOOK

The main goal of this thesis was the investigation of dextran as biocompatible and non-toxic supplement to artificial polymers in amphiphilic block copolymers and to explore their surface-activity and self-assembly behavior (**Figure 72**). With our developed technique, we gained access to nine novel dextran polymer building blocks with functionalities that are chemo- and site-selectively addressable with common methods in bioconjugation chemistry. Furthermore, we provided analytical solutions for the comprehensive characterization of the structure and properties of the resulting monomers and polymers.

Hereby we would like to facilitate and inspire the creation of biocompatible high-performance polysaccharide-hybrid-polymer materials from sustainable resources, such as macrosurfactants, artificially glycosylated enzymes or polysaccharide-coated nanoparticles and surfaces. As our technique should be applicable to virtually any low-molecular weight polysaccharide with an inherent reducing end, we envision our procedure to compliment the tool box of polymer chemistry in future applications, at the interface of polymer synthesis, biochemistry and material science.

4.1 END GROUP-FUNCTIONALIZED DEXTRANS

The combination of two reported approaches of microwave chemistry and organocatalysis in a cosolvent system proved to be very effective to install several *p*-substituted aniline derivatives at the polymer chain end in high end group densities. This strategy led to five different modified dextrans useful for site-selective end-on conjugation (**Figure 72**, **blue**). Moreover, we also identified the full removal of borate-buffer by dialysis to be mandatory for further polysaccharide modification due to its tendency to chelate free hydroxyl groups at the polysaccharide backbone. We further showed that functionalities such as carboxylic acids, thiols or azides can be probed easily in model reactions with small molecules and be quantitatively analyzed by ^{1}H and DOSY NMR. During the project, it was also found that the amount of amine and reducing agent needed can be cut in half respective to the results previously reported in literature.[68b] With our technique we synthesized fully-characterized dextrans with high

chain end functionality in a substantially shortened reaction time and thus provide the foundation for the construction of complex polysaccharide-polymer macromolecules.

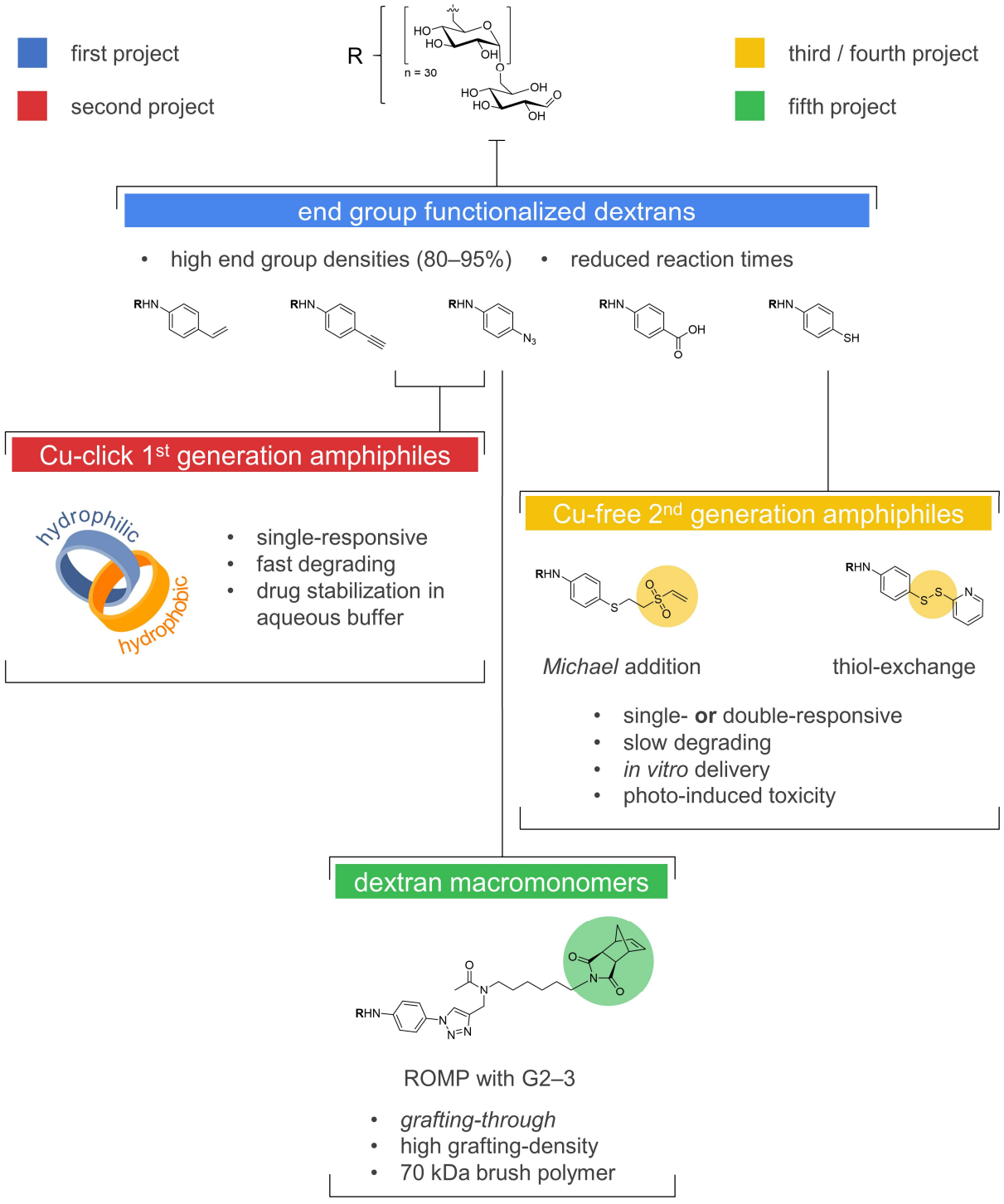

Figure 72. Proceeding from end group functionalized dextran (**blue**) an acetalized alkyne modified dextran **92** was conjugated to an azide-modified dextran **78** by Cu-catalysis. The resulting self-assmbling nanoparticle was studied with DLS (**red**). We then developed a copper-free conjugation method based on thiol-exchange and *Michael*-addition reactions. Hereby we gained access to either pH-responsive **or** reduction- and pH-responsive amphiphiles and performed in-depth analysis of surface-activity and particle morphology (**yellow**). Finally, dextran brush polymers were synthesized by ROMP from norbornene-modified dextran macromonomers. The macromonomer **111/121** was obtained by a Cu-catalyzed reaction of azide-modified dextrans and a bifunctional alkyne-norbornene linker molecule (**green**).

Outlook. In pursuit of this goal, first future experiments could therefore confirm the applicability of our procedure for functional polysaccharides like hyaluronic acid,[7b, 81, 97] heparin,[5] chitosan[84] or chondroitinsulfate.[69] It should also be investigated, whether water-soluble anilines, such as the commercially available 4-propargyloxy aniline, are suitable and posses higher performance than the applied anilines and allow higher chain end modification without the need of co-solvents.[69, 127b] Future applications could include functionalization of dextran **34** with hydroxamic acid[208] or salicyl hydroxamic acid **126** (**Figure 73**).

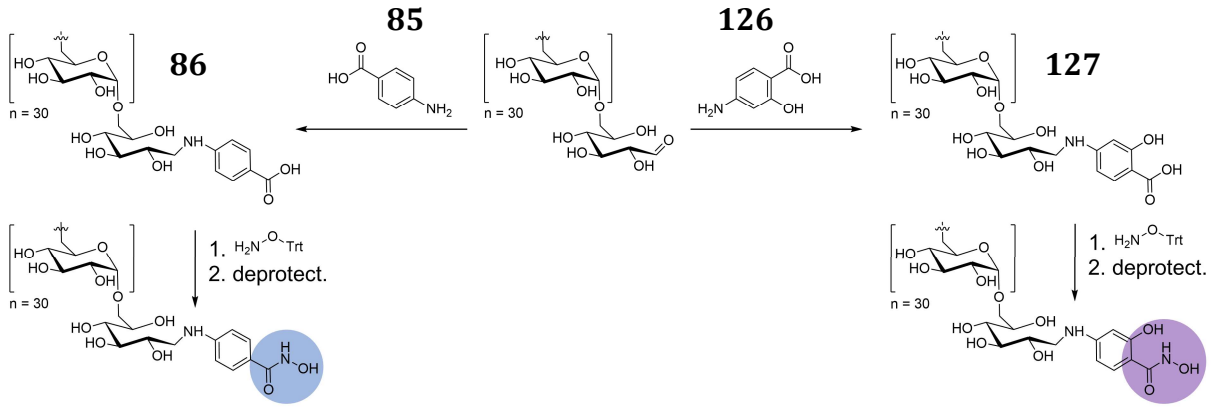

Figure 73. Possible modification of carboxylic acid-modified dextran **86** and sialic acid-modified dextran **127** include the functionalization with *N*-protected hydroxylamine.

Funtionalized dextrans could help stabilizing catalytically active metal and magnetic iron oxide nanoparticles in polar solvents,[209] offering applications as contrast agent[210], in drug delivery[211] or green catalyst in small molecule- or polymer synthesis.[209b] The salicyl hydroxamate functionality allows non-covalent and pH-responsive conjugation of dextran to functionalized surfaces or enzymes.[212] Also it would be interesting to modify dextrans at the reducing end with polymerizable short hydrophobic residues like the norbornene-linker **119**. If these MM were surface-active, they could find application as novel polysaccharide surfmers in emulsion polymerization.[207] This would allow an easy access to polysaccharide-coated polymer nanoparticles.

4.2 CU-CLICK 1ST GENERATION AMPHIPHILES

Building on the newly gained expertise in polysaccharide end group modification, we combined a linear hydrophilic Dex-N_3 block **78** with a linear hydrophobic AcDex-alkyne block **92** (**Figure 72**, **red**). The resulting block copolymer **93** had a low CMC (12 mg L^{-1}) and self-assembled into narrowly dispersed micellar spheres with a diameter of approx.

70 nm (**Figure 74**). The micelles were stable at neutral pH, but degraded under mildly acidic conditions (< pH 5) within 2–4 h.

In vitro experiments confirmed the biocompatibility of the full polysaccharide particles. Furthermore, we showed that the new amphiphilic biomaterial can stabilize the hydrophobic drug curcumin **99** in aqueous solutions, hereby significantly increasing the bioavailability over extended time periods.

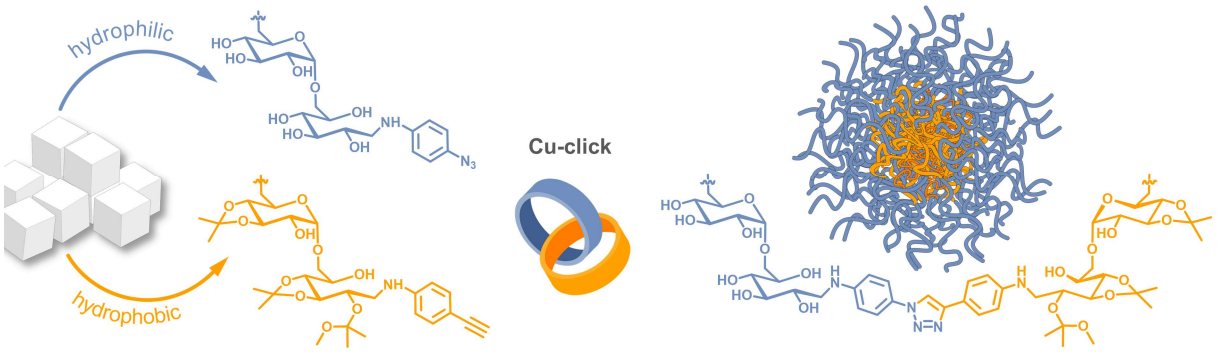

Figure 74. Hydrophilic and hydrophobic dextran building blocks are combined with Cu-click chemistry to form an acid-responsive polysaccharide block copolymer with amphiphilic properties. Adapted from *Breitenbach et. al.*[152] Copyright (2017) American Chemical Society.

We think that full polysaccharide block copolymers represent particularly interesting systems, due to their high biocompatibility, low toxicity and stimuli-responsiveness towards changes in the pH. In addition, other than many synthetic block copolymers, these natural biopolymers also offer remaining functional groups in the backbone of both blocks for a variety of modifications

Outlook. It is therefore essential for future studies to improve and accelerate the purification of the amphiphilic block copolymer. A detailed investigation of solubility in organic solvents could lead to a short precipitation work-up procedure, removing the need for long and tedious dialysis. It is also necessary to further explore the mechanism of self-assembly. Techniques like DLS and SLS but also small angle neutron scattering (SANS) could give a valuble insight in particle behavior and morphology.[25] A detailed understanding of the underlying mechanism could help to obtain full control over nanoparticle design and size distribution. This also includes the in-depth investigation of the surface-active behavior of polysaccharide block copolymers corresponding to varying ratio of hydrophilic to hydrophobic chain length and overall hydrophobicity (tunable by the amount of acetals)[80b, 197] A possible setup would consist of azide-terminated dextran and several acetalated alkyne-functionalized dextrans of varying molecular weight and

acetal content. Additional applications could then include the encapsulation of hydrophobic drugs for cancer therapy[3] or catalysts for catalysis in aqueous media.[186] More generally, it would also be interesting to see weather amphiphilic block copolymers behave schizophrenic and form inverse micelles in organic solvents.[27b, 213] Hereby, enzymes could be encapsulated and stabilized in organic solvents without covalent modification and possible decrease in activity.[7a, 214]

4.3 CU-FREE 2ND GENERATION AMPHIPHILES

Consequently, the family of full polysaccharide block copolymer amphiphiles was further developed with a focus on increasing their biocompatibility and a facilitated synthetic procedure (**Figure 72**, **yellow**-right). Starting from a thiol-modified dextran building block **84**, we exploited the selective reactivity of thiophenols in the fast dipyridyldithiol-mediated thiol-exchange reaction. As a result, we were able to conjugate a hydrophilic Dex-SH **84** and a hydrophobic AcDex-S-S-Py **101** end to end by a reductively cleavable disulfide bridge. The amphiphile **102** had self-assembly properties and a low CMC (12.6 mg L^{-1}) similar to the 1st generation amphiphile **94** (**Figure 75**). With DLS we were able to study nanoparticle degradation in different environments and clearly show two different mechanisms of structure decomposition. While the reduction of the disulfide bridge resulted in a very fast loss of amphiphilic properties and subsequent precipitation of the hydrophobic residue within 3 h, the acid-triggered degradation proceeded over 12 h in a slower, more linear fashion.

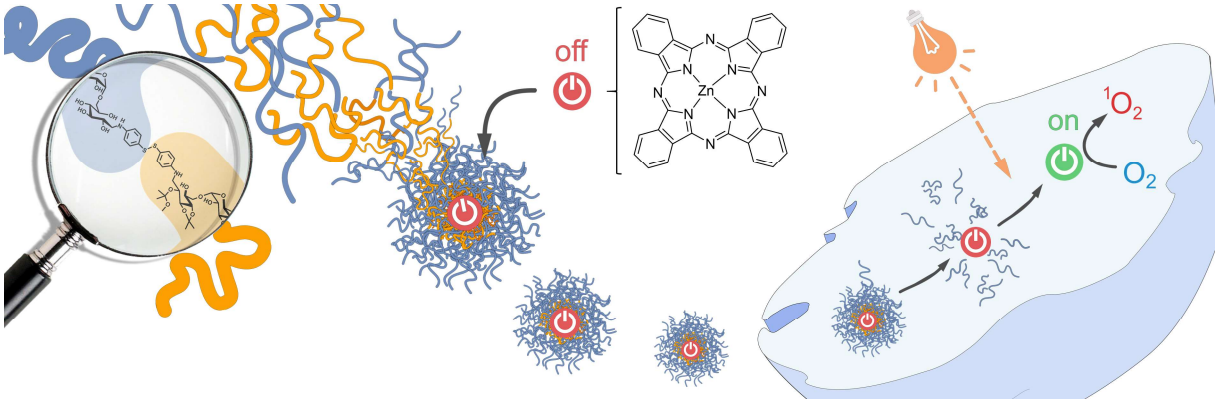

Figure 75. The double-stimulus-responsive dextran amphiphile can stabilize and deliver a hydrophobic 2nd generation photosensitizer into the cytosol of HeLa cells. Hereby, a phototoxic effect can triggered by NIR-light. Adapted from ref.[170] Copyright (2019) Royal Society of Chemistry.

In vitro studies demonstrated that the material successfully stabilizes and effectively transports the hydrophobic 2nd generation photosensitizer PC(Zn) **103** into the cytosol of

HeLa cells. Hereby we were able to trigger a controlled, strong light-induced and concentration dependent toxic effect upon irradiation with NIR light. We think that these results are especially attractive in the field of modern theranostics where polysaccharide-based amphiphiles could synergistically function with high performing photosensitizer molecules as responsive biodegradable nano-photosensitizers.

Outlook. However, for future applications in nanotherapy, particle assembly by dialysis represents a key limitation. Therefore it is necessary to explore other particle formation techniques such as dual asymmetric centrifugation (DAC), microfluidics or emulsion techniques to improve the existing protocol.[141b, 215] Consequently, the crosslinking of assembled particles would increase stability and allow faster work-up with harsher techniques like GPC or centrifugation. The cross-linked micelles could then be treated with acidic buffer to remove the hydrophobic core, leading to polysaccharide nanogels.[216] The polysaccharide scaffold allows further surface functionalization and could be applied as hydrophilic biopolymer-based platform for therapy or imaging. As monomer, both thiol-responsive building blocks **96** and **100** could be conjugated site-selectively to enzymes[151, 199, 217] and RAFT polymers.[182c, 218] RAFT polymers are especially suitable because they generally contain a free thiol end group after removal of the initiating dithioester. Hereby it would be possible to synthesize responsive giant amphiphiles or glycopolymers applicable as nanoreactor or functional polymersomes (possibly in a combination of RAFT and DAC).[7c, 219]

4.4 DIVINYLSULFONES AS ALTERNATIVE TO CUAAC

The chemo-selective reactivity of Dex-SH **84** was further explored with the homo-bifunctional linker DVS **98** (**Figure 72**, **yellow**-left). We found that a four-fold molar excess of DVS **98** was sufficient to suppress crosslinking of two polymer chains as side reaction. The resulting building block **100** enables an additional chemical ligation strategy to the thiol-exchange approach. It is hereby complementing the conjugation of Dex-SH **84** and acetalated dextran from double- to also single-stimulus responsive block copolymers. Contrary to the Cu-mediated synthesis, the reaction of Dex-SH **84** with DVS **98** or AcDex-S-VS **106** proceeded at room temperature within 12 h and without additional catalyst. The surface-activity, surfactant efficiency and effectiveness of the resulting block copolymer was tested and compared to the other polysaccharide

macrosurfactants. We observed that the DVS-conjugated amphiphiles **107** had a higher CMC and a more densely packing at the air/water interface, possibly due to the flexible linkage between the hydrophobic and the hydrophilic domain. It was clearly demonstrated that the divinylsulfone-linked block copolymer **107** was able to stabilize and encapsulate the hydrophobic model compound Nile red with good loading capacities. Particles could be freeze-dried and redissolved without cryoprotectants and loss in particle integrity. Unfortunately, a reproducible CMC determination became increasingly vague with higher acetal content in the hydrophobic block.

In summary, all three amphiphile conjugation strategies resulted in block copolymers with comparable CMC and surface efficiency. From a synthetic point of view, the DVS ligation represents an improvement to the Cu-click reaction. The dextran amphiphiles function as responsive macrosurfactants and can be applied as micellar drug delivery vehicle. Their improved synthesis, high particle stability and slow rate of triggered degradation make them suitable candidates for long circulating drug delivery vehicles.

Outlook. In order to better understand and confirm the results obtained by ringtensiometry, it would be beneficial to perform additional CMC experiments with alternative techniques such as pyrene absorption. Starting from linear amphiphiles, it would then be interesting to explore the influence of block copolymer geometry on the surface excess concentration and surfactant efficiency. Especially for rather stiff polysaccharides with high persistence length (*e.g.* cellulose)[28], the use of *m*-and *o*-substituted anilines would force the hydrophilic and hydrophobic polymer chains into different V-shaped geometries. This might trigger different behavior at the air/water interface. More generally, the influence of steric distribution or three dimensional architecture of polysaccharide polymers could be studied by applying anilines with varying substitution patterns.

4.5 BRUSHES FROM DEXTRAN MACROMONOMERS

The last project of this thesis focused on the synthesis of dextran macromonomers and their application in ROMP. In a *grafting-through* approach we were able to polymerize two different macromonomers and isolate a short polysaccharide brush polymer. We synthesized two norbornene-containing small molecules with an alkyne function and various spacer lengths between the alkyne and the norbornene functionality. Subsequent conjugation to azide-modified dextran in a Cu-click reaction led us to dextran

macromonomers with high end-group densities (85–95%). We found that the distance between the norbornene residue and the dextran polymer chain as well as the monomer concentration and catalyst reactivity play a crucial role for the polymerization of brushes with high molecular weight. Due to the fact that *grafting through* resulted in brushes with a maximum grafting density and sterically demanding propagating monomer species, polymerizations stopped at a DP of 14. For the creation of high molecular weight bottlebrushes, it is therefore necessary to further optimize the macromonomer design and polymerization reaction conditions. Nevertheless, we think that the dextran macromonomers are very valuable intermediates in the bottom-up synthesis of complex polysaccharide structures like proteoglycans.

Outlook. For a systematic reaction optimization, the first improvement would be an upscaled and robust synthesis of dextran MMs. A possible modification could avoid Cu-catalysis and proceed from amine-modified dextran and NHS-activated norbronene (**Figure 76**, **B**).[68b, 220] Since the major problem we encountered was the slow reaction kinetic, the next steps should focus on the application of norbornenes with higher ring strain (**Figure 76**, **C**) [50d, 50e, 221] but also on the steric aspects in macromonomer design.[50a, 50b]

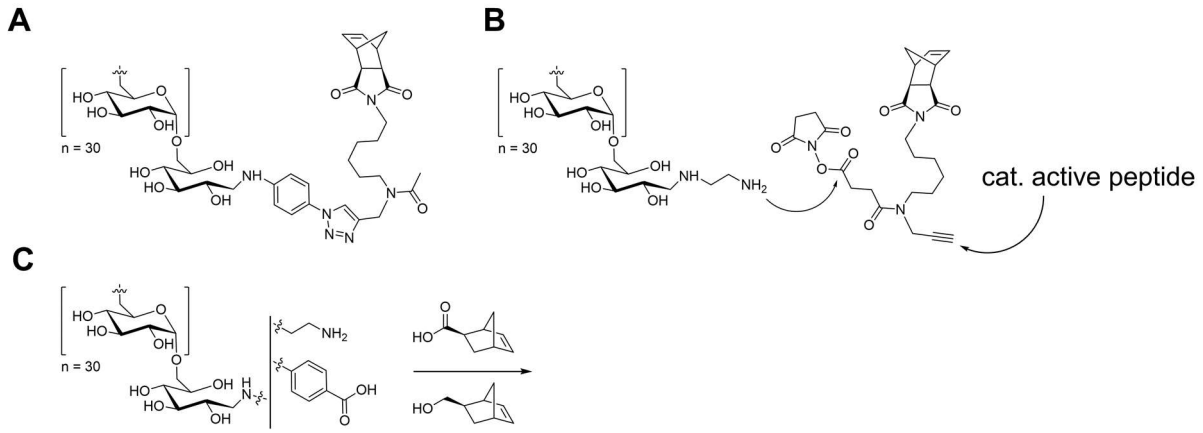

Figure 76. MM design for this thesis (**A**) and for possible future design and application (**B**). The reaction of the secondary amine with acetic anhydride gives access to a branch for peptide or drug conjugation. Possibly improvements in MM conversion would also include an investigation of more reactive norbornene residues (**C**).

Here, microwave-assisted procedures could help improving reaction kinetic.[64, 66] With optimized reaction conditions, future projects could include polysaccharide-*branch*-catalytically active peptide macromonomers (**Figure 76**, **B**).[49, 220] Subsequent ROMP would result in polysaccharide brush enzyme mimics. Furthermore, polysaccharide

bottlebrushes could find application in the field of tissue engineering as rigid biopolymer hydrogels. After sulfonylation of the polysaccharide backbone, a highly osmotic proteoglycan-like polymer (such as polyelectrolytes) could function as artificial cartilage substitute.

5 MATERIALS AND METHODS

5.1 INSTRUMENTATION AND GENERAL REMARKS

5.1.1 SOLVENTS AND REAGENTS

Air-sensitive reagents and reactions

Reagents sensitive to air and moisture were kept under Ar atmosphere throughout the reaction. All glassware was dried at least 24 h in a drying oven at 110 °C. Solvents were degassed by bubbling Ar through the stirred solution for at least 20 min. For more sensitive reactions the solvent was degassed by four freeze-pump-thaw cycles and the reaction vessels were evacuated and backfilled with Ar for at least three times before adding the solvent.

Solvents

All organic solvents were bought technical grade if not otherwise stated and purified by distillation before use. Moisture sensitive reactions were carried out in pre-dried solvents.

Table 18. chemicals used for the experiments in this thesis, including CAS number and supplier information.

chemical	supplier	CAS
11-azido-3,6,9-trioxaundecan−1-amine	Sigma Aldrich	134179-38-7
2,2'-dipyridiyldisulfide	TCI	2127-30-9
2-methoxy propene	Sigma Aldrich	116-11-0
4-aminobenzoic acid	Sigma Aldrich	150-13-0
4-aminothiophenol	TCI	1193-02-8
4-azidoaniline hydrochloride	Sigma Aldrich	91159-79-4
4-azidobenzoic acid	TCI	6427-66-3
4-ethinylaniline	acros chemicals	14235-81-5
4-ethynylbenzoic acid	chempur	10602-00-3
6-amino−1-hexanol	TCI	4048-33-3
acetic acid	Sigma Aldrich	64-19-7
acetic anhydride	Carl Roth	108-14-7
acetone (pure)	Dr. Wieland	67-64-1

chemical	supplier	CAS
ascorbic acid	Canelo	50-81-7
boronic acid	Sigma Aldrich	10043-35-3
cis-5-norbornene-*exo*−1,3-dicarboxylic anhydride	Alfa Aesar	2746-19-1
CuBr, 98 %	Alfa	7787-70-4
curcumin	TCI	458-37-7
$CuSO_4$	Alfa Aesar	7758-99-8
dextrane T5	Pharmacosmos	9004-54-0
dichloromethane anhydrous	Sigma Aldrich	75-09-1
dicyclohexylcarbodiimide (DCC)	TCI	538-75-0
diethyl ether	Carl Roth	69-19-7
dimethyl formamide (99,8 %, anhydrous)	Sigma Aldrich	68-12-1
dimethyl sulfoxide (anhydrous)	Sigma Aldrich	67-68-5
divinyl sulfone (stabilized)	TCI	77-77-0
DL-Dithiothreitol	Alfa Aesar	3483-12-3
ethyl acetate (pure)	Dr. Wieland	141-78-6
ethylenediaminetetraacetic acid	Sigma Aldrich	60-00-4
ethyl-vinylether, stabilized, 99%	Acros Organics	109-92-1
Grubbs catalyst 2nd Gen	Sigma Aldrich	246047-72-3
Grubbs catalyst 3rd Gen	Sigma Aldrich	900169-53-1
HOBt (1-hydroxybenzotriazole hydrate)	Sigma Aldrich	123333-53-9
hydrochloric acid 37%	Carl Roth	7647-01-0
magnesium sulfate	Carl Roth	7487-88-9
methanol (tech.)	VWR	67-56-1
N-Boc-aminoethanethiol	Sigma Aldrich	67385-09-5
N-Boc-ethylenediamine	TCI	57260-73-8
N-methoxycarbonylmaleimide (NMCM)	Sigma Aldrich	55750-48-6
petroleum ether (tech.)	Dr. Wieland	8032-32-4
propargylamine	Sigma Aldrich	2450-71-7
pyridine (tech.)	VWR	11-86-1
pyridinium *p*-toluensulfonate	Fluka	24057-18-1
sodium borohydride	Sigma Aldrich	16940-66-1
sodium chloride	Carl Roth	7647-14-5
sodium cyanoborohydride	Sigma Aldrich	25895-60-7
sodium dihydrogen phosphate	Amresco	7558-80-7

chemical	supplier	CAS
sodium hydroxide	Carl Roth	1310-73-1
sodium sulfate	Carl Roth	7757-82-6
tetrahydrofuran	Carl Roth	109-99-9
tetrahydrofuran (anhydrous)	Sigma Aldrich	109-99-9
toluene (anhydrous)	Sigma Aldrich	108-88-3
triethylamine	Carl Roth	121-44-8
tris-(2-carboxyethyl)-phosphine*HCl	Carl Roth	51805-45-9
zinc phthalocyanine	TCI	14320-04-8

Table 19. Deuterated solvents used for the NMR experiments in this thesis, including CAS number and supplier information.

chemical	supplier	CAS
DMSO-d6	Deutero	2206-17-1
chloroform-d	Deutero	865-49-6
deuteriumoxid	Deutero	7789-10-0
dichlormethan-d2	Deutero	1665-00-5

Buffers and media

All buffers and media were prepared using purified water (Direct-Q®) and filtered through a sterile syringe filter (0.22 μm) (CME membrane, Rotilabo®). Aqueous buffers were stored at 4 °C to prevent contamination.

Borate buffer (0.1 M, pH 8.5). 6.1 g boric acid (*Mw* 61.83 g mol^{-1}) were dissolved in water (0.8 L), then 1 g sodium hydroxide was added and diluted to 1 L.

DMEM buffer. DMEM GlutaMAX™ with phenol red was mixed with 10% FCS, 1% pyruvate and 1% penicillin-streptomycin.

Sodium acetate buffer (0.1 M, pH 5). 13.6 g sodium acetate (*Mw* 61.83 g mol^{-1}) and 3 mL acetic acid (conc.) were dissolved in water (0.5 L). The pH was adjusted with sodium hydroxide (1 M) to pH 5 and the solution diluted to 1 L.

Sodium chloride solution (20 mM, pH 7). 60 mg sodium chloride (*Mw* 58.44 g mol^{-1}) were dissolved in water (50 mL).

Sodium chloride buffer (20 mM, pH 7) with DTT (20 mM). 31 mg dithiothreitol (*Mw* 154.25 g mol^{-1}) were dissolved in NaCl solution (10 mL).

Sodium phosphate buffer (0.1 M, pH 7.4) with EDTA (10 mM). 21.7 g sodium dihydrogen phosphate hepta hydrate (*Mw* 268.03 g mol^{-1}), 80 g sodium chloride (*Mw* 58.44 g mol^{-1}), 2 g potassium chloride (*Mw* 74.55 g mol^{-1}) and 2.59 g potassium dihydrogen phosphate (*Mw* 136.09 g mol^{-1}) were dissolved in water (1 L). Then, 186 mg EDTA disodium salt was dissolved in 40 mL PBS buffer, the pH was adjusted with sodium hydroxide (1 M) to pH 7.4 and the resulting solution filled up to a volume of 50 mL.

5.1.2 DISPOSABLES

consumables	supplier
CELLSTAR® cell culture flasks 175 cm^2, 25 cm^2, 75 cm^2	Greiner Bio One
disposable cuvettes, polystyrene	Carl Roth
disposable hypodermic needles (size: 21 G)	B. Braun
disposable pipettes 2 mL, 5 mL, 10 mL, 20 mL	Sarstedt
disposable syringes 1 mL, 2 mL, 5 mL, 10 mL, 20 mL	B. Braun
filtropur S 0.2 (sterile, non-pyrogenic)	Sarstedt
filtropur S 0.45 (sterile, non-pyrogenic)	Sarstedt
microplate 96-well, flat bottom, clear	Sarstedt
microplate 96-well, flat bottom, clear, UV-Star®	Greiner Bio-One
microplate 96-well, flat bottom, black	Greiner Bio-One
pipette tips 2 μL, 250 μL, 1000 μL	Sarstedt
pipette tips (sterile) 100 μL, 300 μL, 1000 μL	Greiner Bio-One
μ-Slide 8 well plate	ibidi GmbH
tubes 15 mL, 120×17 mm, polypropylene	Sarstedt
tubes 50 mL, 114×28 mm, polypropylene	Sarstedt

5.1.3 INSTRUMENTATION

Absorption and fluorescence-based assays

All measurements involving absorption or fluorescence measurements were carried out on an Infinite® M200 Pro Plate Reader, Tecan Group Ltd., Switzerland. Data analysis was performed with the i-control 1.7 software and Microsoft Excel or Origin 7.5 V5. Absorption measurements were performed with clear 96-well microplates (flat bottom).

Fluorescence measurements were performed with black 96-well microplates (flat bottom).

Bath-Sonicator

Dissolution and resolving of samples was performed with a Sonorex Super RK 102 H, provided by Bandelin electronic. Depending on samples, sonication times were varied.

Biological safety cabinet

All cell culture experiments were performed in a sterile environment using a biological safety cabinet from Herasafe™, Kendro Laboratory Products, Langenselbold, Germany.

Centrifuges

Isolation of modified dextrans and removal of hydrophobic starting material or cargo was carried out using the following devices:

- BECKMAN Type AvantiTM J–15*[a].
- Heraeus™ Megafuge™ 8 R, Thermo Scientific*[b].
- Heraeus™ Multifuge™ X3R, Thermo Scientific*[b].

Centrifugation was performed at 45.000 x *g**[a] or 12.000 x *g**[b] for 20–25 min if not otherwise stated.

Chromatography.

Thin layer chromatography. Analytical thin layer chromatography (TLC) was performed on precoated TLC-sheets ALUGRAM®Xtra SIL G/UV_{254} silica gel 60 with fluorescent indicator UV_{254} provided by *Merck*. Stated ratios of eluents are based on volume fractions before mixing. UV-active compounds were detected with UV-light at a wavelength of λ = 254 nm and λ = 350 nm from CAMAG, Berlin. For further characterization the following dyes were applied:

Ninhydrin-reagent:	solution of 0.6 g ninhydrin in 200 mL ethanol and 6.0 mL acetic acid.
DNPH-reagent:	solution of 12 g 2.4-dinitrophenylhydrazine in 200 mL ethanol, 60 mL sulfuric acid (conc.) and 80 mL water (dest.).

Permanganate-reagent: a solution of 2.5 g sodium permanganate and 5.5 g sodium hydroxide in 250 mL water (dest.).

All TLC plates were developed with a heat gun after staining with the respective solution.

Column chromatography. Every column chromatography was performed using silica gel 60 M (40–63 µm) provided by *Macherey-Nagel*. Ratios of eluents are stated in terms of the volume fractions before mixing.

Size-exclusion chromatography (SEC). Macromolecules were characterized among others by gel permeation chromatography (GPC), a type of SEC were analytes are separated by means of their hydrodynamic diameter. SEC measurements were performed at 25 °C using an Agilent 1260 Infinity system (1260 IsoPump with 1260 LAS injector). For water soluble samples, separation was conducted on a PSS Suprema Linear M column, equipped with a UV/VIS Dual 2487 detector (Waters, Germany) and a RI–101 detector (ERC). Calibration (using dextran standards provided by PSS) and measurements were carried out in water containing 0.1 M $NaNO_3$ at a flow rate of 1 mL min^{-1}. Water unsoluble macromolecules were separated on three conjugated columns: GRAM 1000, GRAM 1000 and PSS GRAM 100 at a flow rate of 1.0 mL min^{-1}, at 60 °C. Sizes were calibrated with PEG standards, provided by PSS in DMF as solvent and the same detector system as in the aqueous system. Data was produced in collaboration with *Sandra Seywald*, Max Planck Institute for polymer research, Mainz, Germany.

In Vitro Drug Release. The release experiments were conducted on a HPLC system (Agilent 1100, Agilent, Germany) with PBS-buffer (1x concentrate) at a flowrate of 1 mL min^{-1}, 25–30 bar and r.t. (25 °C) equipped with a BioRad UNO Q1 column (BioRad, Munich, Germany) filled with Sephacryl S500-HR.

Critical micelle concentration (CMC)

Ring Tensiometry. The critical micelle concentration (CMC) for the block copolymer amphiphiles was determined using a Dataphysics DCAT 11 EC ring tensiometer equipped with a TV 70 temperature control unit, a LDU 1/1 liquid dosing and refill unit, as well as a RG 11 Du Noüy ring. Surface tension data was processed with SCAT v3.3.2.93 software. The CMC presented is a mean value of three experiments. All solutions for surface tension

measurements were stirred for 300 s at a stir rate of 50%. After a relaxation period of 120 s, three surface tension values were measured. The mean values of the three measurements were plotted against the concentration. The slopes of the traces at high concentrations as well as in the low concentration range were determined by linear regression. The concentration at the intersection of the fits determines the CMC.
The Du Noüy ring was rinsed thoroughly with water and annealed in a butane flame.

Dialysis

Purification by dialysis against distilled or double distilled (MiliQ) water was carried out to purify block copolymers or to remove residual buffer from microwave reactions. The following dialysis membranes were used:

- Spectra/Por® 6, regenerated cellulose, MWCO 1 kDa, Carl Roth GmbH.
- ZelluTrans/Roth T2, regenerated cellulose, MWCO 6–8 kDa, Carl Roth GmbH.
- ZelluTrans/Roth V-Serien, regenerated cellulose, MWCO 25.000 g mol^{-1}, Carl Roth GmbH.

Before use, the membranes were left to soak in dest water for 15 min and rinsed before loading with the dissolved samples. The solvent was changed every two hours, dialysis times vary depending on compound and are stated in the respective experimental section.

Inert gas

Also see “Air-sensitive reagents and reactions”. Ar gas was used to degas reaction solutions or to provide an inert, oxygen-free atmosphere. The argon gas bomb was provided by Air Liquide Deutschland GmbH with 99.998% purity N46.

Lyophilizer

Samples were dissolved in 50 mg ml^{-1} and frozen in liquid nitrogen. Typically, 2 mL of solvent were evaporated after 24 h. Depending on the amount of sample, freeze-drying times varied.

Mass spectrometry

Mass spectra of literature unknown compounds (small molecules) were recorded on an Agilent® LC/MSD-ion trap-mass spectrometer coupled to an upstream HP Agilent® 1100 HPLC-system, equipped with a binary pump system, a diode array detector and an

autosampler. Separation was conducted on an Agilent® Poroshell 120 EC-C_{18} column (150x2.10 mm; 4 µm) in MECN/H_2O (+ 0.1% formic acid), samples were ionized by electrospray ionization and prepared at a concentration of 0.1 mg mL^{-1}.

Microscopy

See Cell culture: Fluorescence Microscopy. Live-cell imaging was performed with a Leica TCS SP5 Microscope, equipped with an oil objective lens HC PL APO CS2 63.0x/1.40 OIL UV. The Confocal Microscope was provided by Leica Microsystems, Wetzlar, Germany.

Microwave reactions.

All microwave reactions were carried out using a Discover Benchmate microwave synthesis system (CEM, Canada). Reactions were carried out in 10 mL microwave glass vessels (10 mL, outer diameter: 1.5 cm, length 9 cm) with pressure-resistant, PTFE-coated septa. Temperature control was achieved by external infrared measurement at the bottom of the microwave loading chamber. No specific value for the internal pressure was defined. All data concerning temperature and reaction time are noted in detail in the experimental section.

NIR LED lamp

Radiation of HeLa cells for photo toxicity experiments was conducted using a Flood COB 50 Amber LED, provided by Deko Light Elektronik Vertriebs GmbH. Technical data are: $P_{electric}$ of 52 W corresponding to a P_{photo} of 3.66 W. Photo power (W) was calculated from the light intensity 1819.28 lm, radiation angle 120°, λ = 590–595 nm (λ_{max} 592 nm).[222]

pH measurement

All buffers pH values were adjusted and verified with a SevenCompact™ pH/Ion S220 with a InLab® Micro special electrode from Mettler Toledo, Mettler-Toledo Ltd., Beaumont Leys, Leicester, United Kingdom. Calibration was implemented with commercially available buffer standards (pH 4.00, pH 7.00, and pH 11.00).

Rotary evaporation

For purification and removal of solvents the following equipment was used:

- IKA RV06-ML Janke-Kunkel rotavapor; IKA HB4 water bath; Vacuubrand CVC24 vacuum controller; Vacuubrand 1715550193 Membrane pump.
- IKA RV10 rotavapor; IKA HB10 water bath; Vacuubrand CVC3000 vacuum controller; Vacuubrand VP2 Autovac chemically resistant membrane pump.

Sample concentration or solvent purification by distillation under reduced pressure was achieved by rotary evaporation in a water bath at 40–50 °C. Pressure was adjusted to the respective boiling point of the solvent.

Spectroscopy

IR-spectroscopy. All compounds were measured either as freeze-dried solid or oil without further preparation on the diamond crystal surface of a Nicolet Avatar 330-IR ATR-unit provided by Thermo Electron Corporation.

Raman spectroscopy. For all spectra, a nanosecond-based broadband coherent anti-stocks Raman scattering (CARS) spectroscopy technique was applied. The detail of the setup has been described in detail previously in Billecke et al. and Fleissner et al.[223] 4-ATP **83** was dissolved in methanol at a concentration of 0.5 mg μL^{-1}. All dextran samples were dissolved in water with a concentration of 0.5 mg μL^{-1}. After solutes were fully dissolved, the solution was slowly pipetted into a glass (24 mm x 60 mm #1 MENZEL-GLASER)-double sided tape (05338 tesa)-glass(20 mm x 20 mm #1 MENZEL-GLASER) coverslip sandwich. The glass sandwich was mounted on the CARS microscope stage and the exposure time for the CARS spectra was adjusted depending on the strength of signal, as stated in the figure captions. Specifically, we made sure that the CCD was well below saturation to avoid the non-linear artifacts in the spectra. Since CARS spectra consist of two contributions, a resonant and nonresonant component, we used a phase retrieval method to extract the resonant component, which has been shown to faithfully reproduce the Raman signal in numerous demonstrations.[224] Our implementation was written in Igor Pro 6.37 (WaveMetrics). After resonant component extraction, we spectrally shifted the 4-ATP **83** and the dextran series spectra to 2832 cm^{-1} and 2901 cm^{-1} to remove any day-to-day alignment errors. Afterward, the respective spectra were normalized with the peaks mentioned above and compared to reported values.[225] Measurements were

carried out and analyzed in cooperation with *Yujen Wang*, Max Planck Institute for polymer research, Mainz, Germany.

NMR-Spectroscopy. NMR-spectra for all compounds were recorded on the following devices:

- *Bruker*: *Topspin Fourier 300*: ^{1}H-NMR (300 MHz), ^{13}C-NMR (75.5 MHz), COSY, HSQC, HMBC.
- *Bruker: Avance III HD 400*: ^{1}H-NMR (400 MHz), ^{1}H and DOSY NMR.

For standard analytical purpose and quantification of the end group density, ^{1}H-NMR spectra were recorded with 10 mg substance in 0.55 mL D_2O at 300 MHz and 128 scans. DOSY spectra were recorded with 5 mg substance in 0.55 mL D_2O at 300 MHz and 16 scans. The experiments were performed at room temperature using deuterated solvents in **Table 19**. The chemical shifts were reported in ppm against the solvent signal of TMS. Signals were reported with abbreviations as follows: s = singlet, d = doublet, t = triplet, m = multiplet. Integrals were calculated by using MestReNova Software.

Table 20. Reference values for chemical shifts of all used solvents.[226]

solvent	core	δ in ppm	multiplicity
$CDCl_3$	^{1}H	7.26	s
CD_2Cl_2	^{1}H	5.32	t
	^{13}C	53.84	q
DMSO-d_6	^{1}H	2.50	quin
D_2O	^{1}H	4.79	s
DCl	-	-	-

End group density calculation. Calculation of the functional group density of all modified dextrans was stated as %modified chains (%mc) and calculated as follows:

$$\%mc = \frac{(Q_{real} \times 100)}{Q_{theor.}} \qquad \textbf{eq. 8}$$

where $Q_{theo.} = \frac{\int H_{aromatic}}{\int H_{anomer}}$ like a theoretically 100% modified polymer and Q_{real} is the quotient of the actual integrals with $\int H_{aromatic}$ set to a fixed value of 2.

Degree of acetalization. The degree of acetalation of the modified polysaccharide and the amphiphilic block copolymers was determined by ^1H-NMR. Therefore, approx. 10 mg of modified polysaccharide was dissolved under vortexing in 550 μL D_2O by adding three drops of DCl. Integration of the signals of nascent Acetone and Methanol compared to the signal of all AGU protons allowed the determination of the ratio of cyclic to acyclic acetals with **eq. 9** and **eq. 10**.

$$\text{acyclic acetals} \qquad \frac{I_H(\text{MeOH})}{I_H(\text{Dextran}) \cdot 3} \qquad \textbf{eq. 9}$$

$$\text{cyclic acetals} \qquad \frac{(I_H(\text{Aceton}) - I_H(\text{MeOH})) \cdot 2}{I_H(\text{Dextran}) \cdot 3} \qquad \textbf{eq. 10}$$

With I_H as the integral of the respective signal, where I_H(Acetone) is normalized to 1.

Theoretical molecular weight calculation of acetalized dextrans. The average g mol^{-1} of AcDex-R and Dex-R-AcDex ($M_{n,NMR}$) was calculated by ^1H NMR using equation **eq. 11**:

$$\begin{aligned} \text{n AGU} \times \Big(& 202.22\ \text{g mol}^{-1} \times \frac{\%}{100}\text{cyclic} + 234.26\ \text{g mol}^{-1} \times \frac{\%}{100}\text{acyclic} \\ & + 162.12\ \text{g mol}^{-1} \times \frac{\%}{100}\text{no acetals} \Big)\ \text{g mol}^{-1} \\ & = M_{n,NMR}\ \text{g mol}^{-1} \end{aligned} \qquad \textbf{eq. 11}$$

5.1.4 PARTICLE CHARACTERIZATION

Dynamic light scattering (DLS). Sizes and polydispersities of the self-assembled block copolymer amphiphiles were determined with single angle DLS (90°) with a Malvern Zetasizer Nano ZS instrument. Data analysis was performed with Zetasizer software 7.11 and reported like suggested in recent literature.[185] Settings are displayed in **Table 21**. Particles were suspended at concentrations of approx. 2.5–5 mg mL^{-1} either in NaCl (10 mM) or NaOAc-buffer (50 mM) or DTT/NaCl (10 mM) respectively. Samples were left to shake softly for at least 5 min, then filtered (0.22 μm). Sonication of the solution was avoided due to possible particle degradation. Sample concentrations were individually adjusted to reach an attenuator value between 5–8.

Static light scattering (SLS). Static light scattering measurements were carried out on an ALV spectrometer/goniometer (ALV Langen, Germany) equipped with a He:Ne laser (λ = 632.8 nm) and a multiple-tau full-digital correlator ALV/LSE-5004. Data was produced and analyzed in cooperation with *Christine Rosenauer*, Max Planck Institute for polymer research, Mainz, Germany.

Table 21. Applied standard settings for all DLS measurements on the Zetasizer Nano ZS device.

material:	Polystyrene Latex
	RI 1.590
dispersant:	water
	temperature 20 °C
	viscosity 1.0031 cP
	RI 1.330
cell:	ZEN0117-Disposable Low Volume Cuvette 120 μL
	173° Backscatter (NIBS default)
runs:	3x8

Zeta potential. Zeta potential (surface charge of micelles) was measured on a Zetasizer Nano ZS instrument provided by Malvern. Samples were measured in a clear disposable zeta cell cuvette. Three measurements with 12 individual runs were performed at 25 °C. Particle samples were prepared at concentrations of 2.5 mg mL^{-1} in HEPES buffer (25 mM, pH 7.4). The refractive index (RI) of the dispersant (preset: water) was adjusted to 1.330 and the viscosity to 0.8872 cP with a dielectric constant of 78.5. The RI of the particle material dextran was set to the reference value of polystyrene latex 1.590. The data was analyzed by the model of Smoluchowski with the Malvern Zetasizer software 7.11.

Transmission electron microscopy (TEM) and Cryogenic transmission electron microscopy (Cryo TEM). Tthe nanoparticle solution was drop-casted on a 300-mesh copper carbon grid from Plano GmbH and air-dried. The image acquisition was carried out with a transmission electron microscope Tecnai 12 (FEI, acceleration voltage: 120 kV, electron source: LaB6 BIO-TWIN cathode) equipped with a 4K CCD camera (Tietz). Measurements were performed by *Dr. Lydia Radi*, Group of Prof. Peter R. Wich, Institute of Pharmaceutical- and Biochemistry, Johannes Gutenberg-University, Mainz. Cryo TEM measurements were performed by *Dr. Frank Depoix*, Institute of Zoologie, Johannes Gutenberg-University, Mainz.

Theoretical molecular weight of micelle and aggregation number. By assuming that the micelle is a hard sphere, the amount of block copolymer chains forming the micellar nanoparticle (aggregation number, Na_g) can be estimated from the size of the nanoparticle. The N_{ag} was calculated with **eq. 12**, like previously reported.[105, 177, 227]

$$N_{ag} = \frac{M}{M_0} \qquad \textbf{eq. 12}$$

Where M_0 is the molecular weight of the polymer (by ^1H NMR) and M the molecular weight of the micelle. A direct determination of the molecular weight of a micelle is possible, however difficult to accomplish. M_0 can be approximated with **eq. 13**

$$M_0 = \frac{4\pi N_A R^3}{3\upsilon_2} \qquad \textbf{eq. 13}$$

With R is the radius of the micelle, N_A is Avogadro's number, and υ_2 is the partial specific volume, reported to be approx. 0.611 for dextran.[111] R_H was determined in nm from TEM and CRYO TEM.

Encapsulation efficiency (EE) and loading capacity (LC). The amount of loaded drug into the micellar nanoparticles in percentage was determined by the following **eq. 14** and **eq. 15**. The mol encapsulated drug were determined by an assay, the mass in mg by multiplication of the mol with the molecular weight respectively. The mass of block copolymer amphiphile was calculated from the lyophilized samples in mg after subtraction of the determined encapsulated cargo.

$$\text{EE (mol \%)} = \frac{n_{drug,encapsulated}}{n_{drug,feed}} \times 100\% \qquad \textbf{eq. 14}$$

$$\text{LC (wt. \%)} = \frac{m_{drug,encapsulated}}{m_{drug,encapsulated} + m_{Polymer}} \times 100\% \qquad \textbf{eq. 15}$$

Determination of curcumin loading. The mol and mg of encapsulated curcumin were determined by an external standard calibration using non-encapsulated curcumin. The free curcumin and the micellar nanoparticles containing curcumin were diluted in a Milli Q water: DMSO (1:1) mixture. The absorption of all samples was measured in tripletts of 100 µL at a wavelength of λ = 405 nm on an Infinite® 200 PRO (Tecan) plate reader. The absorbance of the background (water: DMSO) was subtracted from each measurement.

Determination of curcumin release from Dex-click-AcDex micelles. Curcumin **99** was encapsulated in Dex-b-AcDex micelles, like described in the experimental section. To monitor the release of curcumin under acidic conditions from the micelles, four samples of the particle solution (300 μL) were placed in a ZelluTrans/Roth Mini Dialyzer MD300

(MwCO 6000–8000, Carl-Roth, Germany) and dialyzed against 3 ml NaAc-buffer (0.1 M, pH 5.5). The dialysis buffer was exchanged every 2 h. The dialysis was stopped after 2, 4, 8 or 24 h, respectively. The absorbance spectrum of the initial particle solution and each dialyzed sample was recorded as triplet (3 × 100 μL on 96-well microplate, Greiner Bio-One) on an Infinite® 200 PRO (Tecan) plate reader at 405 nm. Quantification of the curcumin content was calculated like described for the curcumin loading.

Determination of PC(Zn) loading.

Briefly, 0.9 mg lyophilized micelles were dissolved in 700 µL DMSO. From the stock solution, triplets of 100 µL were added on a 96 well plate. The external standard was PC(Zn) **103** in DMSO at a concentration of $3.08 \cdot 10^{-5}$mol L^{-1}–$2.41 \cdot 10^{-7}$ mol L^{-1}. The mol PC(Zn) in micelles and free dye were determined by measuring the fluorescence intensity at 690 nm. The initial ratio of mol_{cargo} to $mol_{polymer}$ during particle formation was varied along with the feed (wt%) of cargo to the expected mass of polymer (**Table 10**). The feed of cargo was calculated according to an expected yield of 75% polymer (mol). The $mol_{cargo}/mol_{polymer}$ ratio was calculated with the isolated yield of block copolymer (mg) and the determined amount of cargo in the whole sample. The encapsulation efficiency (EE) and the loading content (LC) in weight percentage were calculated with **eq. 14** and **eq. 15**.

Determination of PC(Zn) release from Dex-click-AcDex micelles.

A stock solution of loaded nanoparticles (10 mg ml^{-1}) was diluted down to a final concentration of 5 mg ml^{-1} in either NaCl (10 mM), NaOAc (50 mM) or DTT/NaCl (10 mM) in three separate vials. After 0-, 1-, 3-, 5-, 8- and 23 h, 100 µL were removed from each vial and injected onto a sephadex column (see GPC). Integration of the area under the curve (signal at 646 nm) allowed the calculation of residual micellar PC(Zn) particles in percent, normalized to 100% at time point 0 h.

Determination of nile red loading.

Briefly, 0.97 mg lyophilized micelles were dissolved in 800 µL DMSO. From the stock solution, triplets of 100 µL were added on a 96 well plate. The external standard was nile red **108** in DMSO at a concentration of $1.56 \cdot 10^{-4}$mol L^{-1}–$2.44 \cdot 10^{-6}$ mol L^{-1}. The mol nile

red in micelles and free dye were determined by measuring the fluorescence intensity at 545 nm. The feed of cargo was calculated according to an expected yield of 75% polymer (mol). The $mol_{cargo}/mol_{polymer}$ ratio was calculated with the isolated yield of block copolymer (mg) and the determined amount of cargo in the whole sample. The encapsulation efficiency (EE) and the loading content (LC) in weight percentage were calculated with **eq. 14**and **eq. 15**.

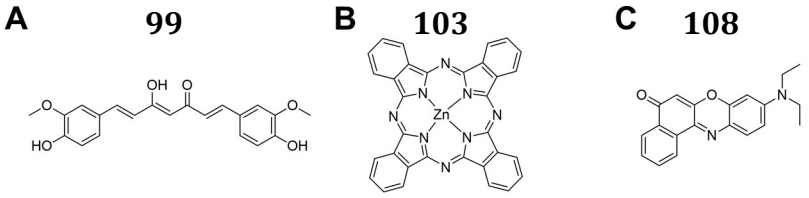

Figure 77. Chemical structures of hydrophobic molecules encapsulated into polysaccharide nanoparticles. Curcumin (**A**), PC(Zn) (**B**) and nile red (**C**).

5.1.5 CELL CULTURE

The original carcinoma cell line was isolated from a sample of cervical cancer tissue of Henrietta Lacks (1951.02.08). Cells with passage numbers of 15–25 were used for all investigations. HeLa cells were grown in Dulbecco's Modified Eagle Medium (DMEM GlutaMAX™) supplemented with 10% (V/V) fetal calf serum (FCS), 1% pyruvate, and 1% penicillin-streptomycin. Cell incubations were performed in a humidified incubator at 37 °C with 5% CO_2 atmosphere. All used buffers were either autoclaved, sterile filtered or already sterile when supplied and were preheated to 37 °C before usage. Cells were grown in 25 cm^2 or 75 cm^2 standard cell culture flasks. Before the assay, HeLa Cells were precultured in DMEM containing 10% FCS and 1% P/S and grown to a concentration of $1.5–1.6 \cdot 10^4$ cells in 100 μL per well, in sterile clear, flat bottom 96-well cell culture microplates. The cells were grown and allowed to attach overnight. All experiments involving cell culture were carried out in cooperation with *Elena Steiert, Ira Schmid* and *Matthias Konhäuser*, group of *Prof. Dr. Peter R. Wich*, Institute of pharmaceutical- and biochemistry, Johannes Gutenberg-University, Mainz.

Cellular toxicity

MTT Assay. Cellular toxicity was evaluated by the MTT assay, reported by *Mosmann* et al.[228]. Empty micellar nanoparticles and curcumin-loaded samples were prepared by mixing the micellar solutions (H_2O-dd, pH 7.4) with DMEM in a concentration range from 10 to 500 µg mL^{-1}. The next day, DMEM was removed from HeLa cells and replaced by

100 µL of the sample solutions as well as H_2O-dd diluted with DMEM as blank in the respective concentrations. All measurements were carried out in triplets. The cells were incubated for 48 hours at 37 °C in 5% CO_2. After 48 h, 40 μL MTT solution (3 mg mL^{-1} in DMEM) was added to each well and incubated at 37 °C for 30 min. After total removal of the medium, a mixture of 200 μL DMSO and 25 μL glycine buffer (0.1 M glycine, 0.1 M NaCl, pH 10.5) was added to each well and shaken for 15 min until full dissolution of the purple formazan salt. 50 μL of this concentrated, purple DMSO solution was added to a second clear, flat bottom 96-well microplate containing a mixture of 17 μL glycine buffer and 133 μL DMSO per well. Finally, the absorbance of the formazan was read using an Infinite 200 PRO (Tecan) plate reader at 595 nm. The background was measured at 670 nm and subtracted from the data obtained from the first read out. Cell viability was normalized to the absorbance of the blank samples and analyzed with excel 2016. Total cell viability was reported in %. All MTT data was produced and analyzed in cooperation with *Ira Schmid*.

WST Assay. Preincubated cells were mixed with empty and PCZn-loaded micelles dissolved in medium for 24 h in a concentration range of 0.0625–0.5 mg mL^{-1}. The cells were washed with PBS, placed on ice and irradiated from the top of the cell culture dish without a plastic cover for 15 min with a lamp at a wavelength of λ = 590–600 nm (3.6 W photo power, 1819.28 Lm light intensity). The samples were placed at a distance of 20 cm, corresponding to a light dose of ca 1 mW cm^{-1} (0.88 J cm^{-1}). The light dose was calculated with **eq. 16.** After irradiation and addition of 100 µl medium, 10 μL WST−1 reagent was added to every well. The absorption was measured after 2 h incubation time at 450 nm with a Tecan Plate reader. The relative viability was calculated as the ratio of the increase in absorption in treated cells to untreated cells. To evaluate the specific phototoxicity, the WST−1 assay was performed in dark, without the light-irradiation step. The cell viability was calculated as cell viability% by **eq. 17**. WST assay data was produced in cooperation with *Matthias Konhäuser* and analyzed in excel 2016.

$$light\ dose\ \left(\frac{W}{cm^2}\right) = \frac{P_{photo}(W)}{\pi \cdot r(cm)^2} \qquad \textbf{eq. 16}$$

with $r(cm) = distance\ from\ sample(cm) \cdot \tan\left(\frac{radial\ angle}{2}\right)$

$$cell\ viability\ (\%) = \frac{A_{sample}}{A_{control}} \times 100 \qquad \textbf{eq. 17}$$

Intracellular drug release

Flow cytometry. HELA cells were seeded in 12-well-plates at a density of approx. 200.000 per well. The cells were allowed to attach overnight, then 0.25 $mg \cdot ml^{-1}$ of PC(Zn)-loaded micelles dissolved in medium were added and the cells incubated for 24 h. Prior to the measurement, the cells were washed three times with PBS, detached with trypsin and washed again twice with PBS. Fluorescence was measured of 10000 cells in a BD© LSRFortessa flowcytometer. Samples were excited at a wavelength of λ = 640 nm and detected at λ = 670–630 nm with a bandpass filter. Data was produced in cooperation with *Matthias Konhäuser* and analyzed with FlowJo_V10.

Fluorescence microscopy. Incubation and preparation of cells with micelles was carried out at 37 °C and 5% CO_2. HeLa cells were seeded overnight in a µ-Slide 8 well plate by ibidi GmbH, Germany. After growing overnight, cells reached a density of $1.6 \cdot 10^4$ cells per well. Cells were incubated with 0.25 $mg\,mL^{-1}$ Dex-S-S-AcDex micelles containing 1.76 wt% PC(Zn) and diluted in 200 µL cell culture medium with FBS. Prior to staining for 30 min with DAPI (2 $\mu g\,mL^{-1}$ in PBS) the cells were washed three times with PBS with additional three washing steps after staining. Analysis of the cells was carried out in cell culture medium with FBS. Live-cell imaging was performed with a Leica TCS SP5 Microscope (see microscopy). The DAPI-stained cells were excited by a 405 nm Diode laser line, emission was collected at a wavelength of λ = 443–485 nm on a HyD detector. The PC(Zn) **103** was visualized by excitation at λ = 633 nm with a HeNe laser, while the emission was collected between 658–800 nm using a PMT detector. Data was produced and analyzed in cooperation with *Elena Steiert* with Fiji software.

5.2 PREPARATION METHODS

If not stated otherwise, reactions were carried out at room temperature and under air.

5.2.1 MICELLATION AND ENCAPSULATION OF GUEST MOLECULES

1st generation amphiphile. Self-assembly of block copolymer **93** was achieved like reported recently.[152] Dex-click-AcDex **93** (5 mg) was dissolved in 200 μL DMSO (or 5 mM curcumin in DMSO) and incubated to swell overnight. The solution was then slowly added into 1.8 mL of H_2O-dd at pH 8 (adjusted with TEA) with a syringe. The solution was vortexed, sonicated (3 s) and residual curcumin removed by centrifugation (12000xg, 5 min, 20 °C). The supernatant was dialyzed for 48 h (MWCO 6–8 kDa) to remove the DMSO. Samples were analyzed by DLS and TEM. The final concentration of micelle solution was determined to be 1.28 mg mL^{-1} (–) and 1.42 mg mL^{-1} (+) by lyophilization of 1 mL of micelle solution and weighing of the residual solid.

2nd generation amphiphile. The crude reaction mixture of amphiphile **102** and **107** was added to a stock solution of PC(Zn) **103** in DMSO to reach a total concentration of 0.6 μM PC(Zn) with a feed of 0.5-, 1-, 2 and 3 wt% cargo to polymer, respectively. Nile red **108** was loaded into the particles by adding a 0.67 μL crude reaction solution to a flask containing nile red to reach a final concentration of 2.5 mM dye. The solution containing block copolymer and free PC(Zn) **103** or nile red **108** was coprecipitated into a 10-fold excess H_2O-dd (pH 8, adjusted with TEA). The slightly colored solution was centrifuged (12000xg, 12 min, 20 °C) and the supernatant was collected in a dialysis bag and extensively dialyzed (MWCO 6–8 kDa) for 72 h against H2O-dd (pH 8) to ensure complete removal of not encapsulated cargo and residual non-modified dextran material. The nanoparticles were lyophilized and stored for later use.

5.2.2 SMALL MOLECULES

Literature known compounds were only characterized by comparing with reported ^{1}H NMR and Rf values. All dextran containing molecules were not characterized with ^{13}C NMR due to the high intensity of polysaccharide backbone carbon compared to introduced linker molecule.

N-propargyl maleimide 87

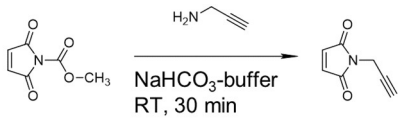

The compound was synthesized by a procedure published by *Nolte* and coworkers.[229] The substance was isolated as yellow to colorless oil and solidified upon standing in the fridge to a white wax-like solid.

Yield: 49 mg (28%, Lit.: 49%)

R*f* = 0.66 (PET/EA 3:1)

^{1}H-NMR (300 MHz, $CDCl_2$): δ = 6.76 (s, CH=CH, 2 H), 4.30–4.29 (d, J = 2.5 Hz, CH_2, 2 H), 2.21 (t, CH, 1 H) ppm

Click-C_1-norbornene linker 109

2-(prop−1-yn−1-yl)-3a,4,7,7a-tetrahydro−1H-4,7-methanoisoindole−1,3(2H)-dione

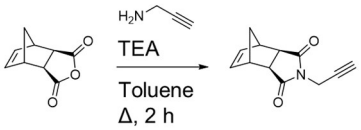

The compound was synthesized like described in recent literature.[200]

Yield: 276 mg (92%, Lit.: 92%)

R*f* = 0.22 (PET/EA 8:2)

^{1}H-NMR (300 MHz, $CDCl_2$): δ = 6.30 (s, CH=CH, 2 H), 4.24 (d, J = 2.4 Hz, CH_{2prop}, 2 H), 3.33 (s, CH_{bridge}, 2 H), 2.72 (s, CH_{Mal}, 2 H), 2.18 (t, J = 2.5 Hz, CH_{prop}, 1 H), 1.59–1.51 (m, $CH_{bridge-top}$, 1 H), 1.30–1.26 (m, $CH_{bridge-top}$, 1 H) ppm

OH-C_6-norbornene linker 125

Exo-N-(6-hydroxyhexyl)-5-norbornene–1,3-dicarboximide

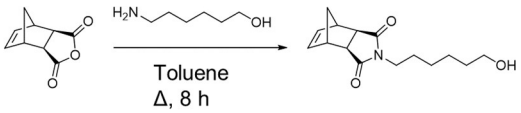

The compound was synthesized like described in recent literature.[49] The substance was isolated as a colorless oil.

Yield: 154 mg (96%, Lit.: 94%)

R_f = 0.39 (PET/EA 1:1)

^1H-NMR (300 MHz, $CDCl_2$): δ = 6.27 (s, CH=CH, 2 H), 3.62 (d, *J* = 12.9 Hz, N-CH_2, 2 H), 3.52–3.40 (m, CH_2-O, 2 H), 3.26 (s, CH_{bridge}, 2 H), 2.67 (s, CH_{Mal}, 2 H), 1.70–1.45 (m, CH_2, 6 H), 1.45–1.25 (m, CH_2, 4 H), 1.23–1.20 (d, *J* = 9.8 Hz, 1 H) ppm

Aldehyde-C_6-norbornene linker 128

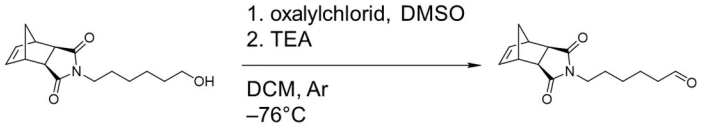

The compound was synthesized like described in recent literature.[49] Isolated as slightly yellow colorless oil.

Yield: 405 mg (84%, Lit.: 89%)

R_f = 0.27 (PET/EA 7:3)

^1H-NMR (300 MHz, $CDCl_2$): δ = 9.74 (s, CHO, 1 H), 6.27 (s, CH=CH, 2 H), 3.45 (t, J = 7.4 Hz, N-CH_2, 2 H), 3.26 (s, CH_{bridge}, 2 H), 2.67 (s, CH_{Mal}, 2 H), 2.42 (t, J = 7.2 Hz, CH_2-CO, 2 H), 1.76–1.43 (m, CH_2, 6 H), 1.43–1.11 (m, CH_2, 4 H) ppm

Propargylamin-C_6-norbornene linker 118

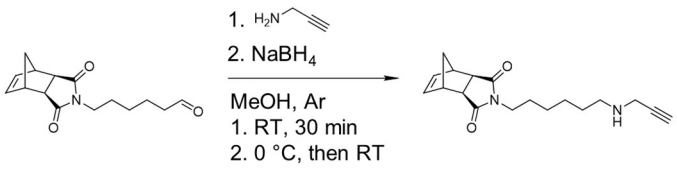

The compound was synthesized like described in recent literature with modified work up procedure.[49]

Yield: 86 mg (74%, Lit.: 78%)

R_f = 0.27 (PET/Aceton 1:1)

^{1}*H*-NMR (300 MHz, $CDCl_2$): δ = 6.27 (s, CH=CH, 2 H), 3.40 (m, CH_2-N-CH_2, 4 H), 3.26 (s, CH_{bridge}, 2 H), 2.66 (s, CH_2 and CH_{Mal}, 2 H), 2.16 (m, CH_2-CO, 2 H), 1.60–1.42 (m, $CH_{2\text{-}hex}$, 6 H), 1.38–1.29 (m, $CH_{2\text{-}hex}$, 5 H) ppm

Propargylamin-*N*(Ac)-C_6-norbornene linker 119

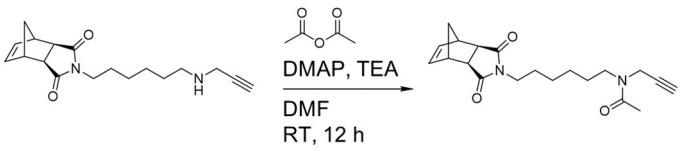

The compound was synthesized in a modified procedure from *Li* et al.[230]

Yield: 123 mg (90%)

R_f = 0.36 (PET/EA 2:8)

^{1}*H*-NMR (300 MHz, $CDCl_2$): δ = 6.28 (s, CH=CH, 2 H), 4.19 (d, *J* = 2.4 Hz, $CH_{2\text{-}prop}$, 1 H), 3.99 (d, *J* = 2.3 Hz, $CH_{2\text{-}prop}$, 1 H), 3.53–3.31 (m, $CH_{2\text{-}hex}$, 4 H), 3.26 (s, CH_{bridge}, 2 H), 2.67 (s, CH_{Mal}, 2 H), 2.24–1.98 (m, $CH_{2\text{-}bridge\text{-}top}$ and Ac, 5 H), 1.67–1.45 (m, $CH_{2\text{-}hex}$, 6 H), 1.44–1.26 (m, $CH_{2\text{-}hex}$, 5 H) ppm

^{13}*C*-NMR (75 MHz, $CDCl_2$): δ = 178.11 (2x C=O), 170.41–170.07 (N**C**OCH_3), 137.88 (2xC=C), 79.31 (**C**≡CH), 71.62 (C≡**C**H), 48.08 ($CH_{2,bridge}$), 45.23 (2x**C**-CO), 42.79 (2xCH_{bridge}), 38.48 (**C**H_2-$N_{phtalimide}$), 34.16 (**C**H_2-N(Ac)), 29.75 (N**C**H_2C≡CH), 28.32 (CH_2), 27.66 (CH_2), 26.66 (CH_2), 26.30 (CH_2), 21.82–21.42 (CO-**C**H_3)

LC-MS (m/z): calculated for [M+H+]: 343.2, found: 343.3

calculated for [M+Na+]: 365.2 found: 365.2

Grubbs mod. 2nd generation catalyst 111

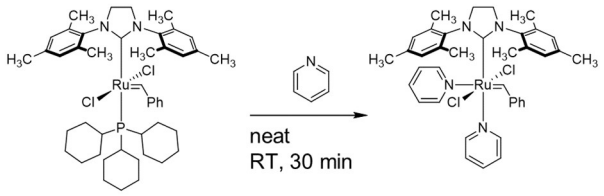

The compound was synthesized like described in recent literature.[231]

Yield: 20 mg (58%, Lit.: 89%)

^{1}H-NMR (300 MHz, $CDCl_2$): δ = 8.57 (s, H_{pyr}, 2 H), 7.78 (s, H_{pyr}, 2 H), 7.67–7.47 (s, H_{pyr}, 5 H), 7.25 (s, $H_{ortho\text{-}para}$, 2 H), 7.17–6.94 (m, meta-CH and CH_{Mes}, 5H), 6.76 (s, CH_{Mes}, 2 H), 4.15–4.04 (m, NCH_2CH_2N, 4 H), 2.61 (s, H_{mes}, 6 H), 2.32–2.20 (m, H_{mes}, 12 H) ppm

5.2.3 REDUCTIVE AMINATION AT THE DEXTRAN REDUCING END

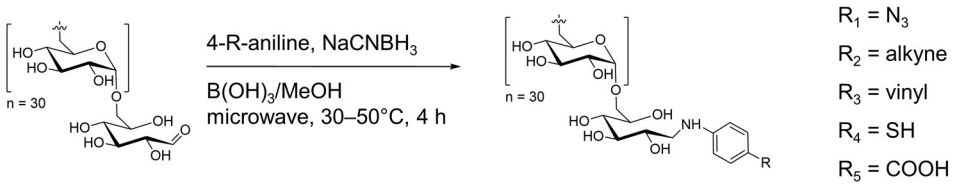

General procedure, method A

All microwave enhanced reductive amination reactions were carried out, applying a modified method of *Verma* et al.[68b] Dextran (200 mg, 0.04 mmol, 1 eq) was dissolved in 1.6 mL $B(OH)_3$-buffer (0.1 M, pH 8.3) in a sealed microwave vial. The aniline derivative (10 eq) was dissolved in 1.6 mL MeOH and slowly added under vigorous stirring to the aqueous solution. The $NaCNBH_3$ (30.2 mg, 0.48 mmol, 12 eq) was added, the vial shortly homogenized in the sonication bath for 3 sec., then placed in the microwave. The reaction was carried out with air-cooling at 50 °C for 4 h. The maximum power was set to 100 W. The product was precipitated in MeOH from a clear, slightly yellow reaction solution, homogenized in the sonication bath and centrifuged down (15000xg, 20 min, 20 °C). The pellet was taken up in 1 mL H_2O-d and precipitated again. This was repeated to a total of 3 times, then the resulting off-white pellet was dissolved in 5 mL H_2O-d and dialyzed against H_2O-d (MWCO 1 kDa) overnight to remove residual buffer salts. After freeze-drying, the purified product was obtained as off-white powder.

General procedure, method B

Reductive amination with *p*-azido-aniline hydrochloride was carried out with different concentrations and the addition of a base (TEA). Briefly, dextran (200 mg, 0.04 mmol, 1 eq) was dissolved in 1.8 mL $B(OH)_3$-buffer (0.1 M, pH 8.3) in a sealed microwave vial. The 4-azidoaniline hydrochloride (68 mg, 0.4 mmol, 10 eq) was dissolved in 0.46 mL MeOH with 61 µL NEt_3 (0.44 mmol, 11 eq) and added slowly while stirring vigorously at room temperature.

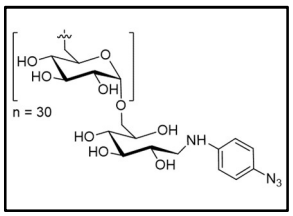

Dex-N_3 78

Due to the photosensitive nature of aromatic azides, all reactions involving azidoaniline hydrochloride were carried out in dark and at temperatures lower than 30 °C. Synthesis after method B.

Yield: 156 mg (78%), 85–90%mc

M_w (GPC, H_2O): 4469.37 g mol^{-1}; **M_w** (NMR): 4972.56 g mol^{-1}

IR (ATR): $\bar{\nu}$ = 3365 (O-H), 2919 (C-H), 2113 (N_3), 1639 (C=C, aromatic), 1515 (C=C, aromatic), 1411, 1338, 1265 (C-H, bending), 993(C-O) cm^{-1}

DOSY NMR (400 MHz, D_2O): D = $9.08 \cdot 10^{-7}$ m^2s^{-1}

^1H-NMR (300 MHz, D_2O): δ = 6.98 and 6.95 (d, H_{arom}), 6.86 and 6.83 (d, H_{arom}), 4.93 (s, H_{anom}), 3.96–3.86 (m, H_{dex}), 3.73–3.65 (m, H_{dex}), 3.56–3.45 (m, H_{dex}) ppm

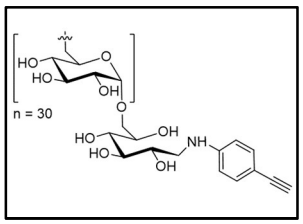

Dex-alkyne 80

Synthesis after method A.

Yield: 158 mg (79%), 73%mc

M_w (GPC, H_2O): 5874.53 g mol^{-1}; **M_w** (NMR): 4937.91 g mol^{-1}

IR (ATR): $\bar{\nu}$ = 3363 (O-H), 2920 and 2985 (C-H), 2104 (C≡C, weak), 1639 and 1608 (C=C, aromatic), 1416, 1344, 1271 (C-H, bending), 1014 (C-O) cm^{-1}

DOSY NMR (400 MHz, D_2O): D = $8.79 \cdot 10^{-7}$ m^2s^{-1}

^1H-NMR (300 MHz, D_2O): δ = 7.48 and 7.45 (d, H_{arom}), 6.85 and 6.82 (d, H_{arom}), 5.03 (s, H_{anom}), 4.06–3.96 (m, H_{dex}), 3.83–3.75 (m, H_{dex}), 3.65–3.49 (m, H_{dex}) ppm

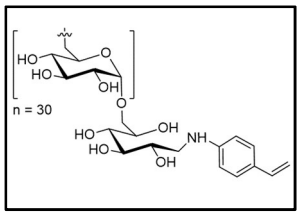

Dex-vinyl 82

Synthesis after method A.

Yield: 191.47 mg (64%), 92%mc

M_w (GPC, H_2O): 7980.84 g mol^{-1}; **M_w** (NMR): 4956.75 g mol^{-1}

IR (ATR): $\bar{\nu}$ = 3560–3126 (O-H), 2910 and 2904 (C-H), 1639 and 1595 (C=C, vinyl and aromatic), 1444–1427, 1356–1327, 1273–1261 (C-H, bending), 1014 (C-O) cm^{-1}

DOSY NMR (400 MHz, D_2O): D = $8.41 \cdot 10^{-7}$ m^2s^{-1}

^{1}H-NMR (300 MHz, D_2O): δ = 7.40 and 7.37 (m, H_{arom}), 6.84 and 6.81 (m, H_{arom}), 6.75–6.65 (m, H_{arom}), 5.68–5.62 (dd, H_{vinyl}), 5.14–5.10 (dd, H_{vinyl}), 4.98 (dd, H_{anomer}), 4.01–3.91 (m, H_{dex}), 3.77–3.70 (m, H_{dex}), 3.59–3.49 (m, H_{dex}) ppm

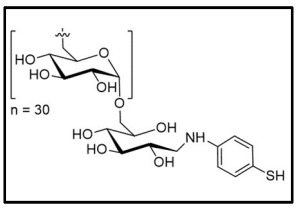

Dex-SH 84

Synthesis after method A. Due to partial oxidation of the free thiol, Dex-SH had to be reduced with either TCEP or DTT after the washing/dialysis steps. Not reduced Dex-SH (150 mg) was dissolved in 2 mL of H_2O-d in a microwave vial and capped with a septum, pierced with a syringe as pressure outlet. The solvent was degassed by bubbling Ar from an Ar-filled balloon through the stirred solution for 10 min. Then TCEP **or** DTT (2 eq to SH) was added to the yellow solution in the Ar backstream and the reaction stirred under Ar at room temperature for 1 h (with TCEP) **or** 3 h (with DTT). By the end of the reaction the reaction solution was completely colorless, and the product was isolated by 3 precipitation- and washing steps in 10-fold excess methanol. The white pellet was taken up in 2 mL H_2O-d and lyophilized directly to avoid reoxidation.

Yield: 158 mg (75%), 90–95%mc

M_w (GPC, H_2O): 6490.40 g mol^{-1}; **M_w** (NMR): 4973.99 g mol^{-1}

IR (ATR): $\bar{\nu}$ = 3340 (OH), 2910 (CH), 1640 and 1600 (C=C, aromatic), 1340 (CH_3), 989 (C-O) cm^{-1}

RAMAN (CARS): $\bar{\nu}$ = 3060 (benzene ring stretch), 2800–3000 (CH_3 stretch), 2456 (SH stretch), 1597 (CH, ring breathing) cm^{-1}

DOSY NMR (400 MHz, D_2O): $D = 9.09 \cdot 10^{-7} m^2 s^{-1}$

^{1}H-NMR (300 MHz, D_2O): δ = 7.29 and 7.26 (m, H_{arom}), 6.82 and 6.79 (m, H_{arom}), 4.98 (s, H_{anom}), 4.00–3.90 (m, H_{dex}), 3.77–3.69 (m, H_{dex}), 3.58–3.48 (m, H_{dex}) ppm

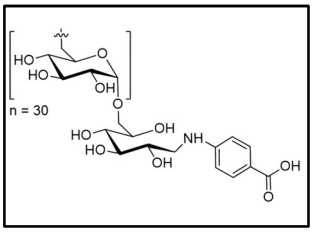

Dex-COOH 86

Synthesis after method A.

Yield: 149 mg (74.5%), 89%mc

M_w (GPC, H_2O): 7349.91 g mol^{-1}; **M_w** (NMR): 4984.94 g mol^{-1}

IR (ATR): $\bar{\nu}$ = 3657–3041 (OH), 2918 (CH), 1645 and 1608 (C=C, aromatic), 1410 and 1342 and 1267 (C-H, bending), 1147 (O-C, acid), 1016 (C-O) cm^{-1}

DOSY NMR (400 MHz, D_2O): *not measured, since not relevant; see compound* **91**

^{1}H-NMR (300 MHz, D_2O): δ = 7.83 and 7.81 (m, H_{arom}), 6.82 and 6.80 (m, H_{arom}), 4.98 (s, H_{anom}), 4.01–3.91 (m, H_{dex}), 3.77–3.70 (m, H_{dex}), 3.59–3.49 (m, H_{dex}) ppm

5.2.4 REACTIONS AT THE MODIFIED DEXTRAN CHAIN END

General Cu(II) click protocol

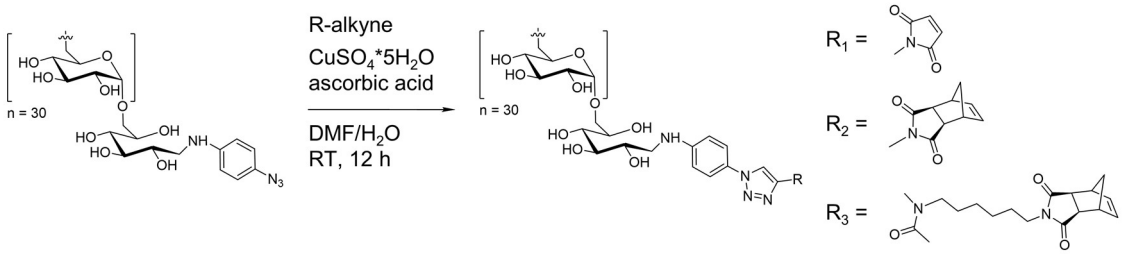

The CuAAC reaction was performed like reported previously.[199] Briefly, Dex-N_3 (100 mg, 0.02 mmol, 1 eq) and $CuSO_4 \cdot 5H_2O$ (2.5 mg, 0.01 mmol, 0.5 eq) were dissolved in a microwave vial 0.4 mL H_2O-d, then the respective alkyne-containing compound (2 eq) was added in 1.5 mL DMF. The green/blue solution was stirred until full dissolution, then ascorbic acid (8.8 mg, 0.05 mmol, 2.5 eq) was added in 0.1 mL H_2O-d to reach a ratio of DMF:H_2O of 3:1. The colored solution became orange immediately and was stirred in dark, at R.T. overnight. The next day, a grey precipitate had formed, the complete solution was precipitated in a 10-fold excess of ice cold MeOH and centrifuged down (15000xg, 20 min, 20 °C), the pellet was taken up in 1 mL H_2O-d and precipitated again. This washing procedure was repeated to a total of three runs. The grey pellet was taken up in 5 mL H_2O-d and dialyzed for 12 h (MWCO 1 kDa). Freeze-drying gave the product as white powder.

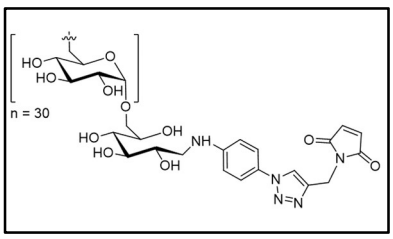

Dex-click-Mal 88

The availability of azide end groups was probed by reaction with the small molecule N-propargyl maleimide. The resulting Dex-click-Mal conjugate was not dialyzed after precipitation due the possible hydrolysis of the maleimide residue. It is necessary to say however, that before acetalization, the compound has to be dialyzed to remove residual buffer or MeOH.

Yield: 85 mg (70.4%), 93%mc

M_w (NMR): 5103.04 g mol^{-1}

IR (ATR): $\bar{\nu}$ = 3589–3049 (OH), 2912 (CH), 1705 (C=O), 1404–1336 and1263 (C=C, aromatic), 1147 (C-N), 1003 (C-O) cm^{-1}

^{1}H-NMR (300 MHz, D_2O): δ = 8.33 (m, $H_{triazol}$), 7.55–7.53 (m, H_{arom}), 6.93 (m, H_{arom} and H_{Mal}), 4.98 (s, H_{anom}), 4.01–3.91 (m, H_{dex}), 3.78–3.70 (m, H_{dex}), 3.609–3.49 (m, H_{dex}) ppm

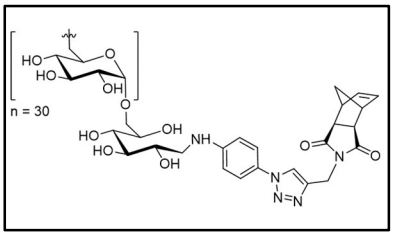

Dex-click-C_1-Norb 110

Yield: 118 mg (75.9%), 86%mc

M_w (NMR): 5183.59 g mol^{-1}

IR (ATR): $\bar{\nu}$ = 3608–3086 (OH), 2924 (CH), 1687 (C=O), 1643–1612 (C=C, alkene), 1414–1342 and1267 (C=C, aromatic), 1147 (C-N), 1012 (C-O) cm^{-1}

^{1}H-NMR (300 MHz, D_2O): δ = 8.33 (m, $H_{triazol}$), 7.56–7.54 (m, H_{arom}), 6.96–6.93 (m, H_{arom}), 6.37 (m, H_{Norb}), 4.98 (s, H_{anom}), 4.01–3.91 (m, H_{dex}), 3.78–3.71 (m, H_{dex}), 3.60–3.53 (m, H_{dex}), 3.23 (m, CH_{Norb}), 2.90 (m, CH_{Norb}), 1.49 and 1.15 (m, $CH_{2\text{-}Norb}$) ppm

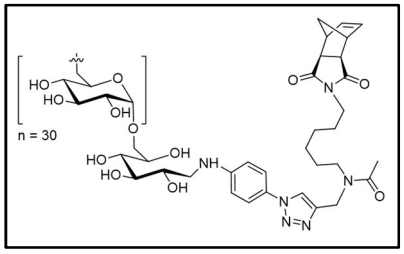

Dex-click-C_6-N(Ac)-Norb 120

Yield: 107 mg (75.3%), 95%mc.

M_w (NMR): 5324.38 g mol^{-1}

IR (ATR): $\bar{\nu}$ = 3608–3034 (OH), 2916 (CH), 1682 (C=O), 1632–1616 (C=C, alkene), 1414–1342 and1267 (C=C, aromatic), 1147 (C-N), 1012 (C-O) cm^{-1}

^{1}H-NMR (300 MHz, D_2O): δ = 8.27 (m, $H_{triazol}$), 7.52 (m, H_{arom}), 6.88 (m, H_{arom}), 6.20 (m, H_{Norb}), 4.96 (s, H_{anom}), 3.99–3.88 (m, H_{dex}), 3.71–3.67 (m, H_{dex}), 3.57–3.50 (m, H_{dex}), 3.05 (m, CH_{Norb}), 2.67 (m, CH_{Norb}), 2.26 and 2.18 (m, $CH_{3\text{-}Ac}$), 1.46–0.99 (m, $CH_{2\text{-}linker}$) ppm

General SH modification protocol

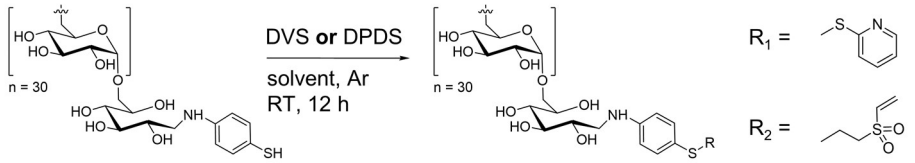

The respective activating agent (DPDS **or** DVS; 2 **or** 4 eq to SH) was dissolved in a microwave vial in 1 mL solvent and capped with a septum pierced with a syringe as pressure outlet. The solvent was degassed by bubbling Ar from a balloon through the solution for at least 15 min. Dex-SH (200 mg, 1 eq) was taken up in 1 mL solvent and added dropwise with a syringe. The clear solution was left to stir overnight. The solution was precipitated in a 10-fold excess of ice cold MeOH and centrifuged down (15000xg, 20 min, 20 °C), the pellet was taken up in 1 mL H_2O-d and precipitated again. This washing procedure was repeated to a total of three runs. The off-white pellet was taken up in 5 mL H_2O-d and dialyzed for 12 h (MWCO 1 kDa). Freeze drying gave the product as white powder.

Note: The syntheses described for the activation of Dex-SH at the thiol function (with DVS or DPDS) started from isolated Dex-SH. However, it is also possible and works faster not to isolate the Dex-SH intermediate and run the reaction, starting from commercially available dextran to the final compound only with precipitation work-up steps after the microwave reaction and the reduction. After the centrifugation, the pellet is simply taken up and dissolved in the next reaction buffer in the desired concentration. Only the final product Dex-S-VS or Dex-S-S-Py has to be dialyzed to fully remove residual buffer salts, MeOH and small molecules.

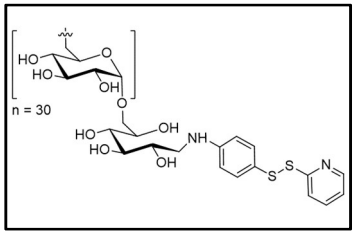

Dex-S-S-Py 96

2,2'-DPDS (11.9 mg, 0.05 mmol, 2 eq) was dissolved in 9 ml DMSO and stirred for 2 min. The reduced Dex-SH (135 mg, 0.03 mmol, 1 eq) was dissolved in 1.4 mL DMSO/H_2O-d (6:1) and added dropwise with a syringe. The clear solution turned bright yellow and was stirred overnight. The product was purified by precipitation (15000xg, 20 °C, 20 min) and two washing steps in 10-fold excess MeOH with subsequent dialysis against H_2O-d (24 h, MWCO 1 kDa).

Note: It was later found, that the reaction also works in a more concentrated setup, like described for Dex-S-VS.

Yield: 95 mg (70%), 90–95%mc

M_w (GPC): 5088.03 g mol^{-1}; **M_w** (NMR): 5079.82 g mol^{-1}

IR (ATR): $\bar{\nu}$ = 3340 (w, OH), 29008 (m, CH), 1639 and 1593 (C=C, aromatic), 1342 (m, CH_3), 1014 (s, C-O) cm^{-1}

RAMAN (CARS): $\bar{\nu}$ = 3060 (benzene ring stretch), 2800–3000 (CH_3 stretch), 1584 (CH, ring breathing).cm^{-1}

DOSY NMR (400 MHz, D_2O): $D = 8.28 \cdot 10^{-7} m^2 s^{-1}$

^1H-NMR (300 MHz, D_2O): δ = 8.42 and 8.41 (d, H_{pyr}), 7.87 (d, H_{pyr}), 7.46 and 7.43 (m, H_{arom}), 7.30 (m, H_{pyr}), 6.74 and 6.71 (m, H_{arom}), 4.96 (s, H_{anom}), 3.99–3.89 (m, H_{dex}), 3.76–3.68 (m, H_{dex}), 3.57–3.48 (m, H_{dex})ppm

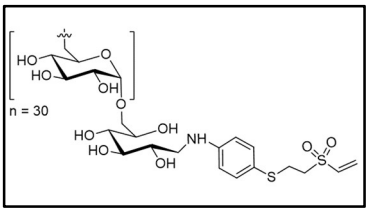

Dex-S-VS 100

The vinyl sulfone terminated dextran was synthesized after a modified procedure by *Grover* et al.[182c] Briefly, DVS (16 μL, 0.16 μmol, 4 eq) was dissolved in 1 mL PBS (10 mM EDTA). Dex-SH was taken up in 1 mL PBS (10 mM EDTA) and added dropwise with a syringe.

Yield: 161 mg (81.7%), 95%mc

M_w (GPC, H_2O): 5137.15 g mol^{-1}; **M_w** (NMR): 5079.82 g mol^{-1}

IR (ATR): $\bar{\nu}$ = 3628–3041 (w, OH), 2916 (CH), 1645 and 1599 (C=C, aromatic), 1406–1338 and 1267 (m, CH_3) 980 (s, C-O)cm^{-1}

DOSY NMR (400 MHz, D_2O): *not measured, since not relevant; see compound* **105**

^1H-NMR (300 MHz, D_2O): δ = 7.41 (d, J = 7.9 Hz, H_{arom}), 6.96–6.74 (m, $H_{arom\ and\ vinyl}$), 6.52–6.28 (s, H_{vinyl}), 5.00 (s, H_{anomer}), 3.97–3.91 (m, H_{ring}), 3.79–3.71 (m, H_{ring}), 3.58 (m, H_{ring}), 3.26–3.12 (m, H_{ethyl}) ppm

Dex-S-VS-SEtNHBoc 105

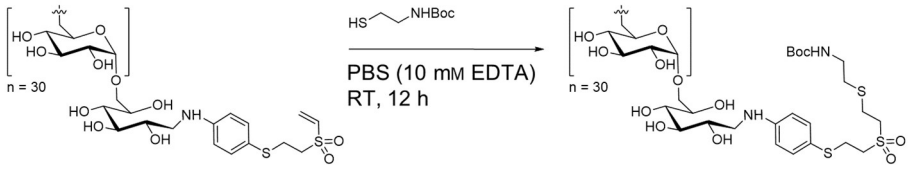

The availability of vinyl sulfone end groups was probed by reaction with the small molecule N-Boc-aminoethanthiol. Dex-S-VS (50 mg, 0.01 mmol, 1 eq) was dissolved in 0.5 mL PBS-buffer (10 mM EDTA), then N-Boc-aminoethanthiol (2.0 µL, 0.012 mmol, 1.2 eq) was added and the solution was left to stir overnight at R.T.. The next day, the colorless solution had turned milky/turbid. The product was purified by precipitation (15000xg, 20 °C, 20 min) and two washing steps in 10-fold excess MeOH with subsequent dialysis against H_2O-d (24 h, MWCO 1 kDa).

Yield: 46 mg (85%), 95%mc

IR (ATR): $\bar{\nu}$ = 3628–3030 (w, OH), 2918 (CH), 1645 and 1597 (C=C, aromatic), 1417–1344 and 1271 (m, CH_3) 1016 (s, C-O)cm^{-1}

DOSY NMR (400 MHz, D_2O): $D = 8.41 \cdot 10^{-7} m^2 s^{-1}$

^{1}*H*-NMR (300 MHz, D_2O): δ = 7.45–7.42 (m, H_{arom}), 6.87–6.84 (m, H_{arom}), 5.00 (s, H_{anomer}), 4.02–3.92 (m, H_{ring}), 3.80–3.72 (m, H_{ring}), 3.61–3.51 (m, H_{ring}), 3.29–3.19 (m, $H_{ethyl\text{-}sulfone}$), 2.92–2.87 (m, $H_{ethyl\text{-}S}$), 2.74–2.64 (m, $H_{ethyl\text{-}N}$), 1.46 (s, H_{Boc}) ppm

Dex-CONHEtNHBoc 91

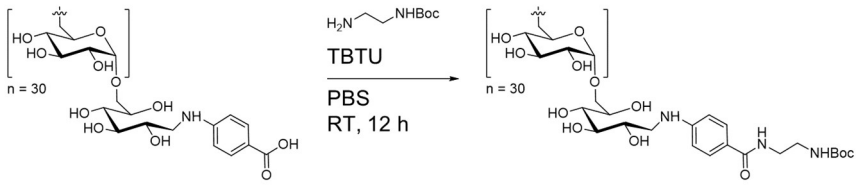

The availability of carboxyl end groups was probed by reaction with the small molecule N-Boc-ethylenediamine. The TBTU-mediated amide coupling was carried out after a modified version of *Watson* et al.[232] Briefly, Dex-COOH (50 mg, 0.01 mmol, 1 eq), DIPEA (3.4 µL, 2 eq) and N-Boc-ethylenediamine (3.2 µL, 0.02 mmol, 2 eq) were dissolved in DMSO and stirred for ca. 5 min. Then TBTU (3.8 mg, 0.012 mmol, 1.2 eq) was added in 50 µL DMSO and the solution turned bright yellow over the next 5 min. The solution was

left to stir overnight at R.T. The product was purified by precipitation (15000xg, 20 °C, 20 min) and two washing steps in 10-fold excess MeOH with subsequent dialysis against H_2O-d (24 h, MWCO 1 kDa).

Yield: 34 mg (68%), 78%mc

IR (ATR): $\bar{\nu}$ = 3610–3032 (w, OH), 2920 (CH), 1641 and 1608 (C=C, aromatic), 1518 (NH_{amide}), 1416–1342 and 1273 (m, CH_3) 1011 (s, C-O)cm^{-1}

DOSY NMR (400 MHz, D_2O): $D = 8.41 \cdot 10^{-7} m^2 s^{-1}$

^{1}H-NMR (300 MHz, D_2O): δ = 7.80–7.67 (d, J = 9 Hz, H_{arom}), 6.86–6.84 (d, J = 9 Hz, H_{arom}), 5.00 (s, H_{anomer}), 4.03–3.93 (m, H_{ring}), 3.80–3.72 (m, H_{ring}), 3.62–3.55 (m, H_{ring}), 3.33 (m, H_{ethyl}), 1.39 (s, H_{Boc}) ppm

5.2.5 ACETALIZATION OF MODIFIED DEXTRANS

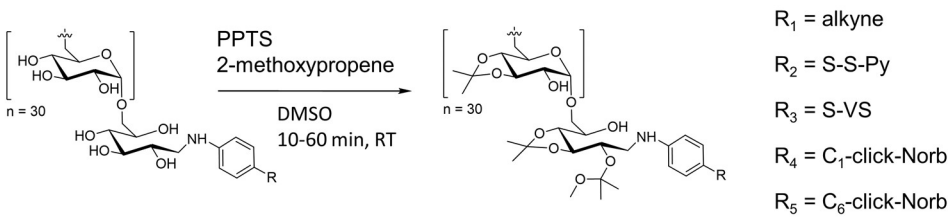

The acetalization was carried out according to a procedure described previously.[22] Modified dextran (158 mg, 0.031 mmol, 1 eq) was dissolved in 1.5 mL anhydrous DMSO in a dried flask under argon atmosphere. PPTS (5 mg, 0.026 mmol, 0.64 eq) was added and the yellow clear solution stirred for 5 min. Then 1.14 mL 2-methoxypropene (12 mmol, 380 eq) was added dropwise and the solution stirred for 10 min. The reaction was quenched by adding 0.32 mL TEA and the product precipitated in H_2O-d (pH 9, adjusted with TEA). The pellet was isolated by centrifugation (12000xg, 20 min, 20 °C) after 3 washing steps including redissolving in MeOH and subsequent precipitation in H_2O-d (pH 9). The slightly yellow pellet was lyophilized and isolated as fluffy off-white solid.

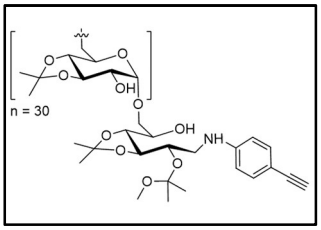

AcDex-alkyne 92

The reaction was quenched with TEA after 10 min or 60 min.

Yield: 166 mg (70.4%), 66.1% acetals

$\mathbf{M_w}$ (GPC, DMF): 5164.06 g mol^{-1}; $\mathbf{M_w}$ (NMR): 6069.39 g mol^{-1}

IR (ATR): $\bar{\nu}$ = 3427 (O-H, weak), 2987 (C-H), 2937 (C-H), 2833 (C-H), 2104 (C≡C, weak), 1659 and 1608 (C=C, aromatic), 1466 (C-H, bending), 1373, 1381 (C-H, bending), 1057 (C-O) cm^{-1}

^{1}H-NMR (300 MHz, D_2O/DCl): δ = 4.89 (s, H_{anom}), 3.91–3.40 (m, H_{Dex}), 3.26 (s, H_{MeOH}), 2.12 (s, H_{Aceton}) ppm

^{1}H-NMR (300 MHz, DMSO): δ = 7.27–7.16 (m, H_{arom}), 7.66–7.59 (m, H_{arom}), 5.48–4.90 (m, OH), 4.72 (s, H_{anom}), 3.79–3.411 (m, H_{Dex}), 3.21–3.15 (m, H_{Dex}), 1.31–1.29 (m, H_{acetal}) ppm

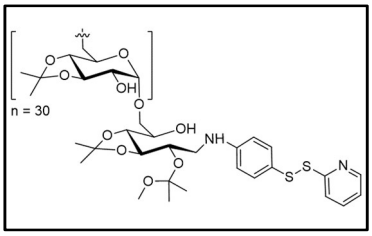

AcDex-S-S-Py 101

The reaction was quenched with TEA after 60 min.

Yield: 100.8 mg (60%), 77.6% acetals

M_w (GPC, DMF): 6601.48 g mol^{-1};

M_w (NMR): 6102.03 g mol^{-1}

IR (ATR): $\bar{\nu}$ = 2987 (C-H), 2935 (C-H), 2831 (C-H), 1655 and 1591 (C=C, aromatic), 1463 (C-H), 1373, 1381 (C-H, bending), 1057 (C-O) cm^{-1}

^{1}H-NMR (300 MHz, D_2O/DCl): δ = 3.74–3.26 (m, H_{Dex}), 3.09 (s, H_{MeOH}), 1.96 (s, H_{Aceton}) ppm

^{1}H-NMR (300 MHz, DMSO): δ = 8.45 (s, H_{arom}), 7.85 (s, H_{arom}), 7.45–7.42 (m, H_{arom}), 7.23 (m, Harom), 6.69–6.65 (m, H_{arom}), 5.51 (m, OH), 5.11 (m, OH), 4.91 (s, H_{anom}), 4.72 (m, OH), 4.29–3.54 (m, H_{Dex}), 3.20–3.14 (m, H_{Dex}), 1.32–1.28 (m, H_{acetal}) ppm

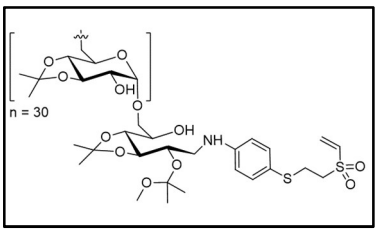

AcDex-S-VS 106

The reaction was quenched with TEA after 60, or 120 min

Yield: 142 mg (93%), 64–82% acetals

M_w (GPC, DMF):5522 g mol^{-1}; **M_w** (NMR): 6310.77 g mol^{-1}

IR (ATR): $\bar{\nu}$ = 2987 (CH), 2940 (CH), 2831 (CH), 1458–1371 (m, CH_3), 1059 (C-O) cm^{-1}

^{1}H-NMR (300 MHz, D_2O/DCl): δ = 3.77–3.20 (m, H_{Dex}), 3.13 (s, H_{MeOH}), 2.00 (s, H_{Aceton}) ppm

^{1}H-NMR (300 MHz, DMSO): δ = 7.20–7.12 (m, H_{arom}), 6.59–6.56 (m, H_{arom}), 4.91 (m, OH), 4.83 (m, OH), 4.67 (s, H_{anom}), 4.50–4.48 (m, OH), 3.74–3.42 (m, H_{Dex}), 3.20 (m, H_{Dex}), 1.33–1.29 (m, H_{acetal}) ppm

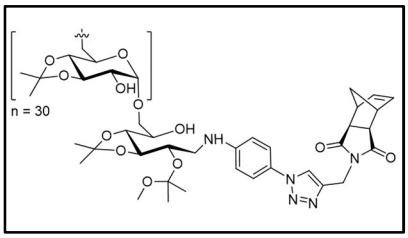

AcDex-click-C_1-Norb 111

The reaction was quenched with TEA after 60 min.

Yield: 270 mg (98 %), 79% acetals

M_w (GPC, DMF): 6601.48 g mol^{-1};

M_w (NMR): 6102 g mol^{-1}

IR (ATR): $\bar{\nu}$ = 2987 (CH), 2937 (CH), 2829 (CH), 1707 (C=O), 1524 and 1458–1371 (m, CH_3), 1207 (C-N), 1054 and 1007 (C-O) cm^{-1}

^1H-NMR (300 MHz, D_2O/DCl): δ = 8.30 (s, $H_{triazol}$), 7.75–7.72 (m, H_{arom}), 7.53–7.51 (m, H_{arom}), 6.09 (s, H_{Norb}), 4.70 (s, H_{anom}), 3.73–3.22 (m, H_{Dex}), 3.13 (s, H_{MeOH}), 2.00 (s, H_{Aceton}) ppm

^1H-NMR (300 MHz, DMSO): *Data not collected, since not necessary.*

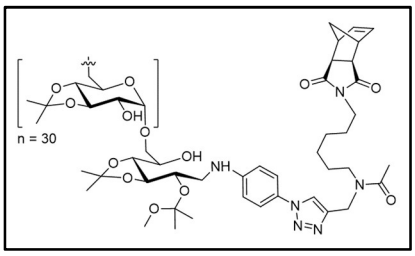

AcDex-click-C_6-N(Ac)-Norb 121

The reaction was quenched with TEA after 60 min.

Yield: 90.62 mg (64 %), 81% acetals

M_w (GPC, DMF): 5382 g mol^{-1};

M_w (NMR): 6559.56 g mol^{-1}

IR (ATR): $\bar{\nu}$ = 2985 (CH), 2931 (CH), 2827 (CH), 1701 (C=O), 1525 and 1454–1371 (CH_3), 1213 (C-N), 1153 and 1032 (C-O) cm^{-1}

^1H-NMR (300 MHz, D_2O/DCl): δ = 8.30 (s, $H_{triazol}$), 7.82–7.80 (m, H_{arom}), 7.61–7.58 (m, H_{arom}), 6.10 (s, H_{Norb}), 4.76 (s, H_{anom}), 3.79–3.27 (m, H_{Dex}), 3.13 (s, H_{MeOH}), 2.89 (s, H_{linker}), 2.58–2.56 (m, $CH_{2\text{-bridge-top}}$), 2.22 (s, H_{linker}), 2.01 (s, H_{Aceton}) ppm

^1H-NMR (300 MHz, DMSO): *Data not collected, since not necessary*.

5.2.6 BLOCK COPOLYMER CONJUGATION

Copper-mediated ligation

Dex-click-AcDex 94

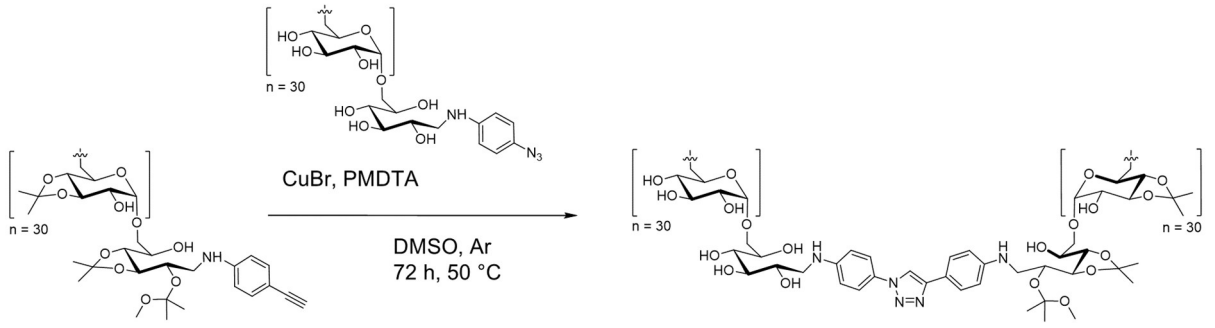

Dex-N_3 (30 mg, 6 μmol, 1 eq), AcDex-alkyne (69 mg, 11.4 μmol, 1.5 eq) and PMDTA (3.7 μL, 18 μmol, 2 eq) were dissolved in 1 mL dry DMSO and the solvent was degassed by three freeze-thaw cycles. Cu(I)Br (1.7 mg, 12 μmol, 2 eq) was added under Ar-atmosphere to the degassed solution and the reaction mixture stirred in dark for 3 d at 50 °C. The dark green solution was added to a 10-time excess of H_2O-dd (pH 9, adjusted by TEA), the unmodified AcDex residue was removed by centrifugation (12000xg, 25 min, 20 °C) and the supernatant was excessively dialyzed (MWCO 6–8 kDa) for 72 h against H_2O-dd (pH 9) to completely remove residual copper and non-modified dextran material. The product was obtained as off white solid.

Yield: 60 mg (90%), 23–30% acetals, depending on starting material.
M_w (GPC, H_2O): 6908.48 g mol^{-1}; **M_w** (NMR): 11069.39 g mol^{-1}
IR (ATR): $\bar{\nu}$ = 3369 (O-H, weak), 2979 (C-H), 2923 (C-H), 2844 (C-H), 1652 (C=C, aromatic), 1454 (C-H, bending), 1205, 1153 (C-H, bending), 1016 (C-O) cm^{-1}
DOSY NMR (400 MHz, D_2O): D = 7.28·10^{-7} m^2 s^{-1}
^{1}H-NMR (300 MHz, D_2O): δ = 8.55 (s, triazole), 7.75 and 7.73 (m, H_{arom}), 7.65 and 7.62 (m, H_{arom}), 7.00-6.94 (m, H_{arom}), 4.98 (s, H_{anom}), 4.19-3.91 (m, H-dex), 3.83-3.70 (m, H-dex), 3.60-3.32 (m, H-dex), 1.50 (s, acetals) ppm
CMC (25 °C, H_2O-dd, pH 8) = 12 mg L^{-1}

Copper-free thiol-mediated ligation: general procedure

Ligation of the Dex-SH and AcDex-S-S-Py (or AcDex-S-VS) building block was achieved as described in the following: The AcDex-R building block (R = S-S-Py, **or** S-VS) (53 mg,

8.7 μmol, 1 eq) was dissolved in 1.3 mL dry DMSO and the solvent was degassed by three freeze-thaw cycles. DTT-reduced Dex-SH (52 mg, 8.2 µmol, 1.2 eq) was added under Ar atmosphere to the degassed solution and the reaction mixture was stirred in dark for 24 h at R.T.. The yellow solution was precipitated in a 10-time excess of H_2O-dd (pH 8, adjusted by TEA). The unmodified AcDex residue was removed by centrifugation (12000xg, 12 min, 20 °C) and the supernatant was excessively dialyzed (MWCO 6–8 kDa) for 72 h against H_2O-dd (pH 9) to completely remove residual non-modified dextran material. The product was obtained after lyophilization as off white solid.

Dex-S-S-AcDex 102

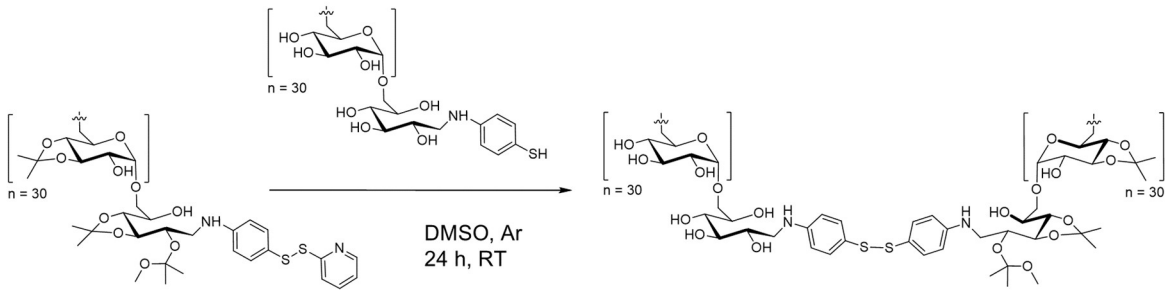

Synthesis like described in general procedure.

Yield: 72.5 mg (75%), 25.6% acetals

M_w (GPC, H_2O): 8236.29 g mol^{-1}; **M_w** (NMR): 10246.81 g mol^{-1}

IR (ATR): $\bar{\nu}$ = 3363 (OH), 2985 and 2928 (CH), 1643 and 1595 (C=C, aromatic), 1371 (CH_3), 1050 (C-O) cm^{-1}

DOSY NMR (400 MHz, D_2O): $D = 6.05 \cdot 10^{-7}$ m^2 s^{-1}

^1H-NMR (300 MHz, D_2O): δ = 7.35–7.32 (m, H_{arom}), 6.77–6.75 (m, H_{arom}), 4.96 (s, H_{anom}), 3.98–3.88 (m, H_{dex}), 3.75–3.67 (m, H_{dex}), 3.56–3.47 (m, H_{dex}), 3.29 (s, acetals), 1.47 (s, acetals) ppm

CMC (25 °C, H_2O-dd, pH 8) = 12.6 mg L^{-1}

Dex-S-VS-S-AcDex 107

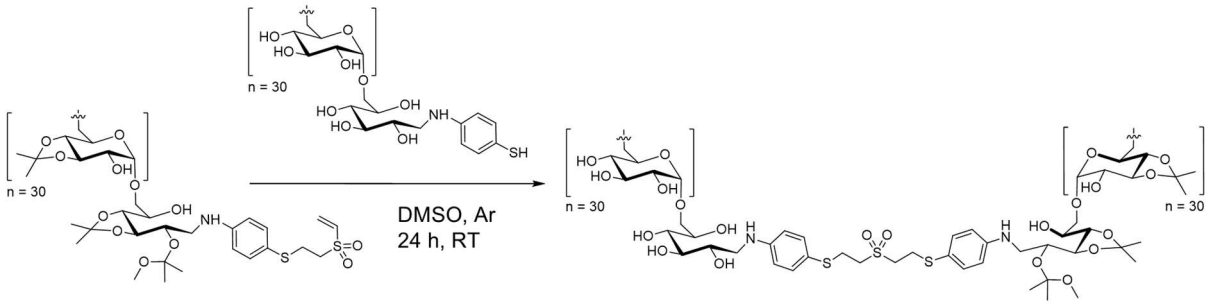

Synthesis like described in general procedure.

Yield: 75–89 mg (67–80%), 30–40% acetals (depending on AcDex-S-VS starting material)

M_w (GPC, H_2O):6736.12 g mol^{-1}; **M_w** (NMR): 11310.77 g mol^{-1}

IR (ATR): $\bar{\nu}$ = 3577–3082 (OH), 2983 and 2920 (CH), 1691 and 1597 (C=C, aromatic), 1373 (CH_3), 1146 (C-N), 1014 (C-O)cm^{-1}

DOSY NMR (400 MHz, D_2O): $D = 6.25 \cdot 10^{-7}$ m^2s^{-1}

^1H-NMR (300 MHz, D_2O): δ = 7.35–7.32 (m, H_{arom}), 6.77–6.72 (m, H_{arom}), 4.96 (m, H_{anomer}), 3.98–3.88 (m, H_{ring}), 3.75–3.67 (m, H_{ring}), 3.57–3.47 (m, H_{ring}), 3.29 (m, H_{acetal}), 1.47 (d, J = 11.9 Hz, $H_{acetone}$) ppm

CMC (25 °C, H_2O-dd, pH 8) = 21.0–30.4 mg L^{-1}. Depending on degree of acetalization

5.2.7 ROMP OF ACDEX MACROMONOMER

poly-(Dex-C_6-Norb) 123

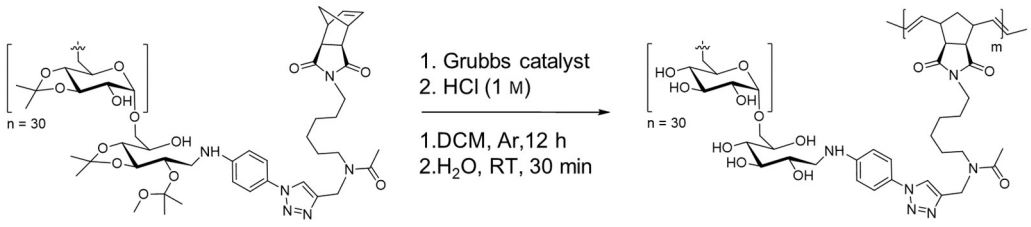

The synthesis was carried out after a modified procedure of *Grubbs* and coworkers.[49] Briefly, AcDex-click-C_6-N(Ac)-Norb macromonomer **121** (150 mg) was added to an oven-dried schlenck tube equipped with a septum. The tube was evacuated and flushed with Ar at least three times. Then, degassed DCM was added to reach a final concentration of MM 0.05 M and a stock solution of the Grubbs catalyst (MM:I; 50:1) was added with a gas tight syringe. The dark orange solution was left to stir overnight at r.t. The DCM was

removed on a rotary evaporator and the resulting oil taken up in MeOH and precipitated in H_2O-dd (15000xg, 20 min, 20 °C) The product was isolated by freeze-drying of the pellet as white powder. The powder was dissolved in 4 mL HCl (0.5 M) and stirred at r.t. for one hour. The slightly brown reaction solution was neutralized with 0.5 M NaOH and isolated in a centrifugal filter unit (MWCO 30 kDa, 6x7 min, 7500xg, 20 °C) with H_2O-d. The product was obtained by freeze-drying as a off-white solid.

Yield: 30 mg (20%)

M_w(GPC, DMF): 70000g mol^{-1} (before deprotection) **PdI** 1.42

M_w(GPC, H_2O): 128304g mol^{-1} (after deprotection) **PdI** 2.67

IR (ATR): $\bar{\nu}$ = 3617–3060 (OH), 2917 (CH), 1693 (C=O), 1624–1614 (C-N_{linker}), 1527 (C=$C_{cis,backbone}$), 1402–1344 and1270 (C=C, aromatic), 1147 (C-N), 1014 (C-O) cm^{-1}

^1H-NMR (300 MHz, D_2O): δ = 7.34 (s_{broad}, H_{arom}), 6.73 (s_{broad}, H_{arom}), 4.97 (s, H_{anomer}), 3.99–3.89 (m, H_{ring}), 3.76–3.68 (m, H_{ring}), 3.58–3.51 (m, H_{ring}), 1.27 (s_{broad}, H_{linker}), 0.85 (s_{broad}, H_{linker}) ppm

6 APPENDIX

6.1 ABBREVIATIONS

abbreviation	meaning
%mc	percent modified chains, means: end group density
°	degree (angle)
°C	degree cellsius
4-ATP	4-aminothiophenol
Å	Ångstrøm
ABA	aminobenzoic acid
abs.	absorbance
Ac	acetyl group
AcDex	acetalized dextran
AceMal	acylated maltose
AcOH	acetic acid
AGU	anhydroglucose unit
AIBN	azobisisobutyronitrile
anhydr.	anhydrous
approx.	approximately
aq.	aqueous
Ar	argon
asc. acid	ascorbic acid
ATRP	atom transfer radical polymerization
BB	bottlebrush
Boc	tert-butyloxycarbonyl group
br	broad
BSA	bovine serum albumine
Bz	benzoyl group
CDCl3	deuterated chloroform
conc.	concentration
COOH	carboxy group
CS	chondroitin sulfate
CuAAC	copper-catalyzed alkyne-azide cycloaddition

abbreviation	meaning
d	dublett
Đ	dispersity
d.nm	diameter in nanometer
D_2O	deuterated water
d_6	deuterated (6-times)
Da	dalton
DAPI	4,6-diamidino-2-phenylindole
DCC	*N,N'*-dicyclohexylcarbodiimide
DCE	dichloroethane
DCl	deuterium chloride
DCM	dichloromethane
dd	dublett of dublett
DET	diethylenetriamine
Dex	dextran
DIPEA	*N,N*-diisopropyl azodicarboxylate
DLS	dynamic light scattering
DMAEMA	2-(dimethylamino)ethyl metacrylate
DMEM	*Dulbecco*'s modified Eagle's medium
DMF	*N,N*-dimethylformamid
DMSO	dimethylsulfoxid
DNA	deoxyribonucleic acid
DOSY	diffusion-ordered spectroscopy
DP	degree of polymerization
DPDS	dipyridyl disulfide
DTAB	dodecyltrimethylammonium bromide
DTT	dithiothreitol
DVS	diviylsulfone
e.g.	*exempli gratia*, means: for example
EA	ethylacetate
EDTA	ethylenediaminetetraacetic acid
em.	emission
eq.	equivalents
Et	ethyl group

abbreviation	meaning
et al.	*et alii*, means: and others
Et_2O	diethyl ether
EtOH	ethanol
ex.	excitation
FTIR	fourier transform infrared spectroscopy
g	gram
G-1-P	*α*-d-glucose-1-phosphate
G2–3	grubbs catalyst 2^{nd}-3^{rd} generation
GAG	glucosaminoglycane
GPC	gel permeation chromatography
GSH	glutathione
h	hour
H	hydrogen
H_2O-dd	double distilled water (MiliQ)
HA	hyaluronic acid
HeLa	tumor cells from the patient *Henrietta Lacks*
HEMAm	2-hydroxyethyl methacrylamide
Hep	heparin
HEPES	4-(2-hydroxyethyl)-1-piperazineethanesulfonic acid
HES	hydroxyethyl starch
HMPA	hydroxypropyl methyl cellulose
HMTETA	1,1,4,7,10,10-hexamethyltriethylene tetramine
HOBt	1-hydroxybenzotriazole
HPLC	high performance liquid chromatography
Hz	hertz
^{i}Pr	isopropyl group
IR	infrared spectroscopy
***J* (NMR)**	coupling constant
J	joule
k	kilo
KBr	potassium bromide
L	liter
Lit.	literature

abbreviation	meaning
m	meta
M	meter
m	multiplett
M	molar
m-	milli
m/z	mass to charge ratio
Mal	maltose
Me	methyl group
MeOH	methanol
min	minute
mL	milliliter
MM	macro monomer
M_n	number average molecular weight
mol	mole(s)
mol-%	mole percent (1 mol-% = 0.01 eq.)
MS	mass spectroscopy
ms	molecular sieve
MSN	mesoporous silica nanoparticles
MTT	3,(4,5-dimethylthiazol-2-yl)-2,5-diphenyl-tetrazoliumbromide
MW	microwave
M_w	weight average molecular weight
MWCO	molecular weight cut-off
N	nitrogen
N	*Newton*
N_3	azide
$NaCNBH_3$	sodium cyanoborohydride
^{n}Bu	n-butyl group
NCA	*N*-carboxylic anhydride
NHS	*N*-hydroxysuccinimide
NIR	near infrared region
NMR	nuclear magnetic resonance
Norb	norbornene
NVP	*N*-vinyl-2-pyrrolidone

abbreviation	meaning
p	para
PAA	poly(acrylic acid)
PAMAM	polyamidoamine
PBA	poly(n-butyl acrylate)
PBLG	poly(γ-benzyl l-glutamate)
PBS	phosphate buffered saline
PC(Zn)	phthalocyanine zinc
PCL	polycaprolactone
PDEGA	poly(diethylene glycol ethyl ether acrylate)
PdI	polydispersity index
PDMAEMA	poly-(2-dimethylamino)ethyl methacrylate
PDMS	poly(dimethylsiloxilane)
PDT	photodynamic therapy
PEG	poly(ethylene glycol)
PEO	poly(ethylene oxide)
PGPR	polyglycerol polyricinoleat
Ph	phenyl group
pH	proton log units
pK_a	acid dissociation constant
PLA	poly(L-lactidic acid)
PLGA	poly(DL-lactide-*co*-glycolide)
PMDTA	*N*,*N*,*N*',*N*'',*N*''-pentamethyldiethylenetriamine
PMOXA	poly(2-methyl-2-oxazoline)
ppm	parts per million
PPTS	pyridiunium *p*-toluenesulfonate
PS (polymer)	polystyrene
PS	photo sensitizer
PTLC	preparative thin layer chromatography
PVA	poly(vinyl alcohol)
PVAc	poly(vinyl acetate)
PVAm	poly(vinylamine)
PVCL	poly-(*N*-vinylcaprolactam)
Py	pyridyl group

abbreviation	meaning
quant.	quantitativ
r.t.	room temperature
RAFT	reversible addition-fragmentation chain-transfer polymerization
R_f	ratio of fronts, retention factor
R_G	radius of gyration
R_H	radius of hydration
RNA	ribonucleic acid
ROMP	ring-opening metathesis polymerization
ROP	ring-opening polymerization
ROS	reative oxygen species
Ru	ruthenium
s	second
s	Singulett
SBB	sodium borate buffer
SEC	size exclusion chromatography
SEM	scanning electron microscope
sept	septett
SFT	surface tension
SH	thiol group
SLS	static light scattering
SPR	surface plasmon resonance
t	triplett
t	time
TBTU	2-(1-*H*-benzotriazol-1-yl)-*N,N,N′,N′*-tetramethylaminium tetrafluoroborate
TCEP	tris(2-carboxyethyl)phosphine
TDI	2,4-toluene diisocyanat
TEA	triethylamine
TEM	transmission electron microscopy
tert	tertiäry
TFE	2,2,2-trifluoro-ethanol
THF	tetrahydrofuran
TLC	thin layer chromatography
TMS	trimethylsilane

abbreviation	meaning
UV	ultraviolet
V	volume
W	Watt
wt%	weight percent
$\boldsymbol{\gamma}$	surface tension
$\boldsymbol{\delta}$	chemical shift
ΔT	difference in temperature
$\boldsymbol{\lambda}$	wavelength
$\boldsymbol{\mu}$	micro

6.2 LITERATURE

[1] H. Ringsdorf, *J. Polym. Sci., Part C: Polym. Symp.* **1975**, *51*, 135–153.

[2] K. Strebhardt, A. Ullrich, *Nat. Rev. Cancer* **2008**, *8*, 473–480.

[3] L. Xiao, L. Huang, F. Moingeon, M. Gauthier, G. Yang, *Biomacromolecules* **2017**, *18*, 2711–2722.

[4] C. Frangville, Y. Li, C. Billotey, D. R. Talham, J. Taleb, P. Roux, J. D. Marty, C. Mingotaud, *Nano Lett.* **2016**, *16*, 4069–4073.

[5] A. Najer, D. Wu, A. Bieri, F. Brand, C. G. Palivan, H. P. Beck, W. Meier, *ACS Nano* **2014**, *8*, 12560–12571.

[6] a) S. Winzen, J. C. Schwabacher, J. Muller, K. Landfester, K. Mohr, *Biomacromolecules* **2016**, *17*, 3845–3851; b) J. Muller, J. Simon, P. Rohne, C. Koch-Brandt, V. Mailander, S. Morsbach, K. Landfester, *Biomacromolecules* **2018**, *19*, 2657–2664.

[7] a) F. Ishizuka, R. Chapman, R. P. Kuchel, M. Coureault, P. B. Zetterlund, M. H. Stenzel, *Macromolecules* **2018**, *51*, 438–446; b) A. M. Carvalho, R. Teixeira, R. Novoa-Carballal, R. A. Pires, R. L. Reis, I. Pashkuleva, *Biomacromolecules* **2018**, *19*, 2991–2999; c) A. K. Khan, S. Gudlur, H.-P. M. de Hoog, W. Siti, B. Liedberg, M. Nallani, *Angew. Chem.* **2017**, *129*, 11916–11920; d) H. Duan, M. Donovan, A. Foucher, X. Schultze, S. Lecommandoux, *Sci. Rep.* **2018**, *8*, 14730–14739; e) H. Zhang, J. Xu, L. Xing, J. Ji, A. Yu, G. Zhai, *J. Colloid Interface Sci.* **2017**, *492*, 101–111.

[8] J. Nicolas, S. Mura, D. Brambilla, N. Mackiewicz, P. Couvreur, *Chem. Soc. Rev.* **2013**, *42*, 1147–1235.

[9] D. Peer, J. M. Karp, S. Hong, O. C. Farokhzad, R. Margalit, R. Langer, *Nat. Nanotechnol.* **2007**, *2*, 751–760.

[10] a) C. Y. Li, Z. J. Liu, P. Yao, *RSC Adv.* **2016**, *6*, 33083–33091; b) W. J. Sun, J. L. Zhang, C. C. Zhang, P. Wang, C. Peng, M. W. Shen, X. Y. Shi, *ACS Macro Lett.* **2018**, *7*, 137–142.

[11] M. Ficker, M. J. M. Theeuwen, A. Janaszewska, M. Gorzkiewicz, S. W. Svenningsen, B. Klajnert-Maculewicz, J. B. Christensen, *Mol. Pharmaceutics* **2018**, *15*, 3573–3582.

[12] D. Gao, P. C. Lo, *J. Controlled Release* **2018**, *282*, 46–61.

[13] Y. Lyu, J. Zeng, Y. Jiang, X. Zhen, T. Wang, S. Qiu, X. Lou, M. Gao, K. Pu, *ACS Nano* **2018**, *12*, 1801–1810.

[14] a) T. Fritz, M. Hirsch, F. C. Richter, S. S. Muller, A. M. Hofmann, K. A. Rusitzka, J. Markl, U. Massing, H. Frey, M. Helm, *Biomacromolecules* **2014**, *15*, 2440–2448; b) Y. Jiang, J. Zhang, F. Meng, Z. Zhong, *ACS Nano* **2018**, *12*, 11070–11079.

[15] T. Sun, Y. S. Zhang, B. Pang, D. C. Hyun, M. Yang, Y. Xia, *Angew. Chem. Int. Ed.* **2014**, *53*, 12320–12364.

[16] S. Mizrahy, D. Peer, *Chem. Soc. Rev.* **2012**, *41*, 2623–2640.

[17] R. Mehvar, *J. Controlled Release* **2000**, *69*, 1–25.

[18] H. Freichels, M. Wagner, P. Okwieka, R. G. Meyer, V. Mailander, K. Landfester, A. Musyanovych, *J. Mater. Chem. B* **2013**, *1*, 4338–4348.

[19] Z. Lin, J. Z. Li, H. Y. He, H. H. Kuang, X. S. Chen, Z. G. Xie, X. B. Jing, Y. B. Huang, *RSC Adv.* **2015**, *5*, 9546–9555.

[20] A. Ghadban, L. Albertin, M. Rinaudo, A. Heyraud, *Biomacromolecules* **2012**, *13*, 3108–3119.

[21] M. S. Alkanawati, F. R. Wurm, H. Therien-Aubin, K. Landfester, *Macromol. Mater. Eng.* **2018**, *303*, 1700505.

[22] E. M. Bachelder, T. T. Beaudette, K. E. Broaders, J. Dashe, J. M. Frechet, *J. Am. Chem. Soc.* **2008**, *130*, 10494–10495.

[23] a) C. Ornelas-Megiatto, P. N. Shah, P. R. Wich, J. L. Cohen, J. A. Tagaev, J. A. Smolen, B. D. Wright, M. J. Panzner, W. J. Youngs, J. M. Frechet, C. L. Cannon, *Mol. Pharmaceutics* **2012**, *9*, 3012–3022; b) S. Suarez, G. N. Grover, R. L. Braden, K. L. Christman, A. Almutairi, *Biomacromolecules* **2013**, *14*, 3927–3935; c) T. Bauleth-Ramos, M. A. Shahbazi, D. F. Liu, F. Fontana, A. Correia, P. Figueiredo, H. B. Zhang, J. P. Martins, J. T. Hirvonen, P. Granja, B. Sarmento, H. A. Santos, *Adv. Funct. Mater.* **2017**, *27*, 1703303.

[24] A. Blanazs, S. P. Armes, A. J. Ryan, *Macromol. Rapid Commun.* **2009**, *30*, 267–277.

[25] C. Schatz, S. Louguet, J. F. Le Meins, S. Lecommandoux, *Angew. Chem. Int. Ed.* **2009**, *48*, 2572–2575.

[26] a) M. M. Kemp, A. Kumar, S. Mousa, T. J. Park, P. Ajayan, N. Kubotera, S. A. Mousa, R. J. Linhardt, *Biomacromolecules* **2009**, *10*, 589–595; b) A. Javid, S. Ahmadian, A. A. Saboury, S. M. Kalantar, S. Rezaei-Zarchi, *RSC Adv.* **2014**, *4*, 13719–13728; c) F. Fontana, M. A. Shahbazi, D. Liu, H. Zhang, E. Makila, J. Salonen, J. T. Hirvonen, H. A. Santos, *Adv. Mater.* **2017**, *29*, 1603239.

[27] a) I. Otsuka, M. Osaka, Y. Sakai, C. Travelet, J. L. Putaux, R. Borsali, *Langmuir* **2013**, *29*, 15224–15230; b) K. M. Zepon, I. Otsuka, C. Bouilhac, E. C. Muniz, V. Soldi, R. Borsali, *Biomacromolecules* **2015**, *16*, 2012–2024.

[28] C. Schatz, S. Lecommandoux, *Macromol. Rapid Commun.* **2010**, *31*, 1664–1684.

[29] V. R. Sinha, R. Kumria, *Int. J. Pharm.* **2001**, *224*, 19–38.

[30] A. Basu, K. R. Kunduru, E. Abtew, A. J. Domb, *Bioconjugate Chem.* **2015**, *26*, 1396–1412.

[31] L. M. Ryno, C. Reese, M. Tolan, J. O'Brien, G. Short, G. Sorriano, J. Nettleton, K. Fulton, P. M. Iovine, *Biomacromolecules* **2014**, *15*, 2944–2951.

[32] J. Chen, C. Travelet, R. Borsali, S. Halila, *Biomacromolecules* **2017**, *18*, 3410–3417.

[33] Y. X. Qiu, T. H. Zhang, M. Ruegsegger, R. E. Marchant, *Macromolecules* **1998**, *31*, 165–171.

[34] S. Asayama, M. Nogawa, Y. Takei, T. Akaike, A. Maruyama, *Bioconjugate Chem.* **1998**, *9*, 476–481.

[35] F. S. Palumbo, G. Pitarresi, D. Mandracchia, G. Tripodo, G. Giammona, *Carbohydr. Polym.* **2006**, *66*, 379–385.

[36] S. Harrisson, G. L. Drisko, E. Malmstrom, A. Hult, K. L. Wooley, *Biomacromolecules* **2011**, *12*, 1214–1223.

[37] K. Nagahama, Y. Mori, Y. Ohya, T. Ouchi, *Biomacromolecules* **2007**, *8*, 2135–2141.

[38] I. Colinet, V. Dulong, T. Hamaide, D. Le Cerf, L. Picton, *Carbohydr. Polym.* **2009**, *75*, 454–462.

[39] T. S. Demina, T. A. Akopova, L. V. Vladimirov, A. N. Zelenetskii, E. A. Markvicheva, C. Grandfils, *Mater. Sci. Eng., C* **2016**, *59*, 333–338.

[40] H. T. Duong, F. Hughes, S. Sagnella, M. Kavallaris, A. Macmillan, R. Whan, J. Hook, T. P. Davis, C. Boyer, *Molecular Pharmaceutics* **2012**, *9*, 3046–3061.

[41] A. K. S. Chandel, B. Nutan, I. H. Raval, S. K. Jewrajka, *Biomacromolecules* **2018**, *19*, 1142–1153.

[42] a) M. Barsbay, O. Guven, M. H. Stenzel, T. P. Davis, C. Barner-Kowollik, L. Barner, *Macromolecules* **2007**, *40*, 7140–7147; b) M. H. Stenzel, T. P. Davis, A. G. Fane, *J. Mater. Chem.* **2003**, *13*, 2090–2097.

[43] Z. A. Sutirman, M. M. Sanagi, J. Abd Karim, A. Abu Naim, W. A. Wan Ibrahim, *Int. J. Biol. Macromol.* **2018**, *107*, 891–897.

[44] O. Garcia-Valdez, P. Champagne, M. F. Cunningham, *Prog. Polym. Sci.* **2018**, *76*, 151–173.

[45] J. Rzayev, *ACS Macro Lett.* **2012**, *1*, 1146–1149.

[46] G. Xie, M. R. Martinez, M. Olszewski, S. S. Sheiko, K. Matyjaszewski, *Biomacromolecules* **2018**, article ASAP.

[47] H. Y. Cho, P. Krys, K. Szcześniak, H. Schroeder, S. Park, S. Jurga, M. Buback, K. Matyjaszewski, *Macromolecules* **2015**, *48*, 6385–6395.

[48] Z. Li, K. Zhang, J. Ma, C. Cheng, K. L. Wooley, *J. Polym. Sci., Part A: Polym. Chem.* **2009**, *47*, 5557–5563.

[49] J. A. Johnson, Y. Y. Lu, A. O. Burts, Y. H. Lim, M. G. Finn, J. T. Koberstein, N. J. Turro, D. A. Tirrell, R. H. Grubbs, *J. Am. Chem. Soc.* **2011**, *133*, 559–566.

[50] a) S. Jha, S. Dutta, N. B. Bowden, *Macromolecules* **2004**, *37*, 4365–4374; b) H. Jung, T. P. Carberry, M. Weck, *Macromolecules* **2011**, *44*, 9075–9083; c) D. A. N'Guyen, F. Leroux, V. Montembault, S. Pascual, L. Fontaine, *Polym. Chem.* **2016**, *7*, 1730–1738; d) S. C. Radzinski, J. C. Foster, R. C. Chapleski, Jr., D. Troya, J. B. Matson, *J. Am. Chem. Soc.* **2016**, *138*, 6998−7004; e) S. C. Radzinski, J. C. Foster, S. J. Scannelli, J. R. Weaver, K. J. Arrington, J. B. Matson, *ACS Macro Lett.* **2017**, *6*, 1175–1179.

[51] M. Gerle, K. Fischer, S. Roos, A. H. E. Muller, M. Schmidt, S. S. Sheiko, S. Prokhorova, M. Moller, *Macromolecules* **1999**, *32*, 2629–2637.

[52] a) J. Zou, G. Jafr, E. Themistou, Y. Yap, Z. A. Wintrob, P. Alexandridis, A. C. Ceacareanu, C. Cheng, *Chem. Commun.* **2011**, *47*, 4493–4495; b) L. Liao, J. Liu, E. C. Dreaden, S. W. Morton, K. E. Shopsowitz, P. T. Hammond, J. A. Johnson, *J. Am. Chem. Soc.* **2014**, *136*, 5896–5899.

[53] A. Ghadban, E. Reynaud, M. Rinaudo, L. Albertin, *Polym. Chem.* **2013**, *4*, 4578–4583.

[54] a) K. Kobayashi, H. Sumitomo, Y. Ina, *Polym. J.* **1985**, *17*, 567–575; b) I. Wataoka, K. Kobayashi, K. Kajiwara, *Carbohydr. Res.* **2005**, *340*, 989–995.

[55] K. Kobayashi, S. Kamiya, N. Enomoto, *Macromolecules* **1996**, *29*, 8670–8676.

[56] K. H. Mortell, M. Gingras, L. L. Kiessling, *J. Am. Chem. Soc.* **1994**, *116*, 12053–12054.

[57] C. Fraser, R. H. Grubbs, *Macromolecules* **1995**, *28*, 7248–7255.

[58] K. Nomura, R. R. Schrock, *Macromolecules* **1996**, *29*, 540–545.

[59] M. Rawat, C. I. Gama, J. B. Matson, L. C. Hsieh-Wilson, *J. Am. Chem. Soc.* **2008**, *130*, 2959–2961.

[60] a) M. Mammen, S.-K. Choi, G. M. Whitesides, *Angew. Chem. Int. Ed.* **1998**, *37*, 2754–2794; b) V. M. Krishnamurthy, V. Semetey, P. J. Bracher, N. Shen, G. M. Whitesides, *J. Am. Chem. Soc.* **2007**, *129*, 1312–1320.

[61] a) Y. I. Oh, G. J. Sheng, S. K. Chang, L. C. Hsieh-Wilson, *Angew. Chem. Int. Ed.* **2013**, *52*, 11796–11799; b) G. J. Sheng, Y. I. Oh, S. K. Chang, L. C. Hsieh-Wilson, *J. Am. Chem. Soc.* **2013**, *135*, 10898–10901.

[62] R. S. Loka, F. Yu, E. T. Sletten, H. M. Nguyen, *Chem. Commun.* **2017**, *53*, 9163–9166.

[63] M. S. Sanford, J. A. Love, R. H. Grubbs, *J. Am. Chem. Soc.* **2001**, *123*, 6543–6554.

[64] F. Fan, C. Cai, L. Gao, J. Li, P. Zhang, G. Y. Li, C. X. Li, G. L. Yu, *Polym. Chem.* **2017**, *8*, 6709–6719.

[65] S. Tang, W. B. Puryear, B. M. Seifried, X. Dong, J. A. Runstadler, K. Ribbeck, B. D. Olsen, *ACS Macro Lett.* **2016**, *5*, 413–418.

[66] F. Fan, C. Cai, W. Wang, L. Gao, J. Li, J. Li, F. F. Gu, T. T. Sun, J. H. Li, C. X. Li, G. L. Yu, *ACS Macro Lett.* **2018**, *7*, 330–335.

[67] Y. L. Zhang, X. W. Dou, T. Jin, *eXPRESS Polym. Lett.* **2010**, *4*, 599–610.

[68] a) M. Moreau METHOD FOR THE REDUCTIVE AMINATION OF POLYSACCHARIDES. US 6,596,861 B1, **2003**; b) M. S. Verma, F. X. Gu, *Carbohydr. Polym.* **2012**, *87*, 2740–2744.

[69] A. R. Fajardo, A. Guerry, E. A. Britta, C. V. Nakamura, E. C. Muniz, R. Borsali, S. Halila, *Biomacromolecules* **2014**, *15*, 2691–2700.

[70] R. J. Ceresa, *Polymer* **1961**, *2*, 213–219.

[71] J. Bernard, M. Save, B. Arathoon, B. Charleux, *J. Polym. Sci., Part A: Polym. Chem.* **2008**, *46*, 2845–2857.

[72] D. Togashi, I. Otsuka, R. Borsali, K. Takeda, K. Enomoto, S. Kawaguchi, A. Narumi, *Biomacromolecules* **2014**, *15*, 4509–4519.

[73] D. M. Haddleton, K. Ohno, *Biomacromolecules* **2000**, *1*, 152–156.

[74] C. Houga, J. F. Le Meins, R. Borsali, D. Taton, Y. Gnanou, *Chem. Commun.* **2007**, 3063–3065.

[75] S. Yagi, N. Kasuya, K. Fukuda, *Polym. J.* **2010**, *42*, 342–348.

[76] R. Novoa-Carballal, A. Pfaff, A. H. E. Muller, *Polym. Chem.* **2013**, *4*, 2278–2285.

[77] G. Ziegast, B. Pfannemüller, *Carbohydr. Res.* **1987**, *160*, 185–204.

[78] K. Loos, A. H. Muller, *Biomacromolecules* **2002**, *3*, 368–373.

[79] G. Ziegast, B. Pfannemüller, *Macromol. Rapid Commun.* **1984**, *5*, 373–379.

[80] a) T. Zhang, R. E. Marchant, *Macromolecules* **1994**, *27*, 7302–7308; b) T. Zhang, R. E. Marchant, *J. Colloid Interface Sci.* **1996**, *177*, 419–426.

[81] K. K. Upadhyay, J. F. Le Meins, A. Misra, P. Voisin, V. Bouchaud, E. Ibarboure, C. Schatz, S. Lecommandoux, *Biomacromolecules* **2009**, *10*, 2802–2808.

[82] Y. I. Jeong, D. H. Kim, C. W. Chung, J. J. Yoo, K. H. Choi, C. H. Kim, S. H. Ha, D. H. Kang, *Colloids Surf., B* **2012**, *90*, 28–35.

[83] M. S. Verma, S. Liu, Y. Y. Chen, A. Meerasa, F. X. Gu, *Nano Res.* **2011**, *5*, 49–61.

[84] F. Ganji, M. J. Abdekhodaie, *Carbohydr. Polym.* **2008**, *74*, 435–441.

[85] J. Rosselgong, M. Chemin, C. C. Almada, G. Hemery, J. M. Guigner, G. Chollet, G. Labat, D. Da Silva Perez, F. Ham-Pichavant, E. Grau, S. Grelier, S. Lecommandoux, H. Cramail, *Biomacromolecules* **2018**, Article ASAP.

[86] J. L. Wang, M. Caceres, S. M. Li, A. Deratani, *Macromol. Chem. Phys.* **2017**, *218*, 1600558.

[87] A. Peyret, E. Ibarboure, A. Tron, L. Beauté, R. Rust, O. Sandre, N. D. McClenaghan, S. Lecommandoux, *Angew. Chem. Int. Ed.* **2017**, *56*, 1677–1677.

[88] R.-S. Lee, Y.-C. Li, S.-W. Wang, *Carbohydr. Polym.* **2015**, *117*, 201–210.

[89] R. S. Lee, Y. C. Li, S. W. Wang, *Carbohydr. Polym.* **2015**, *117*, 201–210.

[90] H. Sun, B. Guo, X. Li, R. Cheng, F. Meng, H. Liu, Z. Zhong, *Biomacromolecules* **2010**, *11*, 848–854.

[91] A. Petrelli, R. Borsali, S. Fort, S. Halila, *Chem. Commun.* **2016**, *52*, 12202–12205.

[92] L. Y. Tang, Y. C. Wang, Y. Li, J. Z. Du, J. Wang, *Bioconjugate Chem.* **2009**, *20*, 1095–1099.

[93] a) Y. Li, K. Xiao, J. Luo, W. Xiao, J. S. Lee, A. M. Gonik, J. Kato, T. A. Dong, K. S. Lam, *Biomaterials* **2011**, *32*, 6633–6645; b) K. Wang, G.-F. Luo, Y. Liu, C. Li, S.-X. Cheng, R.-X. Zhuo, X.-Z. Zhang, *Polym. Chem.* **2012**, *3*, 1084–1090; c) A. Zhang, Z. Zhang, F. Shi, C. Xiao, J. Ding, X. Zhuang, C. He, L. Chen, X. Chen, *Macromol. Biosci.* **2013**, *13*, 1249–1258.

[94] S. M. Black, C. R. Wolf, *Pharmac. Ther.* **1991**, *51*, 139–154.

[95] Y. L. Li, L. Zhu, Z. Liu, R. Cheng, F. Meng, J. H. Cui, S. J. Ji, Z. Zhong, *Angew. Chem. Int. Ed.* **2009**, *48*, 9914–9918.

[96] I. Otsuka, K. Fuchise, S. Halila, S. Fort, K. Aissou, I. Pignot-Paintrand, Y. Chen, A. Narumi, T. Kakuchi, R. Borsali, *Langmuir* **2010**, *26*, 2325–2332.

[97] J. Niskanen, M. Karesoja, V. Aseyev, X.-P. Qiu, F. M. Winnik, H. Tenhu, *J. Polym. Sci., Part A: Polym. Chem.* **2016**, *54*, 425–436.

[98] E. M. Bachelder, E. N. Pino, K. M. Ainslie, *Chem. Rev.* **2017**, *117*, 1915–1926.

[99] Z. Zhang, X. Chen, L. Chen, S. Yu, Y. Cao, C. He, X. Chen, *ACS Appl. Mater. Interfaces* **2013**, *5*, 10760–10766.

[100] Q. Li, W. Liu, J. Dai, C. Zhang, *Macromol. Biosci.* **2015**, *15*, 756−764.

[101] H. H. Kuang, Y. J. Wu, Z. Y. Zhang, J. Z. Li, X. S. Chen, Z. G. Xie, X. B. Jing, Y. B. Huang, *Polym. Chem.* **2015**, *6*, 3625–3633.

[102] Q. Yang, S. K. Lai, *Wiley Interdiscip. Rev.: Nanomed. Nanobiotechnol.* **2015**, *7*, 655–677.

[103] a) H. Kamitakahara, F. Nakatsubo, D. Klemm, *Cellulose* **2005**, *13*, 375–392; b) H. Kamitakahara, F. Nakatsubo, D. Klemm, *Cellulose* **2007**, *14*, 513–528.

[104] a) S. de Medeiros Modolon, I. Otsuka, S. Fort, E. Minatti, R. Borsali, S. Halila, *Biomacromolecules* **2012**, *13*, 1129–1135; b) A. Nakagawa, H. Kamitakahara, T. Takano, *Cellulose* **2012**, *19*, 1315–1326.

[105] S. C. Owen, D. P. Y. Chan, M. S. Shoichet, *Nano Today* **2012**, *7*, 53–65.

[106] L. Cheng, T. Luan, D. Liu, J. Cheng, H. Li, H. Wei, L. Zhang, J. Lan, Y. Liu, G. Zhao, *Polym. Chem.* **2018**, *9*, 1337–1347.

[107] D. Klemm, *Polysaccharides II*, Springer Berlin Heidelberg, **2006**.

[108] A. N. Belder, A. Biosciences, *Dextran*, Amersham Biosciences AB, **2003**.

[109] C. Hiemstra, L. J. Aa, Z. Zhong, P. J. Dijkstra, J. Feijen, *Biomacromolecules* **2007**, *8*, 1548–1556.

[110] J. A. White, W. M. Deen, *Biophys. J.* **2002**, *82*, 2081–2089.

[111] a) K. A. Granath, *J. Colloid Sci.* **1958**, *13*, 308–328; b) T. C. Laurent, J. Killander, *J. Chromatogr. A* **1964**, *14*, 317–330.

[112] a) J. K. Armstrong, R. B. Wenby, H. J. Meiselman, T. C. Fisher, *Biophys. J.* **2004**, *87*, 4259–4270; b) P. Aimar, M. Meireles, V. Sanchez, *Journal of Membrane Science* **1990**, *54*, 321–338; c) K. A. Granath, B. E. Kvist, *J. Chromatogr. A* **1967**, *28*, 69–81.

[113] S. Arnott, W. E. Scott, *J. Chem. Soc., Perkin Trans. 2* **1972**, 324–335.

[114] a) P. E. Marszalek, A. F. Oberhauser, Y. P. Pang, J. M. Fernandez, *Nature* **1998**, *396*, 661–664; b) I. M. Neelov, D. B. Adolf, T. C. McLeish, E. Paci, *Biophys. J.* **2006**, *91*, 3579–3588; c) M. Rief, F. Oesterhelt, B. Heymann, H. E. Gaub, *Science* **1997**, *275*, 1295–1297.

[115] A. P. Goodwin, S. M. Tabakman, K. Welsher, S. P. Sherlock, G. Prencipe, H. Dai, *J. Am. Chem. Soc.* **2009**, *131*, 289–296.

[116] J. Varshosaz, *Expert Opin. Drug Delivery* **2012**, *9*, 509–523.

[117] G. Arturson, G. Wallenius, *Scand. J. Clin. Lab. Invest.* **1964**, *16*, 81–86.

[118] C. J. De Groot, M. J. Van Luyn, W. N. Van Dijk-Wolthuis, J. A. Cadee, J. A. Plantinga, W. Den Otter, W. E. Hennink, *Biomaterials* **2001**, *22*, 1197–1203.

[119] G. Arturson, G. Wallenius, *Scand. J. Clin. Lab. Invest.* **1964**, *16*, 76–80.

[120] E. L. Rosenfeld, I. S. Lukomskaya, *Clin. Chim. Acta* **1957**, *2*, 105–114.

[121] a) K. H. Køster, V. Sele, M. Schwartz, E. Sindrup, *The Lancet* **1957**, *270*, 262–265; b) U. F. Gruber, J. Siegrist, *J. Arch. Klin. Chir.* **1962**, *301*, 128–135.

[122] a) S. E. Bergentz, *World J. Surg.* **1978**, *2*, 19–25; b) D. Bergqvist, S. E. Bergentz, H. Fredin, *Acta Orthop. Scand.* **1984**, *55*, 247–250.

[123] a) H. Hedin, W. Richter, J. Ring, *Int. Arch. Allergy Appl. Immunol.* **1976**, *52*, 145–159; b) C. E. Zinderman, L. Landow, R. P. Wise, *J. Cardiovasc. Surg.* **2006**, *43*, 1004–1009.

[124] S. R. Maple, A. Allerhand, *J. Am. Chem. Soc.* **1987**, *109*, 3168–3169.

[125] M. Pagnotta, C. L. F. Pooley, B. Gurland, M. Choi, *J. Phys. Org. Chem.* **1993**, *6*, 407−411.

[126] a) A. Dirksen, T. M. Hackeng, P. E. Dawson, *Angew. Chem. Int. Ed.* **2006**, *45*, 7581–7584; b) S. M. Agten, D. P. Suylen, T. M. Hackeng, *Bioconjugate Chem.* **2016**, *27*, 42–46.

[127] a) M. Yalpani, D. E. Brooks, *J. Polym. Sci.: Polym. Chem.* **1985**, *23*, 1395–1405; b) A. Guerry, J. Bernard, E. Samain, E. Fleury, S. Cottaz, S. Halila, *Bioconjugate Chem.* **2013**, *24*, 544–549.

[128] a) V. von Braunmühl, R. Stadler, *Polymer* **1998**, *39*, 1617–1629; b) K. Hashimoto, S.-I. Imanishi, M. Okada, H. Sumitomo, *J. Polym. Sci., Part A: Polym. Chem.* **1991**, *29*, 1271–1279; c) T. Zhang, R. E. Marchant, *J. Colloid Interface Sci.* **1996**, *177*, 419−426.

[129] S. Dumitriu, *Polysaccharides: Structural Diversity and Functional Versatility, Second Edition*, CRC Press, **2004**.

[130] S. J. Angyal, in *Adv. Carbohydr. Chem. Biochem., Vol. 42* (Eds.: R. S. Tipson, D. Horton), Academic Press, **1984**, p. 15−68.

[131] R. F. Borch, M. D. Bernstein, H. D. Durst, *J. Am. Chem. Soc.* **1971**, *93*, 2897–2904.

[132] C. F. Lane, *Synthesis* **1975**, *1975*, 135–146.

[133] C. Bonduelle, J. Huang, E. Ibarboure, A. Heise, S. Lecommandoux, *Chem. Commun.* **2012**, *48*, 8353–8355.

[134] a) K. Yoshimura, Y. Miyazaki, S. Sawada, H. Waki, *J. Chem. Soc., Faraday Trans.* **1996**, *92*, 651−656; b) C. Shao, Y. Miyazaki, S. Matsuoka, K. Yoshimura, H. Sakashita, *Macromolecules* **2000**, *33*, 19–25; c) Y. Miyazaki, K. Yoshimura, Y. Miura, H. Sakashita, K. Ishimaru, *Polyhedron* **2003**, *22*, 909−916.

[135] a) S. A. Galema, *Chem. Soc. Rev.* **1997**, *26*, 233–238; b) A. Corsaro, U. Chiacchio, V. Pistara, G. Romeo, *Curr. Org. Chem.* **2004**, *8*, 511–538.

[136] E. A. Yates, M. O. Jones, C. E. Clarke, A. K. Powell, S. R. Johnson, A. Porch, P. P. Edwards, J. E. Turnbull, *J. Mater. Chem.* **2003**, *13*, 2061–2063.

[137] a) M. R. Bockstaller, R. A. Mickiewicz, E. L. Thomas, *Adv. Mater.* **2005**, *17*, 1331–1349; b) P. Samaddar, A. Deep, K.-H. Kim, *Chem. Eng. J.* **2018**, *342*, 71–89.

[138] a) Y. Wang, H. Xu, N. Ma, Z. Wang, X. Zhang, J. Liu, J. Shen, *Langmuir* **2006**, *22*, 5552–5555; b) R. Qu, L. Shen, Z. Chai, C. Jing, Y. Zhang, Y. An, L. Shi, *ACS Appl. Mater. Interfaces* **2014**, *6*, 19207–19216; c) C. Boucher-Jacobs, M. Rabnawaz, J. S. Katz, R. Even, D. Guironnet, *Nat. Commun.* **2018**, *9*, 841–850.

[139] a) B. Jeong, Y. H. Bae, D. S. Lee, S. W. Kim, *Nature* **1997**, *388*, 860–862; b) N. Zhang, P. R. Wardwell, R. A. Bader, *Pharmaceutics* **2013**, *5*, 329–352.

[140] a) C. Gauche, V. Soldi, S. Fort, R. Borsali, S. Halila, *Carbohydr. Polym.* **2013**, *98*, 1272–1280; b) A.-L. Kampmann, M. Luksin, I. Pretzer, R. Weberskirch, *Macromol. Chem. Phys.* **2016**, *217*, 1704–1711.

[141] a) A. M. Le Ray, M. Vert, J. C. Gautier, J. P. Benoît, *Int. J. Pharm.* **1994**, *106*, 201–211; b) M. F. Zambaux, F. Bonneaux, R. Gref, P. Maincent, E. Dellacherie, M. J. Alonso, P. Labrude, C. Vigneron, *J. Controlled Release* **1998**, *50*, 31–40.

[142] a) D. D. Roberts, S. D. Lewis, D. P. Ballou, S. T. Olson, J. A. Shafer, *Biochemistry* **2002**, *25*, 5595–5601; b) D. A. Evans, D. H. Ripin Brown, evans_pKa_table. **2005**, http://evans.rc.fas.harvard.edu/pdf/evans_pKa_table.pdf (accessed 24 august 2018); c) W. Jiang, Q. Fu, H. Fan, J. Ho, W. Wang, *Angew. Chem. Int. Ed.* **2007**, *46*, 8445–8600.

[143] J. H. Boyer, F. C. Canter, *Chem. Rev.* **1954**, *54*, 1–57.

[144] a) B. Iddon, O. Meth-Cohn, E. F. V. Scriven, H. Suschitzky, P. T. Gallagher, *Angew. Chem.* **1979**, *91*, 965–982; b) E. A. Pritchina, N. P. Gritsan, *J. Photochem. Photobiol., A* **1988**, *43*, 165–182.

[145] a) W. Kirmse, *Angew. Chem.* **1959**, *71*, 537–541; b) E. H. F. Escher, H. Robert, G. Guillemette, *Helv. Chim. Acta* **1979**, *62*, 1217–1222.

[146] P. A. S. Smith, J. H. Hall, R. O. Kan, *J. Am. Chem. Soc.* **1962**, *84*, 485−489.

[147] J. Clayden, N. Greeves, S. Warren, *Organic Chemistry*, OUP Oxford, **2012**.

[148] a) A. Boujakhrout, A. Sánchez, P. Díez, S. Jiménez-Falcao, P. Martínez-Ruiz, M. Peña-Álvarez, J. M. Pingarrón, R. Villalonga, *J. Mater. Chem. B* **2015**, *3*, 3518–3524; b) D. Bamberger, D. Hobernik, M. Konhauser, M. Bros, P. R. Wich, *Molecular Pharmaceutics* **2017**, *14*, 4403–4416.

[149] a) J. A. Burns, J. C. Butler, J. Moran, G. M. Whitesides, *J. Org. Chem.* **1991**, *56*, 2648–2650; b) E. B. Getz, M. Xiao, T. Chakrabarty, R. Cooke, P. R. Selvin, *Anal. Biochem.* **1999**, *273*, 73–80.

[150] E. Valeur, M. Bradley, *Chem. Soc. Rev.* **2009**, *38*, 606–631.

[151] M. H. Stenzel, *ACS Macro Lett.* **2012**, *2*, 14–18.

[152] B. B. Breitenbach, I. Schmid, P. R. Wich, *Biomacromolecules* **2017**, *18*, 2839–2848.

[153] P. R. Wich, J. M. J. Frechet, *Aust. J. Chem.* **2012**, *65*, 15–19.

[154] V. K. Tiwari, B. B. Mishra, K. B. Mishra, N. Mishra, A. S. Singh, X. Chen, *Chem. Rev.* **2016**, *116*, 3086–3240.

[155] V. V. Rostovtsev, L. G. Green, V. V. Fokin, K. B. Sharpless, *Angew. Chem. Int. Ed.* **2002**, *41*, 2596–2599.

[156] M. Meldal, *Macromol. Rapid Commun.* **2008**, *29*, 1016–1051.

[157] V. Reukov, V. Maximov, A. Vertegel, *Biotechnol. Bioeng.* **2011**, *108*, 243–252.

[158] P. Leophairatana, C. C. De Silva, J. T. Koberstein, *J. Polym. Sci., Part A: Polym. Chem.* **2018**, *56*, 75–84.

[159] A. Klaikherd, C. Nagamani, S. Thayumanavan, *J. Am. Chem. Soc.* **2009**, *131*, 4830–4838.

[160] a) A. Dag, Y. Jiang, K. J. Karim, G. Hart-Smith, W. Scarano, M. H. Stenzel, *Macromol. Rapid Commun.* **2015**, *36*, 890–897; b) Z. Zhang, X. Chen, X. Gao, X. Yao, L. Chen, C. He, X. Chen, *RSC Adv.* **2015**, *5*, 18593–18600.

[161] Y. Kato, S. Ozawa, C. Miyamoto, Y. Maehata, A. Suzuki, T. Maeda, Y. Baba, *Cancer Cell Int.* **2013**, *13*, 89–97.

[162] a) M. E. Egan, M. Pearson, S. A. Weiner, V. Rajendran, D. Rubin, J. Glockner-Pagel, S. Canny, K. Du, G. L. Lukacs, M. J. Caplan, *Science* **2004**, *304*, 600–602; b) R. K. Maheshwari, A. K. Singh, J. Gaddipati, R. C. Srimal, *Life Sci.* **2006**, *78*, 2081–2087.

[163] a) Z. Ma, A. Haddadi, O. Molavi, A. Lavasanifar, R. Lai, J. Samuel, *J. Biomed. Mater. Res.* **2008**, *86A*, 300–310; b) Y. Jiang, M. Liang, D. Svejkar, G. Hart-Smith, H. Lu, W. Scarano, M. H. Stenzel, *Chem. Commun.* **2014**, *50*, 6394–6397.

[164] M. Callari, P. L. De Souza, A. Rawal, M. H. Stenzel, *Angew. Chem. Int. Ed.* **2017**, *56*, 8441–8445.

[165] a) C. Girard, E. Onen, M. Aufort, S. Beauviere, E. Samson, J. Herscovici, *Org. Lett.* **2006**, *8*, 1689–1692; b) S. I. Presolski, S. K. Mamidyala, F. Manzenrieder, M. G. Finn, *ACS Comb. Sci.* **2012**, *14*, 527–530; c) H. Wu, H. Li, R. T. Kwok, E. Zhao, J. Z. Sun, A. Qin, B. Z. Tang, *Sci. Rep.* **2014**, *4*, 5107–5112; d) N. Jasinski, A. Lauer, P. J. M. Stals, S. Behrens, S. Essig, A. Walther, A. S. Godmann, C. Barner-Kowollik, *ACS Macro Lett.* **2015**, *4*, 298–301.

[166] a) D. C. Kennedy, C. S. McKay, M. C. B. Legault, D. C. Danielson, J. A. Blake, A. F. Pegoraro, A. Stolow, Z. Mester, J. P. Pezacki, *J. Am. Chem. Soc.* **2011**, *133*, 17993–18001; b) K. S. Egorova, V. P. Ananikov, *Angew. Chem. Int. Ed.* **2016**, *55*, 12150–12162.

[167] a) A. Sahu, U. Bora, N. Kasoju, P. Goswami, *Acta Biomaterialia* **2008**, *4*, 1752–1761; b) C. Mohanty, S. Acharya, A. K. Mohanty, F. Dilnawaz, S. K. Sahoo, *Nanomedicine* **2010**, *5*, 433–449; c) J. Sun, C. Bi, H. M. Chan, S. Sun, Q. Zhang, Y. Zheng, *Colloids Surf., B* **2013**, *111*, 367–375.

[168] D. R. Grassetti, J. F. Murray, Jr., *Arch. Biochem. Biophys.* **1967**, *119*, 41–49.

[169] a) G. T. Zugates, D. G. Anderson, S. R. Little, I. E. Lawhorn, R. Langer, *J. Am. Chem. Soc.* **2006**, *128*, 12726–12734; b) C. Boyer, J. Liu, V. Bulmus, T. P. Davis, *Aust. J. Chem.* **2009**, *62*, 830–847.

[170] B. B. Breitenbach, E. Steiert, M. Konhäuser, L. Vogt, Y. Wang, S. H. Parekh, P. R. Wich, *Soft Matter* **2019**.

[171] P. Winterwerber. Amphiphilic Protein Polysaccharide Conjugates with Double Stimuli Responsiveness. Master of Science Johannes Gutenberg-Universität Mainz, **2018**.

[172] C. R. Becer, R. Hoogenboom, U. S. Schubert, *Angew. Chem. Int. Ed.* **2009**, *48*, 4900–4908.

[173] K. Brocklehurst, T. Stuchbury, J. P. G. Malthouse, *Biochem. J.* **1979**, *183*, 233–238.

[174] a) S. Viel, D. Capitani, L. Mannina, A. Segre, *Biomacromolecules* **2003**, *4*, 1843–1847; b) Y. Bakkour, V. Darcos, S. M. Li, J. Coudane, *Polym. Chem.* **2012**, *3*, 2006–2010; c) N. E.

M. Kuz'mina, S. V.; Krylov, V. I.; Yashkir, V. A.; Merkulov, V. A., *J. Anal. Chem.* **2014**, *69*, 953–959.

[175] R. Singh, G. M. Whitesides, in *Sulphur-Containing Functional Groups* **2010**, pp. 633–658.

[176] a) W. Brown, K. Schillen, M. Almgren, S. Hvidt, P. Bahadur, *The Journal of Physical Chemistry* **1991**, *95*, 1850–1858; b) S. Lacelle, F. Cau, *Macromolecules* **1996**, *29*, 170–178.

[177] M. Shi, J. H. Wosnick, K. Ho, A. Keating, M. S. Shoichet, *Angew. Chem. Int. Ed.* **2007**, *46*, 6126–6131.

[178] J. T. Ping, H. S. Peng, W. B. Duan, F. T. You, M. Song, Y. Q. Wang, *J. Mater. Chem. B* **2016**, *4*, 4482–4489.

[179] a) A. Ogunsipe, D. Maree, T. Nyokong, *J. Mol. Struct.* **2003**, *650*, 131–140; b) Y. Chin, S. H. Lim, Y. Zorlu, V. Ahsen, L. V. Kiew, L. Y. Chung, F. Dumoulin, H. B. Lee, *PLoS One* **2014**, *9*, e97894

[180] M. Obata, S. Tanaka, H. Mizukoshi, E. Ishihara, M. Takahashi, S. Hirohara, *J. Polym. Sci., Part A: Polym. Chem.* **2018**, *56*, 560–570.

[181] S. Wang, F. Yuan, K. Chen, G. Chen, K. Tu, H. Wang, L. Q. Wang, *Biomacromolecules* **2015**, *16*, 2693–2700.

[182] a) M. S. Masri, M. Friedman, *J. Protein Chem.* **1988**, *7*, 49–54; b) M. Morpurgo, F. M. Veronese, D. Kachensky, J. M. Harris, *Bioconjugate Chem.* **1996**, *7*, 363–368; c) G. N. Grover, S. N. Alconcel, N. M. Matsumoto, H. D. Maynard, *Macromolecules* **2009**, *42*, 7657−7663; d) J. Morales-Sanfrutos, J. Lopez-Jaramillo, M. Ortega-Munoz, A. Megia-Fernandez, F. Perez-Balderas, F. Hernandez-Mateo, F. Santoyo-Gonzalez, *Org. Biomol. Chem.* **2010**, *8*, 667–675.

[183] a) J. W. Bae, E. Lee, K. M. Park, K. D. Park, *Macromolecules* **2009**, *42*, 3437–3442; b) R. Wang, W. Chen, F. Meng, R. Cheng, C. Deng, J. Feijen, Z. Zhong, *Macromolecules* **2011**, *44*, 6009–6016.

[184] a) G. T. Hermanson, *Bioconjugate Techniques*, Academic Press, **2013**; b) A. Lihme, C. Schafer-Nielsen, K. P. Larsen, K. G. Muller, T. C. Bog-Hansen, *J. Chromatogr. A* **1986**, *376*, 299–305.

[185] S. Bhattacharjee, *J. Controlled Release* **2016**, *235*, 337–351.

[186] S. Buwalda, A. Al Samad, A. El Jundi, A. Bethry, Y. Bakkour, J. Coudane, B. Nottelet, *J. Colloid Interface Sci.* **2018**, *514*, 468–478.

[187] R.-S. Lee, K.-P. Wu, *J. Polym. Sci., Part A: Polym. Chem.* **2011**, *49*, 3163–3173.

[188] P. Raffa, D. A. Wever, F. Picchioni, A. A. Broekhuis, *Chem. Rev.* **2015**, *115*, 8504–8563.

[189] M. J. Rosen, *J. Colloid Interface Sci.* **1976**, *56*, 320–327.

[190] P. Szumala, A. Mowinska, *J. Surfactants Deterg.* **2016**, *19*, 437–445.

[191] K. Holmberg, B. Jönsson, B. Kronberg, B. Lindman, *Surfactants and Polymers in Aqueous Solution*, Wiley, **2002**.

[192] I. Astafieva, X. F. Zhong, A. Eisenberg, *Macromolecules* **1993**, *26*, 7339–7352.

[193] a) K. Ogino, Y. Onoe, M. Abe, H. Ono, K. Bessho, *Langmuir* **1990**, *6*, 1330–1330; b) H. J. Gong, G. Y. Xu, H. Ding, X. F. Shi, Y. B. Tan, *Eur. Polym. J.* **2009**, *45*, 2540–2548; c) O. Theodoly, M. Jacquin, P. Muller, S. Chhun, *Langmuir* **2009**, *25*, 781–793.

[194] H. Yin, E. S. Lee, D. Kim, K. H. Lee, K. T. Oh, Y. H. Bae, *J. Controlled Release* **2008**, *126*, 130–138.

[195] a) P. Alexandridis, J. F. Holzwarth, T. A. Hatton, *Macromolecules* **1994**, *27*, 2414–2425; b) J. P. Marcolongo, M. Mirenda, *J. Chem. Educ.* **2011**, *88*, 629–633.

[196] J. A. White, W. M. Deen, *Macromolecules* **2001**, *34*, 8278–8285.

[197] R. Gref, V. Babak, P. Bouillot, I. Lukina, M. Bodorev, E. Dellacherie, *Colloids Surf., A* **1998**, *143*, 413–420.

[198] N. M. P. S. Ricardo, A. Glendinning, C. Price, *Polym. Eng. Sci.* **1996**, *36*, 182–187.

[199] T. J. Styslinger, N. Zhang, V. S. Bhatt, N. Pettit, A. F. Palmer, P. G. Wang, *J. Am. Chem. Soc.* **2012**, *134*, 7507–7515.

[200] K. B. Daniel, C. E. Callmann, N. C. Gianneschi, S. M. Cohen, *Chem. Commun.* **2016**, *52*, 2126–2128.

[201] J. A. Love, J. P. Morgan, T. M. Trnka, R. H. Grubbs, *Angew. Chem. Int. Ed.* **2002**, *41*, 4035–4037.

[202] B. Yang, B. A. Abel, C. L. McCormick, R. F. Storey, *Macromolecules* **2017**, *50*, 7458–7467.

[203] J. Liu, A. X. Gao, J. A. Johnson, *J. Visualized Exp.* **2013**, 1–7.

[204] a) C. W. Bielawski, R. H. Grubbs, *Angew. Chem. Int. Ed.* **2000**, *39*, 2903–2906; b) C. W. Bielawski, R. H. Grubbs, *Macromolecules* **2001**, *34*, 8838–8840.

[205] S. S. Sheiko, M. Möller, *Chem. Rev.* **2001**, *101*, 4099–4124.

[206] a) J.-P. Laval, A. Lattes, R. Mutin, J. M. Basset, *J. Chem. Soc., Chem. Commun.* **1977**, 502–502; b) C. Edwige, A. Lattes, J. P. Laval, R. Mutin, J. M. Basset, R. Nouguier, *J. Mol. Catal.* **1980**, *8*, 297–311; c) D.-J. Liaw, C.-H. Tsai, *J. Mol. Catal. A: Chem.* **1999**, *147*, 23–31; d) T. M. Trnka, R. H. Grubbs, *Acc. Chem. Res.* **2001**, *34*, 18–29; e) S. Sutthasupa, F. Sanda, T. Masuda, *Macromolecules* **2009**, *42*, 1519–1525.

[207] S. Mekki, S. Saïdi-Besbes, A. Elaïssari, J.-P. Valour, A. Derdour, *Polym. J.* **2010**, *42*, 401–405.

[208] B. Kurzak, H. Kozłowski, E. Farkas, *Coord. Chem. Rev.* **1992**, *114*, 169–200.

[209] a) J. Park, K. An, Y. Hwang, J.-G. Park, H.-J. Noh, J.-Y. Kim, J.-H. Park, N.-M. Hwang, T. Hyeon, *Nat. Mater.* **2004**, *3*, 891–895; b) H. Pang, F. Gallou, H. Sohn, J. Camacho-Bunquin, M. Delferro, B. H. Lipshutz, *Green Chem.* **2018**, *20*, 130–135.

[210] H. L. Chee, C. R. R. Gan, M. Ng, L. Low, D. G. Fernig, K. K. Bhakoo, D. Paramelle, *ACS Nano* **2018**, *12*, 6480–6491.

[211] K. El-Boubbou, *Nanomedicine (London, U. K.)* **2018**, *13*, 929–952.

[212] a) D. Y. Ng, M. Arzt, Y. Wu, S. L. Kuan, M. Lamla, T. Weil, *Angew. Chem. Int. Ed.* **2014**, *53*, 324–328; b) C. Seidler, D. Y. W. Ng, Y. Wu, T. Weil, *Supramol. Chem.* **2016**, *28*, 742–746.

[213] C. Houga, J. Giermanska, S. Lecommandoux, R. Borsali, D. Taton, Y. Gnanou, J. F. Le Meins, *Biomacromolecules* **2009**, *10*, 32–40.

[214] a) S. Shipovskov, D. Trofimova, E. Saprykin, A. Christenson, T. Ruzgas, A. V. Levashov, E. E. Ferapontova, *Anal. Chem.* **2005**, *77*, 7074–7079; b) M. Moniruzzaman, N. Kamiya, M. Goto, *Langmuir* **2009**, *25*, 977–982; c) V. Stepankova, S. Bidmanova, T. Koudelakova, Z. Prokop, R. Chaloupkova, J. Damborsky, *ACS Catalysis* **2013**, *3*, 2823–2836.

[215] a) Z. Q. Xu, B. Yan, J. Riordon, Y. Zhao, D. Sinton, M. G. Moffitt, *Chem. Mater.* **2015**, *27*, 8094–8104; b) U. Massing, S. Cicko, V. Ziroli, *J. Controlled Release* **2008**, *125*, 16–24.

[216] K. S. Soni, S. S. Desale, T. K. Bronich, *J. Controlled Release* **2016**, *240*, 109–126.

[217] K. Velonia, A. E. Rowan, R. J. M. Nolte, *J. Am. Chem. Soc.* **2002**, *124*, 4224–4225.

[218] S. N. Alconcel, G. N. Grover, N. M. Matsumoto, H. D. Maynard, *Aust. J. Chem.* **2009**, *62*, 1496–1500.

[219] a) B. Le Droumaguet, K. Velonia, *Angew. Chem. Int. Ed.* **2008**, *47*, 6263–6266; b) S. Ganda, Y. Y. Jiang, D. S. Thomas, J. Eliezar, M. H. Stenzel, *Macromolecules* **2016**, *49*, 4136–4146.

[220] H. V. T. Nguyen, N. M. Gallagher, F. Vohidov, Y. V. Jiang, K. Kawamoto, H. Zhang, J. V. Park, Z. H. Huang, M. F. Ottaviani, A. Rajca, J. A. Johnson, *ACS Macro Lett.* **2018**, *7*, 472–476.

[221] S. C. Radzinski, J. C. Foster, J. B. Matson, *Macromol. Rapid Commun.* **2016**, *37*, 616–621.

[222] G. Wyszecki, R. W. Blevin, K. G. Kessler, K. D. Mielenz, *Principles Governing Photometry: Principes regissant la photometrie*, International Bureau of Weights and Measures, **1983**.

[223] a) N. Billecke, G. Rago, M. Bosma, G. Eijkel, A. Gemmink, P. Leproux, G. Huss, P. Schrauwen, M. K. Hesselink, M. Bonn, S. H. Parekh, *Histochem. Cell Biol.* **2014**, *141*, 263–273; b) F. Fleissner, M. Bonn, S. H. Parekh, *Sci. Adv.* **2016**, *2*, e1501778.

[224] Y. Liu, Y. J. Lee, M. T. Cicerone, *Opt. Lett.* **2009**, *34*, 1363–1365.

[225] S. Takehiko, *Tables of Molecular Vibrational Frequencies Vol. 1*, National Bureau of Standards, **1972**.

[226] G. R. Fulmer, A. J. M. Miller, N. H. Sherden, H. E. Gottlieb, A. Nudelman, B. M. Stoltz, J. E. Bercaw, K. I. Goldberg, *Organometallics* **2010**, *29*, 2176−2179.

[227] B. Jeong, M. R. Kibbey, J. C. Birnbaum, Y.-Y. Won, A. Gutowska, *Macromolecules* **2000**, *33*, 8317–8322.

[228] T. Mosmann, *J. Immunol. Methods* **1983**, *65*, 55–63.

[229] A. T. Dirks, J. J. Cornelissen, R. J. Nolte, *Bioconjugate Chem.* **2009**, *20*, 1129–1138.

[230] H. Li, B. Cheng, N. Boonnak, A. Padwa, *Tetrahedron* **2011**, *67*, 9829–9836.

[231] J. A. Love, J. P. Morgan, T. M. Trnka, R. H. Grubbs, *Angew. Chem. Int. Ed.* **2002**, *41*, 4035−4037.

[232] D. S. MacMillan, J. Murray, H. F. Sneddon, C. Jamieson, A. J. B. Watson, *Green Chem.* **2013**, *15*, 596−600.

6.3 SUPPLEMENTAL DATA

On the following pages are listed additional ^1H *NMR*, DOSY, and FTIR spectra as well as TEM, DLS and CMC data of compounds prepared in this thesis.

6.3.1 ^1H NMR SPECTRA

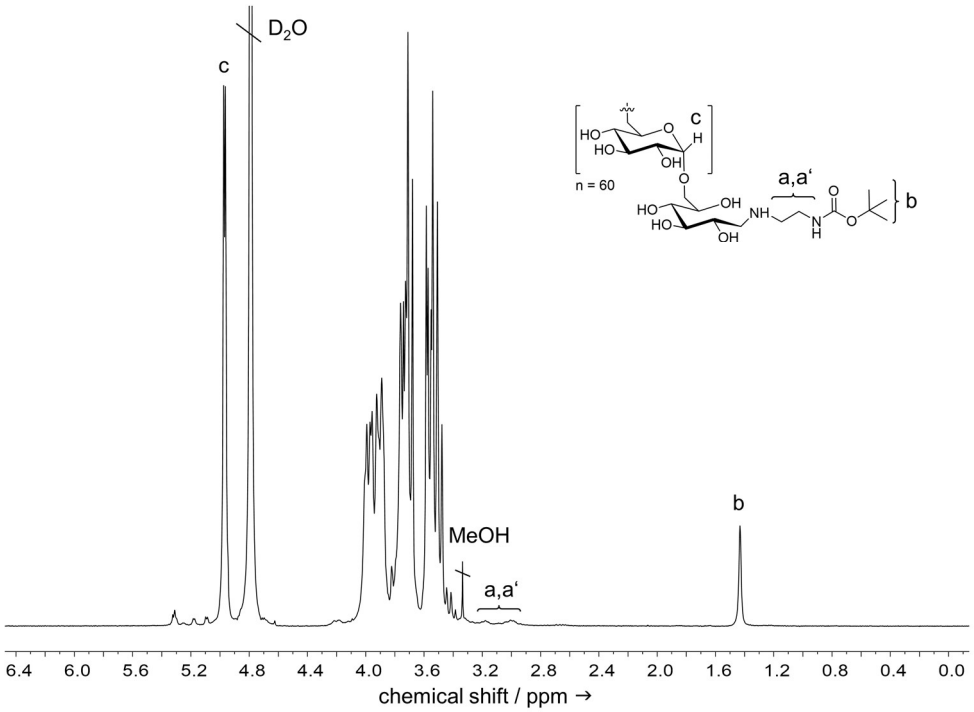

Figure 78. ^1H NMR (D_2O, 300 MHz) of Dex-NHBoc (10 kDa).

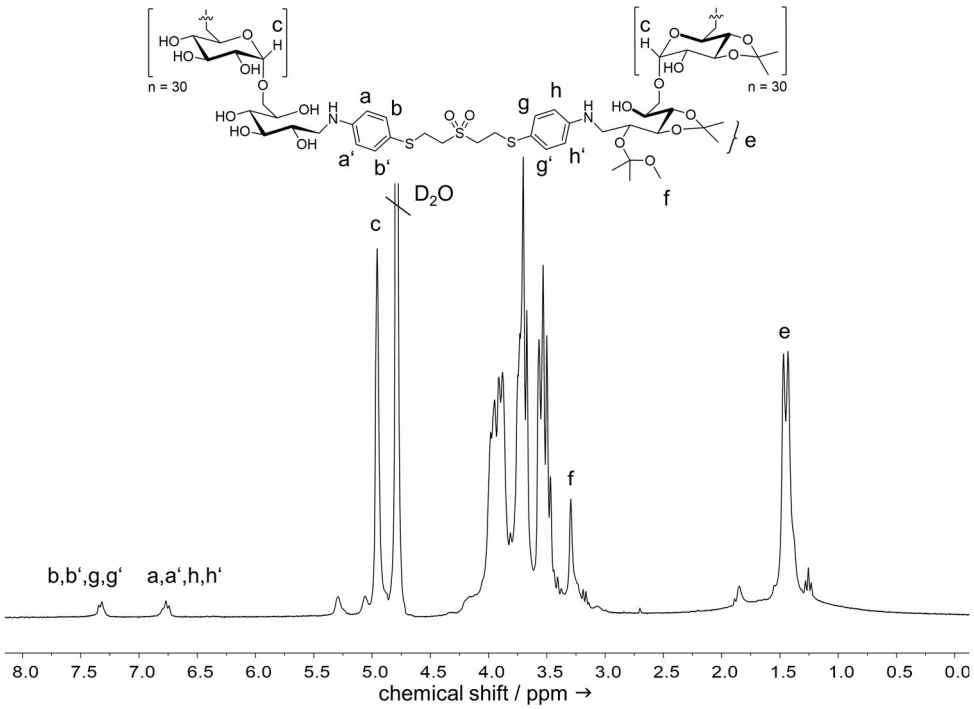

Figure 79. ^1H NMR (D_2O, 300 MHz) of Dex-S-VS-S-AcDex **104** (30% acetals).

6.3.2 DOSY SPECTRA

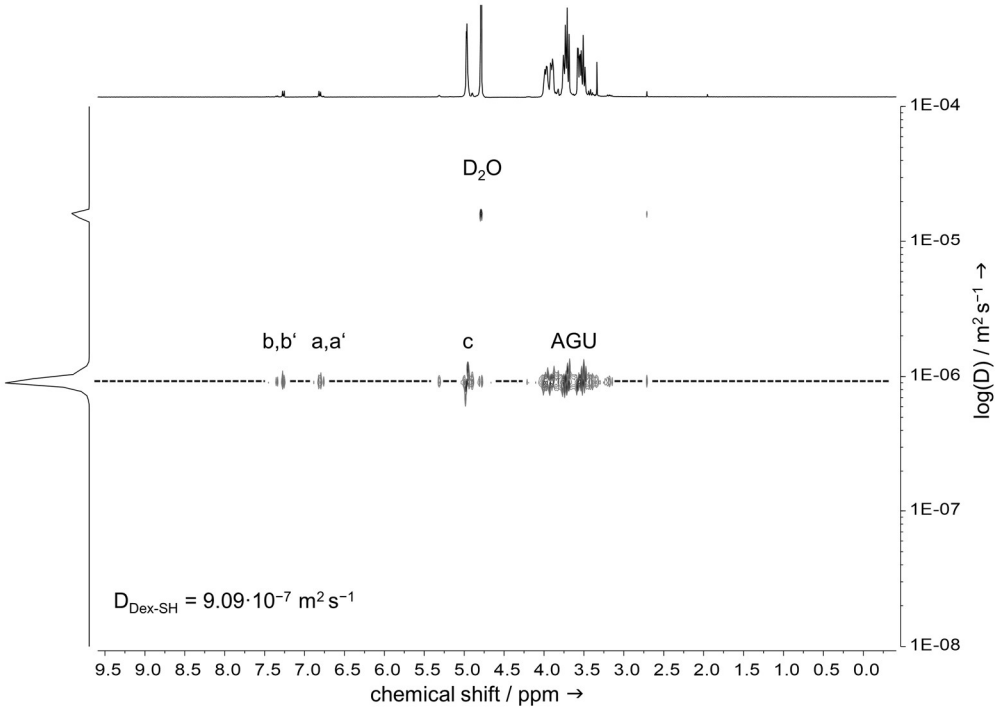

Figure 80. DOSY spectrum (400 MHz, D_2O) of thiol-modified Dex-SH **81**. The proton signals of (b-a') can be assigned to the introduced 4-ATP **80**. The anomeric proton at the dextran backbone is marked with (c) and the polysaccharide ring signals with (AGU).

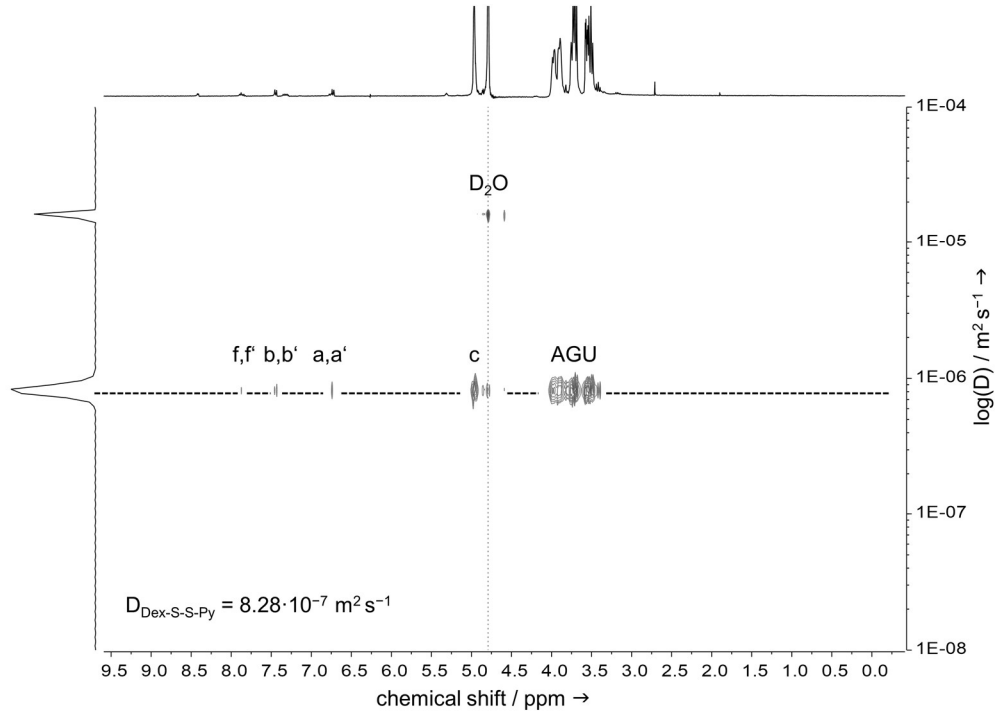

Figure 81. DOSY spectrum (400 MHz, D_2O) of Dex-S-S-Py **93**. The proton signals of (f and f') can be assigned to the introduced pyridyl-residue of DPDS **92**.

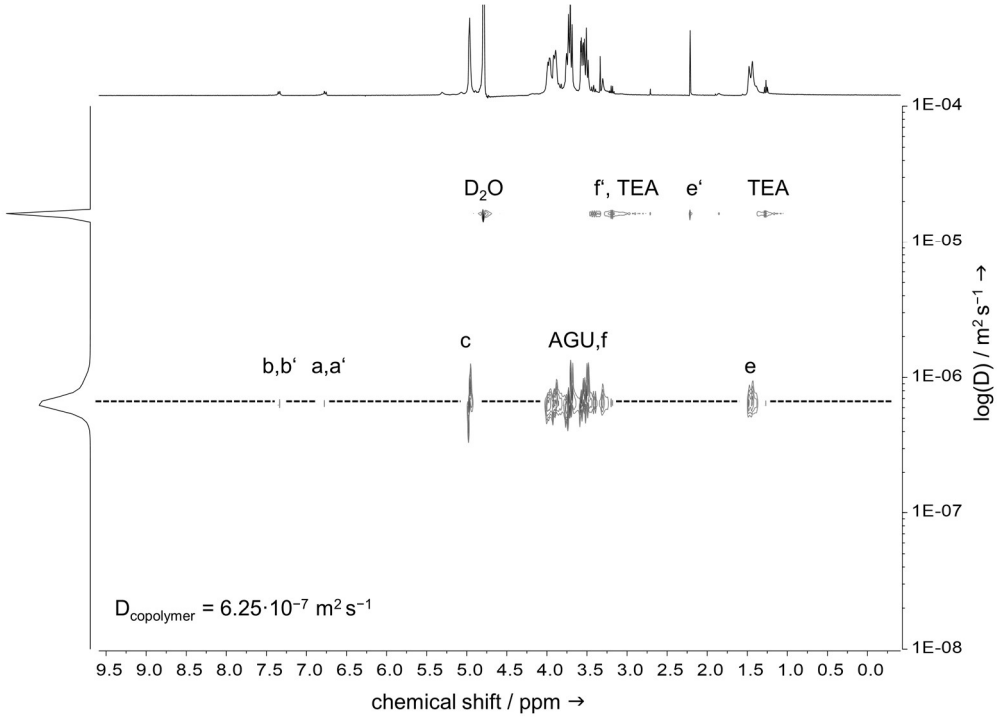

Figure 82. DOSY of Dex-S-VS-S-AcDex copolymer **104** (30%acetals) (400 MHz, D_2O). The proton signals of the acetals (e, f), the anomeric proton (c) and the aniline group (b, b') align at the same diffusion coefficient as the polysaccharide backbone protons (AGU). This strongly suggests a succesfull coblock formation. Due to long measurement times, some of the acetals are hydrolyzed, visible at the MeOH (f') and acetone proton signal (e').

6.3.3 FTIR SPECTRA

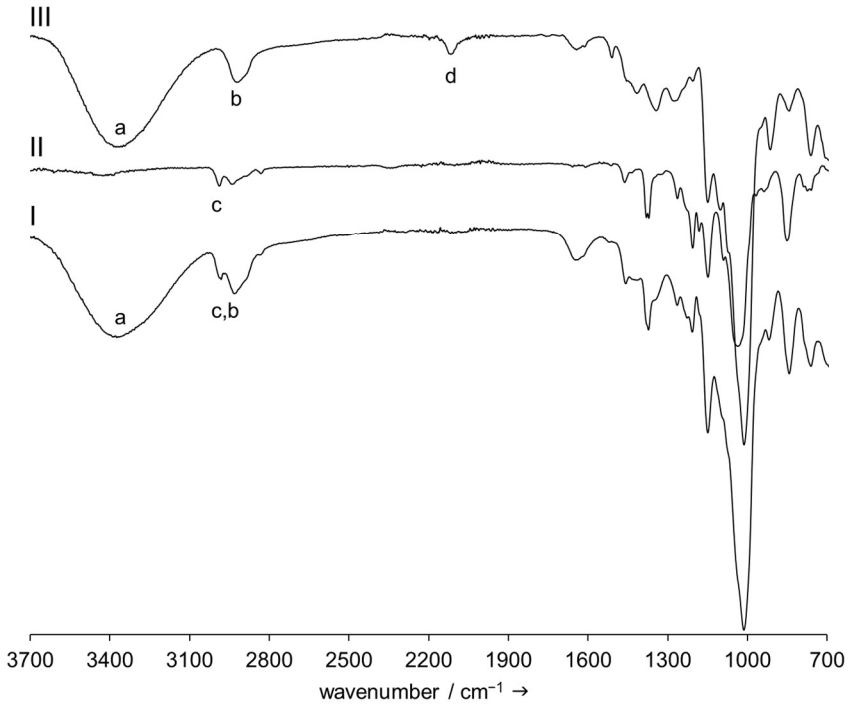

Figure 83. FTIR spectra of Dex-N_3 **75** (III), AcDex-alkyne **89** (II) and copolymer Dex-click-AcDex **91** (I). The absorption spectrum of the block copolymer (I) contains the characteristic O–H stretch signal at 3577-3082 cm^{-1} (a) of the hydrophilic block and the C–H stretch of the CH_3 group present in the introduced acetals at 2920 cm^{-1} (c). The azide group (d) of Dex-N_3 is visible at 2112 cm^{-1}. Reprinted with permission from *Breitenbach et al.*[152] Copyright 2017 American Chemical Society.

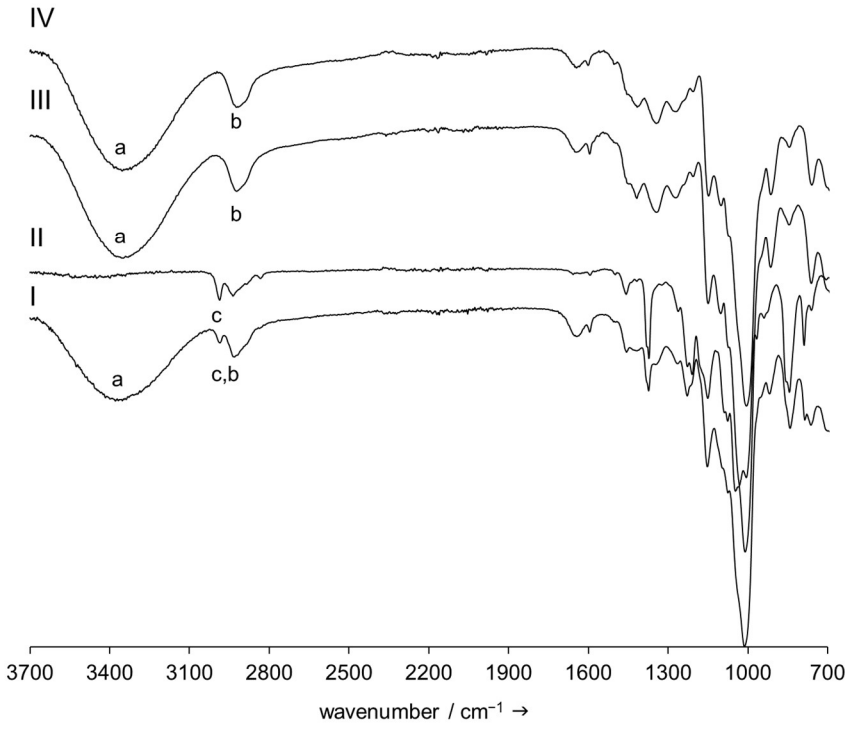

Figure 84. FTIR spectra of Dex-SH **81** (IV), Dex-S-S-Py **93** (III), AcDex-S-S-Py **98** (II) and Dex-S-S-AcDex **99** (I). The absorption spectrum of the block copolymer (I) contains the characteristic O–H stretch signal at 3577-3082 cm^{-1} (a) of the hydrophilic block and the C–H stretch of the CH_3 group present in the introduced acetals at 2920 cm^{-1} (c).

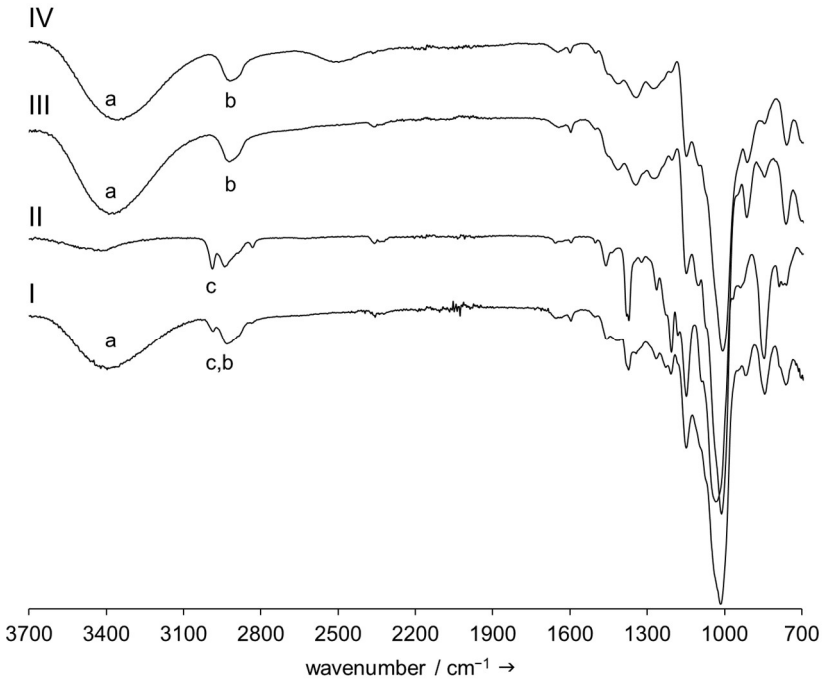

Figure 85. FTIR of Dex-SH **81** (I), Dex-S-VS **97** (II), AcDex-S-VS **103** (III) and Dex-S-VS-S-AcDex **104** (IV). The absorption spectrum of the block copolymer (I) contains the characteristic O–H stretch signal at 3577-3082 cm^{-1} (a) of the hydrophilic block and the C–H stretch of the CH_3 group present in the introduced acetals at 2920 cm^{-1} (c).

6.3.4 SEC DATA

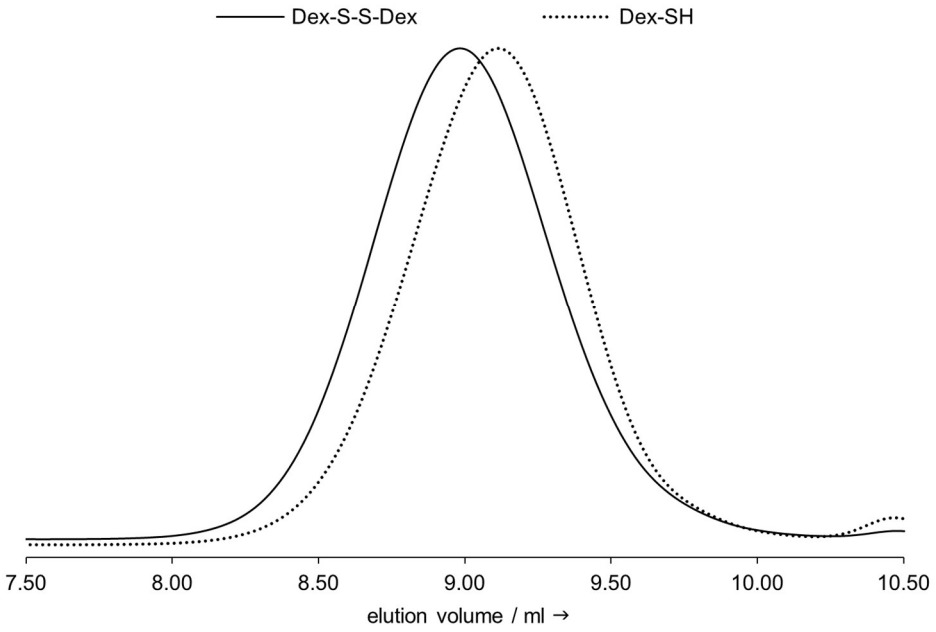

Figure 86. SEC measurement of Dex-SH **81**and two disulfide-linked dextranes (0.1 M $NaNO_3$, 1 mL min^{-1}).

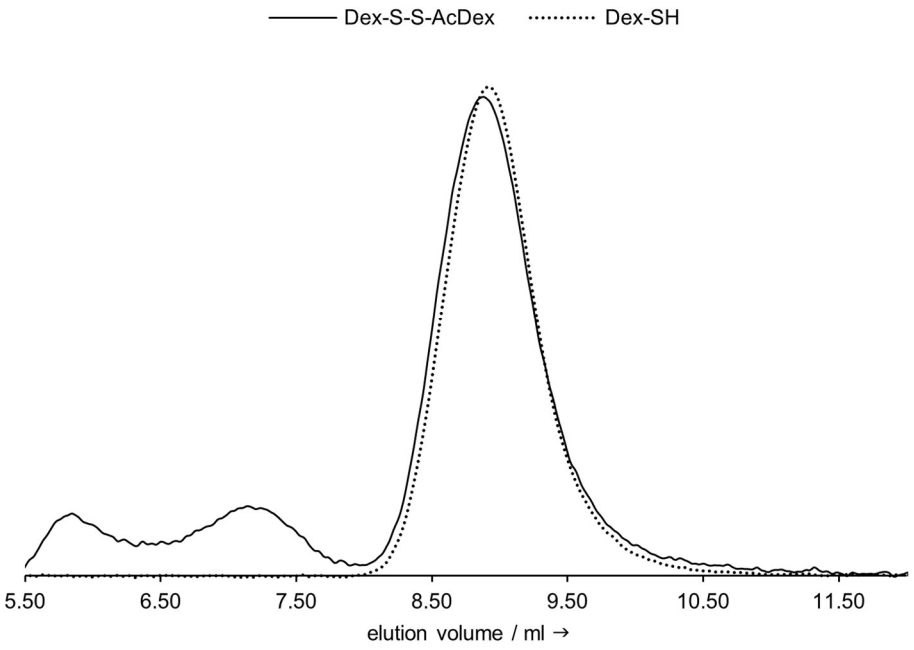

Figure 87. SEC measurement of Dex-SH **81** and block copolymer **99** (0.1 M $NaNO_3$, 1 mL min^{-1}). The amphiphilic polymer does not elute from the column like fully water soluble polymer with the same molecular weight (**Figure 86**). The high molecular weight species at 5.5–7.5 mL elution volume indicates micellation.

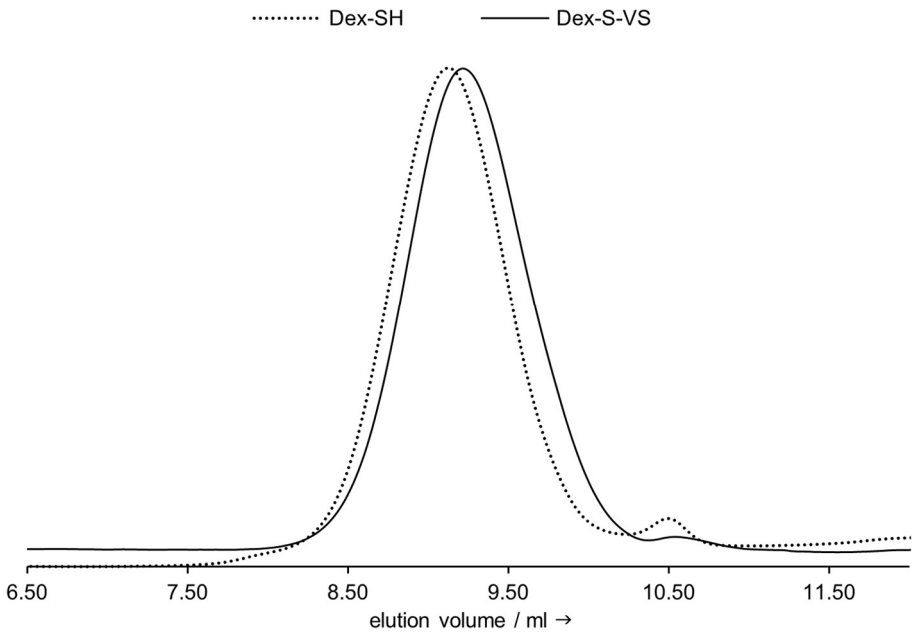

Figure 88. SEC measurement of Dex-SH **81** and Dex-S-VS **97** (0.1 M $NaNO_3$, 1 mL min^{-1}). The GPC traces show that Dex-S-VS has almost the same size as Dex-SH. No increase in mass by crosslinked side products can be observed. The slight retention in elution volume of Dex-S-VS might be due to hydrophobic interactions of the vinylsulfone group with the column material.

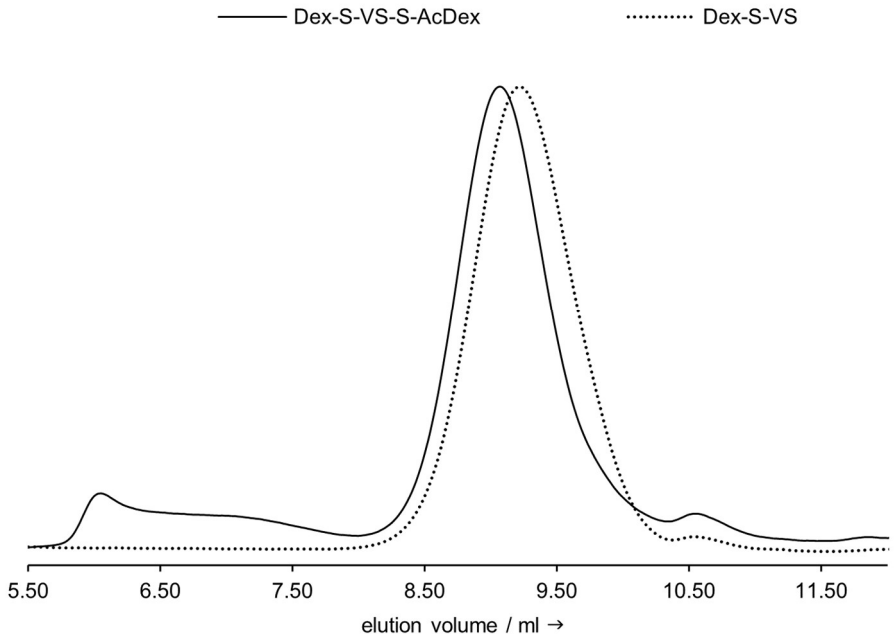

Figure 89. GPC trace of block copolymer **104** and Dex-S-VS **97** (0.1 M $NaNo_3$, 1 ml min^{-1}). The singal at lower retention times 5.8–7.5 mL elution volume indicates higher molecular weight species, probably micelles.

6.3.5 DLS/SLS DATA

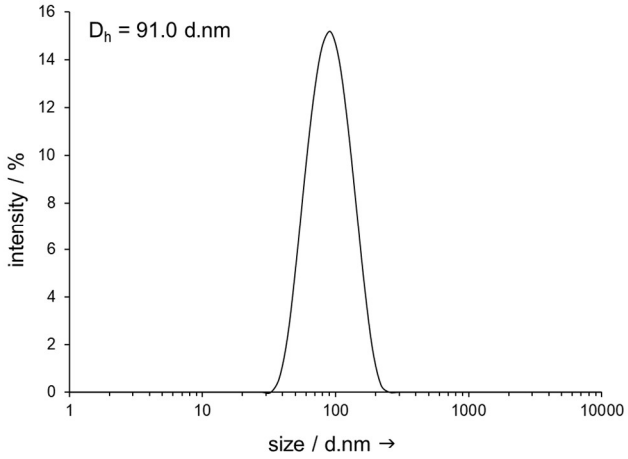

Figure 90. DLS (H_2O-dd, 2.5 mg mL^{-1}, pH 8) of Dex-click-AcDex **91** (23% acetals) sample after work up by dialysis. Adapted from *Breitenbach et al.*[152]

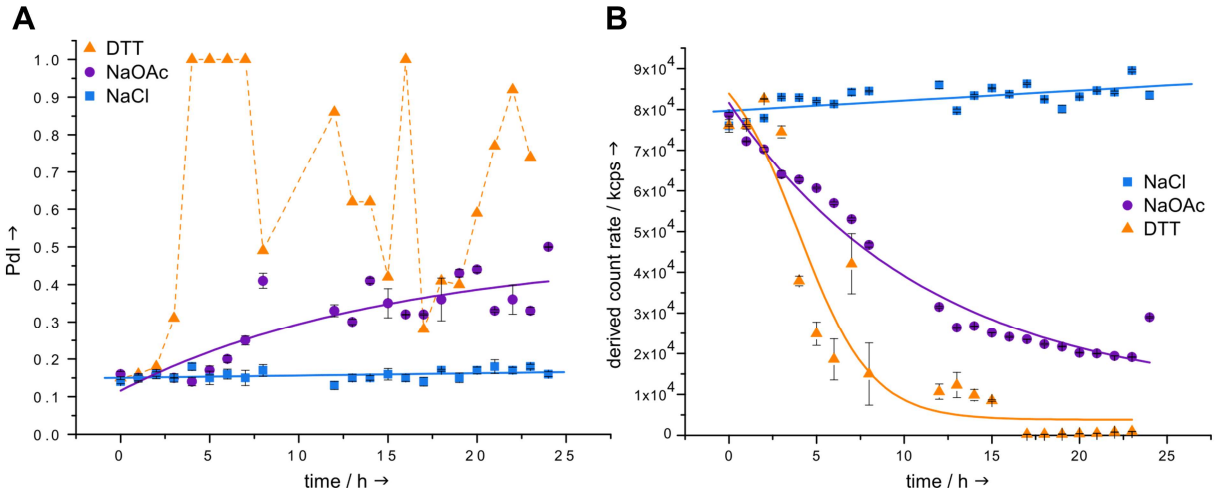

Figure 91. DLS data of PC(Zn)-loaded micellar particles. PdI describes the size distribution of the micellar nanoparticles. Values range from 0 (full monodisperse) to 1 (polydisperse). The particles incubated in NaOAc-buffer or with DTT aggregate and from large ill-definded structures caused by particle degradation (**A**) The derived count rate gives a description of the particle concentration in solution. Particles incubated in NaOAc-buffer (pH 5) or with DTT degrade over time. Over 24 h, the colloidal character of the micellar particle solution gets lost (**B**).

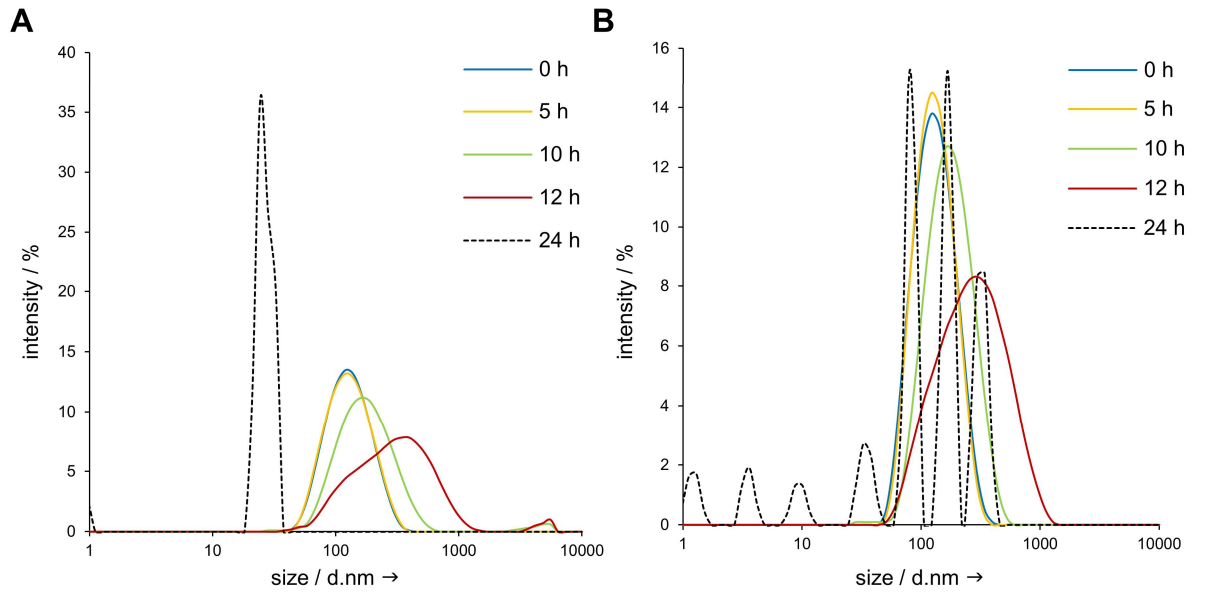

Figure 92. DLS data of Dex-S-VS-S-AcDex micelles in NaOAc (50 mM, pH 5). Micelles with encapsulated Nile red show beginning aggregation after 10 h, the next day, small ill-defined structures with D_H 30–20 nm have formed (**A**). Empty micelles without cargo decompose after 10 h and form larger aggregates until after 24 h the solution becomes strongly polydisperse (**B**).

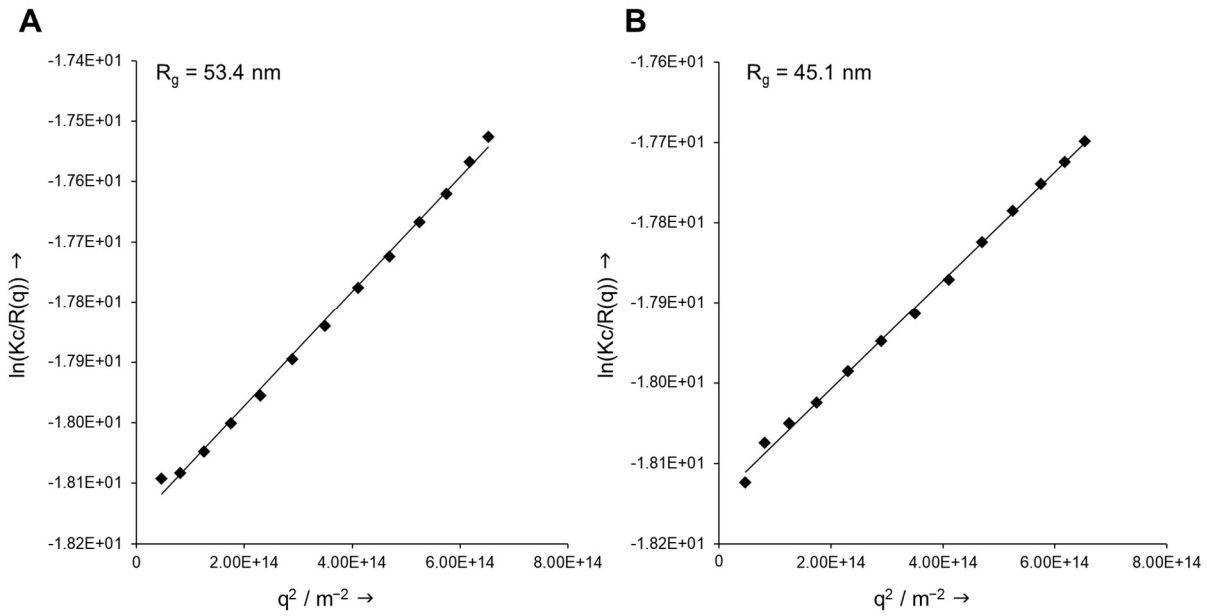

Figure 93. SLS Data for nanoparticles of amphiphile **99** PC(Zn)-loaded (**A**) and empty (**B**). C = 2 mg mL^{-1}, T = 20 °C, λ = 632.8 nm.

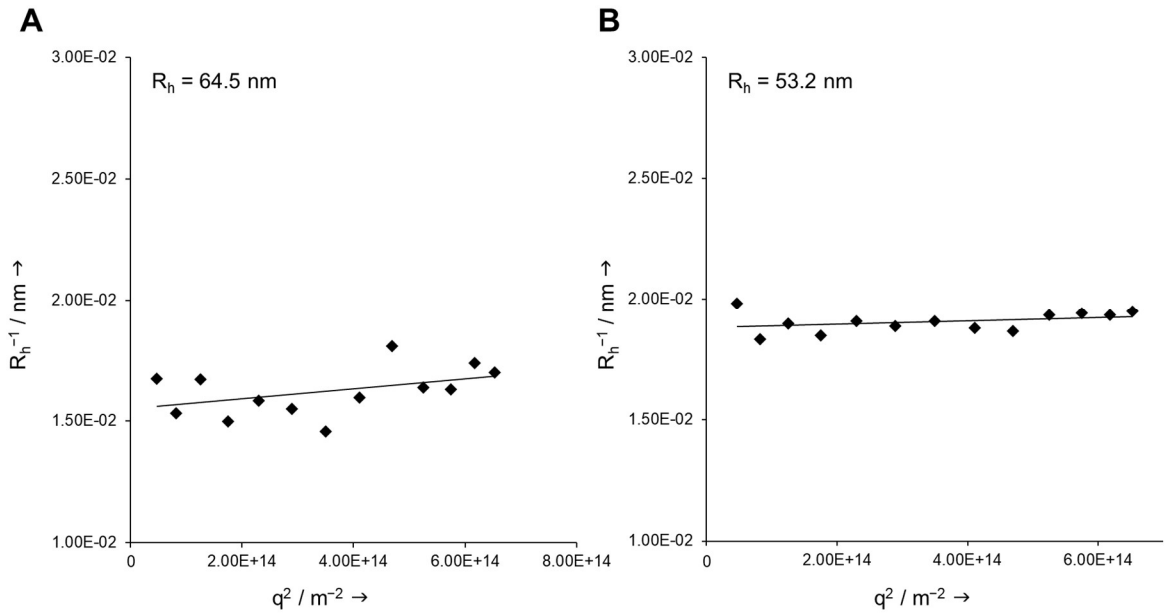

Figure 94. DLS Data for nanoparticles of amphiphile **99** PC(Zn)-loaded (**A**) and empty (**B**). C = 2 mg mL^{-1}, T = 20 °C, λ = 632.8 nm.

6.3.6 TEM/CRYO TEM DATA

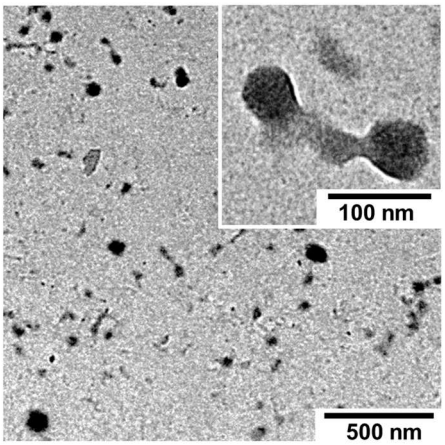

Figure 95. TEM image of block copolymer **91** directly after work up of click reaction. The dried particles have a diameter below 100 nm. Adapted from *Breitenbach et al.*[152]

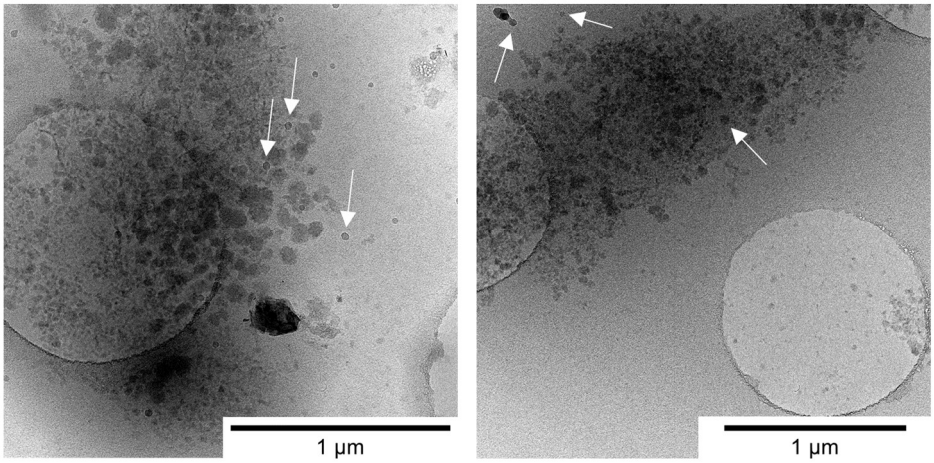

Figure 96. CRYO TEM images of PC(Zn)-loaded Dex-S-S-AcDex micelles (0.25 mg mL^{-1}). During single sided plotting, the particle solution would stream through the notch in the copper grid towards the cellulose membrane of the plotting seal. The solvent stream causes particle aggregation and concentrates around the gap. Marked with arrows are intact particles around the larger structures.

6.3.7 RINGTENSIOMETRIC DATA

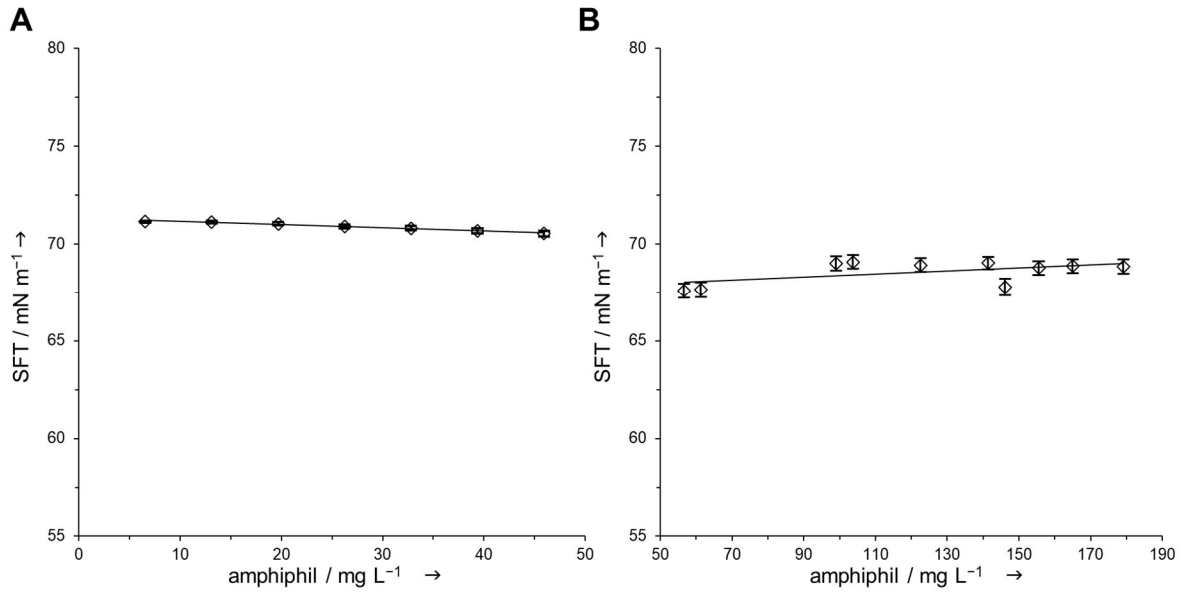

Figure 97. CMC data of Dextran T5 from two independent measurements. First measurement (**A**) the concentration was ranging from 6–46 mgL^{-1} dextran T5. For the second measurement (**B**) the concentration was ranging from 56–184 mgL^{-1} dextran T5.

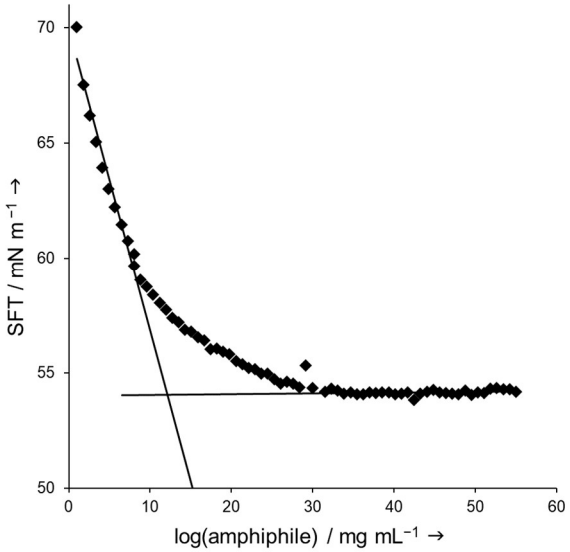

Figure 98. CMC data obtained for Dex-click-AcDex **91** (23% acetals) from three independent measurements in H_2O-dd (pH 8). The CMC is marked at the intersection of the straight lines calculated by linear regression. The final CMC is calculated to be 12 mg L^{-1}. Reprinted with permission from *Breitenbach et al.*[152] Copyright 2017 American Chemical Society.

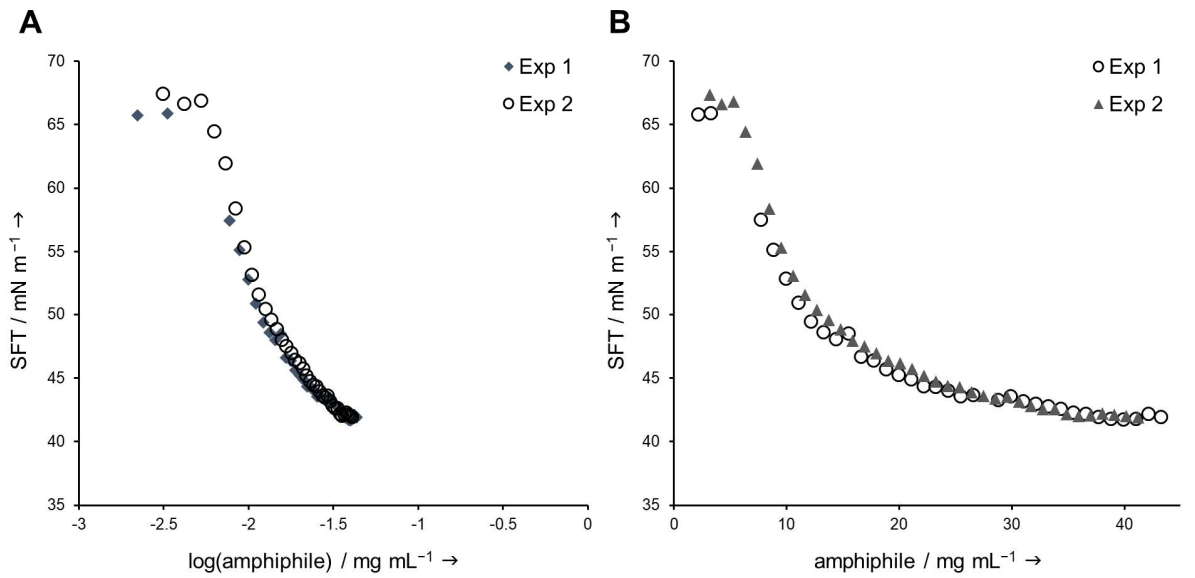

Figure 99. SFT vs. log(amphiphile) plot derived from two independent ringtensiometric measurements with Dex-click-AcDex **91** (30% acetals) for the calculation of pC_{20} and Γ (**A**). SFT vs. amphiphile-plot of the same amphiphile in five independent measurements for the determination of CMC and ΔG° (**B**).

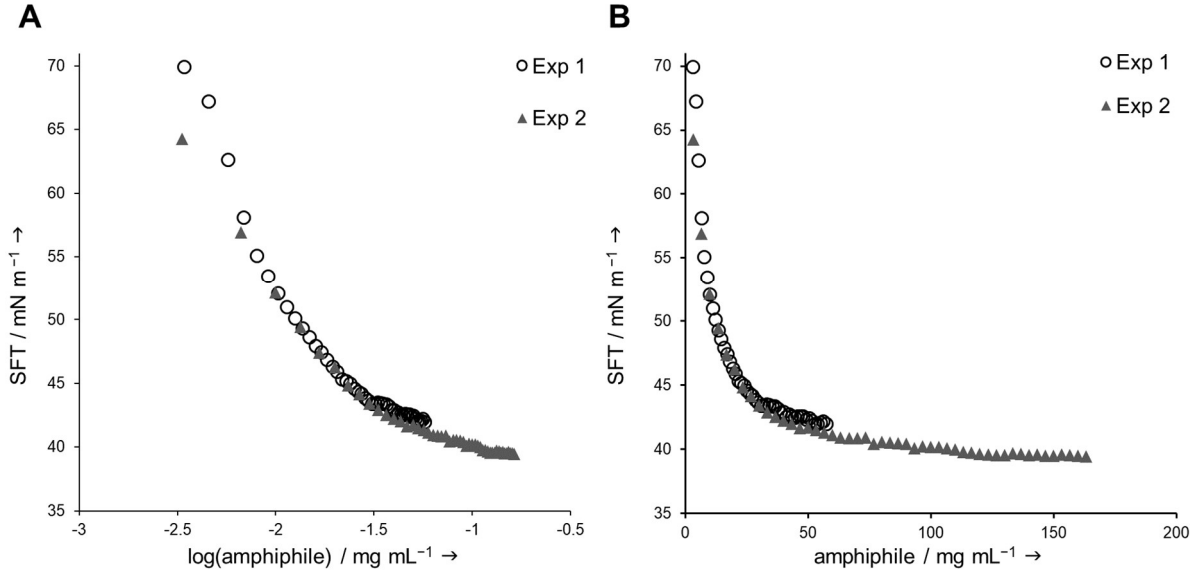

Figure 100. SFT vs. log(amphiphile) plot derived from two independent ringtensiometric measurements with Dex-S-S-AcDex **99** (23% acetals) for the calculation of pC_{20} and Γ (**A**). SFT vs. amphiphile-plot of the same amphiphile in five independent measurements for the determination of CMC and ΔG° (**B**).

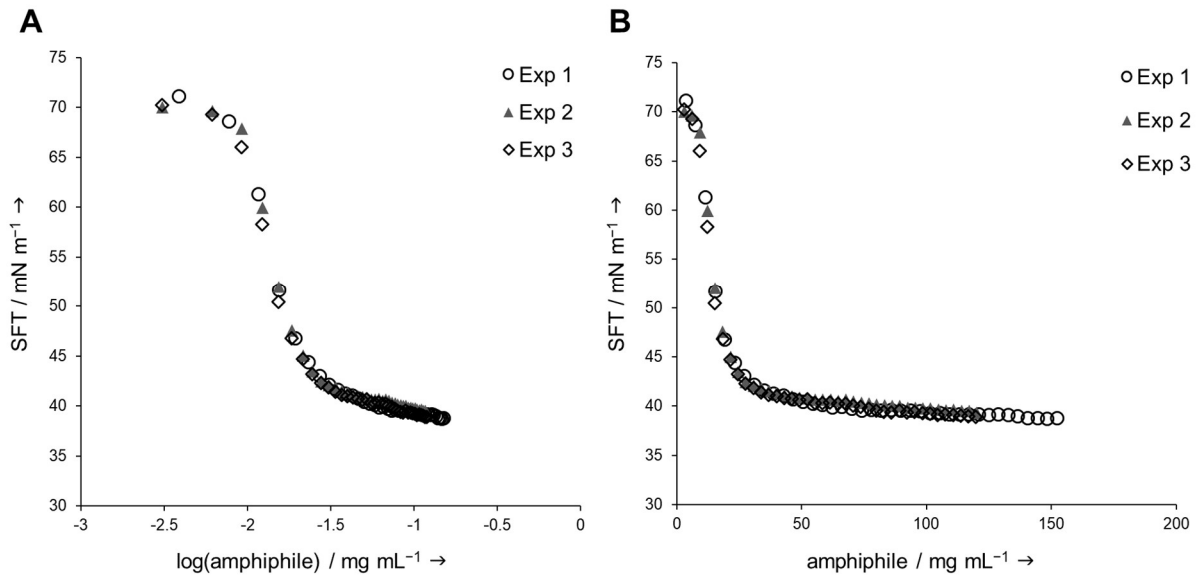

Figure 101. SFT vs. log(amphiphile) plot derived from three independent ringtensiometric measurements with Dex-S-VS-S-AcDex **104** (30% acetals) for the calculation of pC_{20} and Γ (**A**). SFT vs. amphiphile-plot of the same amphiphile in five independent measurements for the determination of CMC and ΔG° (**B**).

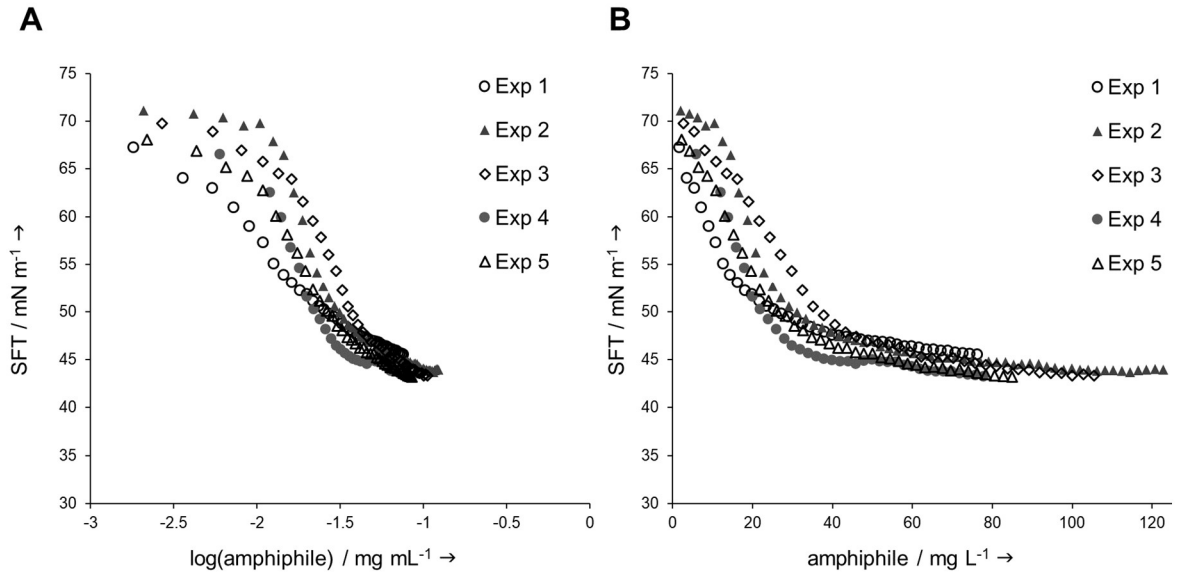

Figure 102. SFT vs. log(amphiphile) plot derived from five independent ringtensiometric measurements with Dex-S-VS-S-AcDex **104** (38% acetals) for the calculation of pC_{20} and Γ (**A**). SFT vs. amphiphile-plot of the same amphiphile in five independent measurements for the determination of CMC and ΔG° (**B**).